UNIVERSIDADE D
COIMBRA

Camila Giacomini Dariva

DEVELOPMENT OF DRUG DELIVERY SYSTEMS BASED ON HIGH WAVELENGTH LIGHT - PHOTOSENSITIVE POLYMERS

Doctoral Thesis of the Doctoral Program on Chemical Engineer supervised by Professor Arménio Coimbra Serra, Professor Jorge Fernando Jordão Coelho and Doctor Ana Clotilde Amaral Loureiro da Fonsceca and submitted to the Department of Chemical Engineering of the Faculty of Sciences and Technology of University of Coimbra

July 2020

Department of Chemical Engineering
of the University of Coimbra

DEVELOPMENT OF DRUG DELIVERY SYSTEMS BASED ON HIGH WAVELENGTH LIGHT - PHOTOSENSITIVE POLYMERS

Camila Giacomini Dariva

July 2020

1 2 9 0

UNIVERSIDADE Đ
COIMBRA

II

Financial Support:

IV

Às minhas famílias, de sangue e de coração.

"Quando cria harmonia em si próprio, o ser humano provoca harmonia nas coisas a sua volta. A questão é perceber que estamos em rede, que tudo esta conectado e que uma atitude benéfica transforma o entorno"

Monja Coen

Agradecimentos

A elaboração desta tese só foi possível graças a contribuição de inúmeras pessoas. Por isso expresso aqui os meus sinceros agradecimentos à todos aqueles que de modo directo ou indirecto contribuíram para o sucesso deste trabalho.

Primeiramente, ao Doutor Arménio Serra, o meu orientador científico, que sempre trouxe inúmeras ideias que me ajudaram a superar os grandes obstáculos encontrados ao longo do projecto. Agradeço também, por toda a sua disponibilidade, as discussões e os conselhos que guiaram-me e mantiveram-me motivada. Sou grata também por ter sido o meu *mentor* no âmbito profissional, modelo de dedicação, profissionalismo e carácter, mas mais que isso, a sua orientação abrangeu também o espectro pessoal, os seus conselhos e toda a sua generosidade tornaram-no para mim um "segundo pai". Também quero estender a minha gratidão à sua esposa, que além dos conselhos profissionais, acolheu-me como uma filha e consentiu em partilhar comigo uma das experiências mas marcantes na minha trajectória. Obrigada por todo apoio e suporte que vocês me deram aqui em Portugal.

Ao Doutor Jorge Coelho, meu co-orientador, obrigada pela oportunidade e confiança que depositou em mim desde o início. Agradeço também a disponibilidade, os conselhos e todo o apoio que deu-me neste trajeto.

À Doutora Ana Clotilde Fonseca, muito obrigada pelas análises de TGA, pelos inúmeros conselhos, ajuda, dicas e correcções. Acima de tudo, muito obrigada pela sua amizade e pelo seu exemplo.

A todo o grupo do PolySyc pelo acolhimento, amizade, apoio e suporte em todos os momentos de desespero e alegria. Todos que se frustraram e desesperaram comigo e mesmo assim sempre tiveram forças para ajudar-me a levantar. Obrigada em especial ao pessoal do B03/B05 pelo adorável ambiente de trabalho que sempre existiu, onde o bom humor deixa as dificuldades das experiências mais leves e o dia mais agradável. Obrigada também pelas inúmeras vezes que a vossa amizade saiu do departamento em inúmeros convívios sob sol ou sob granizo.

Ao João Figueiredo, que aceitou aventurar-se comigo nas tarefas de síntese dos polímeros sensíveis e das micelas. O teu esforço e dedicação foram fundamentais para este projeto.

À Doutora Mafalda Laranjo pelo contributo decisivo nos ensaios *in vitro* e à Catarina Ferreira por ensinar-me, auxiliar-me e acolher-me. Muito obrigada por toda a vossa disponibilidade, paciência, profissionalismo e amizade.

Aos meus colegas do laboratório do Instituto de Biofísica/Biomatemática Unidade de Biofísica (IBILI), que tão bem me acolheram, estando sempre disponíveis para me ajudar.

Ao Dr. Pedro Cruz, do Laboratório de Ressonância Magnética Nuclear (L-RMN) do Centro de Química de Coimbra, pela execução das análises de NMR.

À Professora Maria João Moreno e ao Jaime Samelo pela disponibilidade em marcar e auxiliar no uso do equipamento de DLS.

À Professora Dra. Sílvia Maria Gramacho Alexandre pela ajuda e disponibilidade em usar o espectrofotómetro de fluorescência.

Ao Dr. Rui Fernandes do Instituto de Biologia Molecular e Celular (IBMC) pela execução das análises de TEM.

Ao Departamento de Engenharia Química da Faculdade de Ciências e Tecnologia da Universidade de Coimbra e a todos os seus funcionários, pelas excelentes condições que me proporcionaram para o desenvolvimento do trabalho.

Ao Conselho Nacional de Desenvolvimento Científico e Tecnológico (CNPq) pelo financiamento do projecto.

A nível pessoal, um muito obrigada a todos aqueles que, participaram comigo nesta caminhada, em especial aos meus amigos que viajaram, dançaram, correram, caminharam, partilharam refeições e também secaram as minhas lágrimas neste turbilhão de experiencias que foi viver num novo país e em um novo projeto. Um agradecimento especial à Aline Arim e à Sónia Ribeiro que sempre estiveram presentes e prontas para ajudar-me. Obrigada por terem entrado na minha vida e pelas inúmeras lições que me ensinaram.

Ao Akel e ao André, meus amigos, irmãos e colegas de casa, por todo o suporte que sempre me dão, por partilharem comigo todas as experiências, por ouvir todos os meus lamentos e festejarem todas as minhas vitórias. Não foram poucas as lágrimas que derramamos neste nosso trajecto de crescimento pessoal, profissional e espiritual, mas foram elas que nos fortaleceram e proporcionaram os incontáveis momentos de alegria que sempre ficarão marcados no meu coração. O vosso apoio foi imprescindível para esta etapa e conto convosco para as próximas.

Ao Manuel, que sempre teve paciência e serenidade quando estive stressada. Obrigada por saberes encorajar-me quando estava intimidada, alegrar-me quando estava triste e distrair-me quando estava perto de perder a sanidade. Obrigada pela disponibilidade, atenção e apoio em todos os momentos. Foram inúmeras as vezes em que me ouviste desabafar, mesmo que te custasse noites inteiras em claro. Obrigada pela confidência, por acreditares em mim, ensinar-me a viver uma etapa de cada vez e, principalmente, obrigada por todo o amor e carinho.

X

Por fim, à minha família que me encorajou a entrar nesta aventura e sempre apoiou-me incondicionalmente. Obrigada pelo amor incondicional, carinho, fé e compreensão ao longo da minha vida. Principalmente, obrigada por incentivar-me a correr atrás dos meus objectivos, mesmo que isso signifique estarmos afastados.

Obrigada, do fundo do coração, a todos os que comigo percorreram este caminho!

Abstract

Drug delivery systems have been designed to provide a pharmaceutical compound in a controlled manner, into a specific site. These systems are developed to reduce the drug side effects and control the biodistribution profile in order to improve therapeutic efficacy. One of the most common categories of these systems is the nanoparticle (such as hydrogels, liposomes and micelles). The drug is encaged inside the nanoparticle and driven to the required site (usually by the incorporation of target molecules or taking advantage of the enhanced permeability and retention effect of tissues), where the drug release will occur. In some applications, such as cancer therapy, a burst release of the drug could enhance the efficacy against the cancer cells. A range of stimuli can trigger the process of drug delivery. These stimuli can have internal (reactive oxygen species, pH, temperature) or external causes (ultrasound, magnetic field, light). For cancer therapy, micelles that release the drug upon an external stimulus are more advantageous, as the drug release is independent of the tumor-type or the specificity of the microenvironment of each cancer type/stage. The use of light, particularly, allows a controlled spatio-temporal drug release. In the electromagnetic spectrum, the deepest penetration in biological tissue is achieved by near-infrared light (NIR), which additionally, corresponds to less harmful effects on cells. This low energy radiation can unleash the drug release by generating highly reactive singlet oxygen ($^1O_2$) species through the excitation of a photosensitizer. The $^1O_2$ can react with specific molecules, resulting in a hydrophilicity change or cleavage of the nanoparticle structure, thus promoting a fast drug release. The aim of this work was the development of light-sensitive polymers to be used in the design of nanocarriers for biomedical applications, namely cancer therapy. The strategy involved the synthesis of $^1O_2$ sensitive molecules belonging to the vinyl disulfide family (1,2-bis(2-hydroxyethylthio)ethylene, BHETE and 1,2-bis(carboxyethylthio)ethylene, BCETE), that was covalently inserted into a polymer backbone. Three different types of polymers were developed, namely, two light-sensitive amphiphilic block copolymers, viz. poly(ethylene glycol)-BHETE-Poly(lactic acid) (PEG-BHETE-PLA) and PEG-Poly(1,4-dithio-7,10-dioxa-2-dodecene)-PEG (PEG-PDDD-PEG), and a light-sensitive BCETE based poly(ester amide). Additionally, a new concept of light cleavable molecules was developed.

The PEG-BHETE-PLA copolymers were successfully synthesized under mild conditions, exhibiting a narrow polydispersity. The block copolymers were able to form micellar structures in an adequate size for a drug delivery system and also presenting a reasonable drug loading capacity (considering the physical encaging of doxorubicin inside

a nanoparticle with a PLA core). The kinetic release of doxorubicin was studied and allowed to confirm the light-triggered micelle disassembly. In vitro tests were carried out with MCF7 cell lines and confirmed the non-cytotoxicity of the bare micelles. The anti-cancer efficacy of the micelles loaded with doxorubicin and the photosensitizer was tested in the same cell lines, and the results showed an increase in cell death in the systems that were irradiated with red light.

Considering the advantages over the in situ burst release of drugs in cancer therapy, to enhance the eradication of the tumor cells, a strategy to boost the micelle disassembly was hypothesized. Hence, a new polymer (PDDD) bearing the light-sensitive moiety in each repeating unit was developed. The PDDD was easily synthesized under mild conditions and proton nuclear magnetic resonance (^{1}H NMR) spectroscopy analysis proved that polymer cleavage is initiated by light. The covalent linkage of PEG blocks to PDDD (PEG-PDDD-PEG) yielded an amphiphilic triblock copolymer, that is able to form micellar structures with a drug loading capacity of doxorubicin, similar to the PEG-PLA micelles. The amount of drug released from PEG$_{5k}$-PDDD-PEG$_{5k}$ micelles was found to be 7% higher than the amount released from PEG-BHETE-PLA. It is worth mentioning that the PEG$_{5k}$-PDDD-PEG$_{5k}$ exhibited a burst release in the first 30 minutes.

Light-sensitive poly(ester amide)s were prepared by interfacial polymerization using a diacyl chloride based on BCETE and an α-amino acid based diamine. The number of light-sensitive molecules in the poly(ester amide)s' chain was controlled by varying the content of BCETE from 0 to 100%. The cleavage induced by light was confirmed by ^{1}H NMR and size exclusion chromatography (SEC).

Lastly, a new concept of light-sensitive moiety was evaluated. The cleavage strategy of this molecule was based on Photoinduced Electron Transfer for Reversible Addition-Fragmentation Chain Transfer (PET-RAFT) polymerization methodology, with the difference that a hydrogen donor was used to ensure the stability of the fragments resulting from the cleavage. The 2-(dodecylthiocarbonothioylthio)-2-methylpropionic acid (DDMAT, a commercial RAFT agent) was cleaved by light irradiation in the presence of a photosensitizer. This molecule can have the potential to be used as a new light-sensitive moiety in a polymer for application in drug delivery systems.

Overall, this research work has contributed to the development of light-sensitive polymers and drug delivery systems. Simple polymer synthesis and straightforward nanoparticle preparation were used in order to develop a non-expensive and promising 'magic bullet' system.

XVI

Resumo

Sistemas de entrega de fármacos são projectados para permitir a libertação de maneira controlada e em locais específicos. Estes sistemas pretendem reduzir os efeitos secundários e controlar o perfil de biodistribuição do fármaco com o objetivo de melhorar a eficácia terapêutica. As nanopartículas (tais como hidrogéis, lipossomas e micelas) são uma das categorias mais comuns destes sistemas. Nestas, o fármaco é aprisionado no seu interior e é direcionado para o local alvo (geralmente por meio da incorporação de moléculas específicas ou tirando vantagem do efeito de aumento de permeabilidade e retenção nos tecidos, no caso de doenças tumorais). Em algumas aplicações, como na terapia contra o cancro, a libertação total e instantânea do medicamento pode levar a maior eficácia do tratamento. Para tal, vários estímulos são capazes de desencadear o processo de libertação do medicamento. Estes estímulos podem ser internos (espécies reactivas de oxigénio, pH e temperatura) ou externos (ultra-sons, campo magnético e luz). Na terapia contra o cancro, as nanopartículas capazes de realizar a libertação do medicamento através de estímulos externos podem trazer mais vantagens, já que a libertação do fármaco ocorre independentemente do tipo de tumor ou peculiaridades do microambiente de cada tumor. Em especial, o uso da luz permite a libertação do medicamento através de um controlo espacial e temporal. Dentro do espectro electromagnético, a luz que apresenta uma maior penetração em tecidos biológicos situa-se na zona do infravermelho próximo, a qual demonstra o menor efeito nocivo para as células. Esta radiação com baixa energia pode iniciar a libertação do medicamento com a geração de espécies reactivas como o oxigénio singleto ($^1O_2$) por meio da excitação de fotosensibilizadores. O $^1O_2$ pode reagir com moléculas específicas, resultando na mudança da hidrofilicidade ou na quebra da estrutura das nanopartículas, que promove uma rápida libertação do fármaco.

O objectivo deste trabalho foi o desenvolvimento de nanopartículas poliméricas sensíveis a luz para serem usados em nanotransportadores para aplicações biomédicas, nomeadamente na terapia do cancro. A estratégia usada envolve a síntese de polímeros com base em moléculas sensíveis a $^1O_2$ pertencentes a família dos disulfuretos vinílicos (1,2-bis(2-hidroxietiltio)etileno, BHETE e 1,2-bis(carboxietiltio)etileno, BCETE), os quais são covalentemente inseridos na cadeia principal do polímero. Três tipos diferentes de polímeros foram desenvolvidos, nomeadamente, dois copolímeros de bloco amfifílicos sensíveis a luz, como polietileno glicol-BHETE-poli (ácido lactico) (PEG-BHETE-PLA) e PEG-Poli(1,4-ditio-7,10-dioxa-2-dodeceno)-PEG (PEG-PDDD-PEG), e poli(ester amidas)

sensíveis a luz. Adicionalmente foi desenvolvido um novo sistema de quebra de moléculas pela acção da luz.

Os copolímeros de PEG-BHETE-PLA foram sintetizados sob condições de reacção suaves e apresentaram baixa polidispersividade. Os copolímeros foram capazes de formar estruturas micelares com um tamanho adequado para sistemas de libertação de fármacos e apresentaram uma razoável capacidade de encapsulação de doxorubicina. A cinética de libertação da doxorubicina encapsulada foi estudada e permitiu a confirmação da desestruturação das micelas quando sujeita à acção da luz. Testes *in vitro* com a linha celular MCF7 foram realizados e confirmaram a ausência de toxicidade das micelas. A eficácia anticancerígena das micelas carregadas com doxorubicina e o fotossensibilizador (simultaneamente) foi testada e os resultados mostraram um aumento da mortalidade celular do sistema quando irradiado com a luz vermelha.

Considerando as vantagens de uma libertação completa, imediata e *in situ* de medicamentos para promover a erradicação completa de células tumorais, na terapia contra o cancro, foi pensada uma estratégia para promover a destabilização tão completa quanto possível da nanopartícula transportadora do fármaco. Um novo polímero (PDDD) contendo uma unidade sensível a luz em cada unidade de repetição foi desenvolvido. O PDDD foi facilmente sintetizado sob condições amenas e a análise por espectroscopia de ressonância magnética de protão (^{1}H RMN) provou a quebra do polímero sob a acção da luz. A ligação covalente do PDDD a blocos de PEG (PEG-PDDD-PEG) produziu um copolímero tribloco anfífilico capaz de formar estruturas micelares com uma capacidade de encapsulação de doxorubicina similar a das micelas de PEG-PLA. A quantidade de medicamento libertada pelas micelas de PEG$_{5k}$-PDDD-PEG$_{5k}$ foi 7% maior do que a quantidade libertada para a micelas de PEG-BHETE-PLA. É importante mencionar que o PEG$_{5k}$-PDDD-PEG$_{5k}$ exibiu uma libertação "explosiva" nos primeiros 30 minutos.

As poli(ester amidas) sensíveis a luz foram preparadas por polimerização interfacial usando um cloreto diacil baseado na molécula de BCETE e na diamina baseada em α-amino ácidos. Foram preparados polímeros com diferentes valores de incorporação da molécula sensível à luz. A quebra da estrutura destes polímeros, induzida pela luz, foi confirmada pela ^{1}H RMN e cromatografia por exclusão de tamanho (SEC).

Por último, um novo conceito de unidade sensível a luz foi avaliado. A estratégia de quebra da molécula foi baseada na metodologia de polimerização chamada de Transferência de Electrões Foto-induzida por Transferência Reversível de Cadeia por Adição-Fragmentação (PET-RAFT), com a diferenciação de que um doador de hidrogénio foi usado para estabilizar os fragmentos resultantes da reacção de quebra. O ácido 2-(dodeciltiocarboniltioiltio)-2-metilpropiónico (DDMAT, um agente RAFT comercial) foi

XVIII

quebrado pela irradiação de luz na presença de um fotossensibilizador. Esta molécula pode ter potencial para ser usada como uma nova unidade sensível a luz em polímeros para a aplicação em sistemas de entrega de medicamentos.

Em suma, este trabalho de pesquisa contribuiu para o desenvolvimento de polímeros sensíveis a luz para fazer parte de sistemas de entrega de fármacos. Os processos de síntese desenvolvidos são relativamente simples e os métodos de preparação de nanopartículas utilizados originaram sistemas de libertação efetivos, promissores e não dispendiosos.

Palavras-chave: polímeros sensíveis a luz; sistemas inteligentes de entrega de medicamento; oxigénio singleto; nanopartículas

xx

Thesis Outline

The main goal of this PhD work was the development of biocompatible drug delivery systems sensitive to high-wavelength light, with potential application in cancer therapy. The thesis is organized into four chapters.

Chapter 1 gives an overview of the concept of nanocarriers, their use in drug delivery systems (DDS), especially in cancer chemotherapy centered on the stimuli-responsive systems, namely those that are sensitive to light. Presents the main characteristics required for a polymer to form micelles and the synthesis route for the PLA-PEG micelles. This chapter also presents the light sensitive moieties capable of suffering cleavage or hydrophobicity change when in contact with singlet oxygen and their application in micellar systems for cancer therapy (C.G. Dariva, J.F.J. Coelho, A.C. Serra, Near infrared light-triggered nanoparticles using singlet oxygen photocleavage for drug delivery systems, J. Control. Release. 294 (2019) 337–354. doi:10.1016/j.jconrel.2018.12.042).

Chapter 2 describes the materials and methods used for the synthesis and characterization of the materials.

Chapter 3 presents the results obtained in the course of this work and the respective discussion. This chapter is divided into three sections:

- o 1) synthesis of PEG-PLA with sensitive molecules; the light-sensitive amphiphilic PEG-PLA copolymers were synthesized and characterized, followed by the nanoparticle formation. The properties of the nanoparticles, as doxorubicin carrier, were evaluated by lab experiments and *in vitro* assays;
- o 2) preparation of nanoparticles based on monomers that are light responsive. A polymer containing a structural unit with sensitivity for singlet oxygen was synthesized and characterized. Functionalization with PEG originates an amphiphilic copolymer. Encapsulation of doxorubicin and drug release studies were carried out;
- o 3) synthesis of polymers with light sensitive segments. A poly(ester amide) containing a variable amount of light-sensitive segment was synthesized, characterized and evaluated by its cleavage kinetics under

light irradiation; proof of concept of a new system with light-sensitive segment based on the PET-RAFT polymerization concept was carried out.

Chapter 4: the overall conclusions and final remarks of the work are referred, along with the recommendation for future studies and research lines.

List of Nomenclatures, Acronyms and Abbreviations

Symbols	Definitions
rac-lactide	3,6-Dimethyl-1,4-dioxane-2,5-dione
^{13}C NMR	Carbon-13 Nuclear Magnetic Spectroscopy
^1H NMR	Proton Nuclear Magnetic Spectroscopy
$^1O_2$	Singlet oxygen
^1PS	Singlet photosensitizer excited state
238	*meso*-tetra(2,6-dichlorophenyl) porphyrin
3-MPA	Mercaptopropionic acid
$^3O_2$	Ground triplet state of oxygen molecule
^3PS	Stable excited triplet state of the photosensitizer
4T1	Murine breast cancer cells
A549	Human lung cancer cells
ACS-5	*meso*-tetra(2,6-dichloro-3-sulphonic acid phenyl) porphyrin
ACT	Acetone
AmAc	Aminoacrylate
ANOVA	Analysis of variance
ATN	Acetonitrile
B-16	Murine melanoma tumor cells
BATA	Sensitive bis-(alkylthio) alkene
BCAETE	1,2-bis(chloroalcylethylthio)ethylene
BCETE	1,2-bis (carboxyethylthio)ethylene
BHETE	1,2-bis(2-hidroxyethylthio)ethylene
BPAD	Benzophenylporphyrin monoacid derivative
BxPC-3	Hypoxic and hypopermeable pancreatic tumors cell line
CA4	Combretastatin A-4
CDDP	Cisplatin
Ce6	Chlorin e6
CLF	Chloroform
CMC	Critical micellar concentration
CP	Cysplatin
$C_{polymer}$	Fraction of the polymer in the copolymer chain
CPT	Camptothecin
Đ	Dispersity
δ	Chemical shift
$\Delta G°$	Standard free energy associated with the micelle formation
$\Delta H°$	Standard enthalpy changes
$\Delta S°$	Standard entropy change
DBU	1,8-diazabicyclo[5.4.0]undec-7-ene

DCC	N,N'-Dicyclohexylcarbodiimide
DCM	Dichloromethane
DD	Direct dialysis
DDMAT	(dodecylthiocarbonothioylthio)-2-methylpropionic acid
DDS	Drug delivery systems
DLC	Drug Loading Capacity
DLE	Drug Loading Efficiency
DLS	Dynamic light scattering
DMA	*N, N'*-dimethylacetamide
DMAP	4-Dimethylaminopyridine
DMF	Dimethyformamide
DMSO	Dimethyl sulfoxide
DMTA	Dynamic mechanical thermal analysis
dn/dc	Refractive index increment
DNQ	2-diazo-1,2-naphthoquinone
DOX	Doxorubicin
DOX.HCl	Doxorubicin hydrochloride
DV	Differential viscometer
EDANS	5-[(2-aminoethyl)amino]naphthalene-1-sulfonic acid
EPR	Enhanced permeability and retention effect
EtOAc	Ethyl acetate
f	Volume fraction in the copolymer
FBS	Fetal bovine serum
FDA	Food and Drug Administration
FTIR-ATR	Fourier-transform infrared attenuated total reflection
GPC	Gel permeation chromatography
η	Number of Mols
H&E	Hematoxylin and eosin immunostaining
HB	Hydrophobic
Hep G2	Human liver cancer cell line
HL	Hydrophilic
HMAP	Hexane-1,6-diyl bis(4-methyl-2-(methylamino)pentanoate)
HO$^{\bullet}$	Oxidant hydroxyl radical
HPLC	High performance liquid chromatography
HPTS	Trisodium salt of 8-hydroxypyrene-1,3,6-trisulfonic acid
I	Stirring inside the dialysis bag
IC_{50}	The half maximal inhibitory concentration
ICG	Indocyanine green
IM	Imidazole group
K-1735	Mouse melanoma tumor cells
λ	Wavelength

l_c	Hydrophobic length chain
L-02	Human hepatic cells line
LED	Light emitting diode
M theoretical	Theoretical molecular weight
MCA	Merocyanine
MCF7	Michigan Cancer Foundation-7 Breast cancer cell line
MDA-MB-231	Human breast cancer cell line
M_n	Average Number Molecular Weight
mPEG	Mono methyl ether
mPEG-COOH	Carboxyl-terminated mPEG
MTT	3-(4,5-dimethylthiazol-2-yl)-2,5-diphenyltetrazolium bromide assay
M_w	Molecular weight
N	Number of independents assay carried
N_{agg}	Number of polymers aggregated in each micelle
NCI-H460	Lung cancers cell line
NCP	Nanoscale coordination polymer
NI	Nitroimidazole group
NIR	Near infrared
NP	Nanoparticle
NR	Nile red
O	Stirring outside the dialysis bag
$O_2^{\bullet-}$	Superoxide radial anion
OS	Organic solvent
P	Ratio of effective volume
PA	Poly(ester amide)
PAMAM	Poly(amidoamine) dendrimer
PAsp	Poly(aspartic acid)
PBA	Phenylboronic acid
PBS	Phosphate buffer saline
PC	Photoredox catalyst
PCL	Poly(ε caprolactone)
PDDD	Poly(1,4-dithio-7,10-dioxa-2-dodecene)
PDI	Polydispersity index
PDSe	Polyurethane nanoparticle containing a diselenide oxidation-sensitive negatively charged moiety
PDT	Photodynamic therapy
PE	Polyelectrolyte
PEG	Poly(ethylene glycol)
PEG-A	Poly(ethylene glycol) methyl ether methacrylate
PET	Photoinduced Electron Transfer
PG	Polyglycerol

PGA	Poly(glycolic acid)
PLA	Poly(lactic acid)
PLCA	Pthalocyanine
PMMA	Poly(methylmethacrylate)
P_n	Carbon centered radical
PN-Te	Polyelectrolyte multilayer film composed of cationic tellurium-containing polymeric micelles
PPS	Poly(propylene sulfide)
PS	Photosensitizer
PS_0	Stable ground state of photosensitizer
PSS	Poly(styrene sulfonate)
PTFE	Polytetrafluoroethylene
PTX	Paclitaxel
PUSeSe	Polyurethane with diselenide bonds
PUTe	Tellurium-polyurethane
R	Gas constant
R^2	Coefficient of determination
RAFT	Reversible Addition-Fragmentation Chain Transfer
RES	Reticuloendothelial system
Rh	Rhodamine B
RI	Refractive index
ROP	Ring opening polymerization
ROS	Reactive oxygen species
s_o	Head area
Seb Cl	Sebacoyl chloride
SEC	Size exclusion chromatography
SRB	Sulforhodamine B
T	Temperature
Tan δ	Tangent of the ratio between loss modulus and storage modulus of the polymer
TBM	2,6 di-tert-butyl-4-methylphenol
TCT	Thiocarbonythio
Te	Tellurium containing polymers
TEA	Triethylamine
TEM	Transmission electron microscopy
TET	*meso*-tetra(3-hydroxyphenyl) porphyrin
T_g	Glass transition temperature
TGA	Thermal gravimetrical analysis
THF	Tetrahydrofuran
TK	Thioketal
$T_{melting}$	Melting temperature

TMNP	*meso*-tetra(1-naphtyl) porphyrin
TP	Thiaporphyrin
TPP	*meso*-tetraphenyl-porphyrin
TPPAD	Tetraphenylporphyrin monoacid derivative
υ	Volume
UCNP	Upconversion nanoparticles
UV	Ultraviolet
UV-Vis	Ultraviolet-visible spectroscopy
VDS	Vinyl disulfide
W	Water
WO	Without agitation in the micelle formation
wt%	Percent of the compound in mass
ZnTPP	Zinc *meso*-tetraphenyl-porphyrin

Contents

XXX

List of Figures

XXXVI

List of Schemes

XL

List of Tables

Motivation

At the beginning of the 20th century, the Nobel laureate and "father of chemotherapy", Paul Ehrlich, brought up the concept of "magic bullet", in which a drug could be targeted and delivered into a diseased cell [1]. The dream of "magic bullet" turned real at the end of the 1970s when Peter Paul Speiser and Patrick Couvreur developed a drug loaded biodegradable nanoparticle (NP), which was the first NP that enabled targeted drug therapy. However, the first appearance of the term "nanomedicine" only occurred in 1991, in the book "Unbounding the Future: The Nanotechnology Revolution" by K. Eric Drexler, Chris Peterson and Gayle Pergamit [1], [2]. The "nanomedicine" term designates nanoscale materials used as carrier systems containing drugs and/or image agents for treatment and/or diagnostic with the aim to improve the effects inside the body. Nowadays, these technologies are being used all over the world, especially in the healthcare services, improving treatments and patients' lives in a range of diseases. The growth in the development of nanomedicine has been witnessed by the increase in the number of Food and Drug Administration (FDA) approved NPs and followed by a considerable rise in the number of registered clinical trials, mainly focused in cancer treatment [3].

The majority of the chemotherapeutics have a hydrophobic character which decreases the bioavailability of the drug when in contact with the body fluids. As a consequence, high dose levels are required, with increased risk of side effects and a reduced effect in *in vivo* therapy. A possible way to overcome such issue is to encapsulate the drugs in nanocarriers. In this sense, among all nanocarriers, micelles have the ability to encapsulate hydrophobic therapeutics while presenting higher biocompatibility. Micelles usually have a hydrophobic core, that enables the encapsulation of the drug. It also has a hydrophilic corona to easily pass through the body aqueous medium, without suffering disturbance and thus reaching a maximum specificity at the targeted site.

To be efficiently used as drug delivery systems (DDSs), micelles should have the ability to reach the target site. Additionally, in some therapies, namely cancer therapy, a burst release of the cargo might be interesting to faster produce the desired effects.

Light has been emerging as a promisor trigger in DDS, due to its spatio-temporal activation and non-invasive character. The light around the near-infrared (NIR) region is safe to the human being and allows a deep penetration in human tissues. However, this section of the electromagnetic spectrum has lower energy when compared to the commonly used ultraviolet (UV) to green light region, nullifying the use of typical chromophores. Nevertheless, the lower energy of this high-wavelength light can be useful if

photosensitizers (PSs) are applied. In the presence of light, PSs generate high reactive oxygen singlet species which can interact with sensitive moieties to undergo a photo-oxidation reaction, cleaving apart or changing hydrophobicity. Therefore, a single oxygen ($^1O_2$) sensible micelle should encompass the amphiphilic polymer, a light responsive segment, and the PS. A proper choice of the sensitive segment position is in the polymer backbone that by breaking could change the micelle stability leading to an on-demand and efficient drug release.

This PhD work aims developing sensitive polymers responsive to high wavelength light using PS as an intermediate for the photo-oxidation reaction. To achieve such aim, amphiphilic copolymers, comprising a sensitive segment which allows the copolymer cleavage when irradiated, were developed. Red-light sensitive polymers were designed in order to form micellar structures able to co-encapsulate hydrophobic drugs and PS. With copolymers disruption, the micelle structure is destabilized, releasing chemotherapeutics while the $^1O_2$ generated by the photosensitizer can simultaneously act as photodynamic therapeutic.

1 State of Art
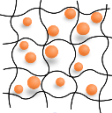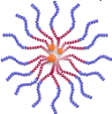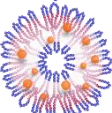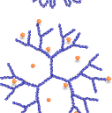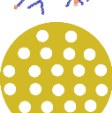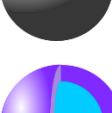
This chapter is structured in three main topics, starting with a review about the most used nanocarriers with a special focus on poly(ethylene glycol)-poly(lactic acid) (PEG-PLA) micellar structures, where the polymers' properties and the methods used for their preparation are discussed. Next, an overview of the reported sensitive segments and their mechanism of reaction with $^1O_2$ are described. Also, examples of NPs with $^1O_2$ sensitive segments are presented and their behavior in the biological environment is shown. This chapter ends with the discussion and future perspectives of these systems.

1.1 Micelles Properties and Synthesis

Since the appearance of the concept of the "magic bullet", nanotechnologies such as nanocarriers have turned up as a key science, mainly, in the field of oncology treatments. Nanocarriers can act as a "Trojan horse", protecting the payload against the degradation promoting target interaction and allowing the release in the specific place and/or time. The most common nanocarriers in cancer therapy are liposomes, micelles, dendrimers, mesoporous materials, hydrogels, metal-based and upconversion NPs (UCNPs) [1], as presented in Table 1. 1.

Table 1. 1 The most usual nanocarriers in cancer therapy

Nanocarrier	Structure	Definition	Size (nm)	Ref
Hydrogel		Cross-linked network made of hydrophilic or amphiphilic polymer, mainly composed by water.	10-100 (mesh size)	[4]
Micelles		Amphiphilic polymers able to self-assemble by hydrophobic interactions.	10-200	[5], [6]
Liposomes/ Polymersomes		Liposomes are a vesicle with an aqueous core within a lipid bilayer. Polymersomes have an architecture similar to liposomes, but they are composed of synthetic polymer amphiphiles.	50-450	[5]–[8]
Dendrimers		Synthetic branched macromolecules with a tree-like structure. Therapeutic molecules can be linked from the core until the surface functional groups.	~5	[5], [7]
Mesoporous materials		Materials with a solid framework containing pores with diameters between 2 and 50 nm and a large surface area.	50-300	[9]
Metal-based-NPs		These NPs usually have a large surface area allowing the drug incorporation. They usually are made of gold, silver, nickel, zinc oxide, iron oxide, titanium dioxide, gadolinium or graphene.	10-100	[10]
UCNPs		NPs composed by transition metals able to absorb one or two photons of low energy converting into one emitting photon of higher energy or into heat.	1-100	[11]

Among all the mentioned nanocarriers, the most extensively explored are liposomes and micelles. These lipids or polymer-based nanocarriers can be considered as one of the simplest nanotechnology platforms. They have simple preparation methods and easy control of composition, size, and stability when compared with other DDSs. Furthermore, the therapeutic agent within/conjugated with these nanocarriers shows an improvement in the therapeutic activity and the pharmacokinetics. These systems have shown the most promising results in clinical applications, including some products that are already in the market [12]. For instance, one of the most important clinical contributions in the anti-cancer nanomedicine field is the injectable liposomal doxorubicin (Doxil®) formulation, which significantly reduced the cardiotoxicity in advanced breast cancer [13]. Liposomes have more than 8 products already approved by the FDA, showing an increased delivery to the tumor site and decreased systemic toxicity. However, the growth in the pharmaceutical market of liposomes products is hindered by some essential problems, such as deficient storage stability and rapid leakage of hydrophilic drugs in the bloodstream [14].

The main advantages of polymeric micelles over liposomes are their smaller size, that favors the rapid accumulation in tumor site [15], and the ability to encage hydrophobic drugs. This last feature is crucial for cancer therapy because the major part of anti-cancer

4

drugs have a hydrophobic character [16]. As liposomes have an internal aqueous compartment, the hydrophilic drugs are easier encapsulated in the inner core, however, the liposoluble drugs can only be imprisoned between the core and shell among phospholipids moieties. In contrast, all the hydrophobic core of the polymeric micelle is able to enclose hydrophobic drugs [17]. Furthermore, have been reported that drug carriers, such as PEG-modified liposomes hardly migrate into deep site of tumors due to their low stability [18],[19] and their surface is hard to modify when compared to polymeric micelles [20]. These last nanostructures have shown the promising capability to encapsulate a vast number of hydrophobic anti-cancer drugs. The stability, tailor-made functionalities and the multiple polymeric structures available, along with the boost progression in the polymer research field turned micelles out to be highly popular as DDS [1],[21].

Amphiphilic polymers have the singular ability to spontaneously self-assemble into a core/shell micelle nanostructure when subjected to an aqueous environment. Theoretically, the formation of these structures in aqueous solution is mainly driven by the decrease of free energy of the system. The self-association hides the hydrophobic segment in the stabilized inner core. Oppositely, the hydrophilic segments undergo repulsive interactions among them [1], [22], [23].

The unique core-shell architecture of micelle regulates the dose and prolongs the bioavailability of the encapsulated drug. The hydrophobic core serves as a reservoir of the water-insoluble drug, a great advantage for cancer therapy due to the high hydrophobic character of most of the available drugs. Hence, polymeric micelles can improve the solubility of the hydrophobic drug and, consequently, induce a lowering off-target biodistribution [1], [13]. Hydrophilic shell controls the *in vivo* pharmacokinetic behavior and offers to the micelle excellent dispersibility in aqueous solution [24]–[26].

The injectable micelle systems are, commonly, designed to target solid tumors by taking advantage of the enhanced permeability and retention (EPR) effect. The small size of the polymer micelles avoids the scavenging by the liver and the filtration by the spleen, resulting in a longer blood circulation time [27]. Additionally, due to the small size, micelles are able to escape renal clearance by leaking into the abnormal-permeable-vasculature system of the affected tissue. Consecutively, the weak-local-lymphatic system enables these nanocarriers to remain there for a longer period. Owing to the mentioned properties, the anti-cancer agent passively accumulates in tumor site [1], [13], [27]. When in the tumor site, the drug can be released out of the polymeric matrix of micelle through erosion or diffusion to aqueous media [28].

Beyond this, micelles should present a set of characteristics to be admitted as DDS. The most required characteristics of an ideal polymeric micelle are:

- biocompatibility and biodegradability for easy and non-toxic elimination from the body;
- small size, targetability, tunable stability, high drug loading capacity (DLC) to enhance the drug residence time into the body, improve drug efficacy and reduce side effects;
- reproducible, easy and low-cost synthesis procedure to enable its commercialization in the market [29].

These characteristics result in an increase in the synergy of the anti-cancer efficacy with the reduced systemic toxicity of the polymeric micelle systems, which propelled the development of formulations that are currently in stages of pre-clinical and clinical development [13], [30].

Table 1. 2 shows the characteristics and development phase of some of the most successful formulations.

Table 1. 2 Polymeric micelles in clinical trials

Product name	Polymer composition	Drug encaged	Size (nm)	Drug loaded (%)	Reported study (development phase)	Ref
Genexol®-PM	mPEG-PDLLA	PXL	20-50	16.7	Non-small cell lung cancer, ovarian cancer, breast cancer and gastric Cancer (III/IV) approved and commercially available in some countries	[24][31]
NK105	PEG-P(α,β-Asp)	PXL	85	23	Gastric/breast cancer (III)	[24][31]
NK911	PEG–b-P(Asp)	DOX	40	17	Various solid tumors (II)	[24][32][33]
NC-6004	PEG-PGlu	Cispatin	30	39	Pancreatic cancer (III)	[24][32]–[34]
NK012	PEG-PGlu	SN-38	20	20	Triple negative breast cancer (II)	[24][32]–[34]
NC-4016	PEG–b-PGlu	Oxaliplatin	30	30	Various solid tumors (I)	[24][32][33]
NC-6300	PEG-b-poly(Asp-Hyd)	Epirubicin	60	20	Various solid tumors (I)	[32][33]
siRNA micelles	PEG-b-polycations	siRNA	40-60		Preclinical	[35]
SP1049C	pluronic polymer-bound doxorubicin	DOX	30	8.2	Carcinoma of the esophagus and in gastric cancer (III)	[1]
DTXL-TNP	PLA-PEG	Docetaxel	100	10	Advanced or metastatic cancer (I)	[27]

mPEG-PDLLA – methoxy-poly(ethylene glycol)-poly(D, L-lactide); PEG-P(Asp) – poly(ethylene glycol)-poly(α,β-aspartic acid); PEG-Pglu – poly(ethylene glycol)-poly(L-glutamic acid); PEG-b-poly(Asp-Hyd) - poly(ethylene glycol)-poly(aspartate – hydrazone).

The most advanced product in the market is Genexol®-PM, produced by Samyang Biopharm. It is a paclitaxel carrier with the micelle structure made of mPEG-*b*-D,L-PLA. It is already approved by the FDA and commercialized in South Korea for the treatment of metastatic breast cancer and advanced lung cancer. Furthermore, it has demonstrated low toxicity and favorable overall response rates of 40 to 68% in many clinical trials in patients with breast cancer or non-small cell lung cancer [1], [36]. These exciting results, combined with the sophisticated upgrade in polymer structure design, are opening a promisor future for micelles in biomedical applications [37].

The micelle formation process and design are of outstanding importance since they can dictate the application of the nanocarrier. Each parameter in the formation process, along with the type of polymer, has a direct influence on the final features of the micelles. The most relevant design properties and micelle formation processes are explored in the following sections, including the hypotheses of how their properties can be manipulated to improve micelle's use in clinical practice.

1.1.1 Important Parameters in Micelle's Preparation

Preparation Method

The main requirement in the polymeric micelle formation is the amphiphilicity character of the polymer. This is usually achieved by synthesis of a block copolymer, composed by, at least, a hydrophobic and a hydrophilic block. The method selected for micelle preparation depends, chiefly, on the solubility of the copolymer and also on the nature of the drug (hydrophobic or hydrophilic) [38], [39].

As higher is the relative molecular weight of the hydrophilic block, the easier is the dispersibility in water and the copolymer will self-assemble into small and monodisperse micelles by a direct process of self-assembly. However, if the molecular weight of the hydrophobic segment is higher than the hydrophilic segment, the copolymer becomes more water-insoluble and the self-assembly process may need to proceed by other methods which allow the use of others solvents (such as organic solvents) [38].

The most used methods for micelle preparation by self-assembly are the direct dissolution, solvent evaporation, emulsion-solvent evaporation and dialysis [26], [40]. For moderately water-soluble copolymers, the direct dissolution method may be employed.

Poorly water-soluble polymers can be prepared by solvent evaporation, dialysis and emulsion-solvent evaporation methods [38].

- Direct dissolution (Figure 1. 1): In this method, copolymer at a concentration above critical micellar concentration (CMC) (the CMC is directly related to the micelle stability, knowing that only above this value the unimers are assembled into micelles) and drug are added, under gentle stirring, to an aqueous solvent. Sometimes this solution needs to be heated to cause micellization occurrence via dehydration of the segment that will form the micelle core [38], [41].
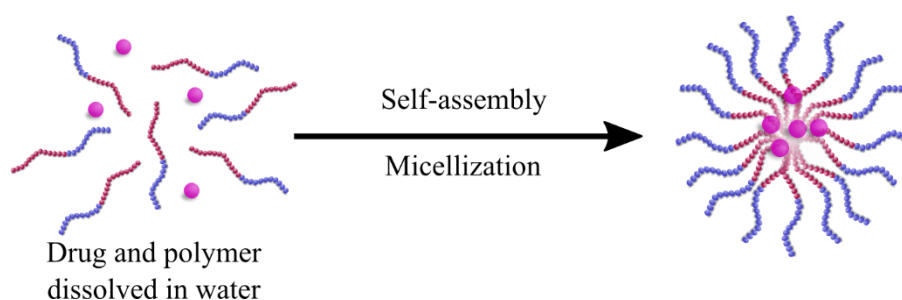
Figure 1. 1 Direct dissolution method

- Solvent evaporation: The drug and copolymer are dissolved in an organic solvent suitable for both, followed by solvent evaporation to produce a thin film. The micelles are formed upon rehydration of the film with a warm buffer or aqueous solution, under gentle stirring (Figure 1. 2). This method is used for copolymers with fairly low aqueous solubility. Amphotericin B and estradiol are some of the drugs successfully loaded by this method [38], [41]–[43]. Also, the drug encapsulation by the evaporation method could be carried out by dissolving the drug and copolymer in a water-miscible organic solvent, where the self-assembly occurs by the addition of an aqueous phase followed by evaporation of the organic solvent. This process is called co-solvent evaporation method (Figure 1. 3) [44]. Due to the vast availability of solvents, this technique allows an appropriate selection of solvent for the polymer-drug system leading in good control over the evaporation. This is important to prevent premature precipitation, keeping the drug as long as possible in solution during micellization, which favors an enhancement in drug loading [45].

8
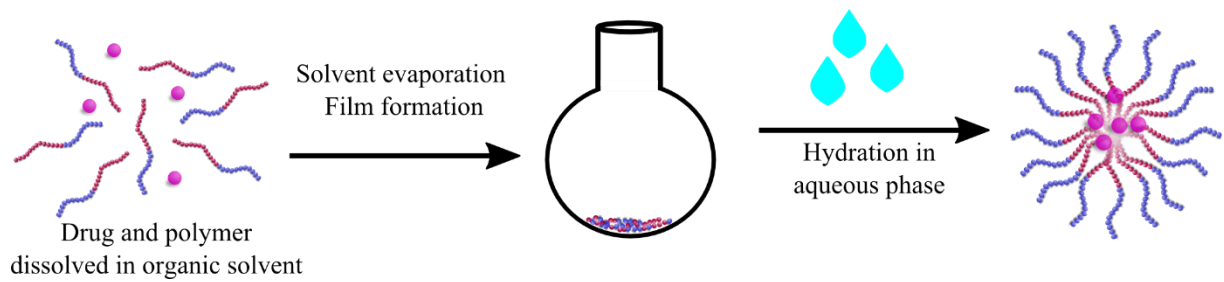
Figure 1. 2 Solvent evaporation method
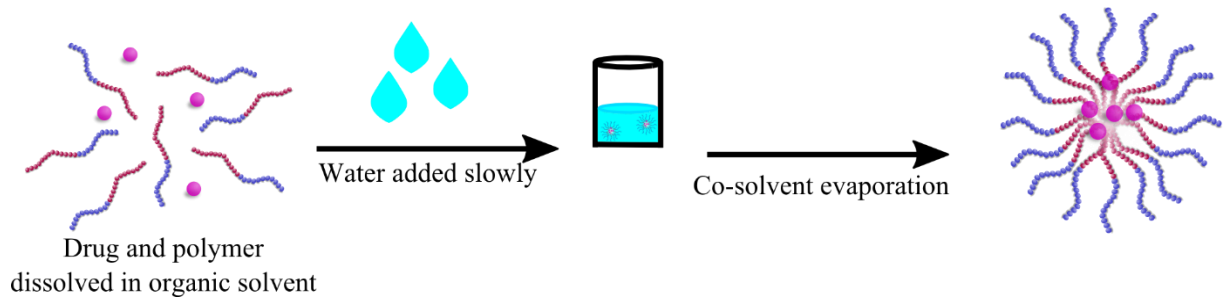
Figure 1. 3 Co-solvent evaporation method

- Emulsion-solvent evaporation (or oil-in-water emulsion process, O/W, Figure 1. 4): A hydrophobic drug is dissolved in a water-immiscible organic solvent (*e.g.*, dichloromethane, ethyl acetate and chloroform). Next, this solution is placed in an aqueous phase (with or without surfactant) under continuous stirring (or under ultra-sound radiation) to form micelles by copolymer assembly. The organic solvent will be removed under low pressure. Hydrophilic drugs, in turn, need to be solubilized in the aqueous phase to be encapsulated by double emulsion (water-in-oil-in-water). However, this technique usually has poor encapsulation rate for hydrophilic drugs and is vastly influenced by nanocarrier and drug load size. By emulsion evaporation technique, particle size distribution can be controlled through the volume ratio of organic to the aqueous phase, nature and amount of surfactants and chemical properties of drug loaded [26], [38], [41], [42].
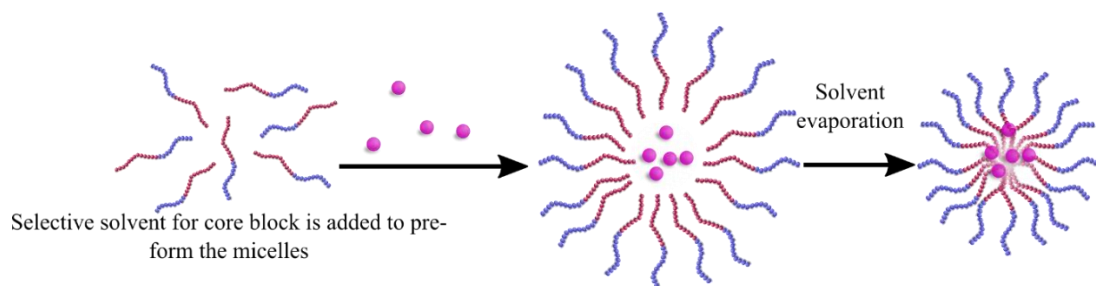
Figure 1. 4 Oil/water emulsion method

- Dialysis method (Figure 1. 5): the polymer and drug are dissolved in a water-miscible-organic-solvent (e.g., *N, N'*-dimethylformamide (DMF), tetrahydrofuran (THF), *N, N'*-dimethylacetamide (DMA) or dimethylsulfoxide (DMSO)), and a small amount of water is added, under stirring, to the solution. The micelle is formed upon the organic solvent removal using the dialysis process [42]. This method is used for copolymers that are insoluble in water. The size of the micelle, along with other characteristics (e.g. amount of drug loading, stability and micelle morphology), is influenced by the solvent used [38], [41]. Amphotericin B and DOX are examples of drugs successfully encapsulated by this technique [43]. DOX is commonly entrapped using DMSO as solvent in dialysis methodology [46]–[48].

Dialysis against water

Micellization

Drug and polymer
dissolved in organic solvent
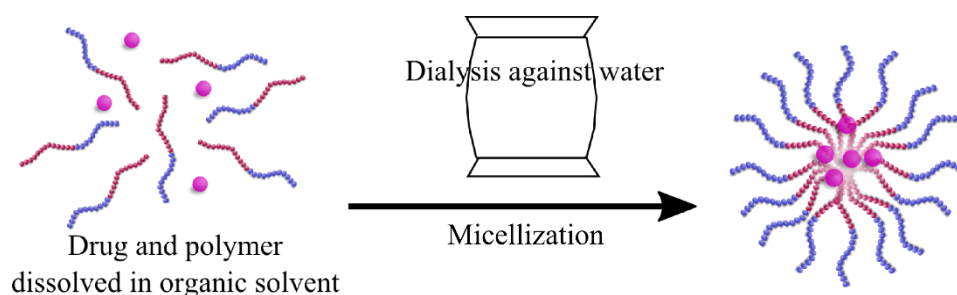
Figure 1. 5 Dialysis method

The choice of a suitable method and solvent could improve the amount of drug encapsulated and influence the micelle size. Miller *et al*. studied the dexamethasone encapsulation in PEGylated poly-4-(vinylpyridine) micelles, finding an encapsulation of < 2% w/w in the direct dialysis from acetone, ~13 % w/w in O/W emulsion technique from dichloromethane and ~19% w/w in cosolvent evaporation method. They regarded that a driven factor in the encapsulation process is the drug and copolymer solubility in the medium. Direct dialysis and O/W emulsion technique have a fast change/interaction with water, which can lead to the hydrophobic drug precipitation. The graduated addition of water can avoid the precipitation of the water-insoluble drug [45].

Polymer composition

Since the spontaneous process of micelles formation is driven by the amphiphilic polymer character, the polymer composition can tune properties for the micelle application, acting as the determinant factor for this DDS. In general, the core structure formed by the hydrophobic polymer is the main responsible for the stability, degradation rate/ release

behavior and loading capacity of micelles [37]. These micelles' features are regulated through properties such as crystallinity, stereoregularity, molecular weight and structure of the hydrophobic block. In turn, the shell formed by the hydrophilic polymer is responsible for the micelle interaction with the body fluids, and it has the role of avoiding a rapid clearance by the reticuloendothelial system (RES) and targeting the NP into a specific site.

The hydrophobic core is generally composed by polyesters. They are the most used family of polymers in the biomedical field, particularly in DDSs. Among them, it is possible to highlight poly(lactic acid) (PLA), poly(glycolic acid) (PGA) and poly(ε-caprolactone) (PCL) due to their excellent biocompatibility and non-toxic degradation products. These polymers have the ability to degrade by hydrolysis of ester bonds, producing non-toxic sub-products that are eliminated by normal cellular activity and urine [26], [49]. Typically, these polyesters are copolymerized with PEG, yielding amphiphilic copolymers that are used to produce the micelles.

PLA is one of the most commonly used polyesters in medical applications such as surgical implants and DDSs. It is suitable and useful because of its good properties like biodegradability, biocompatibility, low-immunogenicity eco-friendliness, and low-cost production [50].

PLA is obtained from lactic acid, which is a naturally occurring hydroxy acid, obtained from the carbohydrate fermentation mediated by microbes. It can also be produced by chemical synthesis by the hydrolysis of lactonitrile by strong acids [50]–[52]. Due to the chiral nature of the lactic acid molecule, it has two isomers, L-lactic acid and D-lactic acid. Both are used for lactide synthesis which exists in three distinct stereo form L-lactide, D-lactide or *meso*-lactide [53], [54]. Figure 1. 6 shows the stereoisomers of lactide.
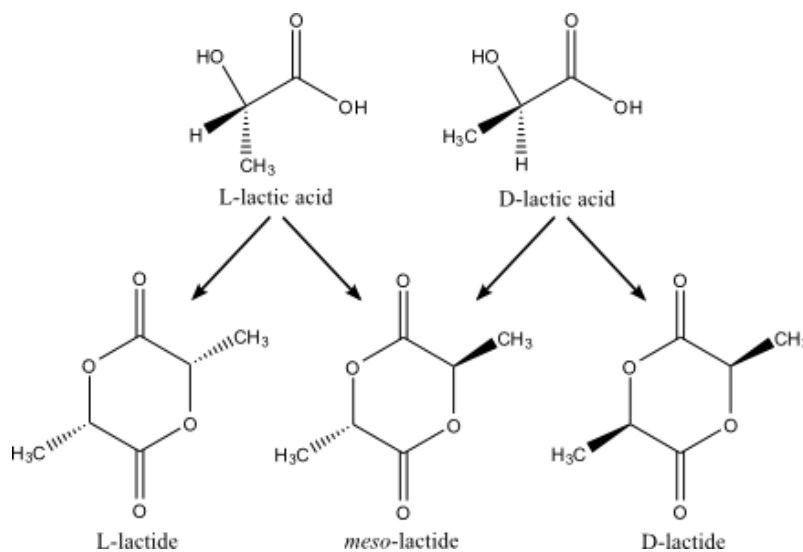
Figure 1. 6 Stereoisomers of lactide

One of the most important advantages of PLA is that its physical and mechanical properties can be manipulated through the polymer composition. Stereochemistry of PLA is an important property that not only affects the physicochemical properties but also the biodegradation. Poly(L-lactic acid) (PLLA) stereo form has an *in vitro* degradation slower than poly(D,L-lactic acid) (PD,L-LA) [55]. The molecular weight also has influence in the properties of PLA; typically, PLA with high molecular weight have improved mechanical properties and PLA with low molecular weight have increased biodegradability [53], [56].

In polymeric micelles, PLA can have a higher influence in a number of proprieties, mainly the NP stability. Jelonek *et al* found a relationship between the CMC and the length of the hydrophobic block in PEG-PLA. They showed that an increase of ~30% in PLA molecular weight can decrease by about 60% of CMC value [57].

The hydrophilic polymer, which forms the micelles' shell, drives the micelle-blood interactions, governing the residence time in the human body. In DDSs with targeting governed by the EPR effect, a prolonged residence time (> several hours) is a decisive factor to allow enough number of particles to pass through the desirable site and accumulating there [58]. However, serum proteins could bind to the particles' surface targeting them to be uptaken by RES. This phenomenon can be minimized or circumvented if micelles are composed by PEG as the hydrophilic block, or if they are decorated with PEG at their surface. This stealth-like nature of PEG is due, mainly, to its high mobility and hydrated nature [13].

12

Besides this, PEG is non-toxic, non-immunogenic, non-antigenic and its use is approved by the FDA. Due to these important characteristics, more than forty-five PEG-drug conjugates are already in the market or under stages of the clinical evaluation or still under active development [42], [59]–[62]. This 'protective' characteristic is influenced by the molecular weight (conventionally between 2 to 15kDa) and the concentration of the PEG chain on the surface [59]. Some studies have shown that the most important factor against protein adsorption and RES uptake is the surface density of PEG molecules (distance below 2 nm between two PEG molecules is ideal for this protection). In this way, longer PEG chain gives a denser hydrophilic corona increasing the circulation time *in vivo* [42], [59].

Changes in the amount of PEG in the block copolymer of PEG-PLA allows controlling the biodegradation rate [63]. The molecular weight of PEG has also an impact on the stability and drug release [60]. These parameters need to be optimized for each composition of block copolymer size and application.

Polyglycerol (PG), a polyether analog to PEG, is also emerging as an alternative to be used as micelles' shell because, such as PEG, is highly biocompatible. Additionally, it presents a controllable structure, functional groups can be easily added and has a facile synthesis [37].

Copolymers comprising PLA and PEG are the most studied diblock copolymers for DDSs due to their proved biocompatibility, nature and stability. As mentioned above, GENEXOL®-PM is a micelle product released in the market in 2007 and is made from PEG-PLA amphiphilic copolymer for encapsulation of paclitaxel [24], [26], [63], [64].

This amphiphilic block copolymer is usually synthesized by the ring opening polymerization (ROP) of lactide, using monohydroxylated PEG-moieties as the macroinitiator and, generally, stannous octoate ($Sn(Oct)_2$) as a catalyst, at 140ºC and vacuum pressure [26]. The polymer synthesis under these typical conditions of ROP, namely high temperatures, reduced pressures and the use of metallic catalysts harms the incorporation of extremely sensitive moieties in the copolymer. Alternative methods with milder conditions have to be used. In this sense, in the last years, considerable efforts have been directed towards the synthesis of PEG and PLA block copolymers, under mild conditions [65]–[69].

Qian *et al*. have developed a new copolymerization method, started by the Waymouth/Hedrick method (developed in 2006), for a racemic mixture of D and L-lactide by the ROP method using PEG as macro initiator and 1,8-Diazabicyclo[5.4.0]undec-7-ene

(DBU) as a catalyst. As a result, the authors obtained an amphiphilic block which polymerization was proceed rapidly at room temperature, with well-controlled molecular weight distribution (polydispersity index (PDI) = 1.05-1.15) [70]. This narrow molecular weight distribution of the copolymers is a high required characteristic to efficiently form micelles [41].

In copolymers of PEG-PLA, the molecular weight of each polymer defines the characteristics of the micelles. As the PLA length increases, the hydrophobic drug load increases. As greater is the interaction between the PLA block and the hydrophobic drug, the slower will be the drug release. An increase in the PEG content increases the hydrophobic drug release and an increase in the PLA molecular weight will lead to a increase in particle stability, an increase of drug content and loading efficiency. The degradation rate of micelles can be modified by varying the length of PLA block polymer due to easily degradation of polyester [26].

Table 1. 3 summarizes some of the consequences of different fractions in PEG-PLA amphiphilic copolymer which should be considered in the polymer design.

Table 1. 3 Parameters influenced by different fractions of a hydrophilic and hydrophobic part in a PEG-PLA copolymer

Fraction of polymer in the copolymer structure	Consequence
Increase in PLA fraction	Increases particle stability, decreases CMC
	Increases hydrophobic drug loading and loading efficiency
	Increase the degradation rate
Increase in PEG fraction	Increases hydrophobic drug release
	Improves the stealth capacity
	Increases the circulation time

Garofalo *et al*. studied the chemical composition and architecture effects in the PEG-PLA copolymer micelles formation and stability. Different mPEG initiators (mPEG$_{2k}$ and mPEG$_{5k}$) and atactic and isotactic poly(lactic acid) with different architectures (linear, two and tri-arms) were evaluated. With the use of AlMe$_3$ as a catalyst in ROP of lactide, perfect control over the polydispersity index (PDI) was achieved (1.02 to 1.22). The authors found that PEG size and PLA structure control the biological interaction between micelle and biological system. The diblock copolymer conjugated with linear mPEG$_{2k}$ and two arms of (PD,L-LA) block formed micelles with high efficiency to stain tumor cells (among linear and tri-arms PD,L-LA block). Their results are explained by the fact that mPEG$_{2k}$

14

micelles showed a better cellular internalization than mPEG$_{5k}$ and the two arms PLA micelles showed a monodispersed distribution, less tendency to aggregate (at pH ranging from 5 to 7.4) and higher stability [55].

Kang *et al*. described that the stereochemistry of PLA can influence micelle stability. They developed micelles made from an amphiphilic PEG$_{5,4k}$-PLA$_{2k\ to\ 7,4k}$ polymer with a different stereo form of PLA (L, D, DL or a racemic mixture of L and D). Interestingly, the micelle of a racemic mixture of L and D PLA showed less tendency to aggregate after the lyophilization process. This aggregation behavior is a common problem among polymeric micelles attributed to hydrophobicity interactions between two parts of the amphiphilic polymer. Stereocomplexated micelles also showed an increase in the number of polymers aggregated in each micelle (N$_{agg}$) that increase the PEG shell density. This thick cover can provide a higher steric repulsion, avoiding the uptake by the mononuclear phagocyte system, increasing the circulation time after I.V. administration [71].

Additionally, Nasongkla *et al*. showed that DOX can easily diffuse through a PDLLA micelle core for fast drug release due to this PLA amorphous character when compared with PEG-PCL micelles (PCL segment can form crystalline regions in the micelle core) [72].

Table 1. 4 Summarizes some of PEG-PLA micelles synthesized for use as drug delivery systems.

Table 1. 4 PEG-PLA micelle for drug delivery system

Polymer	Size (nm)	Micelle formation method	Drug	CMC 10^3 (mg.mL^{-1})	Drug loaded (%)	Ref
PEG$_{5k}$-PLA$_{5k}$	98.7	Co. solv. evap.	DOX	200	11	[73]
PEG$_{5k}$-PLA$_{5k}$	23	Co. solv. evap.	DOX	250	2.73	[74]
PEG$_{2k}$-PLA$_{3k}$	34	Dialysis	DOX	24	2.29	[48]
PEG$_{5k}$-PLA$_{3k}$	43	Dialysis	DOX	23	2.79	[48]
PEG$_{2k}$-PLA$_{5k}$	107	Dialysis	DOX	76	4.65	[48]
PEG$_{5k}$-PLA$_{5k}$	107	Dialysis	DOX	80	3.2	[48]
PEG$_{2k}$-PLA$_{6k}$	67	Co. solv. evap.	DOX	-	10.06	[75]
PEG$_{5k}$-PLA$_{15k}$	115	Co. solv. evap.	DOX	-	19.61	[75]
PEG$_{2k}$-PLA$_{3k}$	41	Dialysis	DTX	1.41	9.27	[76]
PEG$_{2k}$-PLA$_{4k}$	22.46	Co. solv. evap	PTX	10.7	20.32	[77]

Co. solv. evap = co-solvent evaporation; DTX= Docetaxel; PTX = Paclitaxel

Size

Micelle size is an important parameter that can improve the permeability through the tumor blood vessels and increase the accumulation of drug at the tumor site by taking advantage of the EPR effect [19]. Typically, polymeric micelles present diameters ranging from 10 to 200 nm [16],[26]. The particle size will define the way the body will interact with it. Liver and spleen are the most active organs in NPs clearance. Particles less than 100 nm may accumulate in the liver due to the presence of the sinusoidal fenestration (between 50 to 100 nm). On the other hand, micelles with diameters greater than 400 nm, can be cleared by the spleen. Thus, researchers have shown that aggregates near 100 nm are the most appropriate for minimizing clearance, avoiding renal excretion (filtration of particles <6-8 nm [78]) and improving the escape of NP from the RES. This contributes to an increase in circulation time [27],[28]. However, the size which is able to ensure tumor penetration in all kind of tissue is still under investigation. Some studies have revealed that hyperpermeable tumor (like murine colon cancer) has no size restriction in range of 30 to 100 nm, but poorly permeable tumor (like hypovascular human pancreatic cancer) only allows the penetration of particles smaller than 50 nm [19].

To avoid the micelle elimination by the body before the accumulation in the tumor site, polymeric micelles should have a molecular weight greater than 70,000 g/mol which

is the upper limit of renal clearance to protein. For micelles, this molecular weight is easily achieved with amphiphilic polymers and is an advantage against non-polymeric micelles, that usually have molecular weight about 10^6 g/mol. When particle disassembly occurs, the molecular weight of each amphiphilic copolymer needs to be lower than this cut-off limit for glomerular filtration. This favors the excretion and lowers the risk of chronic accumulation in the body [11],[29].

Several conditions can influence the polymeric micelle size like the preparation method, polymer length, amount of drug loaded and the ratio of hydrophilic to hydrophobic segment [13],[17]. Aliabadi *et al*. reported that PEG-PCL micelles showed a unimodal size distribution using acetone as the solvent in the co-solvent evaporation method (this was not achieved with THF or acetonitrile) [79]. Regarding the molecular size of the polymers, as expected, micelle size tends to increase as the polymer size increases. Also, higher hydrophobic micelle association usually has a smaller size than other compositions with less hydrophobic amphiphilic polymer associations. Hagan *et al*. showed that the hydrophobic character of the block copolymer (the PLA) has a significant influence in the micelles' diameters, which decreases with the increase in the hydrophobic block content. The most hydrophobic micelles (1.5:2 PLA:PEG) showed diameters approximately 16% smaller than the less hydrophobic micelles (2:5 PLA:PEG) [63]. Also, the increase in PEG content influenced the micelle size. A higher amount of PEG leads to a higher micelle's size and a less dense core [80], as shown in Figure 1. 7.
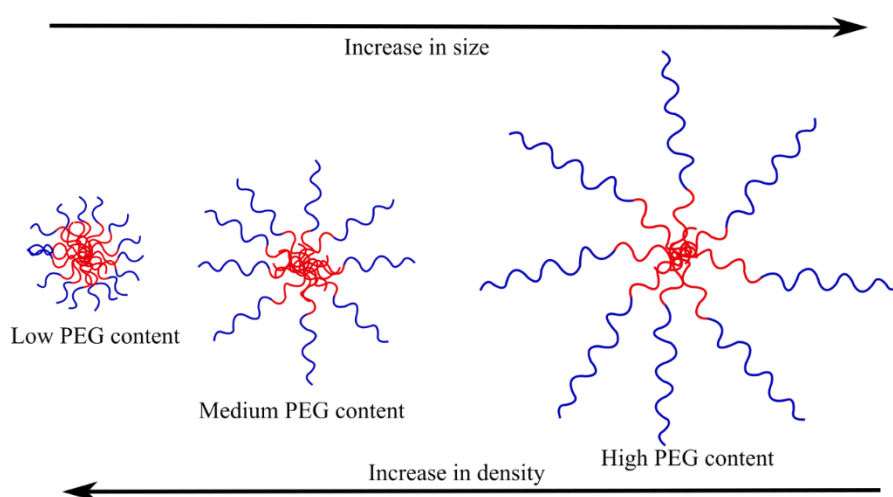
Figure 1. 7 The influence of PEG content in copolymer PEG-PLA in the micelle size. Figure based in [80].

The interaction between the inner core and drug-loaded influence the stability [81] but also interfere in the particle size, which could increase with the increase in the amount of drug loaded.

Morphology

In an amphiphilic copolymer, the balance between hydrophilic-hydrophobic blocks directly influences the morphology of the micelle. If the hydrophilic and hydrophobic segments have approximately the same length, the micelle may present a spherical shape. An increase in the length of the hydrophobic block will lead to the formation of non-spherical forms, like cylinders (rods) or bilayers (lamellae) [41]. Figure 1. 8 shows the different possibilities of micelle shapes.

Spherical

Cylindrical

Bilayer

Vesicle
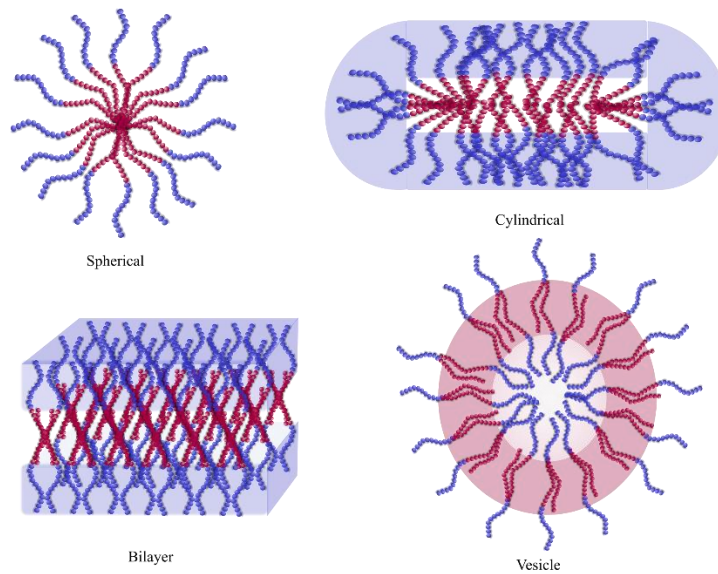
Figure 1. 8 Schematic descriptions of the most common micelle shape. Figure from [82].

Equation 1.1 shows the relation between segment sizes by packing parameter (p):

$$p = \frac{v \cdot s_0}{lc}$$

Equation 1.1

where p is the ratio of effective volume (v), the head area (s_0) and the hydrophobic length chain (lc). Self-assembled spherical structures present $P \leq 1/3$, cylinders $1/3 \leq P \leq 1/2$ and bilayers vesicles $1/2 \leq P \leq 1$ [40].

Alternatively, micelle's morphology could also be simply analyzed through the hydrophilic volume fraction (f) in the copolymer (Equation 1.2, [83]). When f is about 35% of the copolymer, micelles usually presents a vesicle shape and if f is higher than 45%, the micelle tends to acquire a spherical shape [22]. Jelonek *et al.* prepared different micelles from PEG-PLA block copolymers. The authors varied the weight fraction of the PEG block and found that the micelle's morphology changed as this parameter was altered. They synthesized filomicelles using mPEG$_{2k}$/PLA$_{1.6k}$ ($f = 0.55$) and mPEG$_{5k}$/PLA$_{6k}$ ($f = 0.45$)

18

[57]. It is also important to consider that the reduction in the hydrophilic segment length will lead to a decrease in the inter-corona repulsions and allows more copolymers to pack into the micelle. In that way, as the hydrophilic segment decreases the micelle morphology changes from a spherical to a rod form [84].

$$f = \frac{M_{w\ Hydrophilic\ block}}{M_{w\ Copolymer}}$$

Equation 1.2

The micelle's morphology is an important characteristic for DDSs, as it can affect, for example, the drug loading and the pharmacokinetic properties of the micelles [1]. Jelonek *et al*. found a paclitaxel loading capacity 20% higher for PEG_{5k}-PLA_{6k} filomicelles than for micelles with spherical form [57]. Geng et al. showed that filomicelles have a circulation time 10 fold-higher than their spherical analogs [85].

Stability

The stability parameter ensures the physical integrity of the micelle in a period ranging from the time of injection until the desired disassembly. It is highly important to ensure the solidity of the micelle under dilution conditions (e.g. after injection into the blood) to efficiently carry the drug to the target site. To reach this goal, the DDS needs to be formed from solutions with a low concentration of amphiphilic copolymer. The minimal polymer concentration for micelle formation is known as CMC. The CMC term was originally used to evaluate the thermodynamic stability of surfactant micelles, even though most of the literature employs this term to polymeric aggregates [86]. CMC describes the minimum polymer concentration in which below, the polymers exist separately undergoing adsorption at the air-water interface. Above CMC, the self-assembly starts and the system's free energy is reduced [22]. Low values of CMC are better to generate a stable aggregated system. CMC of polymeric micelles is about 1000 times lower than those of low-molecular-weight surfactants, making them rather insensitive to dilution and stable enough to ensure the needed circulation time [26], [40], [42], [87], [88].

Jelonek *et al*. used PEG-PLA diblock copolymers with low CMC values (3-6 x 10^{-3} mg.mL^{-1}) just to ensure the stability at administration and during the dilution in the bloodstream. The PLA blocks with higher molecular weights (PEG_{5k}-PLA_{6k}) showed the lowest CMC. The stability of the PEG/PLA micelles exhibits a promising behavior for prolonged delivery of hydrophobic drugs [57]. Theerasilp and Nasongkla have made a comparative study of PEG-PLA and PEG-PCL micelles and showed that, as PLA forms a less hydrophobic core than PCL, the micelles made from PEG-PLA copolymer presented

smaller sizes (between 20 -30 %, for an M_w of the hydrophobic core ~5k) and higher CMC values (187 % for an M_w of the hydrophobic core ~6k) than PEG-PCL [74].

The micelle formation process is mainly driven by the effective interaction between the hydrophobic block in the amphiphilic polymer [22]. Therefore, as the size of the hydrophobic segment increases, the CMC value decreases [57], whereas the size of the hydrophilic segment does not have a significant influence on CMC value. Interestingly, CMC values usually decrease with an increase in the total molecular weight of PEG-PLA diblock copolymer [81], [86], [89].

It is noteworthy that kinetic stability of the micelle can be changed by blood components causing the dissociation even when the micelle is administered in a concentration far beyond the CMC. Chemical crosslinking could prevent micelle disaggregation because it can dramatically enhance the micelle CMC. However if the crosslinking turns the micelle too stable it may not release the sufficient amount of drug prolonging the circulation time until an unpredictable physiological disruption [31].

Micelle stability is also dependent on thermodynamic factors. The effect of temperature on micelles derives from the equation of the standard free energy $\Delta G°$ associated with the micelle formation (Equation 1.3):

$$\Delta G° = RT * ln(CMC)$$
<div align="right">Equation 1.3</div>

where CMC is expressed in mole fraction, R is the gas constant and T is the temperature in Kelvin. Considering (Equation 1.4):

$$\Delta G° = \Delta H° - T\Delta S°$$
<div align="right">Equation 1.4</div>

where $\Delta H°$ and $\Delta S°$ are the standard enthalpy and entropy changes, respectively. These two equations lead to equation 1.5:

$$ln(CMC) = \frac{\Delta H°}{RT} - \frac{\Delta S°}{R}$$
<div align="right">Equation 1.5</div>

In Equation 1.5 is clearly noticed that the CMC value is dependent on the temperature. Considering the $\Delta S°$ for a polymer with a positive $\Delta H°$ the value of the CMC will decrease with the increasing temperature, namely, this polymer will form micelles at a lower concentration of unimers when subjected to higher temperatures. However, for polymers with negative $\Delta H°$ the CMC will increase with the enhance in the temperature [31]. Yang *et al.* [90] reported that PEG-PLA micelles have a decrease in the CMC value (around 7.5 to 28%) when the temperature is increased from 20 to 37ºC.

20

The kinetic of the micelle dissociation into unimers and exchange of unimers between different micelles influence micelle stability [91]. When in equilibrium the micelle exhibits inordinate kinetic stability. At room temperature and in water, micelles with poly(styrene) core, for instance, have an imperceptible low or none exchange of unimers between micelles, but the exchange rate is altered by changes in temperature or addition of co-solvents or surfactants [31].

Drug Loading

Micelles are highly used to encapsulate low molecular weight drugs, but they can also encapsulate molecules of high molecular weight (e.g., proteins, peptides, DNA, SiRNA, etc). However, in this thesis, we will just focus on encapsulation of low molecular weight drugs (the traditional chemotherapeutics drugs have a molecular weight ranging from 300 to 855 g/mol).

The interaction between polymer and drug needs to be taken into account since the higher is the compatibility between them the higher is the drug loading. Factors like the nature of the micelle core, the core block size, the preparation method, the nature and the size distribution of drug influence the loading efficacy [92], [93]. However, the most important parameter is the compatibility between the polymer hydrophobic segment and the drug (mainly, the hydrophobic interactions [94]). According to Meunier *et al.,* the PLA affinity with active pharmaceutical ingredients can increase the DLC of the PEG-PLA NPs. The authors studied drugs with different hydrophobicity (such as DOX, B-Lapachone and Cabazitaxel, where the last is the most hydrophobic and the first is the less) and they concluded that the drug loading increased from 0.8 to 3.2 % as the PLA affinity with the active pharmaceutical ingredients increases, namely, the hydrophobicity [95]. The drug usually is loaded into the micelle by physical interactions with the core or covalently bonded to the polymer core. For PEG-PLGA block copolymer the higher the hydrophobic segment molecular weight, the better is the drug loading [39], [40], [74].

The influence of size of hydrophobic block in micelle DLC was studied by Jelonek *et al*. In their work, the PLA length block showed no significative change in paclitaxel encapsulation capacity for polymers initiated by PEG$_{5k}$ (PLA varying from 4 to 6.1k), however, the encapsulation increased ~18% as the PLA weight increased from 1.6 to 3k for polymers started with PEG$_{2k}$. They also described that the drug release was faster for copolymers with PLA blocks of shorter lengths and for the copolymer initiated with mPEG$_{2k}$ [57]. The decrease of micelle density caused by the higher molecular weight of

PEG may be the reason for the undifferentiation of DLC due to the PLA M_w. On the other hand, the mPEG$_{2k}$ increases the micelle density and thus the influence of the length of PLA block in the drug encapsulation is more noticeable.

For a PEG$_{5k}$-PLA$_x$ copolymer micelle, when the molecular weight of the core segment is between 3k and 30k the particle size remains unchanged after encapsulating the drug (the model drug studied was procaine HCl). However, when the PLA molecular weight is within 75k to 110k range, the particle size increases 10 to 15%. This result can be explained by the fact that a PLA with higher molecular weight could be entangled and form a relatively more compact core. In this way, when the drug is loaded, an inevitable increase in the micelle size occurs due to the space that is occupied by the drug. Cores with a low ratio of PLA are more loose, thus having enough space to accommodate the drug, avoiding changes in the micelles' size [93].

For PEG$_{5k}$-PLA$_{6k}$, the encapsulation of paclitaxel is influenced by using a different methodology based in co-solvent evaporation (using CHCl$_3$ as solvent). When the drug was added after the micelle formation process, the DLC increased from 25% to 31% when compared with the simultaneous addition of drug and polymer in the solution used to form the micelle. However, no significant difference could be observed in micelles' morphology comparing dialysis (THF) and co-solvent evaporation for PEG$_{5k}$-PLA$_{3-6k}$ [57].

The ability to load a significant amount of drug is indispensable for a good treatment, however, this has been considered one of the major drawbacks of micelles [45]. Micelles usually have low DLC, PEG-PLA micelles carrying DOX present a DLC around 1 to 10% in weight of DOX per polymer weight. Since the driven force of drug incorporation in the micelle is the hydrophobic interaction between polymer and drug, the low drug encapsulation is usually credited to undesired drug aggregation during the self-assembly process. This cluster of the hydrophobic drug decreases the drug loading efficiency (DLE) and increases the heterogeneity of the formulation [94].

A lot of efforts have been direct to boost the DLC [1]. A usual way to improve the micelle drug capacity is by the introduction of suitable molecular forces. The functionalization of the hydrophobic part of the amphiphilic polymer, by attaching the drug to the polymer or by the attachment of a functional group that has an affinity to the drug, are strategies to increase the DLC. With an interesting approach, Song *et al*. showed that the ring structure of poly(tetrahydropyranyl glycidyl ether) used as hydrophobic block of the micelle inner core can increase the loading capacity of Nile Red (14.9%, ~1.4 times higher) when compared with its acyclic analog, 1-ethoxyethyl glycidyl ether [37]. The cyclic structure is more hydrophobic than the acyclic one, enhancing the affinity of drug

22

and inner core. This behavior was also predicted by Meunier using Monte-Carlo "docking" method, Hildebrand solubility parameter (δ), and the solvation free energy of the drug in the PLA polymer models [95].

With a distinct strategy, Lv *et al*. prepared polymeric micelles with an ultrahigh DLC via the introduction of coordination interactions between the drug and polymeric carrier. They synthesized an amphiphilic copolymer PEG-b-poly- [(N-2-hydroxyethyl)-aspartamide] containing pendant phenylboronic acid (PBA). The PBA group acts as an electron acceptor unit which afforded donor-acceptor coordination with the electron donor group of DOX (the primary amine). The DLC achieved was approximately 50% of DLC and DLE was ~95%. Furthermore, they extended the current platform to efficiently encapsulate (DLC ~50%) other drugs with electron-donating groups (e.g., epirubicin and irinotecan) [94].

It is noteworthy that the incorporation of hydrophobic drugs changes the hydrophobic-hydrophilic balance, due to enhanced interactions between inner core and drug. Usually, when the amount of loaded drug decreases, the stability of micelles increases.

Table 1. 5 show the parameters and sizes of some PEG-PLA micelles accordingly by the used preparation methodology; solvent evaporation, thin-film hydration, dialysis and direct dissolution.

Table 1. 5 Summary of micelles synthesized through different methodologies.

Polymer	Solvent	Concentration (mg.mL^{-1})	Addition order	Speed rotation (rpm)	Diameter (nm)	Drug/substance	Obs	Ref
					Evaporation methodology			
PEG$_{5k}$-PLA$_{3k}$	ACT	10	OS in W	400	28.73 ^{D}	Haloperidol	Micelle achieved a DLC of 20% (w/w)	[96]
					52.23 ^{Dp}		Dp micelle achieve a DLC of 3.5 % (w/w) formed in a non-drug-saturated solution	
PEG$_{5k}$-PLA$_{4.8k}$	THF	-	OS in W	sonication	24.6 ^{D}	Semi-synthetic andrographolide analog	Micelle synthesized by fil formation showed higher DLC	[97]
					17.3 ^{D}	b-lap	-	
PEG$_{10k}$-PLA$_{10k}$	ACT		W in OS	-	83.2 ^{D}	bovine serum albumin (BSA)-	5% mannitol as cryoprotectant and ultrasonication are effective methods to control the size and distribution and agglomeration after the freeze-drying process	[98]
PEG$_{5k}$-PLA$_{4.5k}$	ACT	-	W in OS	2500	66 ^{D}	Lavender oil	The hydrophobic oil was efficiently encapsulated with a DLE of 70 to 75%. The higher DLE was achieved with the copolymer with the higher M_w	[99]
					78			
PEG$_{5k}$-PLA$_{10k}$					18 ^{D}			
					23			
PEG$_{2k}$-PLA$_{2k}$	THF	2	W in OS	Sonication 2 min	42.13	salinomycin	The *in vivo* results showed a significant tumor eradication with the highest survival in mice treated with drug-loaded micelles	[100]
					154.5 $^{D\ 10\%}$			
					127.1 $^{D\ 5\%}$			
PLA$_{2k}$-PEG$_{6k}$-PLA$_{2k}$	ACT	1.2	OS in W		118	Lisinopril	The Dp-micelle showed a lower DLC (1.9%) than the physically entrapped drug-micelle (8.2%). The release profile of Dp-micelle was dependent on medium pH	[101]
PLA$_{2k}$-PEG$_{6k}$-PLA$_{2k}$ ^{Dp}					162			
PEG$_{5K}$-PLA$_{2k}$*	ACT	3.33	OS in W		26		Micelle present spherical form. The micelle formation behavior is strongly dependent on polymer composition. Micelles composition with PLA chain of 45k or higher	[102]
PEG$_{5K}$-PLA$_{3k}$*					28.2			
PEG$_{5K}$-PLA$_{4k}$*					34.9			
PEG$_{5K}$-PLA$_{6k}$*					41.1			

Copolymer	Solvent		Method		Size	Drug	Observations	Ref
PEG$_{5K}$-PLA$_{9k}$ *					46.7		showed to have the size influenced by the polymer concentration in the formation solution	
PEG$_{5K}$-PLA$_{15k}$ *					50.6			
PEG$_{5K}$-PLA$_{30k}$ *					63.8			
PEG$_{5K}$-PLA$_{45k}$ *					80.7			
PEG$_{5K}$-PLA$_{75k}$ *					118.7			
PEG$_{5K}$-PLA$_{110k}$ *					156.6			
PEG$_{5K}$ -PLA$_{5K}$	ACT	1	OS in W	50	375.6	All-trans-retinoic acid (5:2 w/w)	The drug release is higher dependent on copolymer composition, with the faster release in micelles with lower M$_w$ and DLC. Micelles showed a promisor behavior in *in vivo* assays for injection administration.	[103]
PEG$_{5K}$ -PLA$_{10K}$					442.1			
PEG$_{5K}$ -PLA$_{20K}$					302.3			
PEG$_{2K}$ -PLA$_{16K}$					295.8			
PEG$_{2K}$ -PLA$_{32K}$					374.7			
PEG$_{5K}$ -PLA$_{3K}$	ACT	0.667	OS in W		32	-	The thickness and structure of the PEG shell are dependent on PLA M$_w$. Higher PLA amount leads to a more radially and homogeneous PEG shell.	[104]
PEG$_{5K}$ -PLA$_{15K}$					48.4			
PEG$_{5K}$ -PLA$_{45K}$					110.8			
PEG$_{5K}$ -PLA$_{5.8K}$	CLF	1	OS in W	500	< 33 ^{D}	paclitaxel	The micelle showed faster degradation at acidic pH than at pH 7.4, and PDLLA-PEG spherical micelle degrades faster than PLLA-PEG filomicelles	[105]
PEG$_{5K}$ -PLA$_{6.1K}$					< 40 ^{D}			
Thin film hydration methodology								
PEG$_{5k}$-PLA$_{4.8k}$	THF	-	-	Sonication 1min	49.4	Semi-synthetic andrographolide analog	These micelles increased ~280x the amount of drug in aqueous solution, compared with the free drug	[97]
					29.6 ^{D}	b-lap		
PEG$_{2k}$-PLA$_{2k}$	THF	2		Sonication 2 min	32.13	salinomycin	Drug-loaded micelles showed a suitable size and DLC. Micelles also increased the cell mortality and apoptosis in PC-1 cell line	[100]
					~ 225 $^{D\ 10\%}$			
					~ 135 $^{D\ 5\%}$			
PEG$_{5k}$-PLA$_{5k}$	ATN	5			44.7	Nile red	The dynamin- and caveolin-dependent but clathrin-independent endocytosis was involved in micelle cellular uptake and the micelle is colocalized with lysosome and microtubulin after internalization.	[106]
PEG$_{2k}$-PLA$_{2k}$	ATN	2.7	Water addition at 100 ºC with gently stirring		93	paclitaxel	Micelles formed by Peg and hydrotropic moieties showed higher DLC and enhanced long-term stability than PEG-PLA.	[107]
PEG$_{2k}$-PLA$_{3k}$	DCM	10	Water addition at 60 ºC overnight 1250 rpm, followed by 30 min sonication		78.3		Copolymers of PEG/PLA with relatively higher M$_w$ tend to have higher encapsulation and provide sustained release of DOX	[75]
PEG$_{2k}$-PLA$_{6k}$					63.59			
PEG$_{5k}$-PLA$_{7k}$					480			
PEG$_{5k}$-PLA$_{9k}$					371			
PEG$_{5k}$-PLA$_{15k}$					119.			
Dialysis methodology								

PEG$_{5K}$ -PLA$_{5K}$[#]	ACT	1	OS in W		375.6	All-trans-retinoic acid (5:2 w/w)	The drug release is higher dependent on copolymer composition, with the faster release in micelles with lower M$_w$ and DLC. Micelles showed a promisor behavior in *in vivo* assays for injection administration	[103]
PEG$_{5K}$ -PLA$_{10K}$[#]					442.1			
PEG$_{5K}$ -PLA$_{20K}$[#]					302.3			
PEG$_{2K}$ -PLA$_{16K}$[#]					295.8			
PEG$_{2K}$ -PLA$_{32K}$[#]					374.7			
PLA$_{4.4k}$-PEG$_{4k}$-PLA$_{4.4k}$	DMF	1	OS in W		63.8	paclitaxel	The increase in PLA difficulted the micelle formation. The hydrophobic drug showed better DLC and release profile than hydrophilic one (5-Fluorouracil)	[108]
					75.0 [D]			
PLA$_{4.9k}$-PEG$_{4k}$-PLA$_{4.9k}$					138.0			
					179.1 [D]			
PLA$_{6.5k}$-PEG$_{4k}$-PLA$_{6.5k}$					210.7			
					219.4 [D]			
PLA$_{3k}$-PEG$_{2k}$-PLA$_{3k}$					93.3			
PLA$_{7k}$-PEG$_{2k}$-PLA$_{7k}$					93.8			
PLA$_{4.5k}$-PEG$_{8k}$-PLA$_{4.5k}$					168.8			
Acetal-PEG$_{5.1k}$-PLA$_{5.3k}$	DMA	5 in OS	DD		33.1	-	The surface-modulated PEG–PDLLA micelle has a suitable size with a narrowly distributed and present a promising potential as a long-circulating carrier system with desirable biocompatibility and biofunctionality	[109]
Aldehyde-PEG$_{5.1k}$-PLA$_{5.3k}$					34.2			
tyrosine-PEG$_{5.1k}$-PLA$_{5.3k}$					37.4			
tyrosine-glutamic acid-PEG$_{5.1k}$-PLA$_{5.3k}$					38.9			
PLA$_{6.5k}$-PEG$_{4k}$-PLA$_{6.5k}$	DMF	1	OS in W		210.7	paclitaxel	The diffusion-controlled drug release (DLE 30-40%) is slower for PEG-PLA-PEG and dependent on the PLA length	[110]
PEG$_{5k}$-PLA$_{19.5k}$-PEG$_{5k}$					63			

Copolymer	Solvent		Method		Size	Drug	Observations	Ref
PEG$_{5k}$-PLA$_{36.8k}$-PEG$_{5k}$					80			
PEG$_{1.1k(x3)}$-PLA$_{6.7k}^+$	ACT	15 in OS	OS in W		50.6	DOX	NP showed that size and dispersity are dependent on magnetic stirring and organic/aqueous media composition. The control drug release is pH-dependent and effectively deliver MCF-7 cell line	[46]
	DMF				80.5			
	DMSO				232.7			
	THF				95.2			
	DMSO/THF (1:1)				220.6			
	DMSO/ACT (1:4)				133.3			
	ACT		W in OS		118.1			
	DMF				107.6			
	DMSO				121.9			
	THF				195.1			
	DMSO/THF (1:1)				199.5			
	DMSO/ACT (1:4)				135.9			
PEG$_{5k}$-PLA$_{1k}$	DMSO		DD			DOX	Mixed micelles of Vitamin E containing graft copolymer poly(hydroxypropyl methacrylamide)-g-a-tocopheryl succinate and PEG-PLA were synthesized and showed an enhanced cell uptake and cancer cell cytotoxicity.	[47]
PEG$_{5k}$-PLA$_{2.5k}$								
PEG$_{5k}$-PLA$_{3.5k}$								
PEG$_{2k}$-PLA$_{3k}$	DMSO	1.25			34	DOX	This PEG-PLA co-polymer with double disulfide linkage in the backbone are redox-responsive. *In vitro* assay confirms the destruction of micelles inside the cells and inhibition in the cell proliferation.	[48]
PEG$_{5k}$-PLA$_{3k}$					43			
PEG$_{2k}$-PLA$_{5k}$					107			
PEG$_{5k}$-PLA$_{2k}$					107			
Direct dissolution methodology								
L-PLA$_{0.9k}$ -PEG$_{4.6k}$-L-PLA$_{0.9k}$					107.0 / 204.9 [D]	paclitaxel	The L- and D-PLA/PEG mixed micelles by direct dissolution method present many advantages over dialyzes, such as faster drug release, easy formulation, and absence of toxic organic solvents. DLC, DLE is not influenced by direct dissolution or dialysis method.	[111]
L-PLA$_{0.9k}$ -PEG$_{4.6k}$-L-PLA$_{0.9k}$ and D-PLA$_{0.9k}$ -PEG$_{4.6k}$-D-PLA$_{0.9k}$	-	5			129.8 / 178.0 [D]			
L-PLA$_{.1.5k}$ -PEG$_{20k}$-L-PLA$_{1.5k}$ and D-PLA$_{1.5k}$ -PEG$_{20k}$-D-PLA$_{1.5k}$					226.8 / 276.4 [D]			
PEG$_{5k}$-L-PLA$_{1.8k}$ and PEG$_{5k}$-D-PLA$_{1.8k}$					101.4 / 207.8 [D]			
L-PLA-PEG and D-PLA-PEG varying PLA and PEG length	-				50-100		The mixed micelles L- and D-PLA/PEG are more stable than the separate composition due to the strong interaction between isomers forms of PLA	[90]
PEG$_{2k}$-L-PLA$_{3k}$	-				15°C 25°C 35°C			[112]

							Description	Ref
					58.3	62.9	72.1	Mixed micelles of L- and D-PLA/PEG shower smaller size than L-PLA/PEG due to the stereocomplexation effect between both isomers blocks. Increases in temperature and hydrophobic length increases the micelle size. These micelles exhibit a looser structure at higher temperatures due to water swelling effect.	
PEG_{2k}-DL-PLA_{3k}					49.2	58.5	65.6		
PEG_{5k}-L-PLA_{3k}					65.4	72.8	88.6		
PEG_{5k}-DL-PLA_{3k}					56.8	64.4	78.8		
PEG_{5k}-L-PLA_{4k}					64.8	69.4	83.4		
PEG_{5k}-DL-PLA_{4k}					53.0	60.6	69.6		
PEG_{2k}-$(L,D)PLA_{0.86k}$	-				105			The micelle composition influences the degradation rate. Longer hydrophobic blocks exhibit fewer size changes due to a more compact structure. Micelles formed by dialysis showed to be more stable than the direct dissolution	[113]
PEG_{5k}-$(L,D)PLA_{0.79k}$					90			Because the different micellization methods form a more compact structure. However, the LA fragments produced by degradation disfavors the crystallization of PEG blocks, resulting in a reduction of melting temperature and melting enthalpy	
PEG_{5k}-L-$PLA_{1.9k}$					120				
PEG_{5k}-$(L,D)PLA_{1.9k}$					100				

* Only copolymers with PLA bigger than 45kDa increase the size with increasing the concentration (1-20 mg.mL^{-1})

dialysis bag was stirred at 50 rmp;

+ Micelle size synthesized in DMF, DMSO and DMSO/acetone are affected by polymer solution dilution.

^{D} size measured with encapsulated drug

^{Dp} Pro-drug micelle

Acetone =ACT; Chloroform = CLF; Acetonitrile = ATN; organic solvent = OS; Water = W; direct dialysis =DD

28

As specified in Table 1. 5, the PEG-PLA micelles synthesis are highly influenced by PEG or PLA chain length, methodology, solvent, and experimental conditions.

Polymeric micelles are a challenging field in academic, industry and clinical sectors. However, the increase in the number of NPs in clinical trials and FDA approved in the last years shows the improvements generated by researchers' efforts. With the broad route for functionalization and application of micelles, it is expectable a huge number of new products released in the near future [3].

There is a closer relation between properties and micelles structural parameters (Table 1. 6).

Table 1. 6 Most important properties and parameters to micelle-based DDS

Basic properties of the micelles	Important parameters
Biological criteria and circulation time	Polymer biocompatibility
	Amount and nature of the hydrophilic segment
	Micelle total weight
	Particle size
	Chain length
	The ratio of the hydrophilic and hydrophobic segment (principally molecular weight fraction of the hydrophobic segment)
	Amount of drug load
	Micelle preparation method
	Superficial charge
Drug load	Morphology
	Micelle core and drug interaction
	Nature of hydrophobic chain
	Length of the core chain
	Preparation method
Release Kinetics	Stability
	CMC
	Amount of each block segment
	The inner core and compact conformation
	Size and amount of drug loading
	Micelle core and drug interaction
	Polymer degradation rate

Most drug-carrying NPs for cancer treatment have been designed to take advantage of the EPR effect of cancer cells. This effect results from unusual physiological aspects of

rapidly growing tumor tissue which enables macromolecules to penetrate and accumulate in the tumor interstitium for long periods of time [2]. However, for practical effectiveness, it is necessary not only accumulate but also to release the NP content into specific regions of affected tissues. In cancer therapies, for instance, fast-cellular destruction, achieved by a boost drug release, would improve the treatment. An interesting purpose in nanocarriers is the possibility to tailor the release profiles with spatial, temporal and dosage control. Owing to impressive progress in materials science, the development of stimuli-responsive systems became feasible through the design of biocompatible materials susceptible to undergo a dynamic modification in response to a specific stimulus (internal such as pH and redox potential or external such as temperature changes, magnetic fields, ultrasounds and light) [114].

1.2 Stimuli-responsive nanoparticles for drug delivery

The majority of the existing DDSs in cancer therapy are based on *in situ* response due to a specific and the particular environment of cancer cells (e. g. pH, temperature and reactive oxygen species (ROS) levels). The drawbacks of these systems are related to the variety of body reactions against an unknown particle, the different possible tumor stages and the specificities of the target tissue and cellular microenvironment, such as the levels of cell receptors [115],[114]. Consequently, developing new release systems for DDSs that do not depend on pathophysiology-based receptors or particular cell environment is a major step forward in order to overcome the influence of the heterogeneity of tumor environments.

A DDS that can be triggered using external stimuli-response is a promising approach. External stimuli such as light, ultrasound, and electric pulse are unaffected by the heterogeneous nature of target cells, tissues, and microenvironments. Particularly, light is a promising source for external stimulus due to the possibility of controlling the spatio-temporal release, the light modulation, the irradiation intensity, and duration. These advantages and the use of innocuous sources of light allow the possibility of consecutive treatment cycles without the need for a new injection of the drug dose. With light-responsive DDSs the drug is distributed over the body in an encapsulated form and is only activated/released in the target tissue by the localized light irradiation. Thus, this method could reduce drug side effects and improve drug specificity.

Most of the developed photo-responsive nanocarriers are based on the one-photon excitation system, which uses UV or visible light and a wide plethora of photoactive

chromophores [115]–[117]. Although UV irradiation has enough energy to cause efficient photochemical processes of cleavage, isomerization or rearrangement in a broad number of molecules, this energy may be toxic for some healthy surrounding tissues. Moreover, the clinical application is hindered due to poor tissue penetration of this type of radiation and the risk of damaging of DNA and proteins. Also, natural tissue chromophores, such as haemoglobin, absorb UV and visible light, contributing to reduced tissue penetration.

Considering the electromagnetic spectrum in the visible region and below, the light depth in tissue penetration reduces with the decrease in wavelength. On the other hand, in the other extreme of the spectrum, radiation over 900 nm has low penetration due to its absorption by water molecules. Therefore, the most suitable light source for irradiation, with tissue penetration values at the centimeter scale, is settled between 650-900 nm, and is known as first NIR-window [118]–[120]. For these wavelengths, the radiation may not have enough energy to directly cause a photo-reaction in common photochromic groups such as azobenzene, spiropyran, coumarin, and 2-diazo-1,2-naphthoquinone (DNQ) [116].

1.2.1 NIR-responsive nanoparticles

The use of NIR light to break, isomerize or rearrange molecules is mainly achieved by: 1) the two-photon excitation process that, requires high-power sources and focused lasers to achieve a photo-reaction at an acceptable rate, limiting the use of *in vivo* applications [119] (these systems may require a femtosecond pulse laser with high power density for two-photon absorption, and results in the increase of application costs [116]); 2) the NIR-to-UV upconversion process, that is usually synthesized from toxic precursors or composed of highly toxic rare-earth elements, which may be unsafe for biological uses and enhance the risk and cost of the process [121], [122].

To overcome this challenge, photothermal (generation of heat) and photodynamic (production of ROS) mechanisms are being used to activate the drug release process through different nanostructures. In photothermal systems, the NIR radiation is absorbed and the energy is converted into heat. In this case, a photothermal agent (such as gold NP or graphene nanosheets) is needed. It has the ability to absorb the energy of a NIR photon and get excited to a new vibrational state. When it relaxes, returning to the ground state, the surplus of vibrational energy is converted into heat. This heat changes the physico-chemical properties of the thermosensitive component in the nanocarrier, resulting in the release of the drug. However, there are some concerns regarding the use of photothermal agents. The generated heat can warm the whole intracellular environment leading to cell

membrane disruption or may cause changes in protein structures. These factors can cause unexpected side effects. Indeed, systems based on this approach have not reached the clinical stage for cancer therapy purposes [118].

In photodynamic based systems, the high reactivity of $^1O_2$ is exploited by the same species that mediate photodynamic therapy (PDT). After irradiation, the PS generates $^1O_2$ from molecular oxygen that reacts with specific molecules in the nanocarrier. This interaction leads to a structural change, able to promote the drug release. The PS molecule is capable of absorbing a photon from a certain wavelength, resulting in a higher-energy electronic configuration state (Jablonski diagram, Figure 1. 9) known as singlet photosensitizer excited state (^1PS). This is a very unstable state with a short lifetime between nano to picoseconds. ^1PS can be deactivated (the molecule goes back to the stable ground state (PS_0)) by losing its energy either through fluorescence emission or heat production (internal conversion). However, ^1PS can, alternatively, turn into the slightly more stable excited triplet state (^3PS) by a process known as 'intersystem crossing'. In this case, the ^3PS can decay back to the ground state by emitting phosphorescence, however as it is a 'forbidden process' by quantum selection rules, this process is very unlikely to occur. Therefore, in the most common process the ^3PS, with a lifetime in the microseconds scale, loses its energy via two other different mechanisms [123], [124]:

Type I mechanism: ^3PS could either gain or donate an electron to form a radical cation or anion, which further can interact with oxygen, generating radical oxidants such as the superoxide radical anion ($O_2^{\bullet-}$) and the powerful oxidant hydroxyl radical ($HO^\bullet$).

Type II mechanism: ^3PS could transfer energy to an oxygen molecule (in the ground triplet state $^3O_2$) leading to the formation of $^1O_2$. The $^1O_2$ has high cytotoxicity but a very limited diffusion distance (~20 nm due to its very short lifetime around 40 ns). In the literature, it is pointed out that $^1O_2$ diffusion is long enough to reach and be active at any site within a 100 nm liposome [125].

Type I and Type II reactions can occur simultaneously, and the amount of oxygen reactive species generated by each type varies according to the environment conditions, such as: the structure of the PS (which determines the energy of triplet and singlet states); cellular localization of PS; and the concentration of oxygen or other species. However, in PDT it is generally accepted that photochemical reactions via type II are more predominant than type I. Hence, most of the cellular damage is supposed to be induced through cytotoxic $^1O_2$ generated in the Type II reaction [124], [126]–[128].
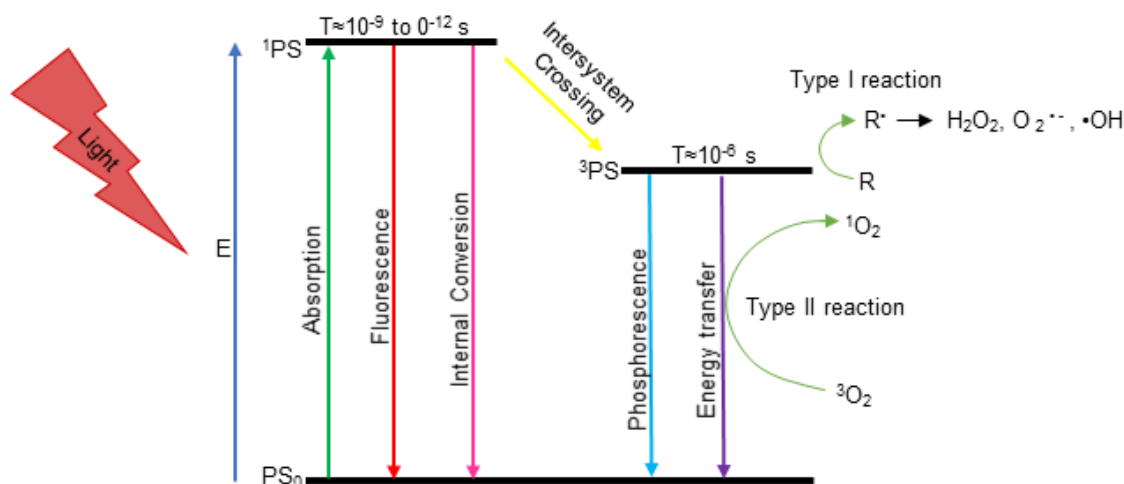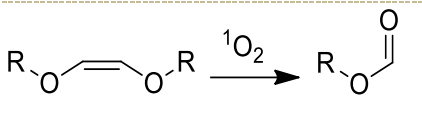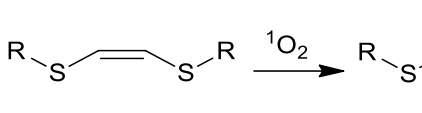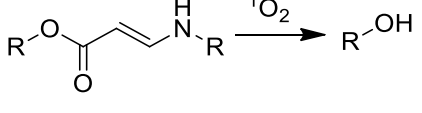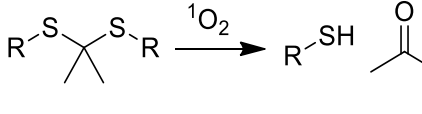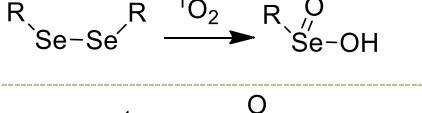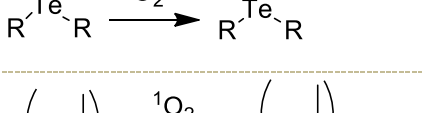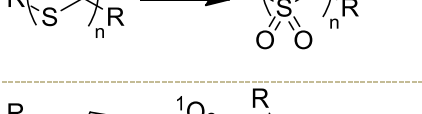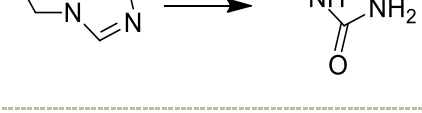
Figure 1. 9 An example of a Jablonski diagram. When irradiated, the photosensitizer absorbs a photon which results in the transformation from the ground state (PS_0) to excited singlet state (^1PS). Due to the high instability of the ^1PS state, it can return to the ground state or alternatively turn into a long-lived excited triplet state through intersystem cross flipping of an electron. In this state radicals and molecules can interact with PS and generate high oxidative species.

Polymeric based nanostructures activated through photodynamic mechanisms must be composed by PS and ROS-sensitive moieties strategically located in the polymeric structure. To provide an efficient spatial-temporal drug release mediated by light, the DDS requires the following characteristics: an efficient $^1O_2$ production of the PS by NIR irradiation; a sensitive segment with high responsiveness to ROS and a suitable location for the sensitive segment in the polymer backbone [118]. The induced photochemistry process in a proper position will favor efficient and fast disassembly of the micelle structure, cleavage of pro-drugs or disruption of aggregates or NPs [129]. The sensitive segment can generally react with $^1O_2$, undergoing a bond cleavage process or a change in the polymer hydrophobicity. Both processes are capable of destabilizing the nanostructure leading to the cargo release [118]. The sensitive segment should also be stable in aqueous media, inert in common biological environments and have simple chemistry of incorporation into a wide number of polymeric molecules [130].

There are many different types of $^1O_2$ sensitive structures such as olefin linkers (lipids, vinyl ether, vinyl disulfide, and aminoacrylate), thioketal linker, selenium-containing polymers and hydrophobicity changeable polymers (tellurium containing polymers), poly(propylene sulfide), and polymers containing imidazole (and derivatives) groups. Table 1. 7 summarizes these structures, which are discussed in the following sections.

Table 1. 7 Summary of sensitive linker groups and their mechanism of reaction with $^1O_2$.

Sensitive linkers group		Disruption mechanism	Ref
Olefins linkers	Vinyl ether		[131]
	Vinyl disulfide		[132]
	Aminoacrylate		[133]
Thioketal			[134]
Sellenium			[135]
Hydrophobicity change	Tellurium		[136]
	Poly(propylene sulfide)		[137]
	Imidazole		[138]

1.2.2 Olefins linkers

The first use of $^1O_2$ for photo-oxidable material leading to a payload release was described using olefin compounds [139]. When an unsubstituted alkene is exposed to $^1O_2$, it undergoes a [2+2] cycloaddition reaction through the formation of an unstable dioxetane intermediate (Scheme 1. 1), which spontaneously decomposes to give two carbonyl type products. This process of dioxetane decomposition can be catalyzed *in vivo* by the presence of amines and traces of metals [140].
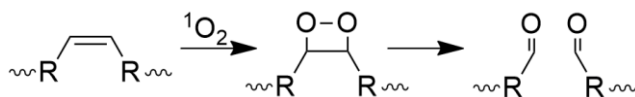
Scheme 1. 1 [2+2] Cycloaddition reaction of an alkene, forming the unstable dioxetane intermediate that decomposes to carbonyl (carboxyl) derivatives [131].

Lipids

Peroxidation of lipid membranes is a well-established process that occurs through ROS attack [141]–[145]. The process of photodynamic sensitization of a lipid membrane is known to promote oxidation and cleavage of the unsaturated part of the carbon-carbon chain [146]. Based on this strategy, in 1999, Berg *et al*, developed a process known as photochemical internalization (PCI). In this process, the ROS generated by PS is able to induce the rupture of the lipidic membrane of endocytic vesicles inside the cells in order to enhance the endosomal escape of entrapped compounds (Figure 1. 10) [142]. This relevant discovery led many researchers to exploit the PCI process for the controlled leakage of payload in DDSs through photosensitizer stimulation or ROS rich environment caused by cancer cell metabolism [118]–[120], [147]–[152]. Among them, Chen *et al*, designed a photo-responsive liposome with a PS (verteporfin) encapsulated inside a liposomal bilayer. The liposome was able to overcome the lipid biological cellular barriers of endolysosomal membranes and release the entrapped compound through destabilization of lipids of both membrane layers (liposome and endosome/lysosome) being the whole process mediated by $^1O_2$ [153]. In a similar approach, Park *et al*. engineered a Pluronic F127® micelle with chlorin e6 (Ce6) conjugated in the outer end of the micelle and holding doxorubicin (DOX) in the inner core. After red light irradiation, the $^1O_2$ generation disrupted the cellular membrane by lipid peroxidation, increasing the cellular uptake of the drug, reducing side effects and overcoming the drug resistance in cancer cells [154].
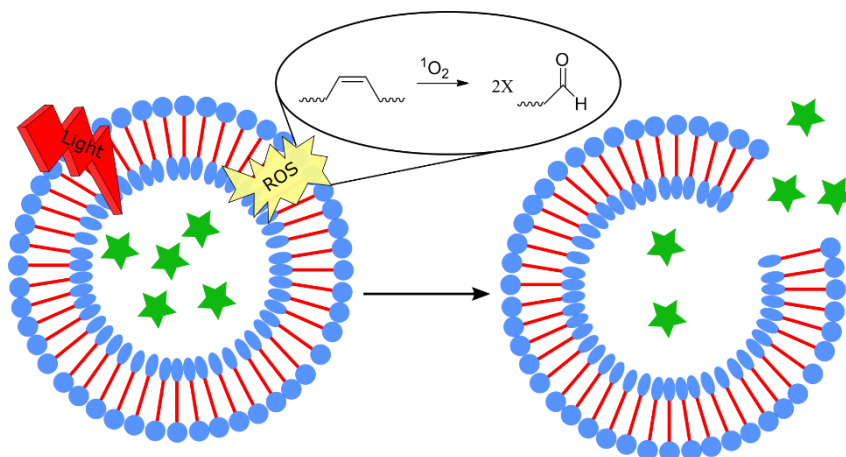
Figure 1. 10 Illustration of the impact of $^1O_2$ on lipid oxidation leading to the endosomal escape of the entrapped compound.

Inspired by the lipid peroxidation process, Anderson *et al*. published in 1992 the first work using $^1O_2$ as a potential release agent through cleavage of the plasmalogen vinyl ether linker [139]. Since this seminal work, his research group has present several works with this linker in photosensitizer $^1O_2$ processes and lipid layer peroxidation to induce spatio-temporal drug release [125], [155], [156].

The controlled leakage of payload occurs through the cleavage of the vinyl bond present in the constitutive lipid of the liposome NP. This photodegradation alters the structure of the lipid membrane organization generating defects in the lipid membrane. As an example of liposome transformation, the plasmenylcholine oxidation originates fatty aldehydes and lysolipids (as lysophospholipid) (Scheme 1. 2) [156].
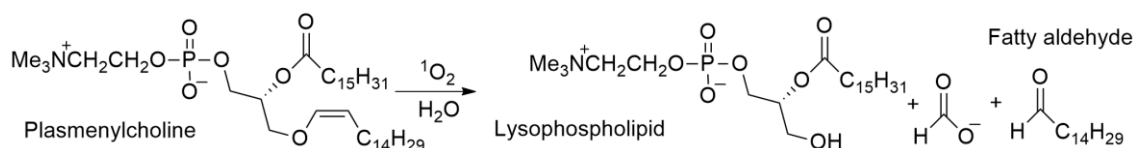
Scheme 1. 2 Plasmenylcholine cleavage into single-chain surfactants via sensitized photooxidation of the plasmalogen vinyl ether linkage [156].

Vinyl ether linker

A similar alkene linker (vinyl diether compound) was reported by Yang and Bauld in 1999 [157] as a promising electron-rich dienophile to react with $^1O_2$. Later, Zamadar *et al*. [131] used this compound as a $^1O_2$ sensitive spacer between a photosensitizer and an optic fiber. This fiber optical-guided sensitizer was designed for specific delivery of a photosensitizer molecule. They also studied the optimal PS concentration and the distance

between the probe tip and sensitive linker to enhance effective cleavage considering the short diffusion distance of $^1O_2$. The optical fiber was composed of pyropheophorbide-*a*, as PS, conjugated with the Z-vinyldiether linker as a photocleavable segment. The sensitive group can react with $^1O_2$ through a [2+2] cycloaddition reaction separating it from probe tip (Figure 1. 11). The maximum photocleavage effect was observed for an amount of 60 nmol of loaded sensitizer and 17 nm distance between probe and linker (light intensity of 50 W and wavelength below 540 nm).
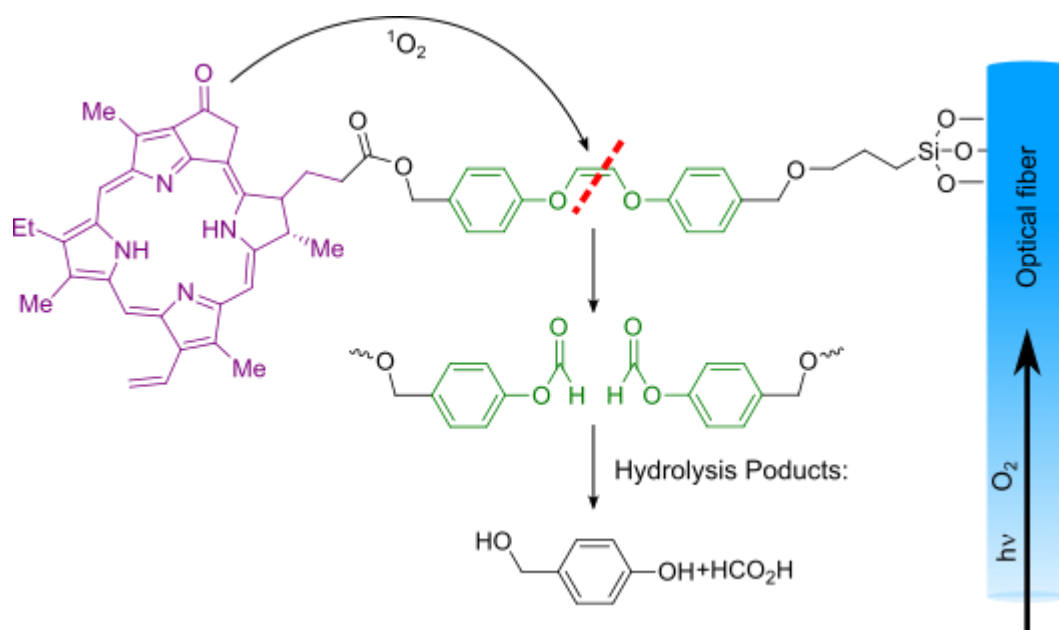
Figure 1. 11 The concept of oxygen singlet fiber optic of Zamadar *et al*. Oxygen flow through fiber optic and the light excite the photosensitizer producing $^1O_2$ which is able to cleave the vinylic bond (adapted from [131]).

Vinyl disulfide linker

In 1999, the Breslow group [158] modified the vinyl ether linker of plasmalogen using sulfur substituents at each side of the vinylic linker, increasing the reactivity of the double bond. The electron-rich alkene linker reacts with $^1O_2$ forming a dioxetane derivative, which is decomposed leading to two carbonyl group derived fragments. The authors proposed a nanostructure composed of PS (zinc phthalocyanine) protected with a cyclodextrin dimer linked through $^1O_2$ sensitive vinyldithioether linker. The sensitive linker was completely cleaved after 10 min of irradiation [159].

Lee *et al.* developed a highly light-sensitive DDS incorporating a PS (zinc phthalocyanine) and a $^1O_2$ sensitive crosslinker into mesoporous silica NP. The surface of

the particles was decorated with the model drug 5-[(2-aminoethyl)amino]naphthalene-1-sulfonic acid (EDANS) through a bis-(alkylthio)alkene $^1O_2$ sensitive group. They found that the close proximity of PS and linker in the designed system has a crucial role for the cleavage mediated by the generated $^1O_2$ and consequently, leading to drug release upon light irradiation (Figure 1. 12 a). EDANS showed a release profile of only 10% in dark condition contrasting with the cumulative release of ~60% after 2 h irradiation (100 mW.cm^{-2}, >525 nm, Figure 1. 12 b) [160].
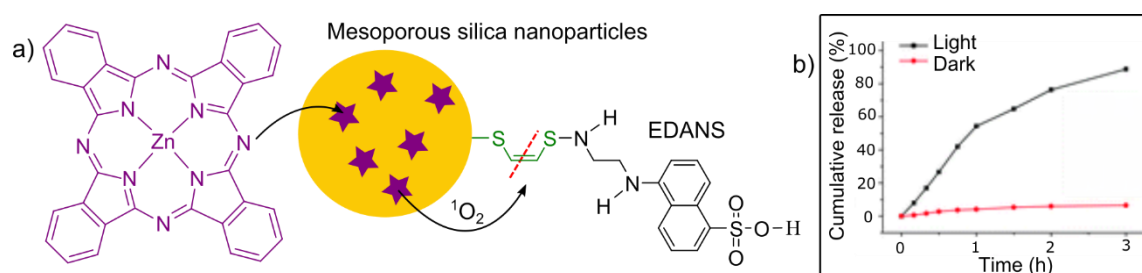
Figure 1. 12 Scheme of the Lee *et al* mesoporous silica NP with surface decorated by EDANS through a sensitive linker. $^1O_2$ is generated by zinc phthalocyanine photosensitizer and cleaves the sensitive vinylic bond releasing the model drug a); comparison of the NP release profile under dark and light conditions b) (published by permission of The Royal Society of Chemistry) [160].

Saravanakumar *et al*. developed a light-induced micelle with a vinyldithioether linker located in the middle backbone of the copolymer composed by PEG and PCL, (Figure 1. 13 a). Spherical micelles with average size about 124 nm were prepared through a self-assembly process induced by the polymer amphiphilicity. DOX and Ce6 were loaded in the inner core of micelles with incorporations of 3.4 and 5.2 wt% respectively, correlated with copolymer mass. The unleashing of the release process was confirmed by irradiating for 2 h at 660 nm with an intensity of 50 mW.cm^{-2}. After 7 h, micelles released 32% of the encapsulated DOX, which is about 1.4 times more than the ones kept in the dark (Figure 1. 13, b). *In vitro* tests prove that this DDS showed no significant cytotoxicity under dark conditions, however, when irradiated it reduces cancer cell viability up to 37% compared to micelles that were not irradiated and was 53% lower than micelles without sensitive segment. With high biocompatibility, the developed micelles showed promising characteristics for co-delivery of hydrophobic drugs and PS [132].
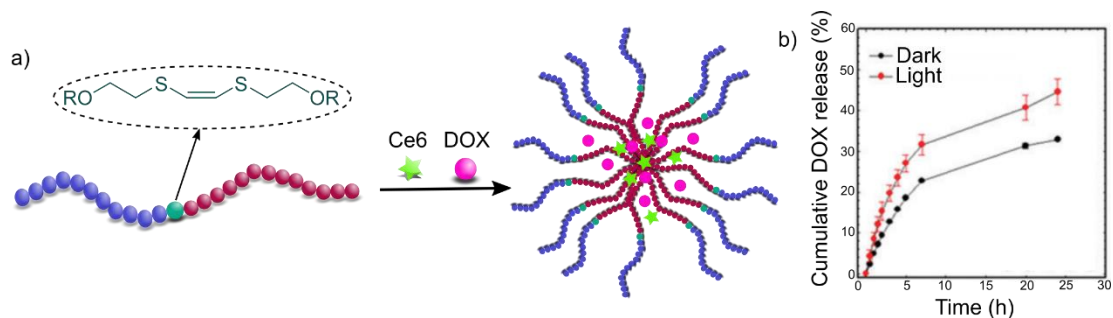
Figure 1. 13 Schematic illustration of the Ce6 and DOX co-loaded micelles developed by Saravanakumar *et al* (a) and the release profile of DOX (b) (published by permission of The Royal Society of Chemistry) [132].

Liu *et al.* developed particles based on a nanoscale coordination polymers (NCPs) that are responsive to red light (660 nm) for controlled delivery of DOX and at the same time present a PDT effect due to a PS that was co-loaded with the drug (Figure 1. 14). The carboxylic vinyl disulfide linker and Hafnium ions complex to afford the sensitive NCP NPs. The NPs were then soaked in a solution with Ce6 and DOX in order to load the drugs and PS. Lastly, the NCPs surface was functionalized with PEG affording NCP particles with a size of 90 nm. The DLC of Ce6 and DOX were approximately 23 wt% and 45 wt% respectively and after 1 h of light emitting diode (LED) irradiation (5 mW.cm^{-2}) the system released 30.4% of entrapped DOX. They also verified the effective light-triggered release using *in vitro* assays with 4T1 murine breast cancer cells. The capacity of the NP to be used as a contrast agent for *in vivo* computed tomography imaging of tumors was also studied due to the presence of Hafnium. *In vivo* tests carried out by injection of the NP in mice bloodstream and followed by laser irradiation (30 min of 5 mW.cm^{-2}) showed a decrease of tumor volume after 12 days of the irradiation period. Although high levels of accumulation of NP were found in the reticuloendothelial system (RES) organs, mice treated with this DDS did not show an appreciable post-treatment body weight drop. Complementary, the histological examination of hematoxylin and eosin stained main organ slices demonstrate that NP exerted no noticeable organ damage, contrasting with conventional treatment with free DOX/Ce6 which caused serious damage to the mouse heart tissues [161].
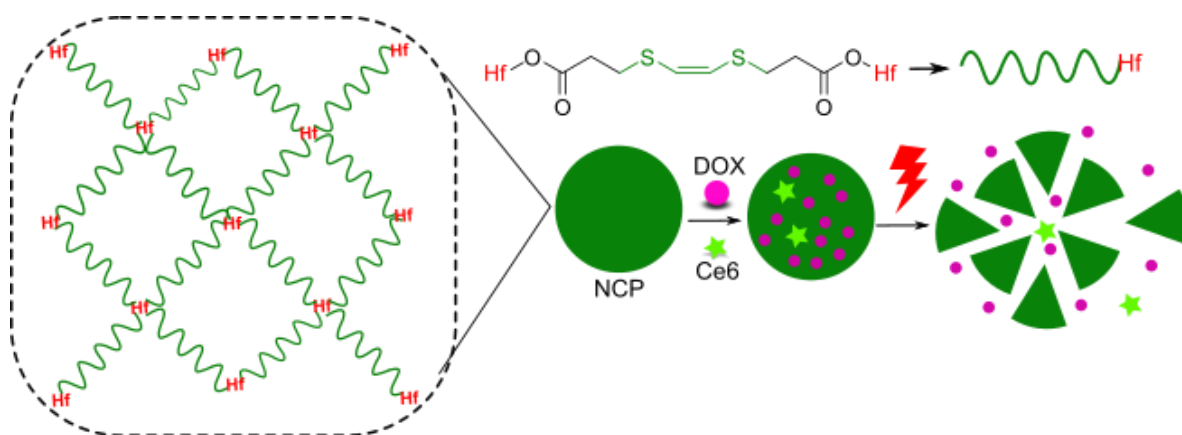
Figure 1. 14 NCPs for red light controlled DOX delivery designed by Liu *et al*. NCPs were co-loaded with Ce6 and had the surface modified by PEG. After red light irradiation and the action of $^1O_2$, the sensitive vinylic bond cleave and DOXs are released [161].

Olefin photo-oxidation mechanism

The You's group studied different types of olefin reactivity towards $^1O_2$. A molar ratio of 1:1 of olefin and photosensitizer (5,10,15-triphenyl-20-(4-hydroxyphenyl)-21H,23H-porphyrin, TPP-OH) in deuterated chloroform (CDCl₃) solution was exposed to 200 mW.cm^{-2} of 400-800 nm wavelength light. The photo-oxidation time and conversion product were analyzed by proton nuclear magnetic resonance (^1H NMR) and high performance liquid chromatography (HPLC) [162]. The authors found out that $^1O_2$ reactivity was enhanced when the olefin compound has:

i. disubstituted heteroatoms O and S (such as 2,3-dihydro-1,4-dioxine and 5,6-diphenyl-2,3-dihydro-1,4-oxathiine), because the strong electron-donating effects of these atoms provide high yields of the oxidation product. Olefins substituted by hetero atoms are more prone to be directly attacked by $^1O_2$ through one side of the double bond, a process known as "*cis*-directing effect". The absence of allylic hydrogens in the case of disubstituted heteroatoms double bonds results in less steric hindrance for the $^1O_2$ attack (Figure 1. 15 i);

ii. amine than amide group near to vinyl bond (Figure 1. 15 ii), due to the availability of the electron lone pair of nitrogen that increases the electron density of the double bond, thus increasing the $^1O_2$ reactivity. However, in amides, the density of the π bond can be reduced by keto-amine resonance, which leads to a retardation of the 1,2-cycloaddition reaction;

iii. C=C bond that is used instead of C=N. All imine groups showed reduced reactivity to $^1O_2$ (Figure 1. 15 iii);

40

Figure 1. 15 summarizes and exemplifies some substituent groups able to increase or decrease the $^1O_2$ reactivity towards olefins.
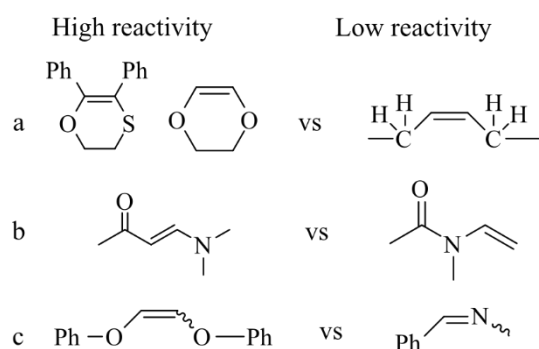
Figure 1. 15 Chemical structures of some olefins substituted by side groups which can improve or not the $^1O_2$ reactivity [162].

The reactivities of dioxygen in comparison to disulfur substituted olefins were also analyzed. The degradation rate of the sulfurated compound (1,2-bis(phenylthio)ethene), was greater than dioxygenated olefin ((Z)-1,2-diphenoxyethene) considering the degradation rate of the substrate or the conversion of initial olefin to oxidized products: 88% for S-C=C-S-compound and 80% for O-C=C-O-compound. Even though the faster reaction kinetics observed for the disulfur compound, not all of the degradation products were detected by ^1H NMR. Thus, authors assumed that dioxygen compound was a more suitable linker for the $^1O_2$-cleavable DDS. Nevertheless, the formyl group that results from the photo-cleavage process could originate a formylated drug that might interfere with the drug activity [162].

Dinache *et al* also studied the $^1O_2$ reactivity towards several olefins. The experiment was performed in a solution of dichloromethane with a molar ratio of olefin compound and photosensitizer (Verteporfin) of 250:0.05 using irradiation light (500-800 nm) of 145 mW during 2 h. The photo-oxidation product was investigated through Fourier-transform infrared spectroscopy (FTIR) and possible photoproducts were suggested. The results were in agreement with You's work [162] showing that hetero substituted olefins (S or O) have a higher rate of [2+2] cycloaddition reactions. These substituents near to the carbon-carbon double bond increase its reactivity with $^1O_2$ [163].

Jiang and Dolphin worked on an olefin linkage to ensure high chemoselectivity during photo-oxidation in order to develop a site-specific prodrug release. They studied the stereoselectivity of $^1O_2$ addition related to the attached side groups in the sensitive linker. A conjugated drug-photosensitizer was prepared, incorporating a spacer with a $^1O_2$-

sensitive vinyl group. The [2 + 2] cycloaddition reaction of $^1O_2$ with the vinyl double bond leads to bond cleavage and site-release of the drug (Figure 1. 16). The best photo-oxidable linker, was a 1,2-dihetero-substituted alkene, preferably in Z-configuration. In the work, simple esters, amides or methyl esters of non-steroidal anti-inflammatory drugs were linked to the photosensitizer by the intercalation of the chosen linker group. No interdependence between solvent and photo-oxidation process was observed using 4 different solvents (deuterated benzene, deuterated chloroform, deuterated methanol and deuterated acetone). Also, tetraphenylporphyrin monoacid derivative (TPPAD) and benzophenylporphyrin monoacid derivative (BPAD, verteporfin analog photosensitizers) were tested, showing equal efficiency of drug release [140].
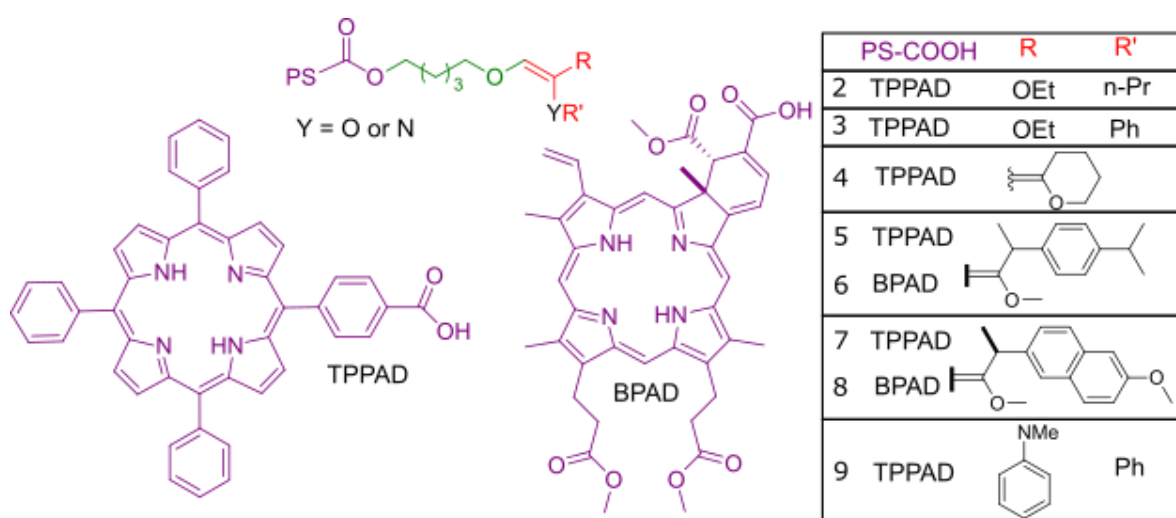
Figure 1. 16 Schematic illustration of the studied structures of Jiang and Dolphin's prodrug [140]. Purple shows the photosensitizer, green the extension chain and in red the linker and the drug, ibuprofen (complexes 5-6) or naproxen (complexes 7-8).

The most interesting result was the difference in the E and Z configuration reactivity of structure 2. The E configuration showed approximately 60% lower photo-oxidation product yield than the Z isomer. This behavior is explained by the hindrance caused by the electron cloud. In the E configuration, the alkoxy substituents hamper the approach of the $^1O_2$ to the olefin from both sides (back and front) of double bound. However, in the Z configuration, the back side of the C=C bond is unprotected from $^1O_2$ attack. In this reaction, the chemoselective attack of $^1O_2$ to the olefin is proposed to depend mainly on the HOMO-LUMO interactions [140].

Intriguingly, in the case of structure 9, the configuration does not show such dependence. The E configuration showed a photo-oxidation only slightly slower than the Z configuration. This behavior can be justified by the higher activating effect of the

42

enamino nitrogen, which surpasses the stereochemical bulkiness caused by the *E* configuration [140].

Although the researches about the break of vinyl ether linker-mediated by $^1O_2$ have been started over 20 years ago, the synthetic routes for vinyl diethers or dithioethers are scarce, usually with low efficiency and nonstereospecificity [164]. This problem was overcome by the work of Nkepang *et al.* that reported a facile synthetic method for producing the vinyl diether linkers and analogs with sulfur and nitrogen, with yields ranging from 40 to 90%, with a purity higher than 90% [165].

Aminoacrylate linker

With the aim to overcome the difficulties of using vinyl-based linkers, You's group developed a new $^1O_2$-cleavable linker stable in aqueous media using an easier synthetic approach, and that has fast cleavage. The aminoacrylate linker (β-enamino ester) was synthesized through esterification in high yields (Figure 1. 17-1). The β-aminoacrylate analogs with sulfur or oxygen replacing the nitrogen atoms (β-thio-acrylate and β-oxy-acrylate, respectively) were prepared following the same route with the aim of comparing their oxidation rate when irradiated by a diode laser (690 nm, 200 mW.cm^{-2}, 25 min) in the presence of a photosensitizer, 5-(4-methoxyphenyl)-10,15,20-tetraphenyl-21,23-dithiaporphyrin. Only β-aminoacrylates showed reactivity towards $^1O_2$. The higher reactivity is due to nitrogen electron donation originating a more electron rich bond for the $^1O_2$ addition. In the case of amine/amide groups attached to both sides of the vinylic bond (aminoacrylamide, Figure 1. 17-2c) the reaction with $^1O_2$ is faster than analogs with oxygen (aminoacrylate, Figure 1. 17-2a) or sulfur (aminoacrylthioate, Figure 1. 17-2b). However, the linker chosen for further experiments was the aminoacrylate (Figure 1. 17-2a) based on the derivative products of the oxidation process. The selected linker forms 4-phenylphenol and 1-formyl piperidine after irradiation, originating fewer side products than 2b and 2c. This aminoacrylate is 72% faster in the reaction with $^1O_2$ than vinyl dithioether (comparing to (Z)-1,2-Bis(phenylthio)ethylene). Subsequently, they designed a model prodrug with hydroxyl-dithiaporphyrin (as a PS) and estrone as a drug which was successfully released after irradiation, with 90% of linker photo-oxidation in 10 min (Figure 1. 17-3). Finally, they developed an aminoacrylate linker conjugated with two photosensitive moieties, a PS and a rhodamine B (PS-L-Rh, Figure 1. 17-4) which showed a faster linker cleavage (~100% in 10 min) than the structure in Figure 1. 17-3. However, the decomposition rate of PS-L-Rh is slower in Dulbecco's Modified Eagle Medium, with 5% fetal bovine serum,

than in CHCl$_3$ due to the reduced oxygen concentration and a shorter lifetime of $^1O_2$ in aqueous media [164].
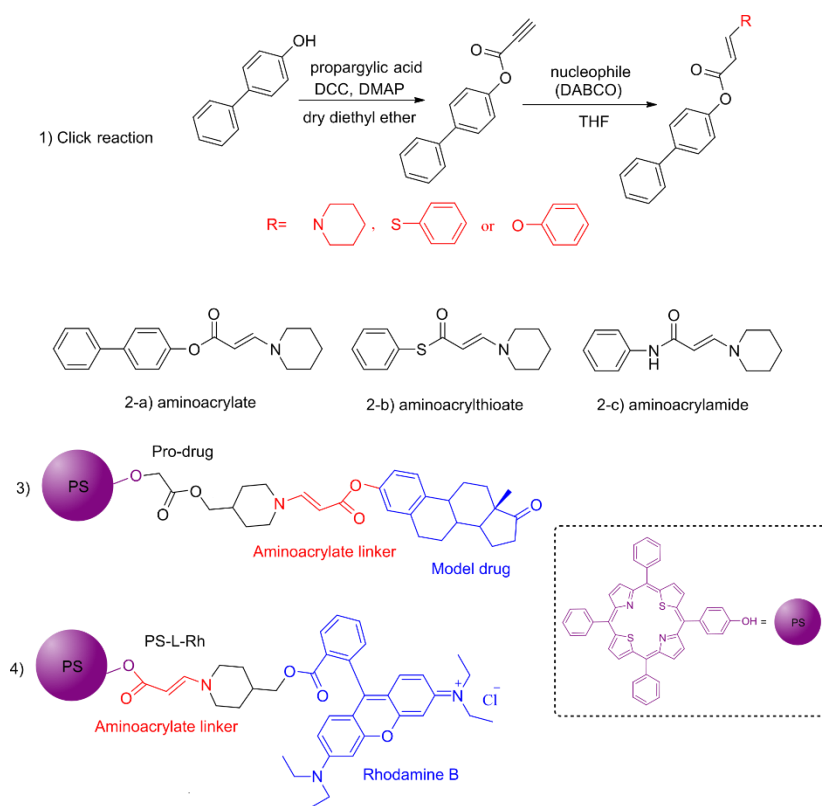
Figure 1. 17 The synthesis of aminoacrylate linkers through click reaction, and the pro-drug developed by the Youngjae You group [164].

The promising results obtained encouraged further studies of the application of aminoacrylate based linkers in $^1O_2$-mediated release strategy in other DDSs. A double activatable prodrug system (drug-linker−deactivated photosensitizer which is activated by intracellular esterase) using very low-intensity radiation (0.8 mW.cm^{-2}, 30 min) achieved a drug release of 99% [166]. They demonstrated that aminoacrylate linker does not suffer oxidation by others superoxide radical but only by $^1O_2$. The reaction of aminoacrylate linker with $^1O_2$ shows a second order rate constant (k) of 2.5 X 10^7 M^{-1} s^{-1}. Using dithiaporphyrin as a photosensitizer, a prodrug system following the same linker with combretastatin A-4 (CA4), as the drug, achieved 80% release of CA4 after 10 min of irradiation. They also proved by *in vivo* tests, the good efficacy of the light-responsive prodrug with a significant colon-26 tumor volume reduction [167]. Other prodrugs were developed with different approaches [168], [169] and also a bioprobe for real-time monitoring $^1O_2$ generation during PDT [170].

44

Saravakamura *et al.* also engineered a miktoarm amphiphilic block copolymer (PEG-*b*-PCL) with a $^1O_2$-labile stereospecific β-aminoacrylate linker for DOX and Ce6 loaded NP (Figure 1. 18 a). Among the different synthesized copolymers, the PEG_{2k}-*b*-PCL_{2k} was selected for further studies. Their results showed that DOX release in PBS medium at red light irradiation (660 nm, 30 min) was 1.2 times higher when a light power of 100 mW.cm^{-2} was used instead of light power of 50 mW.cm^{-2} (68 % of drug release, Figure 1. 18 b). Nanostructures showed no significant cytotoxicity under dark conditions however, the cell viability was reduced to below 20% after treatment with light (10 min of 50 mW.cm^{-2}) [133].
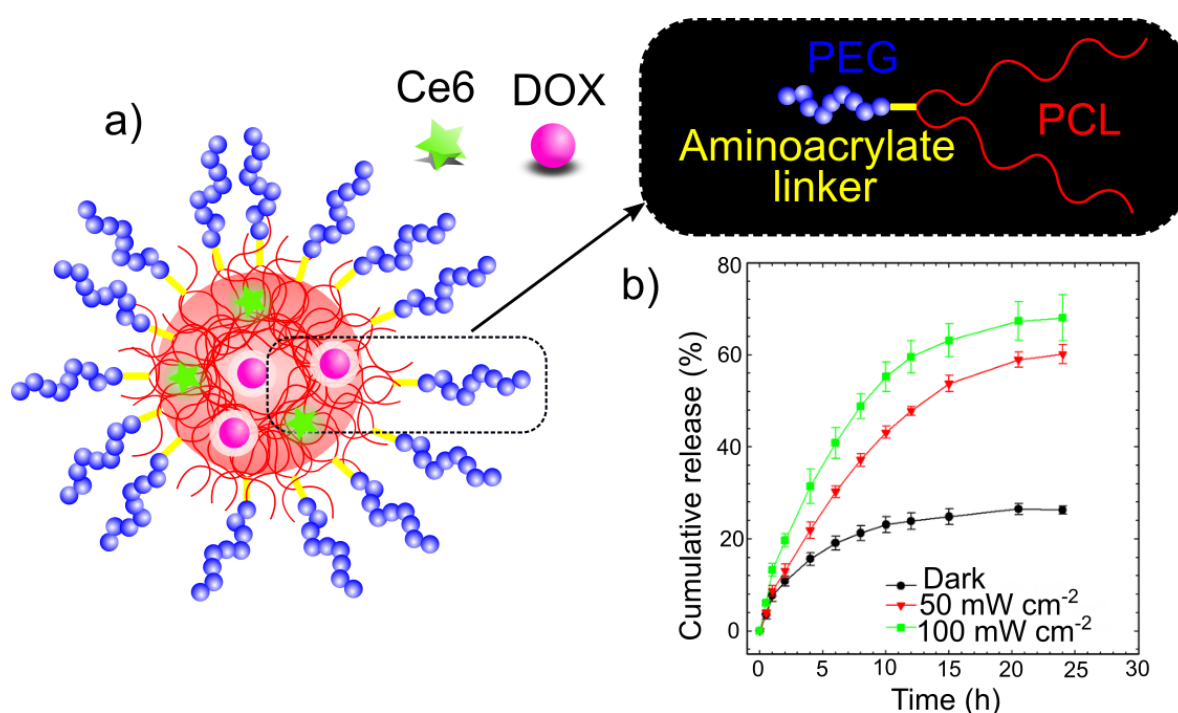
Figure 1. 18 Schematic illustration of the NP made by miktoarm amphiphilic block copolymer with Ce6 and DOX co-loaded (a) and the cumulative release profile of DOX (b) (adapted with permission from American Chemical Society) [133].

1.2.3 Thioketal linker

Thioketal is a well known protective group commonly used due to its stability, easy synthesis and strong responsiveness of redox potential [130].

In mid 1996, Colonna *et al*. studied the oxidative reaction of dithiolane compounds [171]. A plausible product for dithiolane oxidation indicates that compounds such as 1,3-dithiolanes can suffer a superoxide anion mediated cleavage through the oxidative

mechanism, presented in Scheme 1. 3 [171]–[173]. However, the thioketal group as a linker for DDSs only appeared in 2010. Inspired by the mentioned study, Wilson *et al.* developed an oral delivery ROS responsive NP [174]. Thioketal linker showed high sensitivity to ROS species and was further used for internal stimuli drug delivery systems [134], [175].

$$\begin{array}{c}\diagdown C \diagup_{S}^{S}\end{array}\Big] + \bar{O}_2 \longrightarrow \diagdown C{=}O + \Big(_{S^{\ominus}}^{S^{\ominus}} + O_2$$
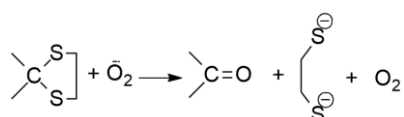
Scheme 1. 3 Cleavage of thioketal linker mediated by superoxide ion [172]

Only four years later, Yuan *et al* synthesized a thioketal linker-polyprodrug able to undergo a cleavage process mediated by $^1O_2$. The structure was constituted by a polyelectrolyte (PE) which acts as a PS generating $^1O_2$ after appropriate light irradiation. The proximity between PE and the sensitive linker enhance drug delivery with spatial and temporal precision [176]. Other thioketal light-sensitive prodrugs have been designed with high efficiency and other functionalities as tumor imaging agents [177], [178]. The first thioketal NP designed to disrupt in the response of $^1O_2$ oxidation was reported in 2016 by Seah *et al*. who developed a polythioketal-based ROS sensitive polymeric micelle (see Figure 1. 19 a) loading paclitaxel (as drug) and *meso*-tetraphenylporphyrin (TPP, as PS) [179]. The developed PPS NP showed a faster release of the encapsulated drug after irradiation (1.5-2.5 faster than PPS degradation when exposed to superoxide anion $O_2^{-•}$). Successful *in vitro* tests were carried out by light irradiation at 650 nm (70 mW.cm^{-2}, over 20 min) in HeLa cells. The NP in dark conditions showed no cytotoxicity and showed the half maximal inhibitory concentration (IC$_{50}$) two times higher than free paclitaxel (5.6 nM and 2.6 nM). When NP was exposed to light the IC$_{50}$ decreased dramatically to 0.11 nM, and importantly, the degradation products of PPS polymer leads to no cytotoxicity. The *in vivo* test (in nude mice *nu/nu*) indicated an increased therapeutic effect with tumor growth suppression in relation to the non-irradiated sample. Even NP with low levels of encaged porphyrin (2.15 wt%) showed efficient light-triggered drug release effect (Figure 1. 19 b). Treated mice did not show any significant change in the body weight in 15 days and no cytotoxicity in the organs, analyzed by hematoxylin and eosin (H&E) immunostaining, was detected [180].
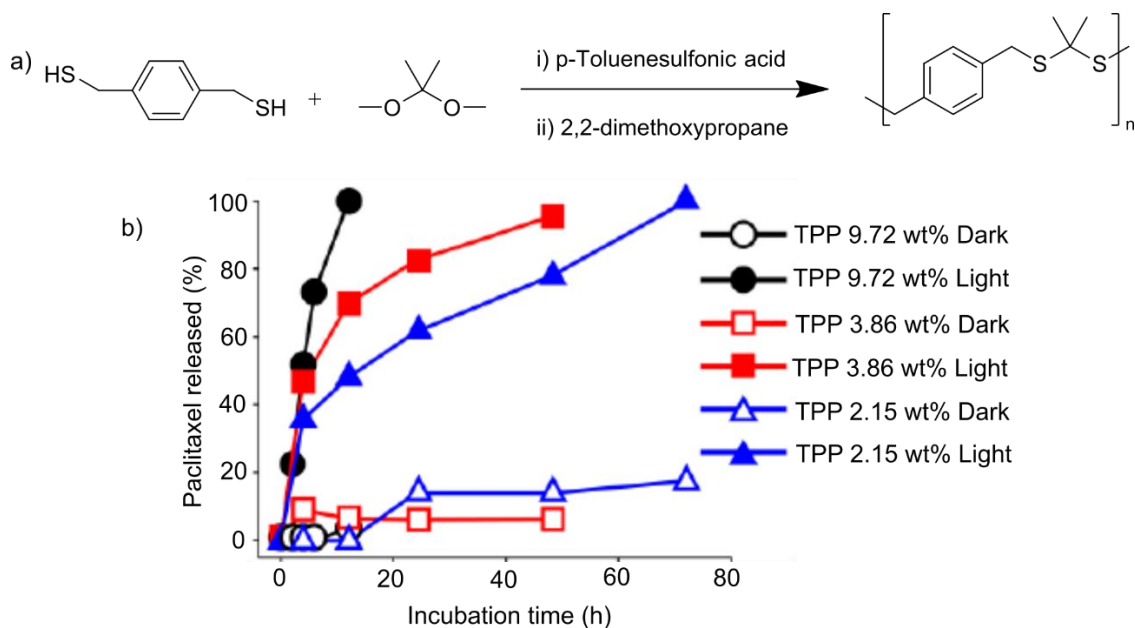
Figure 1. 19 The synthetic route for the polythioketal-sensitive polymer reported by Seah *et al* [179] a); The NP release profile with different concentration of encaged TPP, in dark and light conditions(adapted with permission from Elsevier) [180].

Yue *et al.* developed UCNP (NaYF$_4$:Yb,Er) loading a photosensitizer Ce6, camptothecin (CPT) conjugated with a thioketal linker and carboxyl-mPEG (Figure 1. 20 a). Under 980 nm laser irradiation UCNP is able to emit light in the 645-675 nm region which is absorbed by Ce6, generating oxygen singlet, cleaving the thioketal bond and releasing the drug. After 24 h of the irradiation (30 min, 0.6 W cm^{-2}), the NP released more than 70% of the encapsulated drug (Figure 1. 20 b). *In vitro* tests with NCI-H460 lung cancers showed that cells were totally eliminated by this system when irradiated at 980 nm. The total ablation of the tumor was also proved in *in vivo* tests (NCI-H460 tumor-bearing mice). The biodistribution of NP was also analyzed showing that their uptake and retention took place primarily in the liver and spleen, with partial accumulation in lung within 24 h post-injection. In order to evaluate the *in vivo* biodistribution of NPs, a follow-up study after 50 days of starting treatment in healthy mice was undertaken. The results showed no abnormalities in the liver, spleen, lung, and kidney tissue slices, and hepatic and kidney function. Furthermore, authors also showed the ability of Ce6 to act, parallelly, as photodynamic and fluorescence image agent due to the PS high $^1O_2$ generation and near-infrared fluorescence emission [181].
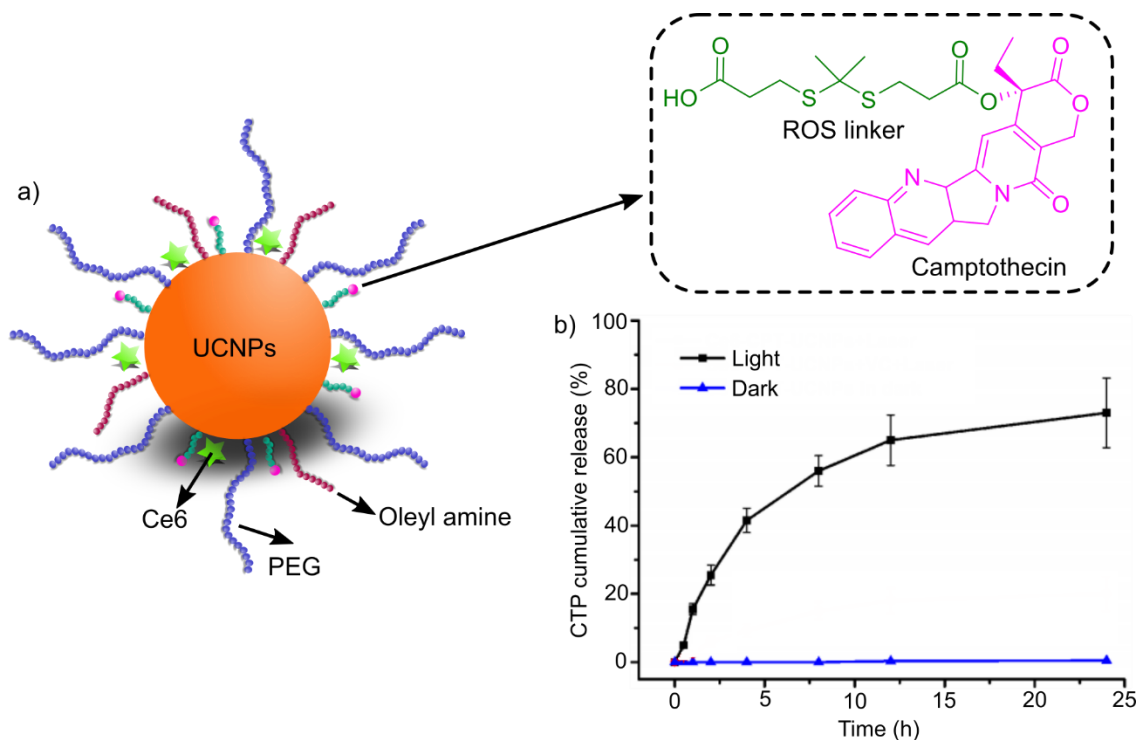
Figure 1. 20 UCNPs developed by Yue *et al*. Linker and camptothecin chemical structure highlighted in the dashed box (a); cumulative release profile of NP under light and dark conditions (b) (adapted with permission from Ivyspring International Publisher) [181].

Similarly, Wang *et al*. synthesized UCNP conjugated with merocyanine 540 (a PS), which is sequentially bonded by thioketal linkers with DOX and folic acid. Under 980 nm of light irradiation (0.5 W cm^{-2}) NP are able to emit light at 540 nm, matching the photosensitizer absorption band, generating $^1O_2$ and consequently cleaving the thioketal linker releasing the DOX. The *in vitro* tests in B-16 melanoma cells line showed no cytotoxicity under dark conditions and excellent anti-tumor activity after light irradiation [182].

Li *et al*. developed a clustered-vesicle able to overcome the hindrance of $^1O_2$ generation in hypoxic tumor. This NP supplies oxygen from hydrogen peroxide when submitted to light and triggers the drug release process through ROS formation. The authors prepared a clustered vesicles from an ABA copolymer (PEG$_{2000}$-thioketal polymer-PEG$_{2000}$) loaded with a fifth-generation poly(amidoamine) dendrimer (PAMAM), conjugated with Ce6 and cypate (as model drug) co-assembled with hydrogen peroxide in a thioketal triblock polymer (Figure 1. 21). Upon cycles of light irradiation at 805 nm (1 W cm^{-2}, 3 min) and 660 nm (100 mW.cm^{-2}, 10 min) the H$_2$O$_2$ is decomposed into O$_2$ and the Ce6 generates almost 2 times more $^1O_2$ compared to samples not subjected to irradiation cycles. The subsequent photodynamic process leads to disruption of the thioketal linker,

48

releasing the dendrimer (~80% of drug release after 1 cycle of irradiation). The main results were the uniform distribution of the PAMAM and cypate over cells and the total ablation of BxPC-3 hypoxic and hypopermeable pancreatic tumors in nude mice, after 5 irradiation (805/660 nm) cycles over 24 days. The success of these NP was justified by the boost of ROS generation, caused by the self-supply of oxygen, and the deep penetration of the dendrimer [183].
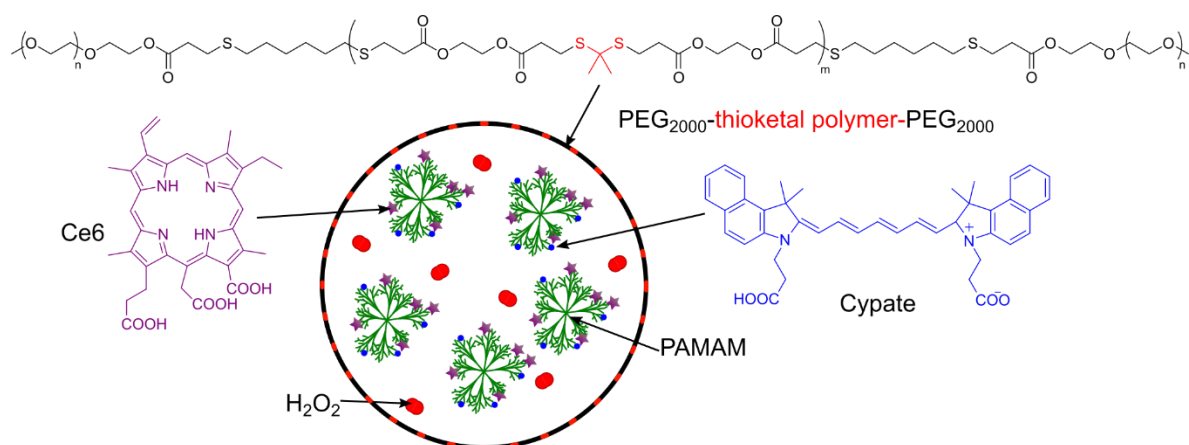
Figure 1. 21 Schematic illustration of photo triggered clustered vesicles with oxygen self-supply proposed by Li *et al* [183].

Liu *et al*. developed a dextran-based polymeric drug conjugate micelle, able to efficiently generate $^1O_2$ and DOX release after 10 min of light irradiation (40 mW.cm^{-2}, 400-700 nm). The dextran was chemically conjugated with DOX by a thioketal linker and a 5-(4-aminophenyl)-10,15,20-triphenylporphyrin conjugated by an ester linker in the backbone of dextran (Figure 1. 22 a). This molecule self-assembled into micelles that incorporated 2.5 to 7.2% of DOX and 13.4% of porphyrin. After light irradiation, micelle size distribution becomes broader and the hydrodynamic radius increased almost 2 times. More than 75% of DOX could be released during 50 h after two cycles of 5 min irradiation spaced by 12 h (Figure 1. 22 b). The *in vitro* results showed a higher cellular uptake compared to no-irradiated NP and a reduction of cellular viability to below 20% (~74% lower than non-irradiated NP) [184].
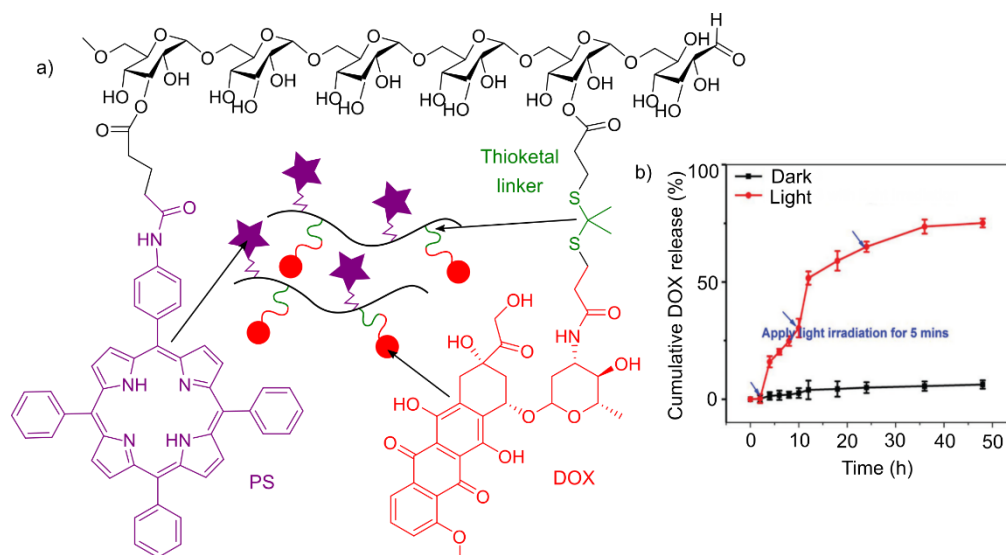
Figure 1. 22 Chemical structure and schematic illustration of a dextran-based polymeric drug conjugate developed by Liu *et al* (a); cumulative release profile of NP under light and dark conditions (b) (adapted with permission of The Royal Society of Chemistry) [184].

Cao *et al* developed a nanocarrier composed of a singlet-oxygen-responsive poly(thioketal phosphoester) and amphiphilic di-block copolymer PEG-*b*-PCL which encaged Ce6 and DOX (2.5 wt% and 5.9 wt%, respectively) and is able to burst release the drug when activated by red light (660 nm) (Figure 1. 23). During light irradiation, Ce6 generates singlet oxygen that rapidly degrades the thioketal polymer core into oligomers or small molecules. This cleavage leads to a shrink of the NP from 154 ± 4 to 72 ± 3 nm resulting in drug release. After 30 min of irradiation (660 nm laser, 0.3 W cm^{-2}) more than 70% of encapsulated DOX could be released during 20 h. However, using lower laser intensity (0.06 Wcm^{-2}) the amount of DOX released is substantially lower (only 30%) at the same time. NP also showed an enhanced release of DOX inside the cells nuclei, higher induced apoptosis (~43%) and anticancer activity in MDA-MB-231 cells (0.3 W cm^{-2} and 30 min) [134].

50
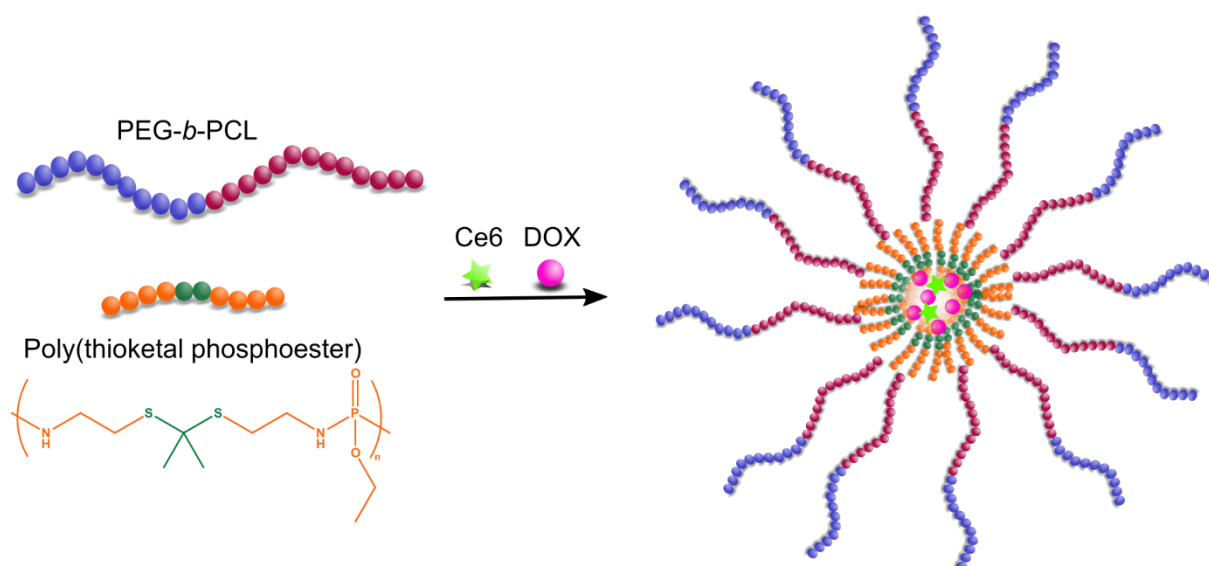
Figure 1. 23 Scheme illustration a chemical structure of Cao's research group shrinkable light responsive NP [134].

Lamb and Barbas III studied the reactivity of several structures containing thioketal $^1O_2$-sensitive linkers in the presence of a photosensitizer under light irradiation from a compact fluorescent bulb (~20 mW.cm^{-2}). After singlet oxidation, the ketone product formation rate from the arythiolanes group was investigated and they concluded that the best structures contain a 1,3-oxathiolane thioketal group and an active α-aryl group (Scheme 1. 4 a and b). The protic and aprotic nature of the environment also has a strong influence on photo-oxidation of arythiolane molecules. Only in protic solvents the ketone was formed, whereas aprotic media yields mainly sulfoxide products. Contrasting with what is described in the literature about the high reactivity of thioketal polymer-based groups with ROS species, arythiolanes showed negligent oxidation in peroxide, superoxide and Fenton conditions. Authors attribute the reactivity difference to $^1O_2$ selectivity for the cyclic structure rather than for the acyclic one. Thereafter, they synthesized a pro-drug with a sensitive linker capable of cleavage in the presence of an amine, hydroxyl or carboxylate functional groups. The molecule has a 2-(4-methoxyphenyl)-2-methyl-1,3-dioxolane conjugated to DOX (Scheme 1. 4 c) and in the presence of photosensitizer and light (white light, 20 mW.cm^{-2}) almost of the 1,3-oxathiolane is transformed into the 3-oxopropyl group. The ketone product instantaneously suffers a β-elimination reaction in serum-containing media. In the absence of the light or photosensitizer, the arylthiolane moiety remains stable in the biological environment [130].
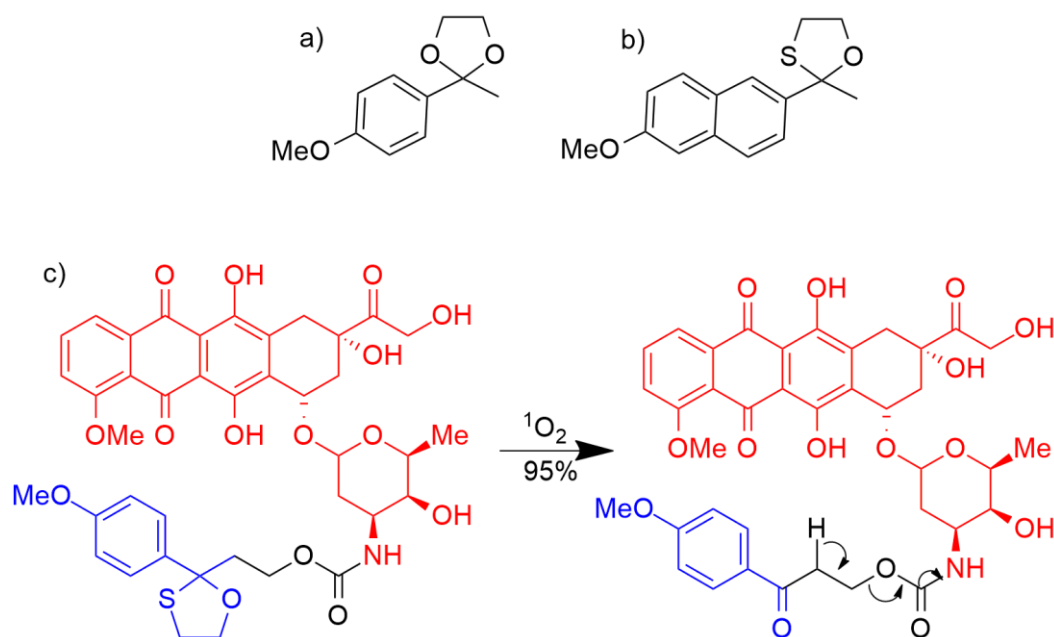
Scheme 1. 4 The optimal thioketal structure for the sensitive segment (a) and (b). Prodrug degradation mechanism in the presence of photosensitizer/light in fetal bovine serum medium (c) [130].

1.2.4 Selenium containing polymers

Recently, selenium containing polymers started to be used as responsive materials able to disassemble under mild conditions due to selenium's unique chemical properties. Compared to sulfur, the selenium atom is bigger and has a lower electronegativity, leading to lower bond energy between C-Se or Se-Se (244 kJ/mol and 172 kJ/mol, respectively, comparing to C-S, 272 kJ/mol, and S-S, 240 kJ/mol). Moreover, selenium atoms are more susceptible to oxidation than sulfur [185]. Diselenide bonds can be cleaved either by oxidation or reduction, generating selenic acid or selenol, respectively [135].

Xu's group have been working on selenium containing polymers for smart drug/gene delivery systems proving that diselenide bonds can disrupt by oxidative reaction with ROS even under mild conditions such as 0.1% H_2O_2 solution [135], [186]–[193]. Due to the ease selenium's oxidation, they hypothesized that the diselenide bond will be sensitive to $^1O_2$. They developed ABA block copolymers with diselenide bonds (PEG-PUSeSe-PEG) with different polymer chain lengths (PEG$_{0.75k}$-PUSeSe$_{12.5k}$-PEG$_{0.75k}$, PEG$_{1.9k}$-PUSeSe$_{31.2k}$-PEG$_{1.9k}$, PEG$_{5k}$-PUSeSe$_{48k}$-PEG$_{5k}$) and prepared micelles with approximately 10 wt% of water-soluble *meso*-tetra(4-sulfonatophenyl)porphyrin (Scheme 1. 5). After 5 h of red light irradiation (600 to 780 nm, 300 W), the authors found that the Se-Se bond was oxidized by $^1O_2$, generating selenic acid as product. They also reported

that PEG length interferes directly with micelle disruption. The increase in PEG chain may prevent the $^1O_2$ approach to the diselenide bond or may participate in $^1O_2$ quenching processes. From all copolymers, $PEG_{1.9k}$-$PUSeSe_{31.2k}$-$PEG_{1.9k}$ was chosen due to its higher stability for micelle formation. In DLS measurements, the synthesized polymeric aggregate showed a decrease in the count rate value with an increase in the light irradiation time (26% after 5 h of irradiation) evidencing the disassembly of the micelles. Importantly, they proved the absence of cytotoxicity of the degraded polymer through *in vitro* tests with human hepatic cells line L-02 (above 90% of cell viability) [194].

PEG-PUSe-Se-PEG

meso-tetra(4-sulfonatophenyl)porphyrin
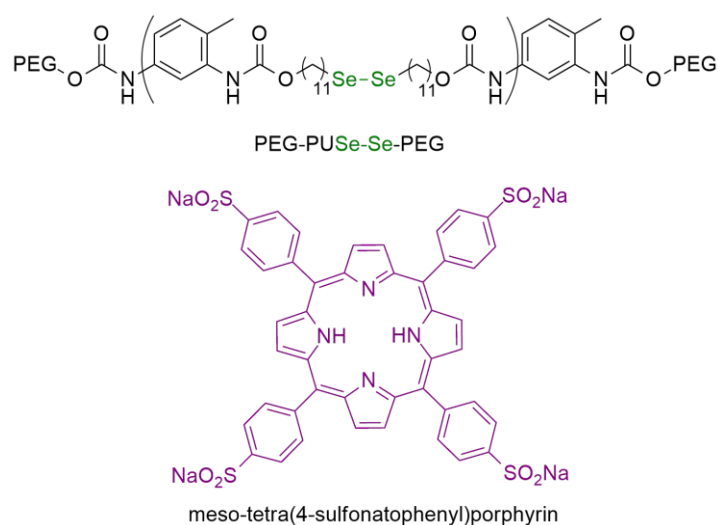
Scheme 1. 5 Chemical structure of Xu's diselenide polymer and the photosensitizer used in the photo-triggered micelles [194].

Influenced by these results, Xu's group also synthesized a layer-by-layer film with the goal of enhancing diselenide linker oxidation by assuring the proximity between photosensitizer and the sensitive bond through charge attraction. The structure was composed of polyurethane NP containing a diselenide oxidation-sensitive negatively charged moiety (PDSe) and a positively charged porphyrin (Figure 1. 24). Film was doped with a polyanion (poly(styrene sulfonate) (PSS) and a cationic photosensitizer (5,10,15,20-tetrakis-(4-trimethylammoniophenyl)porphyrin tetra(toluene-4-sulfonate)) with a higher ratio of PSS (0.02) in relation to the cationic photosensitizer. The negatively charged trisodium salt of 8-hydroxypyrene-1,3,6-trisulfonic acid (HPTS) was used as a fluorescence indicator to easily quantify the process of load and release. In deionized water saturated with oxygen, 83% of the film was degraded after 5 h of irradiation of visible light (400–700 nm, 800 – 1500 mW.cm^{-2}). For the same time but with less irradiation intensity, 110 and 50 mW.cm^{-2}, HPTS can also be released, showing around 80% and 60% of free

payload, respectively. To evaluate the influence of porphyrin amount and location, the film was irradiated with different equivalents of PS dissolved in water or assembled in the film. The rise in the disruption rate is proportional to the amount of porphyrin. However, interestingly, with more than 100 equivalents of PS in solution, the disruption rate is lower than with 1 equivalent of PS incorporated into the film. This result showed the high influence of the PS location on the photodynamic process. Also, films showed little dark cytotoxicity and good biocompatibility in L-02 cell line [195].
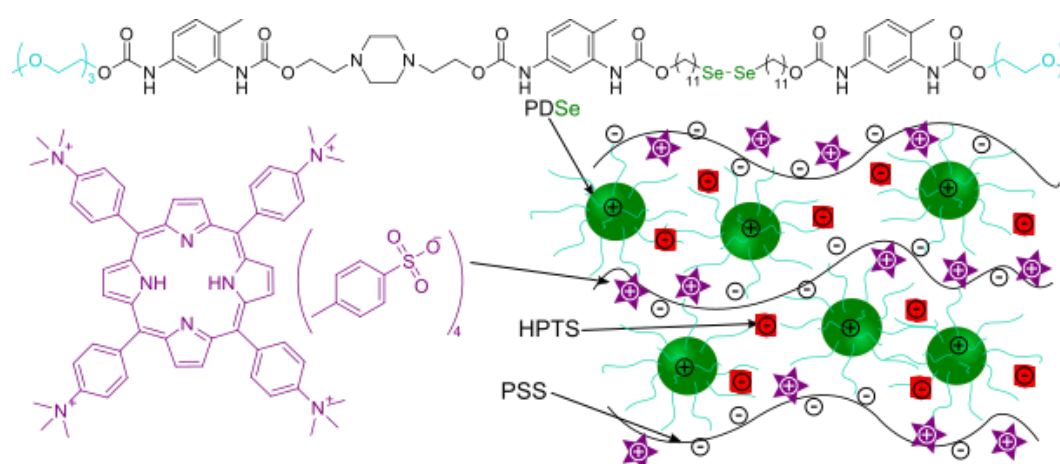
Figure 1. 24 Chemical structure and schematic illustration of PDSe polymer micelles arranged in the layer-by-layer film doped with porphyrin, engineered by Xu's group [195].

More recently, Xu's group developed a different approach for drug releasing materials through diselenide bond oxidation mediated by $^1O_2$. A polyurethane containing diselenide bond was attached to each arm of *meso*-tetra(p-hydroxyphenyl) porphyrin and PEG ($M_w = 5000$) as a terminating group to produce a selenium/porphyrin-containing hyperbranched polymer able to form NP through emulsification and susceptible to suffer cleavage after $^1O_2$ generation (Figure 1. 25). The concentration of porphyrin in the polymer was 18.6 µg/mg. After 1 h of irradiation (xenon lamp, wavelength >420 nm) the partial dissociation of NP was proven by a change in the average diameter of particles from 308 to 220 nm. Surprisingly, the oxidation product of the diselenide bond, selenic acid, might cause apoptosis in both MDA-MB 231 cells and A549 human lung cancer cells tested (decrease of cell viability to 50% when irradiated with NP concentration of 100 µg/mL), increasing the anti-tumor effect of the NP [196].
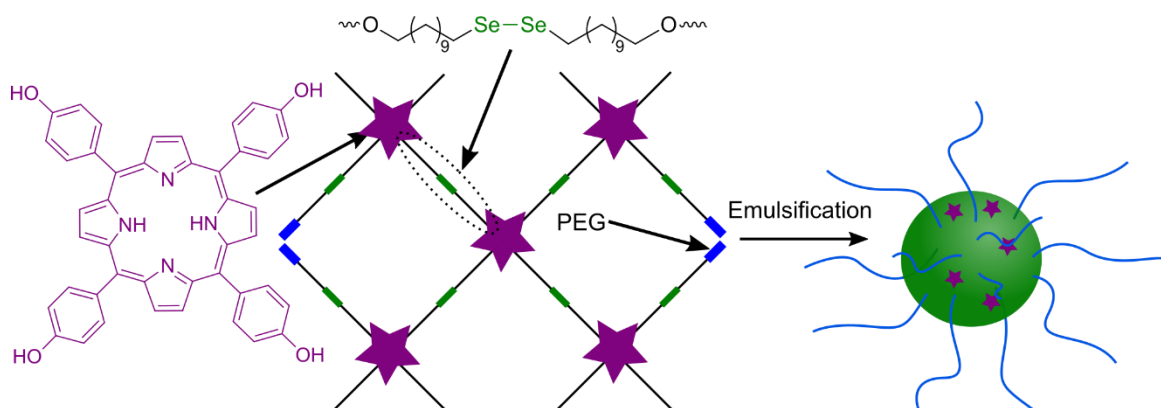
Figure 1. 25 Schematic illustration of the selenium/porphyrin-containing hyperbranched polymer polymeric micelle developed by Xu's research team [196].

1.2.5 Hydrophobic changeable polymers

Recently new $^1O_2$ sensitive groups have appeared taking advantage of hydrophobicity changes of some groups after oxidation. These changes from hydrophobic to the hydrophilic character and vice-versa could be induced by reactive oxygen species, such as $^1O_2$. The most studied polymers with these groups are: tellurium containing polymers; poly(propylene sulfide) polymer; and polymers containing imidazole (and derivatives) groups.

Tellurium containing polymers

Similarly to selenium, tellurium has unique proprieties for stimuli-responsive materials. Compared to selenium, the lower electronegativity of tellurium gives Te a higher ROS sensitivity. Xu's group proved the strong oxidative sensitivity of tellurium in extremely low concentration H_2O_2 solutions (such as 100 µM) [197]–[199]. Encouraged by this result, Xu's group designed a polyelectrolyte multilayer film composed of cationic tellurium-containing polymeric micelles (PN-Te), which have an anionic tetrasodium *meso*-tetra(sulfonatophenyl) porphyrin, as a PS and PSS as an anionic building block, to enhance the film stability (Figure 1. 26). The tellurium-containing polymers formed micelles by self-assembly with a size of 500 nm. Oxidation response was analyzed after 5 h of blue irradiation (5000 lux) in a solution with PS concentration of 50 wt% of micelle mass. After oxidation, the tellurium containing micelles swelled to 4000 nm. This increase in size is explained by the generation of Te=O which changes the amphiphilicity of the film inducing structural changes. However, the morphology of the film did not exhibit obvious

disruption, probably because the change in amphiphilicity was not enough to disassemble the micelle, keeping the film integrity. Tellurium polymer cytotoxicity was analyzed by *in vitro* testing, indicating promising results for biological applications. Hence, this tellurium film after irradiation showed cytotoxicity with cell viability (Hep G2 cells) decrease to 50% compared to the dark control. Also, when Nile Red was used as a model encaged drug, it could be gradually released from the film into water [136].
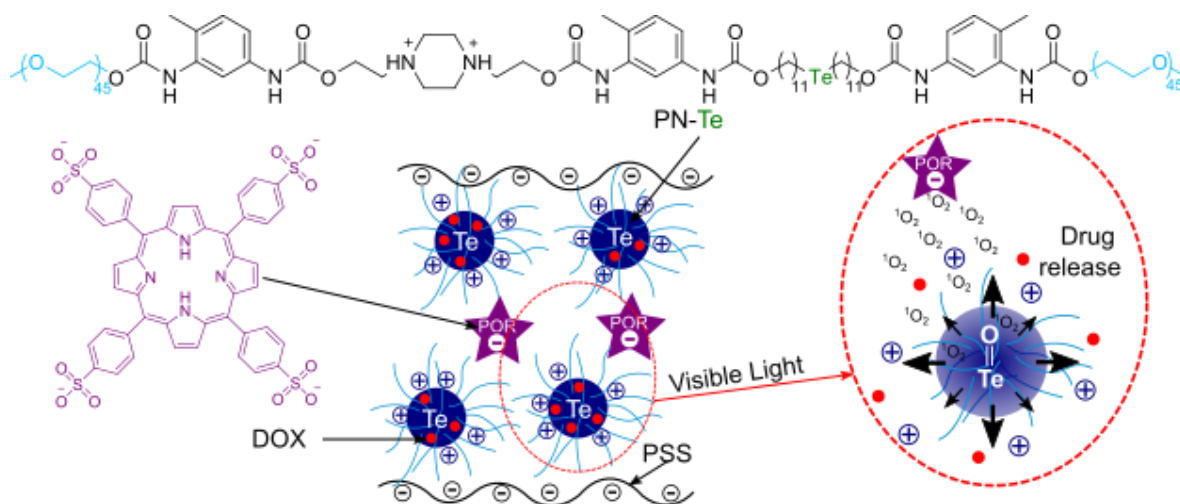
Figure 1. 26 Scheme of drug release of the visible light tellurium-containing multilayer film engineered by Xu's group [136].

Xu's group developed a NIR light-responsive NP for synergistic therapy. Cisplatin (CDDP) (a common anti-cancer drug) and indocyanine green (ICG) (as photosensitizer) were simultaneously encapsulated in the inner core of a nanocarrier formed by amphiphilic tellurium containing ABA triblock polymer (PEG_{5k}-Tellurium-polyurethane-PEG_{5k}) (PEG-PUTe-PEG) (Figure 1. 27 a). Researchers took advantage of the coordination chemistry between platinum and tellurium to guarantee higher stability and prolonged circulation time *in vivo*. After irradiation (4 min, 808 nm, 8 W cm^{-2}) the $^1O_2$ generated by indocyanine green oxidizes the tellurium bond and weakens the coordination interaction with cisplatin, releasing the drug (over 60% of the drug was released after 10 min, Figure 1. 27 b). ICG also has a synergistic antitumor effect through the photothermal effect which, combined with the chemotherapeutic effect of NP achieves high antitumor efficacy in *in vivo* testing with human breast carcinoma cells, with reduced side effects [200].

56
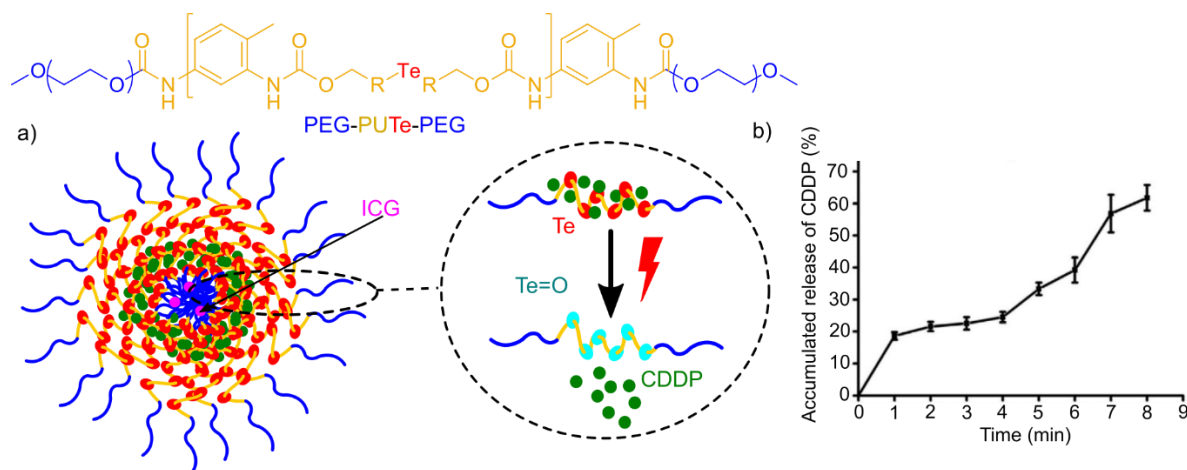
Figure 1. 27 Chemical structure and schematic illustration of PEG-PUTe-PEG based NP release mechanism developed by Xu's group (a); Drug release profile at room temperature and light irradiation (b) (adapted with permission of Elsevier) [200].

Despite the good response of Se and Te linkers to $^1O_2$ species, some drawbacks still need to be addressed aiming further clinical application. As Se/Te-containing compounds have been closely related to the concentration of reactive oxygen species and to the importance of these species in cellular metabolism. Therefore, it is important to evaluate the real biological effects of these metals for the *in vivo* applications. More studies by chemistry, biology, and medical communities are required to clarify the concerns about physiological metabolism, biocompatibility and possible toxicities of this kind of organometallic compounds [185].

Poly(propylene sulfide) polymers

Poly(propylene sulfide) (PPS) is a well-known polymer that is able to change its hydrophobicity after oxidation by ROS. Kim *et al*. hypothesized that a micelle made by an amphiphilic PEG-PPS polymer could be oxidized by $^1O_2$ and lead to a drug release due to the oxidation of the hydrophobic PPS to the more hydrophilic sulfoxide or sulfone (Figure 1. 28 a). The photosensitizer Ce6 was linked to the end of the PEG-PPS chain and DOX was encapsulated in the inner core of the micelle formed (DLC = 3.8%). Following 500 seconds of irradiation (650 nm, 6 mW.cm^{-2}), 60% of the drug was released after 48 h (Figure 1. 28 b). The *in vivo* and *in vitro* tests showed that the Ce6 $^1O_2$ generation also facilitated the endo/lysosomal rupture and could also have a photodynamic effect [137].

57
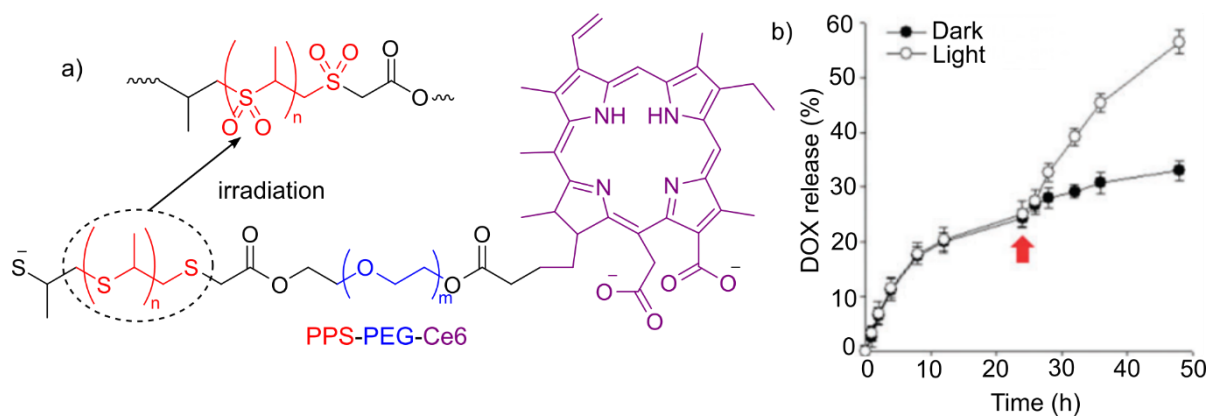
Figure 1. 28 Chemical structure of PPS-PEG-Ce6. In detail, the modified structure of poly(propylene sulfide) polymer after undergoing the hydrophilicity change caused by light irradiation in the NP (a); accumulative DOX release profile from NP, the red arrow indicates the moment of irradiation (b) (Adapted with permission of Royal Society of Chemistry) [137].

Polymers containing imidazole (and derivatives) groups

In a different approach, Li *et al* developed a micelle capable of undergoing a change in the hydrophilic/hydrophobic balance by attaching responsive moieties to the polymer backbone. An imidazole (IM) group was conjugated in the backbone of poly(aspartic acid) which formed an amphiphilic copolymer with methoxyl poly(ethylene glycol) (mPEG-PAsp-IM) The synthesized polymer is able to form micelles by self-assembly in an aqueous medium. Zn^{2+} was used as an ionic crosslinker through imidazole-metal coordination. Ce6 was physically encapsulated in the inner core of the micelles with a loading capacity of 3.3% (w/w, mPEG.PAsp-IM micelle). After laser irradiation (20 min, 660 nm, 100 mW .cm^{-2}) Ce6 generated $^1O_2$ which oxidized imidazole to urea. The urea formation eliminates the coordination complex with Zn^{2+}, increasing the water solubility of the polymer (Figure 1. 29). In addition, the H-bonding donor and NH_2/C=O acceptor properties of urea give the molecule a greater capacity to absorb water by forming a urea-water hydrogen bonding network. The water absorption leads to a large increase in micelle size. In spite of the lack of micelle disruption, Ce6 was rapidly released. Moreover, the reaction product contains multiple hydrogen donors and acceptors inducing the formation of a three-dimensional hydrogen bonding network (dashed box in Figure 1. 29). Further, *in vitro* study showed that generated $^1O_2$-induced cytotoxicity in 4T1 murine breast cancer cells. An enhanced therapeutic effect in *in vivo* (BLAB/c mice) assays was observed using this kind of micelles [138].

58
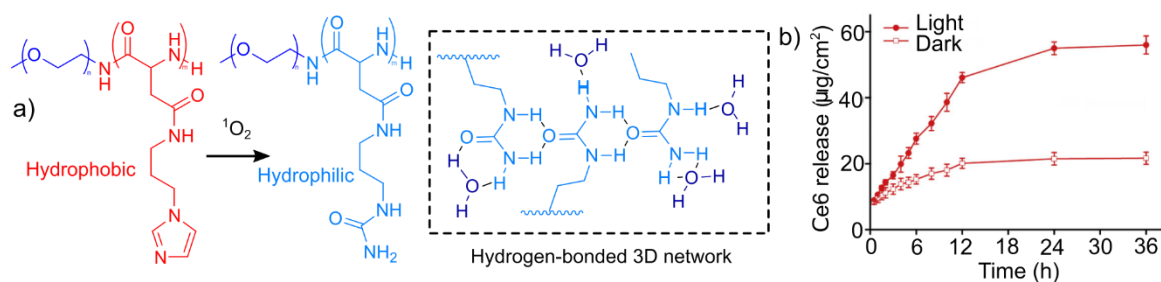
Figure 1. 29 Chemical structure of the amphiphilic copolymer (mPEG-PAsp-IM) synthesized by Li *et al* before and after exposure to light irradiation. In detail the hydrogen-bonded 3D network formed in the expanded micelle, leading to leakage of the Ce6 (a); Cumulative drug release of Ce6 from NP in light and dark conditions (b) (adapted with permission of Elsevier) [138].

The same research group also used this $^1O_2$ responsive polymer to improve mitochondria-targeted nanoplatform loaded with two linked photosensitizers, triphenylphosphonium-pyropheophorbide (TPP-PPa). The combined PSs improved the cumulative *in vitro* release in about 1.2 times compared with nanocarriers loaded with only TPP-PPa [201]. They also re-designed mPEG-PAsp polymer with a nitroimidazole (NI) group instead of the IM group. NI additionally implements a hypoxia response property to $^1O_2$, turning this compound into an alternative to overcome the problems associated with the non-uniform cargo release in the heterogeneous hypoxic tumor sites. $^1O_2$ reaction with NI produces, as a major end product, the hydrophilic oxamic aldehyde with lower conversion (65%). The change in micelle hydrophilicity and the formed three-dimensional hydrogen-bonding network induce a swelling up of micelles causing a size increase from 112 nm to 401 nm, allowing water penetration and leaching out the entrapped drug 64% faster than samples that have not been subjected to light (10 min, 660 nm, 100 mW.cm^{-2}). The NP showed cellular internalization and no cytotoxicity under dark conditions in 4T1 murine breast cancer cells line. After irradiation, the NP expressed lower cytotoxicity than free Ce6. Authors justify this behavior due to the generation of $^1O_2$ by Ce6 in the inner core of micelle and the necessity to react with NI moieties and cargo release in a more complex process [202].

The main *in vivo* result for light-responsive NPs are summarized in Table 1. 8.

Table 1. 8 Summary of the *in vivo* experiments their most relevant results. All NP were dosed through intravenous injection (i.v.).

Linker	Nanocarrier structure	Irradiation conditions			PS	Drug	Tumor cell/Animal model	Outcomes	Ref
		Intensity (mW.cm^{-2})	Wavelength (nm)	Time (h)					
VDS	NCP NP	5	660	0.5	Ce6	DOX	4T1/ Balb/c mice	Relative tumor volume remained unchanged past 12 days, while free drug and PS or control increased 7% and 10%, respectively; Mice showed no body weight drop and no noticeable organ damage in histological examination.	48
AmAc	Prodrug	10-200	660	0.17-0.5	TP	CA4	colon 26 cells/ BALB/c mice	Prodrug showed superior antitumor effect, tumor volume was ~85% little than control sample 15 days post-injection; Animals do not show body weight lost.	54
AmAc	Prodrug	5.6	690	0.5	PLCA	CA4	subcutaneous colon 26 cells/ BALB/c mice	Less skin damage and 75% reduction of tumor area in 96 h, compared to control; Almost all tumor become necrotic and even the bottom layers of cancer cell disappear after 15 days	55
AmAc	Prodrug functionalized with folic acid and PEG	100	690	0.5	Modified TPP or PLCA	CA4	SC colon 26 cells/ BALB/c mice	Higher selective distribution and tumor uptake of prodrug (256% more than prodrug without a linker), mice were all tumor free past 75 days; mice showed no weight loss.	56
TK	UCNP	600	980	0.5	Ce6	CPT	NCI-H460/ BALB/cathymic nude mice	NP showed enhanced tumor target and circulation time (compared to free Ce6); no tumor recurrence or metastasis was observed past 50 days. Mice returned to normal body weight past 3 weeks and no obvious abnormality was observed in liver, spleen, lung, and kidney.	68
TK	UCNP	500	980	0.083	MCA	DOX	B-16 melanoma/ BALB/c mice	Tumor volume was 80% smaller than control mice 20 days post-injection; NP showed long blood circulation and higher accumulation in tumor tissue; higher apoptosis and smaller tumor volume after 3 weeks.	69
TK	Polymeric vesicle	1000/100	805/660	0.05/0.17	Ce6	Cypate	BxPC-3/ BALB/c nude mice	Uniform distribution and preferential accumulation into the tumor tissue at 2 - 24 h post injection; The relative tumor volume, 24 days post injection, was ~95% smaller in mice treated with NP than PBS or free Ce6 dosed mice; The system reached a total ablation of the hypoxic hypopermeable pancreatic tumor.	70
TK	Polymeric micelle	300	660	0.83	Ce6	DOX	MDA-MB-231/ BALB/c nude mice	NP showed higher accumulation in tumor tissue (55%) than free DOX, 24 h post injection; Tumor volume was ~90% smaller than in mice treated with PBS or free Ce6; Mice do not show body weight loss;	21
Te	Nanoplatforms generated by amphiphilic polymer	8000 and 1400	808	0.15 (1 min interval each 2min of irradiation)	ICG	CDDP	MDA-MB-231/ BALB/c nu/nu mice	Preferential accumulation in tumor site compared to free ICG; Tumor was completely disappeared after 26 days; NP showed efficiently alleviation of the damage in organs such kidney when used as the therapeutic instead free CDDP.	87
PSS	Polymeric micelle	6	650	0.056 / 0.14	Ce6	DOX	K-1735 cells/ BALB/c mice	A significant decrease of the tumor (~70% smaller than mice treated with PBS or ~55% for free DOX) with no change in body weight;	24
IM	Polymeric micelle	100/200	660	0.017-0.33, 0.5	Ce6	-	4T1/ BALB/c mice	Tumor volume was smaller in mice treated with NP than ones treated with PBS (~72%) and Ce6 free (~65%); NP higher accumulate in Liver, kidney and tumor tissue even though no adverse or inflammatory lesion; Mice showed no body weight loss during treatment.	25

Abbreviations: vinyl disulfide = VDS; Aminoacrylate = AmAc; Thioketal = TK; Tellurium containing polymers = Te; poly(propylene sulfide) = PPS; Imidazole = IM; Pthalocyanine = PLCA; thiaporphyrin = TP; merocyanine = MCA; Paclitaxel = PTX; Camptothecin = CPT; Cysplatin = CDDP; combretastatin A-4 = CA4; human breast carcinoma cells = MDA-MB-231; lung cancer cells = NCI-H460; murine breast cancer cells = 4T1; human pancreatic tumor cancer cell = BxPC-3; murine melanoma tumor cells = B-16; mouse melanoma tumor cells = K-1735.

1.3 Final remarks and future perspective

Polymeric micelles have been showing an impressive potential to solve one of the major challenges in the pharmaceutical industry, namely, the low bioavailability of the poorly water-soluble drugs (mainly in cancer therapy). These nanocarriers can act as a solubilizing agent for the hydrophobic drugs, driving and releasing the medicine in the damaged, inflamed or infected tissue. Additionally, micelles have shown an evident improvement in drug biodistribution, reduced systemic toxicity and enhanced therapeutic effectiveness.

Micelles made by the amphiphilic PEG-PLA copolymer have already reached the clinical applications due to its high biocompatibility, controlled degradation rate, simple and easy synthesis. Complexities in the architectural design and difficulties in the scaling-up can hamper the application of these systems outside laboratories [114]. Moreover, PEG induces steric repulsion of blood opsonins leading to a longer retention time of the nanocarrier in blood circulation. PLA is a widely studied polymer that facilitates its manipulation in order to achieve different crystallinity and molecular weight, tuning the final micelles' properties such as size, stability, drug loading and degradation.

Although the successful applications showed by micelles in DDSs, for a significative boost in the pharmaceutical market, these nanocarriers still need to be improved. The poorly encapsulation efficiency [92], drug leakage and NPs aggregation before or after the freeze-drying process are some barriers that are still limiting the micelles clinical transition [20]. Ideally, a nanocarrier should have a shelf life of 2 years, which requires a freeze-drying process due to the water character of micelles. However, this process generally increases the micelles' size and sometimes the freeze-drying stresses can also rupture the fragile membrane of the NP [20].

The design and formation processes should be exhaustively studied and understood for each particular polymer composition. Micelle parameters such as size, shape, and surface in *in vivo* behavior are not fully understood [203]. Drug delivery systems driven by EPR effects are not well established due to its variability among tumor types and patients [14]. Particles just based on EPR or endogenous stimuli (pH, temperature, redox potential and concentrations of enzymes or specific analytes) have their translation to clinics hampered by the structural heterogeneity of the biological targets [114].

Light as an exogenous stimulus for triggering the release of NPs is a promising strategy to reach the clinical application. The external spatial-temporal control for drug

release can enhance the application for wide types and stages of tumors, independent of the biological heterogeneity. NIR wavelengths are the more appropriate for human application, with less interference in cells/cells environment and is the frequency which shows the deepest penetration in tissues.

The PS strategy to overcome the challenge of generating an active shift in the sensitive moieties using the low energy of the NIR wavelength has promising applications. Many of the described $^1O_2$-responsive DDSs showed a light on/off controlled release profile, which benefits the *in situ* drug administration systems when combined with proven strategies, such as EPR effect or specific target. The problem of the $^1O_2$ interaction with the drug is possible, however, some studies in systems with coumarin, CA4, SN-38 and DOX have already demonstrated that, before and after exposure to the $^1O_2$ rich environment, no degradation occurs (by NMR or fluorimetry analysis) [166], [194].

An advantage of these systems comes from the fact that $^1O_2$ triggered nanocarriers usually co-encapsulate the drug and the photosensitizer. As a result, these nanocarriers could act simultaneously through chemotherapy and PDT. Furthermore, the fluorescence of some photosensitizers (such as Ce6) allows these systems to work as imaging agents.

Many of the described systems have already improved anti-cancer results in *in vitro* and *in vivo* tests when compared to bare drugs or non-irradiated NPs. However, no therapeutic methods are presented in the clinical trial phase. As for practical applications, many improvements are still required. Most of the developed light-triggered nanosystems demand a long period of light exposure and/or a powerful laser for biological efficacy. The issue related to the penetration depth, even for NIR responsive systems, needs to be improved in order to allow the use in more hidden tumors. The advancements in light conductors' technologies, such as optical fibers, may boost the application of these systems. Additionally, the lower capacity of drug encapsulation and the accumulation of NPs in RES organs need a significant enhancement.

The short life of the $^1O_2$ requires a careful analysis of the position and ratio of the sensitive linker in the polymer chain to ensure an efficient nanocarrier destabilization. To the best of our knowledge, until now, no evidence for accumulation of degraded moiety of sensitive segments in RES organs was described in the literature. However, the interaction or path of the degraded moiety of the NP until elimination from the body was poorly studied and stand in need of more attention. The specific response to $^1O_2$ needs to be evaluated, considering that many linkers (principally thioketal, Se and Te) are also sensitive to other ROS that could lead to premature release of the therapeutic in the body.

62

$^1O_2$ sensitive linkers are not widely explored. There is a lack of knowledge concerning their chemical structure and its influence on the linker reactivity, especially at low-intensity light. Therefore, in this context, further improvements are required. Also, for the sensitive linker, a stable, economic and easy synthetic route needs to be established.

To sum up, this topic describes the most relevant NPs for drug delivery applications. PEG-PLA amphiphilic co-polymer has proven high biocompatibility and residence time inside the body, and it allows high tuneability of the micelle characteristics, such as size, morphology, stability and drug loading. Micelle formation methods are also reviewed, and micelles' characteristics are briefly showed. The *in situ* drug release is an important ability of the NP to improve some treatments, such as cancer. Among the triggered drug delivery applications, the $^1O_2$-sensitive systems are highly auspicious and were extensively described here. The intermediacy of photosensitizers enables the use of low energy light, affording systems with the ability of spatio-temporal drug release. The intensified research in the development of NIR responsive photosensitizers in the PDT field brought a promising tool for this kind of DDSs. Consequently, there is a wide variety of photosensitizers, with a high generation capacity of $^1O_2$, responsive to the NIR window, which is the most suitable energy level for biological applications. The highly reactive $^1O_2$ can easily interact with specific sensitive moieties causing instability in the nanomaterial structure, and thus inducing the delivery of the loaded drug. The $^1O_2$ triggered delivery system is a promising strategy to overcome the lower energy of NIR light while still getting the benefit of its spatio-temporal control and innocuous nature. However, this recently developed concept still needs attention to achieve the trial phase and further translate to clinics.

2 Material and Methodology

2.1 Materials

The *rac*-lactide (3,6-Dimethyl-1,4-dioxane-2,5-dione, 98%, Sigma-Aldrich) was purified by recrystallization in toluene before use. Poly(ethylene glycol) mono methyl ether (mPEG, M_w 2000 and 5000, Sigma-Aldrich) and Poly(ethylene glycol) (PEG, M_w 4000, Hoechst) were dried through azeotropic distillation in toluene. Dichloromethane (DCM, 100%, VWR Chemicals (Prolabo®)), dimethylformamide (DMF, 100%, Fisher Scientific) were dried in CaH_2 and distilled. 1,8-diazabicyclo[5.4.0]undec-7-ene (DBU, 98%, TCI Europe), isopropanol (99.94%, VWR Chemicals (Prolabo®)), diethyl ether (99.98%, José Manuel Gomes dos Santos LTDA), methanol (100%, José Manuel Gomes dos Santos LTDA), sodium sulfate anhydrous (99%, Acros Organics), succinic anhydride (95%, Acros Organics), sodium methoxide 5.4 M 30 wt% in methanol (Acros Organics), 2-mercaptoethanol (99%, Acros Organics), 3-mercaptopropionic acid (3-MPA, 98%, TCI Europe), cis-1,2-dichloroethylene (98%, TCI Europe), ethyl acetate (EtOAc, 99.94%, José Manuel Gomes dos Santos LTDA), toluene (99.97%, Fisher Scientific), hexane (98%, José Manuel Gomes dos Santos LTDA), potassium bisulfate (99%, Acros Organics), 4-dimethylaminopyridine (DMAP, 99%, TCI Europe), N,N'-dicyclohexylcarbodiimide (DCC, 99%, Acros Organics), tetrahydrofuran (THF, 99.5%, VWR Chemicals (Prolabo®)), ethanol (100%, Chem-Lab), dimethyl sulfoxide (DMSO, 99.97%, Merck & Co., Inc.), nile red (NR, TCI Europe), acetone (99.6%, José Manuel Gomes dos Santos LTDA), triethylamine (TEA, 99%, Sigma-Aldrich), acetonitrile (99.99%, Fisher Scientific), tablets of phosphate buffered saline (PBS, Sigma-Aldrich), 3,6-dioxane-1,8-octanedithiol (95%, Aldrich Chemistry), carbon disulphide (99%, Aldrich Chemistry), chloroform (99.98%, José Manuel Gomes dos Santos LTDA), poly(ethylene glycol) methyl ether methacrylate (mPEG$_{0.48k}$-A, Aldrich Chemistry, with commercial name oligo(ethylene oxide) methyl ether acrylate, OEOA), sebacoyl chloride (95%, TCI Europe), sodium carbonate (Na_2CO_3, 99.7%, PanReac AppliChem), oxalyl chloride (98%, TCI Europe), tribromophosphine (99%, Acros Organic), acryloyl chloride (96%, Alfa Aesar) chlorin e6 (Ce6, Cayman Chemical Company), doxorubicin hydrochloride (Dox.HCl, LC Laboratories), deuterated chloroform (CDCl$_3$, 99,8%, Eurisotop), deuterium oxide (D$_2$O, 999.9%, Eurisotop), deuterated dimethyl sulfoxide (DMSO-d_6, 99.9%, Aldrich Chemistry), deuterated methanol (CD$_3$OD, 99.8%, Eurisotop) were used as received. Purified water (Milli-Q®, Millipore, resistivity > 18MΩ.cm) was obtained by reverse osmosis. The dialysis

membrane (M$_W$CO 3.5k, 1k, and 8k, Orange Scientific) were immersed in water 30 min before use.

Bis(α-amino acid) ester based on L-leucine and 1,6-hexanediol (BAAE) was previously synthesized in our group (PolySyc group) through Lamas *et al*. methodology [204].

2.2 Characterization

^{1}H and ^{13}C nuclear magnetic resonance (NMR) spectra were recorded on a Bruker Avance III 400 MHz spectrometer, with a 5 mm TXI triple resonance detection probe, in CDCl$_3$, DMSO-d_6, CD$_3$OD or D$_2$O. Chemical shifts were reported relatively to the deuterated solvent used. The polymers' chain length was determined by integration of certain polymer signals using MestReNova software version: 6.0.2-5475.

Fourier-transform infrared attenuated total reflection (FTIR-ATR) spectra were acquired in the range of 600 – 4000 cm^{-1} at room temperature using an Agilent Technologies Cary 630 spectrometer, equipped with a Golden Gate Sigle Reflection Diamond ATR. Data were recorded with 4 cm^{-1} spectra resolution and 64 accumulations.

The melting temperature was obtained by visualization of the compound melting transition inside a glass capillary. Analyses were carried in triplicate using the FALC melting point equipment.

The chromatographic parameters of the samples were determined by Size exclusion chromatography (SEC), with refractive index (RI) (Knauer K-2301), differential viscometer (DV) and right-angle light scattering (Viscotek 270 Dual Detector) detectors. The column set consisted of a PL 10-µL guard column (50 x 7.5 mm^2), followed by two MIXED-B PL columns (300 x 7.5mm^2, 10 µL). The HPLC pump was set with a flow rate of 1 mL.min^{-1} and the analyses were carried out at 60 °C using an Elder CH-150 heater. The eluent was DMF, containing 0.3% of LiBr. The samples were filtered through a polytetrafluoroethylene (PTFE) membrane with 0.2 µm pore size before injection (100 µL). The system was calibrated with narrow PMMA standards. The *dn/dc* of polymers in DMF at 60 °C was determined at λ = 670 nm, using an automatic refractometer (Rudolph Research, J357 NDS-670-CC). The Mn, GPC, and dispersity (*Đ*) of the synthesized polymers were determined by using a multidetector calibration system (OmniSEC software

version: 4.6.1.354).

High performance gel permeation chromatography (HPSEC) was carried using a Viscotek (ViscotekTDAmax) with a DV, right-angle laser-light scattering (RALLS, Viscotek), and RI detectors, using column set of a PL 10 μm guard column followed by one MIXED-E PLgel column and one MIXED-C PLgel column. Previously filtered THF was used as an eluent at a flow rate of 1 mL.min^{-1} at 30 ℃. The samples were filtered through a PEFE syringe membrane with 0.2 μm pore before injection and the system was calibrated with narrow PS standards. The *dn/dc* of polymers in THF at 30 °C was determined (for λ = 670 nm) using a RUDOLPH RESEARCH J357 Automatic Refractometer (J357-NDS-670-CC). The $M_{n,SEC}$ and Đ of synthesized polymers were determined by using a multidetectors calibration (OmniSEC software version: 4.6.1.354).

Dynamic light scattering (DLS) measurements were performed on a Malvern Instrument Zetasizer Nano-ZS (Malvern Instruments Ltd., UK). The particle size distribution (in intensity), average hydrodynamic particle size average (z-average) and polydispersity index (PDI) were determined with Zetasizer 7.03 software. Measurements were made at 25 °C and using a backward scattering angle of 173°.

Transmission electron microscopy (TEM) was used to observe the size and morphology of the nanoaggregates before and after irradiation. 8 μL of micellar solution (1 mg.mL^{-1}) was mounted on 400 mesh copper grid, inside, and the excess of water was gently removed with a paper filter. The sample was cooled down in liquid nitrogen and freeze-dried to remove the water traces. The samples were negatively stained with uranyl acetate 1% wt aqueous solution and then examined using a Jeol JEM 1400 transmission electron microscope (Germany).

Fluorescence studies were performed using a Perkin Elmer (LS 45) fluorescence spectrophotometer. For the measurements, 2.0 mL of solution was placed in a 10 mm^2 quartz cell. An excitation wavelength of 550 nm was used, and the emission spectra were recorded in the 575-750 nm wavelength range at a scan rate of 500 nm min^{-1} for NR assays. For DOX assays, an excitation wavelength of 480 nm was used, and the emission spectra were recorded in the 550-700 nm wavelength range at a scan rate of 500 nm min^{-1}

Ultraviolet-visible (UV-Vis) spectroscopy was carried out using a Jasco V-530 spectrophotometer. The analyses were carried out in 2 mL of DMSO in fixed wavelength

measurement at room temperature. Absorption spectra were measured at 405 nm with a resolution of 2.0 nm in a 10 mm^2 quartz cell.

For cellular analysis, the fluorescence intensity was determined by fluorescence spectroscopy with a Perkin Elmer LS45 (88107) Plate Reader spectrophotometer using 480 nm excitation wavelength. The absorbance in MTT and SRB assays were measured in the same equipment using 570 nm with a reference filter of 620 nm and 540 nm with a reference filter of 690 nm, respectively.

The statistical analysis was performed in Microsoft® Excel® for Office 365 MSO (16.0.11727.20222) 64-bit using ANOVA single factor. P-Value < 0.05 were considered statistically significant in all analysis.

The light intensity of the lasers beams was analysed through an irradiance detector Gigahertz-Optik X9-7.

The viscoelastic properties of the copolymers were measured by dynamic mechanical thermal analysis (DMTA) with a Tritec 2000 DMA, from Triton Technology, Ltd. The samples were analyzed in the single cantilever bending geometry using stainless steel material pockets. All DMTA measurements were carried out in a -120ºC to 180ºC temperature range, in multifrequency mode, using a heating rate of 2ºC.min^{-1}. The T_g of the synthesized polymers was determined from the maximum of tan δ, at 1 Hz.

2.3 Procedures

2.3.1 Sensitive Segment

1,2-bis(2-hidroxyethylthio)ethylene (BHETE)

Synthesis of BHETE was carried out by a modified methodology of Baugh *et al.* [159] and Lee *et al.* [205]. The synthesis is divided into two steps. First, 2-mercaptoethanol (1.7 mL, 19.5 mmol) is transferred to a hermetically sealed flask followed by slow addition of NaOMe 30 wt% in methanol solution (7.34mL, 43 mmol). The mixture was left in an ice bath over 2 h followed by 1 h at room temperature. The solvent was evaporated, and

the formed salt was dried in vacuum overnight. Scheme 2. 1 shows the scheme of the first step of the reaction.
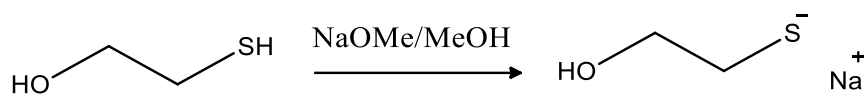
Scheme 2. 1 First step of the BHETE synthesis.

The salt was dispersed in a solution of dried DMF (30 mL), *cis*-1,2-dichloroethylene (781 µL, 10.3 mmol) and ethanol (500 µL). The mixture was stirred in the dark over 48 h at room temperature (Scheme 2. 2). The mixture was diluted in 100 mL of brine, extracted with diethyl ether, washed with brine, stirred in drying agent and evaporated. The product is a dark yellow oil (0.88-1.05 g, yield= 50 to 60%).

Scheme 2. 2 Second step of BHETE synthesis

1,2-bis (carboxyethylthio)ethylene (BCETE)

BCETE was synthesized using the Lee *et al.* [205], methodology. Briefly, 3-MPA (1.7 mL, 19.5 mmol) was added into a solution of NaOMe/MeOH (7.34 mL, 39.14 mmol), while stirring and over an ice bath. The solvent was evaporated, and the salt was dried overnight under vacuum (Scheme 2. 3).
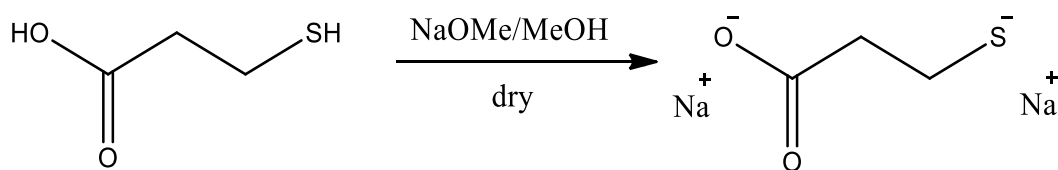
Scheme 2. 3 First step of the BCETE synthesis.

The disodium salt formed was dispersed in dry DMF and a solution of *cis*-1,2-dichloroethylene (0.781 mL, 10.3 mmol) in ethanol (0.5 mL) was added dropwise. The reaction was carried over 18 h at room temperature. Then, the mixture was diluted in water (50 mL) and acidified until pH 3 with KHSO$_4$ solution (1 M). The BCETE was extracted with ethyl acetate (3 x 100 mL), washed with water (2 x 100 mL) and brine (1 x 100 mL). The organic phases were dried with Na$_2$SO$_4$ and the solvent was evaporated. The resultant

68

product was washed with diethyl ether, recrystallized with ethyl acetate/ hexane and dried under vacuum to form a yellowish-white powder. The average yield of this reaction was 50% (Scheme 2. 4).
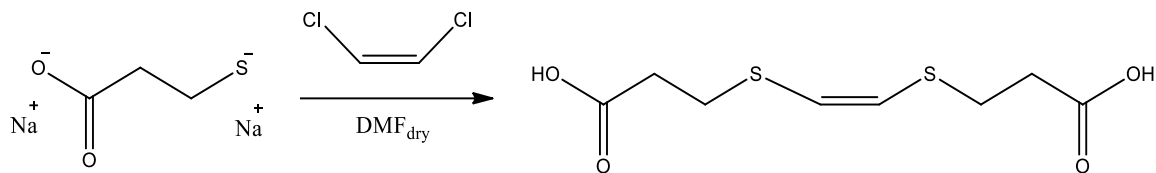
Scheme 2. 4 Second step of BCETE synthesis

2.3.2 Polymers' synthesis

PEG-*b*-PLA

The polymer was synthesized following the methodology of Waymouth and Hedrick [70]. mPEG was used as macroinitiator and PLA was synthesized by ring opening polymerization (ROP) of *rac*-lactide. Briefly, mPEG and *rac*-lactide were dissolved, separately, in DCM (0.5 and 0.1 g.mL^{-1}, respectively). The *rac*-lactide solution was added to the mPEG solution under stirring at 27ºC in a hermetically sealed flask. Then, DBU catalyst (1-10% mol of *rac*-lactide) in DCM solution was added in the flask. The reaction was carried out under room temperature over 24 h. The solution was then evaporated until ~20% of the initial volume. The copolymer solution was precipitated by addition of isopropanol, filtered and washed with ethyl ether. The white copolymer was dried in vacuum at 50ºC. The theoretical molecular weight of the copolymer was calculated through Equation 2.1:

$$M_{n\ theoretical} = \frac{M_{n\ monomer\ unit} * n_{monomer}}{n_{initiator}} + M_{n\ initiator} \qquad \text{Equation 2.1}$$

PEG-BHETE-PLA

The synthesis of the sensitive copolymer was divided into two steps: synthesis of sensitive macroinitiator (PEG-BHETE) and ROP of *rac*-lactide to form the amphiphilic copolymer PEG-BHETE-PLA.

First, a carboxyl-terminated mPEG was synthesized. This reaction was carried out through PEG esterification using succinic anhydride and using DMAP as catalyst. mPEG

(4 g for mPEG$_{2k}$ or 10 g for mPEG$_{5k}$, 2 mmol) was dissolved in DCM (40 mL) and succinic anhydride (0.8 g, 8 mmol) and DMAP (0.5 g, 4 mmol) were added, and the reaction was stirred over 24 h, at room temperature. The solvent was evaporated, and the resultant mass was dissolved in water. mPEG-COOH was extracted with DCM, the extracts were dried with anhydrous Na$_2$SO$_4$, filtered and the solvent was evaporated. mPEG-COOH was dried under vacuum (yield= 87 %) (Scheme 2. 5).
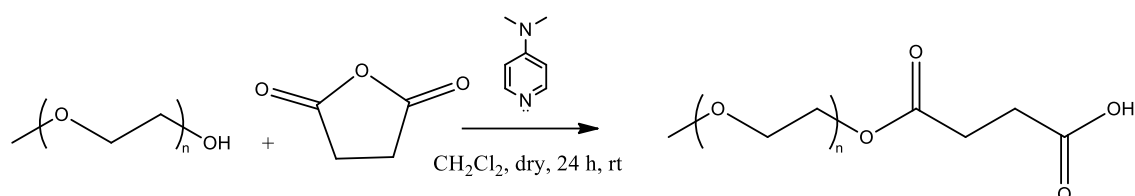
Scheme 2. 5 Scheme of the PEG functionalization with succinic anhydride

mPEG-COOH was attached to BHETE by the *Steglich* esterification (Scheme 2. 6), following the Saravanakumar *et al.* methodology [206]. Briefly, mPEG-COOH (0.4 mmol) was added into the BHETE (1.4 mmol) solution in DCM (30 mL). DCC (1.177 mmol) and DMAP (0.586 mmol) were dissolved in DCM (~ 4 mL) and added slowly. The reaction was stirred for 48 h at room temperature. The solution was evaporated, and the residue washed in diethyl ether. The product (mPEG-COOH-BHETE) was dried in vacuum (yield = 81 %).
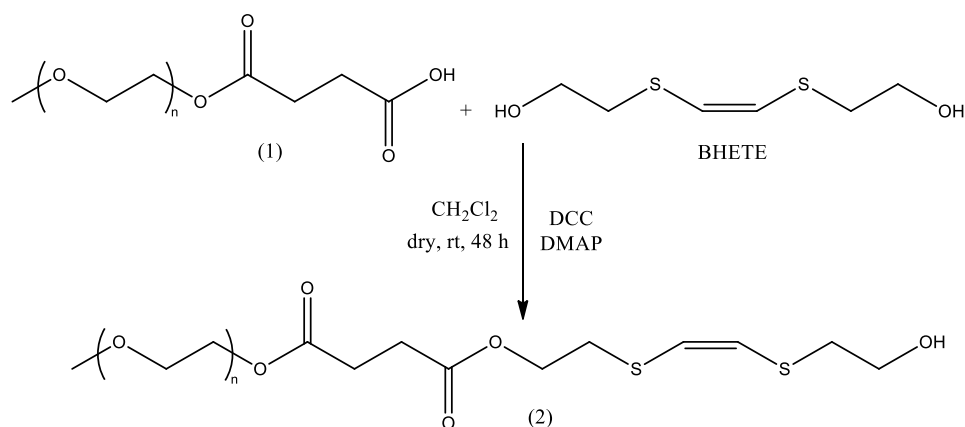
Scheme 2. 6 Scheme of the macroinitiator synthesis.

Next step is the ROP of *rac*-lactide using mPEG-COOH-BHETE as macroinitiator and isolation of the final polymer following the procedure previously described in "PEG-*b*-PLA" (Scheme 2. 7).

70
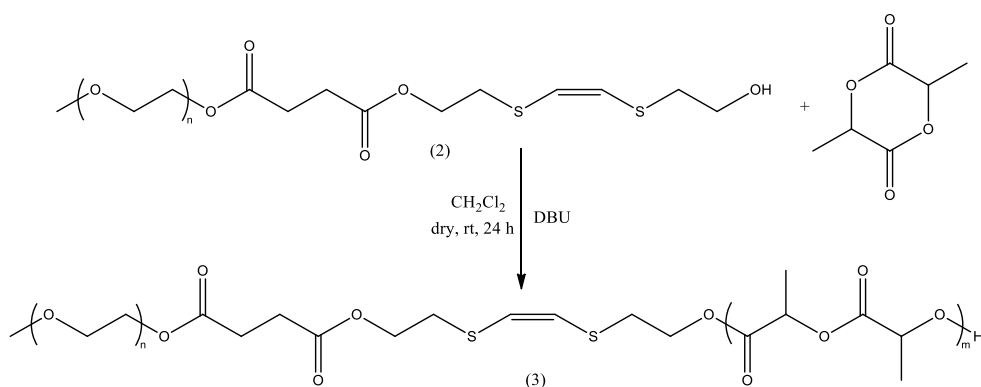
Scheme 2. 7 ROP synthesis route to obtain the sensitive amphiphilic polymer (PEG-BHETE-PLA).

The product was characterized through [^1]H NMR, [^13]C NMR, and FTIR.

Poly(1,4-dithio-7,10-dioxa-2-dodecene) (PDDD)

The PDDD sensitive polymer was synthesized by using the methodology of the BHETE and BCETE synthesis, with some modifications [159], [205]. Briefly, 3,6-dioxane-1,8-octanedithiol (3.5 mL, 19.5 mmol) was mixed with a sodium methoxide solution (30 wt%, 7,34 mL) in an ice bath over 2 h. The solvent was evaporated and dried in vacuum overnight. The formed salt was resuspended in DMSO (12 mL) and a solution of methanol and *cis*-1,2-dichloroethylene (1.49 mL, 19.5 mmol in 1 mL of methanol) was added, slowly and the mixture was stirred for 48 h under a nitrogen atmosphere, in dark and at room temperature. The polymer was then precipitated in water, dialyzed to remove the DMSO and freeze-dried (Scheme 2. 8).
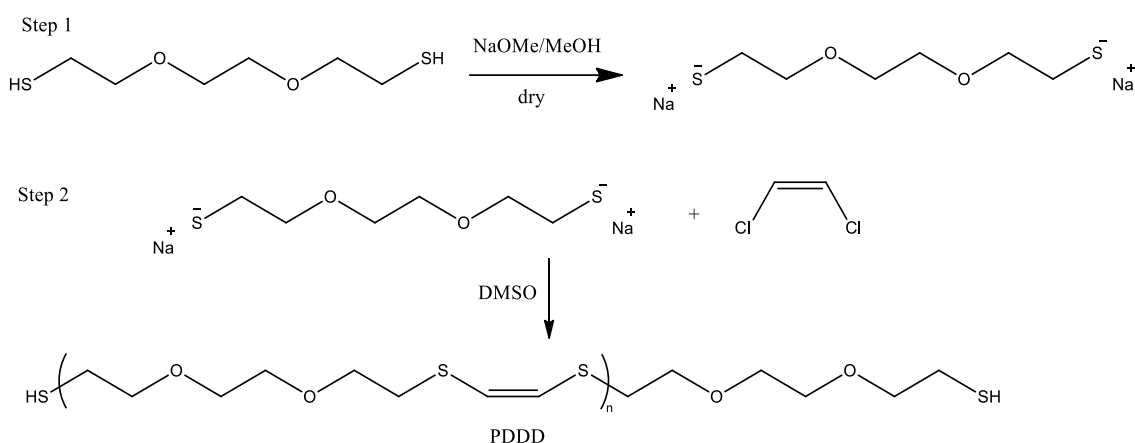
Scheme 2. 8 Sequence of the PDDD synthesis.

The PDDD was characterized by [^1]H NMR, [^13]C NMR, and FTIR.

PEG-PDDD-PEG copolymer synthesis

In order to form an amphiphilic copolymer, PEG was linked into both extremities of PDDD, resulting in an ABA (hydrophilic-hydrophobic-hydrophilic) block copolymer. Firstly, the mPEGs-Acrylate (mPEG-A) was synthesized following the Sundararajan *et al* methodology [207]. Briefly, into a sealed flask, dry mPEG-OH (4 g for PEG$_{2k}$ or 10 g for PEG$_{5k}$, 2 mmol) was dissolved in dry THF and dry triethylamine (418 µL, 1.5 eq) solution was added. The solution was allowed to stir over 15 min under N$_2$ atmosphere and acryloyl chloride (162 µL, 1 eq) was added slowly. The reaction was kept over 24 h under 45ºC. The reaction mixture was filtered to remove the triethylamine hydrochloride salt, followed by polymer precipitation in diethyl ether. Scheme 2. 9 shows the scheme of the reaction.
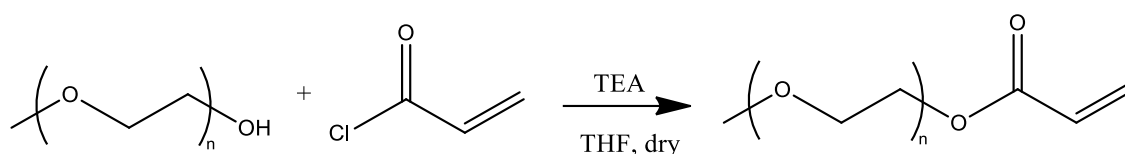
Scheme 2. 9 mPEG-acrylate synthesis route

PDDD (0.526 g, ~0.351 mmol) and PEG-acrylate (mPEG-A, 3.509 g of mPEG$_{5k}$-A or 1.409 g for mPEG$_{2k}$-A or 0.547 g for the commercial mPEG$_{0.48k}$-A, 0.702 mmol) were linked through Michael addition reaction as described in Frias *et al* [208] (Scheme 2. 10). Briefly, both polymers were dissolved in 20 mL of DMSO. The reaction mixture was carried under a nitrogen atmosphere, at 30ºC and magnetic stirring during 18 h. The product was dialyzed against water to remove the DMSO and unreacted polymers (the membrane cut-off used was 1kDa, 3.5kDa and 8kDa for mPEG$_{0.48k}$-A, mPEG$_{2k}$-A, and mPEG$_{5k}$-A, respectively). Samples were freeze-dried.
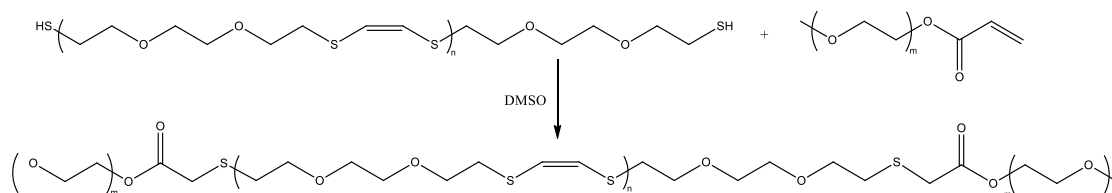
Scheme 2. 10 PEG-PDDD-PEG polymer synthesis route.

Poly(ester amide) based on BAAE and BCETE

The BCETE was converted to a diacyl halide (1,2-bis(chloroalcylethylthio)ethylene, BCAETE) and made to react with a bis(α-amino acid)

72

ester from L-leucine and 1,6-hexanediol (diamine monomer, BAAE). Briefly, the sensitive segment BCETE (0.514 g, 2.18 mmol) was dispersed in DCM (7 mL) and stirred in an ice bath. Then oxalyl chloride (0.467 mL, 5.44 mmol) in 3 mL of DCM was added dropwise using an addition ampoule followed by addition of 2 drops of DMF. The reaction was allowed to stir at room temperature until complete dissolution of the segment (about 2 h, yielding a yellowish-orange solution). The reaction was carried over 3 hours to ensure the functionalization of BCETE.

A pre-determined amount of sebacoyl chloride (0.694 mL to 0 mL, 2.903 to 0 mmol) was added to the formed solution (a pre-determined amount varying from 0 to 2.903 mmol). Meanwhile, BAAE (2 g, 2.903 mmol) and sodium carbonate (0.923 g, 18.87 mmol) were dissolved in 150 mL of water at room temperature. The solution of the BCAETE /sebacoyl chloride (until form 2.903 mmol) was added dropwise to the diamine aqueous solution using an addition ampoule and under stirring. The reaction was allowed to proceed overnight. A light-yellow viscous polymer was formed. The polymer was vigorously washed with water and dried at 50ºC. Scheme 2. 11 shows the scheme of the reactions for the sensitive poly(ester amide) synthesis.
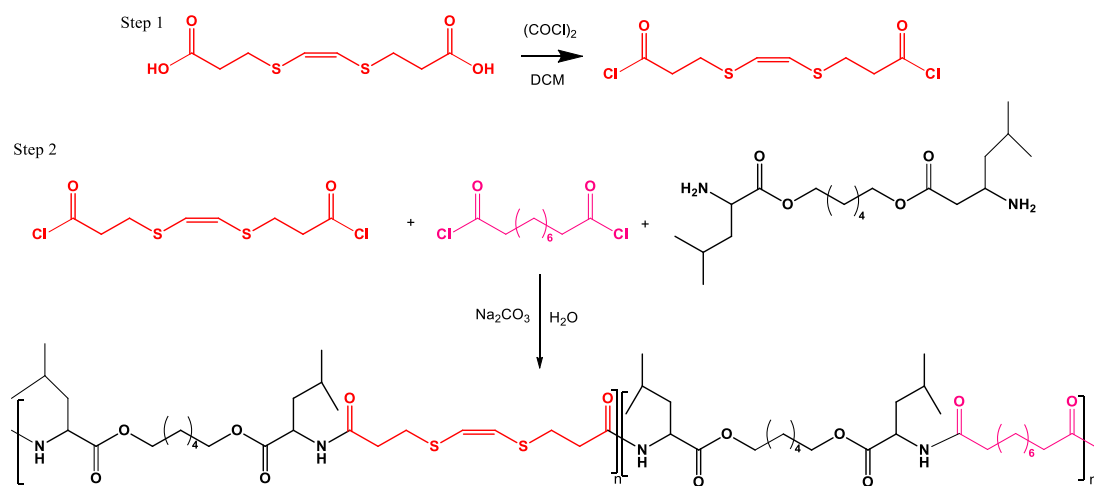
Scheme 2. 11 Synthesis route for poly(ester amide) based on BAAE and BCETE

The reaction product was characterized by FTIR and NMR.

Cleavage studies

The cleavage studies of the sensitive copolymers were carried by ^{1}H NMR before and after light irradiation with or without photosensitizer (Ce6, 1:1 molar of the copolymer). A solution of copolymer (5-10 mg) and Ce6 dissolved in DMSO-d_6, under stirring, was subjected to a pre-determined period of irradiation (through a glass vial wall,

1 cm distance between sample and laser, 650 nm, 80 mW.cm^{-2}). The NMR was recorded before and after each pre-determined irradiation period.

2.3.3 Nanoparticle Formation

For PEG-*b*-PLA and PEG-BHETE-PLA

Micelles were prepared through dialysis methodology. Briefly, 1 mg of polymer is dissolved in DMSO (1 mL). To this solution, predetermined amounts of Ce6 and/or DOX (previously dissolved in DMSO solution containing triethylamine, TEA, (3 times the molar amount of DOX)) were added and mixed. This final solution was slowly dropped (using a micro-syringe) in 1 mL of pure water under stirring (~700 rpm). The solution was allowed to homogenize for 30-60 min and then, was placed in a dialysis bag (cut-off M$_w$ 3.5k) and dialyzed against water (pH=7.5). A magnetic stirrer was placed inside the dialysis bag to promote the homogenization of the inner solution. Dialysis was carried over one day under stirring (~300 rpm) and water was changed 8 times. The solution was filtered through a 450 µm PTFE syringe filter to remove the unencapsulated compounds and the excess of polymer that did not form micelles.

For PEG-PDDD-PEG

The micelles with PEG-PDDD-PEG polymer were formed by dialysis method as described above for PEG-PLA micelles, however, the cut-off of the dialysis bag was altered considering the copolymer molecular weight (cut-off = M$_w$ 1, 3.5 and 8k for PEG$_{0.48k}$-PDDD-PEG$_{0.48k}$, PEG$_{2k}$-PDDD-PEG$_{2k,}$ and PEG$_{5k}$-PDDD-PEG$_{5k}$, respectively).

Determination of the Critical Micellar Concentration

The critical micellar concentration (CMC) was measured using the hydrophobic-selective-Nile Red (NR) fluorescence technique [209]. Briefly, 1 mg of NR was added to 1 mL of THF and was allowed to solubilize in dark over 5 h. The solution was diluted until a concentration of 0.05 mg.mL^{-1} and 22 µL of this solution was dropped in vials. Polymeric solution with concentrations ranging from 1×10^{-7} to 1×10^{-1} mg·mL^{-1} was dropped in each vial and the solution was completed until 2.5 mL. Sequentially, 2.5 mL of high purity water

was dropped to each vial while stirring. The organic solvent (THF) was allowed to evaporate overnight. Fluorescence detection of each sample was carried out. Figure 2. 1 shows the solutions with different amount of polymers used in CMC assay.
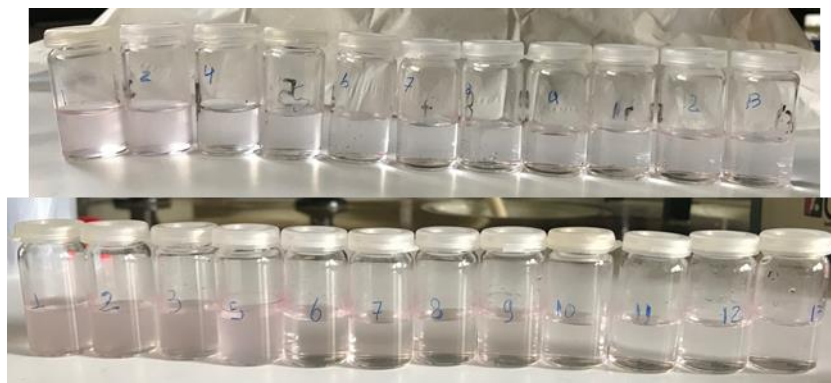
Figure 2. 1 Photographic of the two experiments for CMC measurement (note that solutions turn more blurred from left to right, vials with higher polymer concentration have more micelles and thus present a more blurred aspect).

The obtained values of fluorescence are shown in a graphic of intensity emission versus logarithmic of polymer concentration. At low copolymer concentration, a low NR intensity is observed and at higher concentration, the measured NR intensity suddenly increase. Thus, two linear fitting showing different slopes are drawn for each linear segment. The CMC value is found in the intersection point of these two segments.

Loading capacity study

The micelles for loading capacity studies were prepared following the same methodology described in nanoparticle formation, however, the DOX and Ce6 amount was adjusted as pre-determined for each assay. (usually 10-100 wt% of DOX and 5, 15 wt% or 1:1 molar of Ce6)

The amount of DOX encapsulated was measured by fluorescence, using the maximum intensity of emission (589.5 nm) and the equation of linear fitting in DOX calibration curve. For the DOX measurement, a sample of 100 µL of micelles with encapsulated DOX was mixed with 1,9 mL of DMSO (to destroy micelles) and placed in a 10 mm^2 quartz cell. An excitation wavelength of 480 nm was used, and the emission spectra of DOX were recorded in the 400-750 nm wavelength range at a scan rate of 500 nm min^{-1}.

DOX calibration curve was performed using DOX concentration range from 0 to 0.1 mg.mL^{-1} in DMSO.

DLC (Drug Loading Capacity) and DLE (Drug Loading Efficiency) were calculated using the following equations:

$$DLC\ (\%) = \frac{mass\ of\ probe\ loaded * 100}{mass\ of\ copolymer}$$

<div align="right">Equation 2.2</div>

$$DLE\ (\%) = \frac{mass\ of\ probe\ loaded * 100}{mass\ of\ probe\ used}$$

<div align="right">Equation 2.3</div>

The Ce6 concentration was calculated through maximum intensity absorbed (530 nm) taking into account the equation of linear fitting in Ce6 calibration curve. The amount of Ce6 loaded in micelles and the loading efficiency was calculated using Equation 2.2 and Equation 2.3, respectively. For the measurement, 100 µL of micelle aqueous solution was mixed with 1.9 mL of DMSO and placed in a 10 mm^2 quartz cell. The absorption spectra were recorded on 405 nm wavelength spectrum (the higher intensity absorption band of Ce6)

The Ce6 concentration for the calibration curve was measured using Ce6 concentration range from 3.125 x 10^{-6} to 0.025 mg.mL^{-1} in DMSO.

2.3.4 Drug Release Studies

The drug release assays were performed adapting the procedures described in the literature [206], [210]–[214]. Briefly, a solution with micelles (copolymer with DOX and Ce6) was split into two equal volumes and one was subjected to 2 h of red-light irradiation (650 nm, 80 mW.cm^{-2}) under stirring while the other was kept in the dark (as control sample). The two samples were poured in a dialysis bag (cut-off M_w = 12-14k) and placed in water at 37ºC. At pre-determined periods, a sample of the dialysis inner solution was taken out (75 µL), diluted until 2 mL with DMSO and analyzed in the fluorimeter. The outer aqueous solution was replaced by fresh water at every period of 0.5, 1, 1,5, 3, 5 and 24 hours. Figure 2. 2 shows the scheme of the drug release assay.
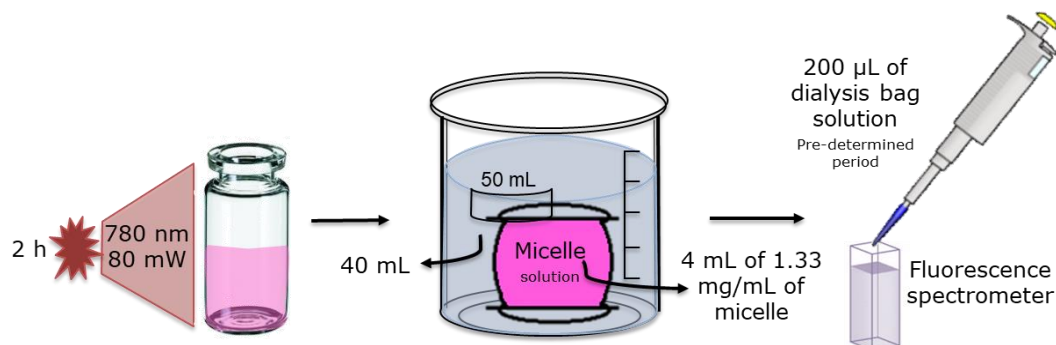
Figure 2. 2 Illustrative scheme of the drug release assay

2.3.5 Cell Studies

Culture conditions

Breast cancer cell line, MCF7 (ATCC® HTB-22™) was acquired from American Type Culture Collection (Rockville, MD, USA). The human cancer cell line was cultured in suitable medium supplemented with 5% heat-inactivated fetal bovine serum (FBS, Sigma), 1% antibiotic/antimycotic (100 U.mL^{-1} penicillin and 10 µg.mL^{-1} streptomycin, Sigma), 100 µM sodium pyruvate (Gibco Invitrogen Life Technologies; Gibco 1360). Cells were grown at 37 °C with 95% air and 5% CO_2. The detachments of the cells were made using a solution of 0.25% trypsin-EDTA (Gibco).

Cellular uptake study

On a glass cover slips of 6-well culture plate, 5×10^5 cells were seeded on each well and incubated overnight. Solutions of free DOX or PEG-BHETE-PLA-DOX-Ce6 were added to form a DOX final concentration of 5 µM in each well. Cells were incubated for 4 h followed by red light irradiation (10 min of 80 mW.cm^{-2}) and afterward, they were incubated for more 4 hours. For dark control, the seeded cells were also subjected to the same therapeutic dose and incubated for 4 hours. Thereafter, cells were washed with PBS and the remaining cells were shaved with DMSO (to ensure cell rupture and full disaggregation) followed by centrifugation at 1800 xG. The fluorescence intensity was determined by fluorescence spectroscopy with a Perkin Elmer LS45 (88107) spectrophotometer using 480 nm excitation wavelength. The concentration of DOX for each well was determined based on a calibration curve of DOX obtained from the fluorescence spectroscopy in DMSO solutions.

In vitro Cytotoxicity

MTT

Cells were plated in a 24 well culture plate in a density of 1×10^5 per mL and incubated overnight to allow cells attachment. Solutions of free Dox, PEG-BHETE-PLA-DOX-Ce6 or PEG-BHETE-PLA-DOX were added to form a DOX final concentration of 2.5 μM in each well, while a solution of PEG-BHETE-PLA-Ce6 or PEG-BHETE-PLA was added in the same volume of PEG-BHETE-PLA-DOX. The control (cells without treatment) were also tested. Cells were incubated for 4 h, followed by red light irradiation (10 min of 80 mW.cm^{-2}) or incubated under dark conditions. Cell culture plates were incubated overnight, washed with PBS and incubated with a solution of MTT (0.5 mg.mL^{-1}, Sigma), in the dark at 37°C for, at least, 4 h. To solubilize formazan crystals, a 0.04 M solution of hydrochloric acid in isopropanol was added. Absorbance was measured using a Perkin Elmer LS45 (88107) Plate Reader. Cytotoxicity was expressed as the metabolic activity of cultures subjected to therapeutics correlated with cultures without any treatment.

SRB

The cell plate, therapeutic doses, and irradiation proceeded as MTT assay. However, after the last period of incubation, cells were washed with PBS and fixed with a solution of 1% acetic acid in methanol over 45 min at 4°C. The organic solvent solution was discarded and a solution of 0.4% SRB (Sigma Aldrich, EUA) dissolved in 1% acetic acid (Sigma Aldrich, EUA) in methanol (Sigma Aldrich, EUA) was added and incubated for 1 h in the dark. Thereafter cells were carefully washed with running water and the formed SRB crystals were dissolved in 10 mM Tris-NaOH, pH 10. Absorbance was measured using a Perkin Elmer LS45 (88107) Plate Reader. Cytotoxicity was expressed as the protein content of cultures subjected to therapeutics correlated with cultures without any treatment. The experiments were performed in triplicate.

Cell images

For the cell image, cells were plated in 6 well culture plates at a density of 5×10^5 cells per well and incubated overnight to allows cell attachment. The solution of free DOX or PEG-BHETE-PLA-DOX-Ce6 were administrated to have a final DOX concentration of 2.5 μM in each well. Cells without treatment were used as control. Thereafter, cells were allowed to incubate for 4 h and irradiated by red light irradiation (10 min of 80 mW.cm^{-2}). The cells' images were made by iPhone 7 camera after 24 h incubation.

3 Results and Discussions

3.1 Synthesis of PEG-PLA with Sensitive Molecules

3.1.1 PEG-*b*-PLA

The methodology of Waymouth and Hedrick (ROP methodology) [70] was chosen to carry out the synthesis of PLA due to mild reaction conditions used in the ROP. Additionally, the use of DBU as catalyst provides a controlled copolymerization, yielding copolymers with a narrow polydispersity. A library of copolymers was synthesized with different molecular weights (Table 3. 1).

In the selected ROP methodology, an N_2 atmosphere is not required but the presence of water is highly prejudicial for the copolymer synthesis. Therefore, all glass materials used were previously dried in an oven at 50ºC overnight, the macroinitiator mPEG was dried through azeotropic distillation with toluene and the *rac*-lactide was re-crystallized in toluene, dried and kept in a desiccator in the fridge.

The success of this synthesis was proved by ^{1}H and ^{13}C NMR analysis (Figure 3. 1 and Figure A 1 in the appendix, respectively).
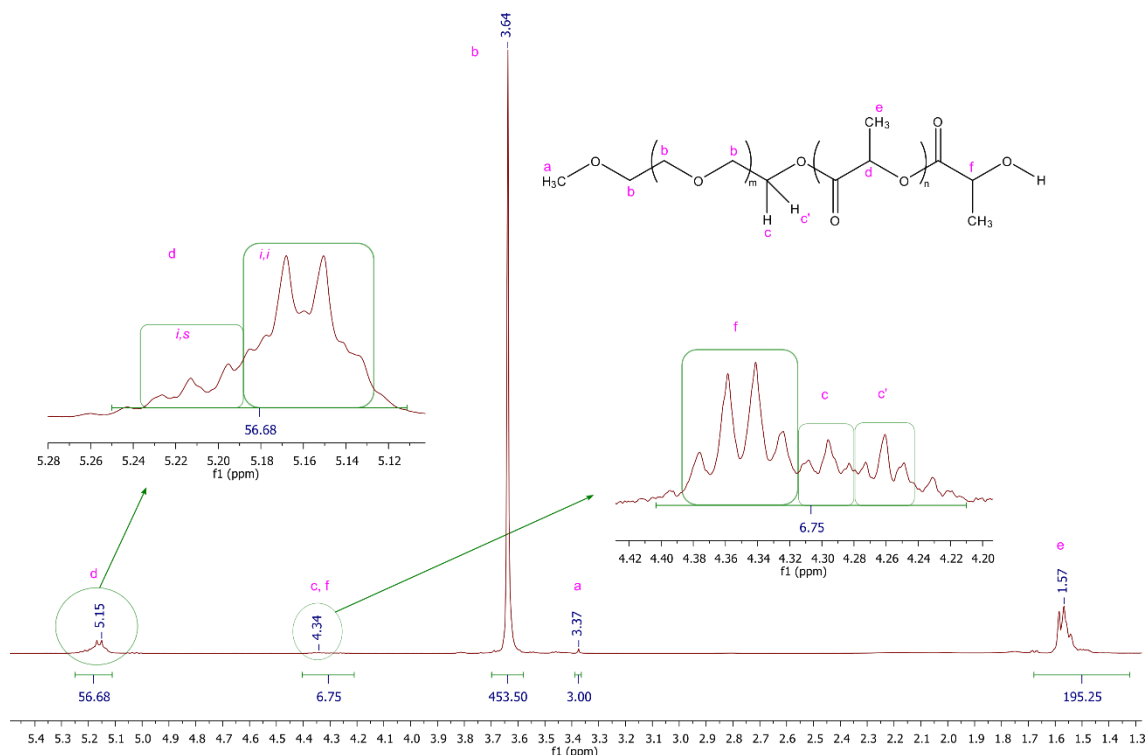
Figure 3. 1 ^{1}H NMR (400 MHz) spectrum of PEG$_{5k}$-PLA$_{5k}$ in CDCl$_3$.

The chemical shift related to the methine (C**H**-CH3, **d**) and the methyl (C**H**3-C-O, **e**) groups of PLA are at *ca.* δ 5.15 ppm and δ 1.57 ppm, respectively [215]. The carbinol resonance peak (C**H**-C-OH, **f**) at the end of the chain and the methylene peaks (C**H**2-O-C=O, **c** and **c'**) at the linkage point between PEG and PLA shift to 4.34 ppm, proving the success of the ROP of *rac*-lactide using mPEG as a macroinitiator. The multiplet resonances of methine (**d**) at ca. δ 5.28 and 5.12 ppm indicate that the ROP of *rac*-lactide monomer led to a PLA with preferential formation of isotactic, isotactic sequences (*i,i,* δ 5.14-5.19 ppm) rather than isotactic, syndiotactic (*i,s,* δ 5.20-5.26 ppm) sequence [70]. This PLA tacticity was favored by the use of DBU as a catalyst [70]. The Mn of the copolymer was determined by comparing the methine proton signal of PLA (**e**) and the methylene proton signal of PEG (**b**), using the methyl proton signal of PEG (C**H**3-O, peak **a**) as a reference in integration analysis. The determination of the molecular weight was obtained following Equation 3.1.

$$M_n = \frac{n_{monomer}}{n_{initiator}} * M_{w\ repeting\ unit}$$

Equation 3.1

Using Equation 3.1, the Mn of PLA calculated was 4.081 kg/mol and the Mn of commercial mPEG used was confirmed as 4.983 kg/mol. The ^{1}H NMR for other synthesized polymers is shown in Figure A 2 in the appendix.

The SEC analysis was used to determine the molecular weight distribution of synthesized copolymers.

Table 3. 1 shows the measured dn/dc, the polydispersity and the molecular weight (analyzed by NMR and SEC) for each polymer.

Table 3. 1 The theoretical and measured molecular weight (SEC-THF) of synthesized copolymers.

Sample	M_W PEG	Mn NMR	Mn PLA NMR	dn/dc THF (* 10^{-3})	Mn SEC- THF	Đ SEC-THF
PEG_{2k}-PLA_{4k}	2000	5700	3700	64.16	6128	1.066
PEG_{2k}-$PLA_{1.2k}$	2000	3200	1200	58.0	3285	1.191
PEG_{5k}-PLA_{4k}	5000	8700	3900	54.52	8756	1.068
PEG_{5k}-PLA_{2k}	5000	6700	1700	77.45	8650	1.037
PEG_{5k}-PLA_{1k}	5000	6200	1200	66.3	7088	1.051

The narrow polydispersity of the synthesized polymers is in conformity with what was expected from a ROP using DBU as a catalyst [70]. This low value of Đ favors the formation of micelles with more homogeneous size and morphology [218].

With a successful PEG-PLA polymerization, under atmospheric conditions and at room temperature, the next step was the synthesis of the sensitive linker to insert it in the block copolymer.

3.1.2 PEG-BHETE-PLA

The light-sensitive PEG-PLA copolymer can be designed by the insertion of a singlet oxygen ($^1O_2$) sensitive moiety. BHETE was previously used in light-triggered drug delivery systems showing a controlled release of the payload [219]. These systems usually consist of a nanoparticle co-loaded with the drug and the photosensitizer, which is activated by light-generated singlet oxygen species. These last species react with the sensitive BHETE leading to cleavage of the segment molecule releasing the drug [161], [205], [206].

In the case of amphiphilic PEG-PLA micelles, the disassembly of the nanoparticle can be reached through the rupture between the hydrophilic and the hydrophobic block. Thus, the strategy used in this work consists of positioning the sensitive segment BHETE between the hydrophilic PEG and hydrophobic PLA. The segment cleavage disrupts the copolymer linkage leading to a destabilization of the micelle structure and, consequently, the drug release.

BHETE synthesis

The first step of the process is the preparation of a sensitive segment with two functional groups. In one of them, PLA was linked, whereas, in the other extremity, a PEG molecule was linked. Figure 3. 2 shows the BHETE structure.
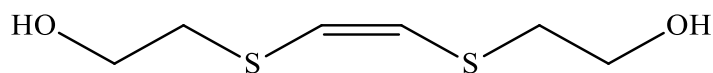
Figure 3. 2 BHETE structure.

The BHETE was synthesized through an adapted methodology [159] [205]. The BHETE was obtained in yields from 50 to 60% and was characterized by FTIR and NMR [159]. The ATR-FTIR spectrum of BHETE is shown in Figure 3. 3
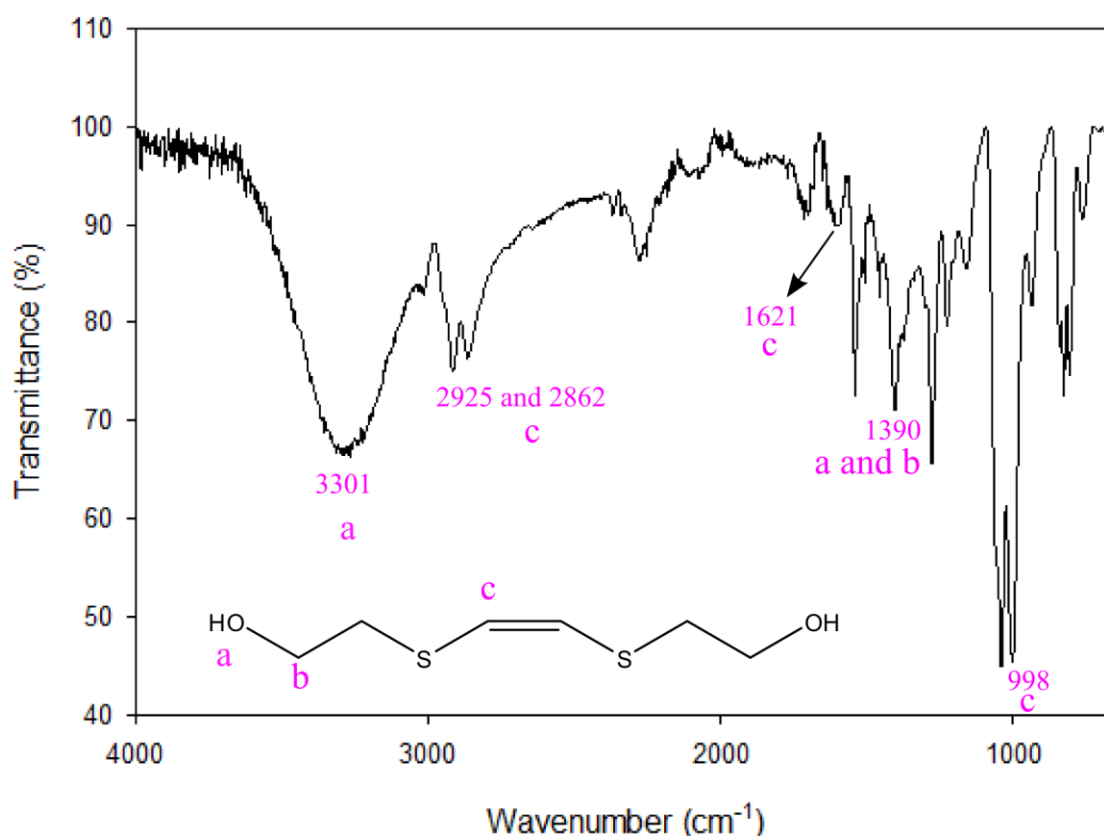
Figure 3. 3 ATR-FTIR of BHETE.

The product presents the characteristic frequency band of O-H stretching of alcohol group at 3301 cm^{-1}, C-H stretching of alkane groups at 2925 and 2862 cm^{-1}, C=C stretching of alkene disubstituted (*cis*) at 1621 cm^{-1}, C-H bending and O-H bending of alcohol group at 1390 cm^{-1} and C=C bending of disubstituted alkene at 998 cm^{-1}. The ^{1}H NMR spectrum

82

of BHETE in CDCl$_3$ is shown in Figure 3. 4 and the ^{13}C NMR is presented in the appendix (Figure A 3).
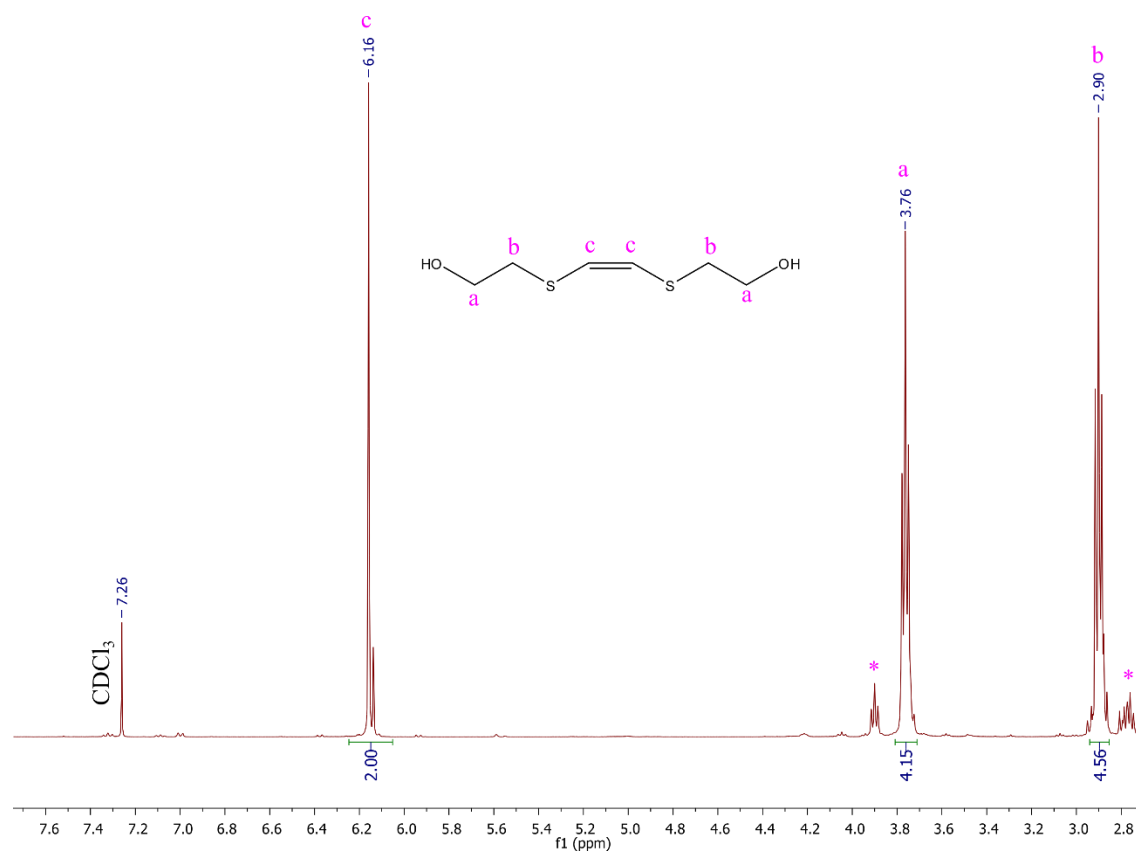
Figure 3. 4 ^{1}H NMR (400 MHz) spectrum of BHETE in CDCl$_3$.

The chemical shift of the protons belonging to the methylene groups are at δ 3.75 (OH-C**H**2-, **a**) and δ 2.89 (-C**H**2-S-, **b**) ppm and the protons of the methine group of the sensitive double bond (-C**H**=C**H**-, **c**) are at 6.15 ppm. The spectrum also shows small resonance peaks (*) that correspond to the protons of unreacted 2-mercaptoethanol. Attempts to perform the purification of this product by column chromatography, using silica gel resulted in the degradation of the product. This may be attributed to the slight acidity present in the silica used as filling of the column (^{1}H NMR in the appendix, Figure A 4).

To confirm the sensitivity of the molecule to the [1]O$_2$, the BHETE was exposed to red light irradiation (2 h, 80 mW.cm^{-2}) in a solution of DMSO-*d$_6$* and Ce6 as the photosensitizer (5 wt% of BHETE). Figure 3. 5 shows the spectra.
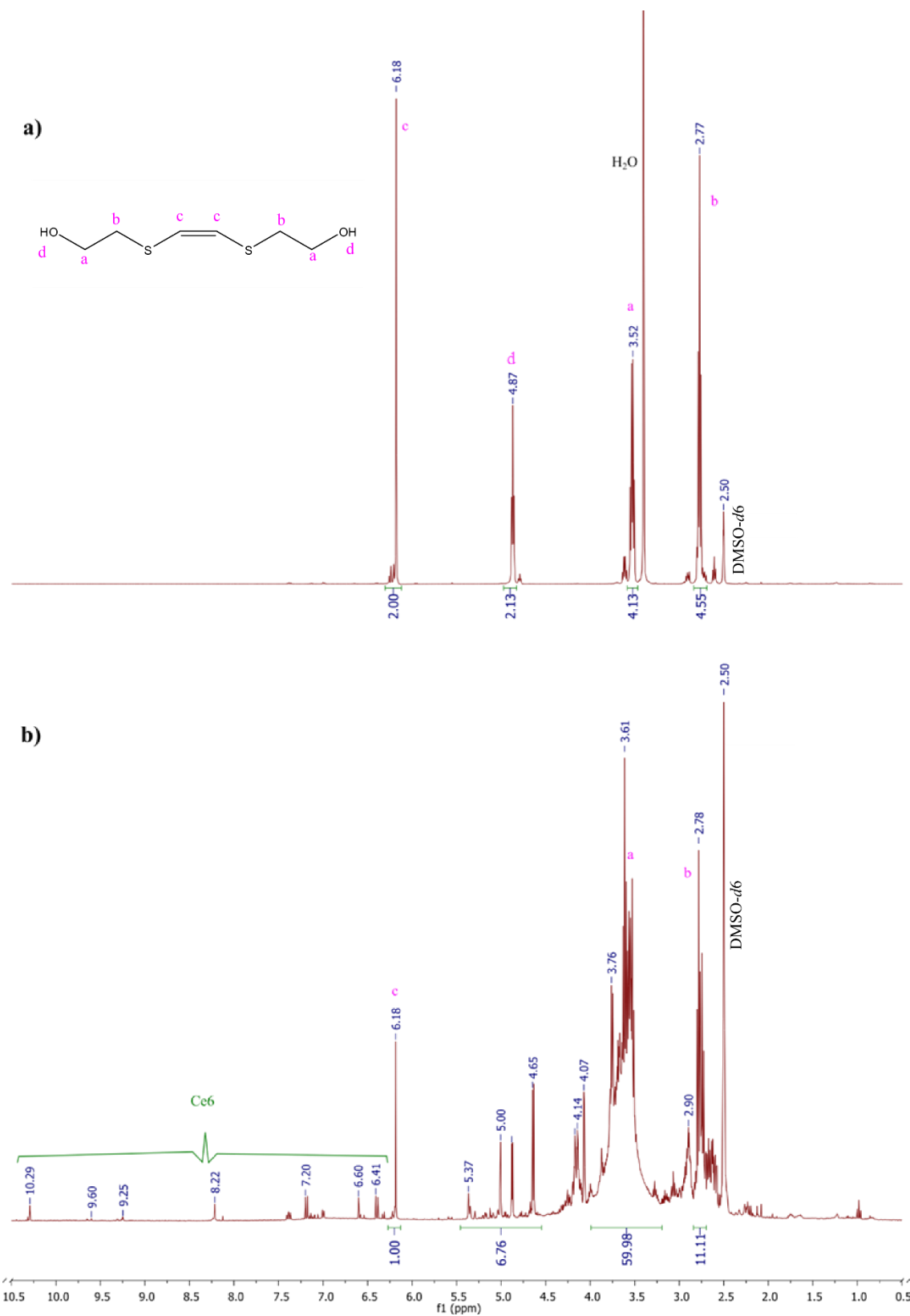
Figure 3. 5 ^{1}H NMR (400 MHz) spectrum of BHETE in DMSO-d_6 in the initial conditions (a) and after 2 hours of irradiation with the presence of the photosensitizer Ce6 (b).

Although BHETE presents a slight deviation of the chemical shifts of the peaks of the methylene protons from NMR spectrum in CDCl$_3$ (Figure 3. 4) and in DMSO-d_6

84

(Figure 3. 5, a), the integration area of each peak remained with almost the same value. The spectrum of BHETE after irradiation shows peaks overlaid in the region of protons belonging to the methylene groups (Figure 3. 5, b, peaks identified as **a** and **b**, HO-C**H**2- and -C**H**2-S-, respectively) and to the methine groups (**c**, -C**H**=C**H**-). The ratio of the integrals of (**c**):(**a** or **b**) is much smaller than the initial ratio, which was 1:2 (Figure 3. 5, b). This modification in the spectrum after irradiation indicates the degradation of the BHETE, triggered by light. Additionally, the new peak at 4.65 ppm might indicate the presence of dioxetane (as predicted by ChemDraw Ultra 12.0.2.1076), that is the intermediate derivative product of the $^{1}O_2$ mediated cleavage [206].

The next step to prepare the PEG-BHETE-PLA sensitive polymer is the reaction between PEG and the BHETE. First, it was necessary to change the OH terminal group of PEG to a carboxylic acid group. Hence, mPEG-OH was transformed in mPEG-COOH (**1**), through an esterification reaction with succinic anhydride. Next, the carboxylic ended PEG was bonded with the BHETE by *Steglich* esterification (mPEG-BHETE, **2**). Compound **2** was used as macroinitiator for ROP of *rac*-lactide, yielding the sensitive amphiphilic copolymer (**3**). Figure 3. 6 shows the structure of the final copolymer PEG-BHETE-PLA (the route synthesis is showed in Scheme 2. 7).

(3)
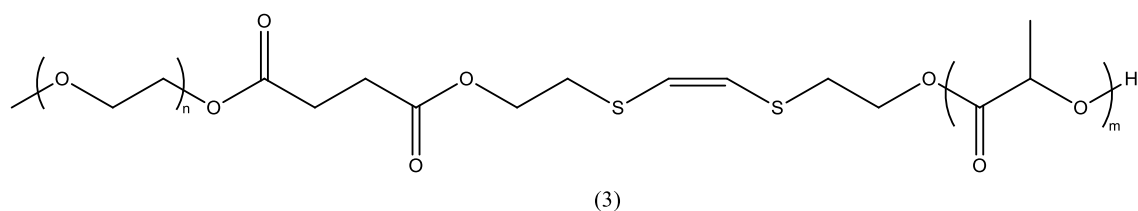
Figure 3. 6 Structure of the amphiphilic PEG-BHETE-PLA (3) achieved by ROP of *rac*-lactide.

The resultant products from each step of the reaction route were characterized by ATR-FTIR. The spectra are shown in Figure 3. 7.
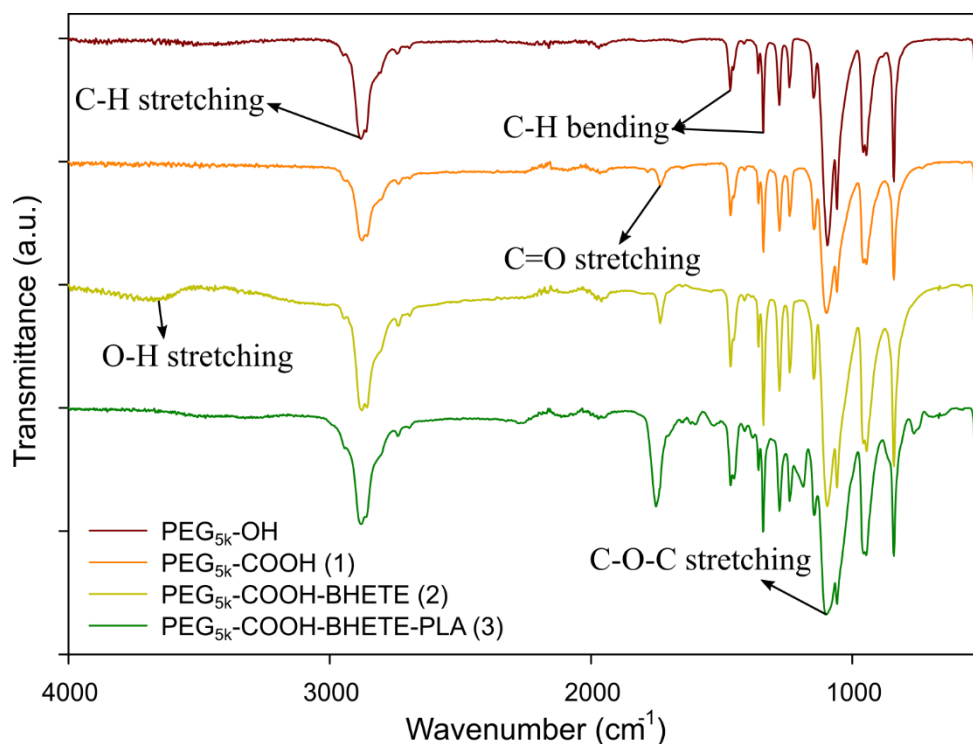
Figure 3. 7 ATR-FTIR of polymers in each step of the polymerization.

PEG$_{5k}$-OH is characterized by the strong absorption peak at 1083 cm^{-1} (C-O-C stretching) and also by the aliphatic C–H stretching at 2873 cm^{-1}, 1466 and 1340 cm^{-1}, which is attributed to the C–H bending vibrations [220]. The PEG functionalized with the carboxylic group shows a new band at 1739 cm^{-1} due to the characteristic C=O$_{ester}$ stretching vibration [220]. The sensitive BHETE was conjugated to mPEG-COOH via an ester bond. The product of the reaction, mPEG-COOH-BHETE, exhibited an increase in the intensity of the band at 1735 cm^{-1} (C=O$_{ester}$ stretching vibration), which indicates the formation of the ester bond between mPEG-COOH and BHETE. The new broad band at 3671 cm^{-1} relative to the O-H stretching of BHETE confirms the success of the covalent conjugation [221]. Finally, the synthesis of the block copolymer PEG-BHETE-PLA is proved by the disappearance of the O-H stretching peak at 3671 cm^{-1}. The success of the reaction is, furthermore, indicated by the increase of the C=O$_{ester}$ stretching vibration at 1750 cm^{-1}, which is due to the presence of the ester groups, not only from the PEG-BHETE, but also from the PLA [222].

The polymers were also characterized by ^{1}H NMR as shown in Figure 3. 8.
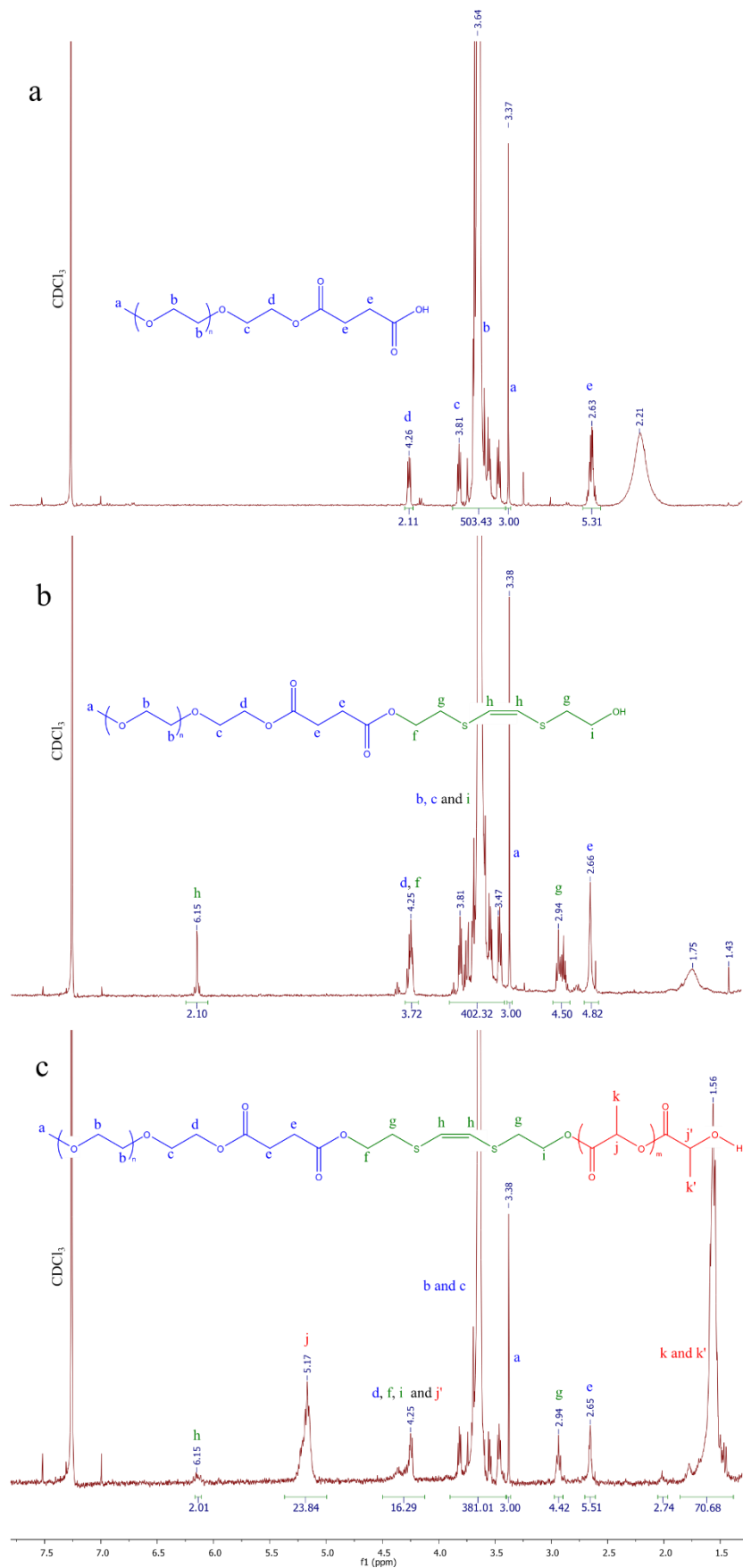
Figure 3. 8 ^{1}H NMR (400 MHz) spectrum in CDCl3 of mPEG$_{5k}$-COOH (compound 1, a); mPEG$_{5k}$-COOH-BHETE (2, b) and mPEG$_{5k}$-COOH-BHETE-PLA$_{1k}$ (3, c)

The structure of mPEG$_{5k}$COOH was confirmed by ^{1}H NMR and is shown in Figure 3. 8 **a**. The spectrum shows the characteristic sharp PEG signal (-**CH**$_2$-O, **b**) at 3.65 ppm. The signal of protons of methylene groups close to the carbonyl groups (-**CH**2-**CH**2-COOH, **e**) can be seen at 2.63 ppm and protons of the methylene group (-**CH**$_2$-O-C=O, **d**) present a signal at 4.26 ppm, thus, confirming the carboxylic functionalization. The initial methyl group of PEG (**a**) at 3.31 ppm was used to set the integration value and evaluate the polymer molecular weight.

The success of the *Steglich* esterification was proved by analyzing the spectrum of compound 2 (Figure 3. 8**b**). The characteristic peak of methine protons (-**CH**=**CH**-, **h**) is found at 6.15 ppm. The methylene group **g** (-**CH**2-S-) has the signal at 2.94 ppm and the signal of methylene **i** (-**CH**2-OH) is found overlaid to the **b** signal. At last, an increase in the value of the integration area under the peak identified as **d** proves the bonded reaction between mPEG$_{5k}$COOH and BHETE. The chemical shift of methylene group **f** (-O-**CH**2-) is dislocated from 3.76 ppm (Figure 3. 4) to 4.25 ppm.

Finally, the synthesis of the sensitive amphiphilic polymer PEG-BHETE-PLA was confirmed by analyzing Figure 3. 8 **c**. The spectrum shows the methyl group of PLA (-CH-**CH**3, **k** and **k'**) at the region of δ=1.56 ppm and the methine group (-**CH**-CH3, **j**) at 5.17 ppm. The shift in the BHETE methylene **i** (-**CH**2-OH) signal could not be detected because the signal is overlaid under mPEG$_{5k}$COOH methylene peak (**d**, -**CH**2-COO-) and the increase in the integration area is also unnoticeable due to the presence of the methine terminal groups of the PLA molecule (-**CH**-CH3, **j'**). The PLA molecular weight in the copolymer, measured through the signal integrations, is approximately 1500 g/mol. The ^{1}H NMR spectra of others synthesized sensitive copolymers are presented in Figure A 5 and Figure A 6 in the appendix.

The polydispersity and molecular weight of sensitive block copolymers were analyzed by SEC- THF. Table 3. 2 shows the Mn values measured by SEC and NMR.

Table 3. 2 The theoretical and measured molecular weight (SEC-THF) of synthesized sensitive copolymers

Sample	M$_w$ PEG	Mn $_{NMR}$	Mn $_{PLA\ NMR}$	dn/dc $_{THF}$ (* 10^{-3})	Mn $_{SEC-THF}$	Đ $_{SEC-THF}$
PEG$_{2k}$-BHETE-PLA$_{2k}$	2000	6200	4280	79.62	4800	1.099
PEG$_{5k}$-BHETE-PLA$_{1k}$	5000	6000	1500	72.3	6755	1.283
PEG$_{5k}$-BHETE-PLA$_{10k}$	5000	16000	11000	76.93	14787	1.012

The Đ values of the sensitive PEG-BHETE-PLA copolymers were similar to the non-sensitive copolymer (showed in Table 3. 2), with narrow molecular weight distribution ($Đ < 1.5$), which is considered good criteria for the synthesis of the micelles [46].

To evaluate the sensibility of the prepared copolymer, PEG_{5k}-BHETE-PLA_{2k} was exposed to 30 min of red-light radiation (650 nm, 80 mW.cm^{-2}) in a solution of DMSO-d_6 and 5 wt% of Ce6 (relatively to the polymer). Figure 3. 9 shows the polymer spectrum after irradiation.
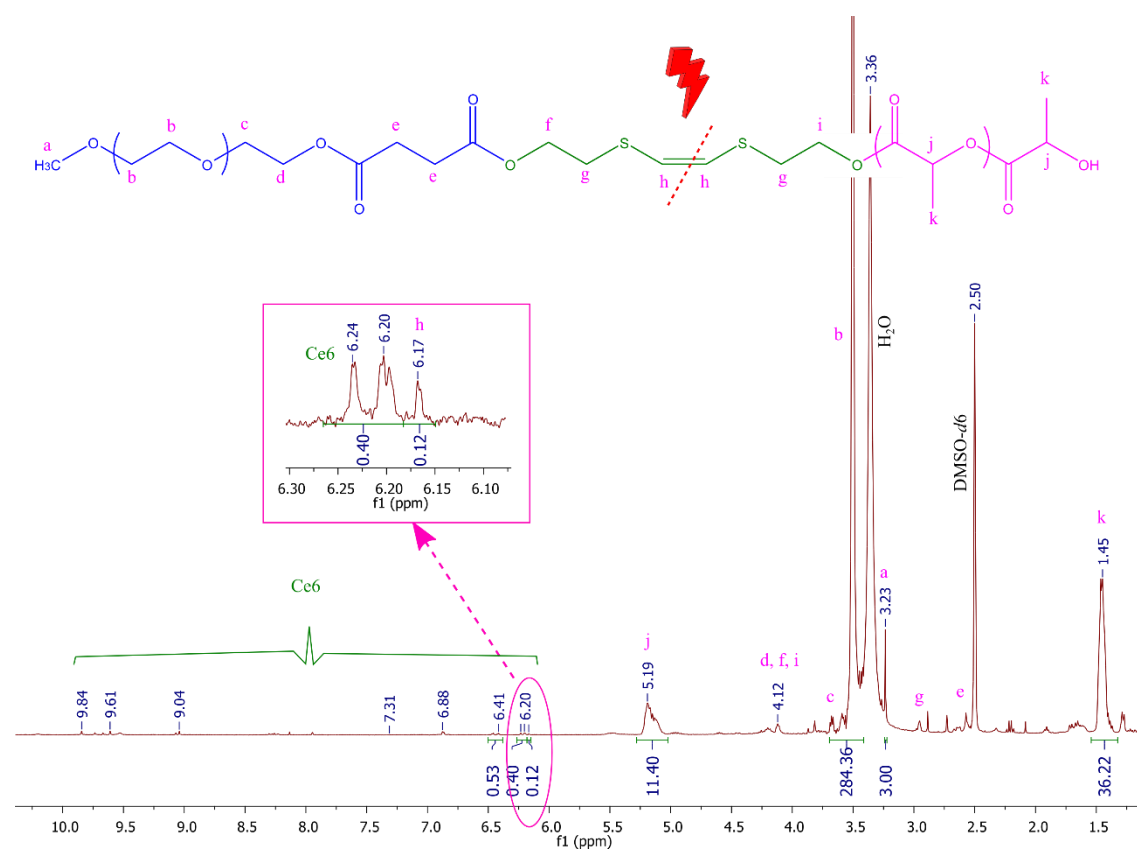
Figure 3. 9 ^{1}H NMR (400 MHz, DMSO-d_6) spectrum of the amphiphilic sensitive copolymer PEG_{5k}-BHETE-PLA_{1k} after 30 min of red-light irradiation (650 nm, 80 mW.cm^{-2}) with ~5 wt% of Ce6 (relatively to the copolymer).

Taking the comparison between the spectra of Figure 3. 8 **c** and Figure 3. 9, the resonance peak at $\delta \sim 6.15$ ppm corresponding to the methine protons of BHETE segment (**h**), show a reduction of the integration area from ~2.29 to 0.12, maintaining the methyl proton from the PEG initial chain (**a**, at $\delta \sim 3.38$ ppm) with the same integration area. This observation suggests that the copolymer breaks with red light irradiation. After 30 min of irradiation, almost no sensitive linker can be seen in the spectrum.

A green light (532 nm, 20 mW.cm^{-2}) was also used to break the sensitive copolymer. The laser used has higher power than red light, approximately 300 fold, so shorter exposition time (10 min) was used in the experiment. Sample breaking analysis was done by NMR. Figure 3. 10 shows the ^{1}H NMR for 10-minutes of irradiation.
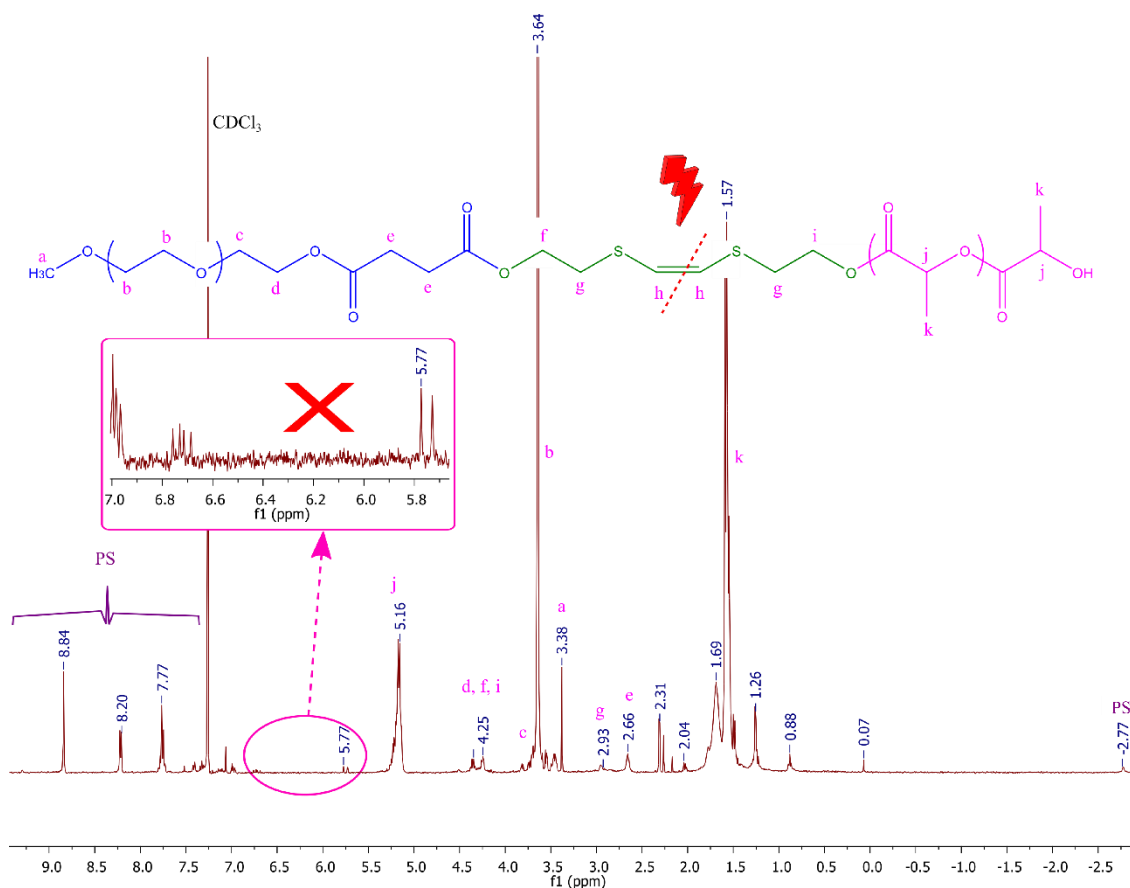
Figure 3. 10 ^{1}H NMR (400 MHz, CDCl$_3$) spectrum of the amphiphilic sensitive copolymer PEG$_{2k}$-BHETE-PLA$_{2k}$ after 10 min of green irradiation.

Once more, after irradiation, there is no visible evidence of the BHETE (c.a. 6.00 to 6.30 ppm corresponding to the resonance peak for alkene group, **h**), suggesting the cleavage of the copolymer.

In another experiment, a much lower power source of the light beam (635 nm, 3.5 mW.cm^{-2}, ~ 4 fold weaker than the previous red-light source) was tried. The cleavage of the amphiphilic polymer was also observed after 4 h of irradiation. The spectrum of the cleaved polymer is shown in Figure A 7 in the appendix.

3.1.3 Micelle Formation of PEG-PLA Copolymers with or without Photosensitive Segments

Giving the amphiphilicity of the PEG-PLA, this copolymer can self-assemble in micellar structures when placed in an aqueous environment [14]. The stability of the micelle in the diluted environment can be measured by the analysis of the CMC. This value is the minimal concentration of polymer needed for the creation of micellar structures (a process known as micellization). Below this concentration, the reduced amount of polymer does not allow each of the individual blocks of the copolymers (unimer) to re-organize in micellar structures, remaining disperse in the liquid and in the liquid-air surface. The single value concentration point established as CMC defines the transition in which the unimers start to form micellar structures. However, this micellization can occur in a broad range of concentrations near the CMC, in some cases, the CMC value can vary 3-10 times depending on the employed method to determine the CMC [223].

The CMC of the PEG-PLA copolymers were measured following the described procedures [209]. The process is based on the difference of the NR emission in the presence of hydrophobic or hydrophilic medium. The NR only presents fluorescence when in a hydrophobic environment, such as in the interior of micelles. As a consequence, when NR is in a polymeric solution, with a concentration higher than CMC, the micellization will be occurring and the NR encaged will display fluorescence (as shown in Figure 3. 11). The NR dispersed in aqueous phase does not exhibit fluorescence.
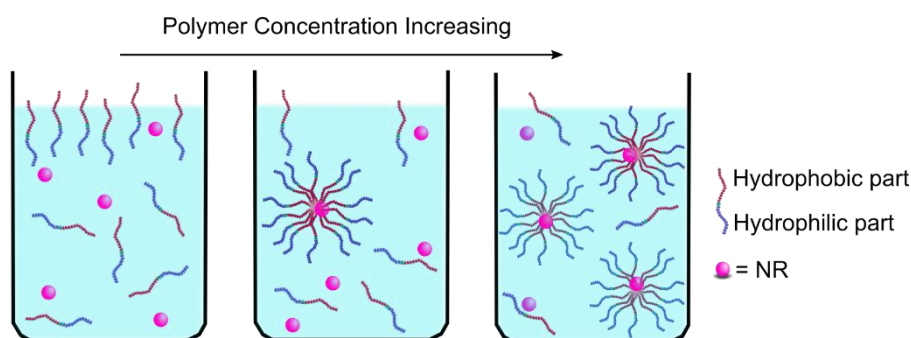
Figure 3. 11 Illustration of the critical micellar concentration assay.

The fluorescence emission spectra of a polymer solution containing NR, excited at 550 nm (Figure 3. 12, A), show a sudden increase in intensity with the increase of the polymer concentration. This is due to the formation of micellar structures and the migration of the NR to the inner core of the structures. The CMC value is then determined by the intersection of linear fittings obtained from the plot of relative fluorescence intensity at ca.

550 nm (λ_{max}) versus the logarithm of polymer concentration. The results of fluorescence spectroscopy for sensitive PEG$_{2k}$-BHETE-PLA$_{2k}$ polymer assay are shown in Figure 3. 12 and Table 3. 3 shows the CMC results for the sensitive polymers.
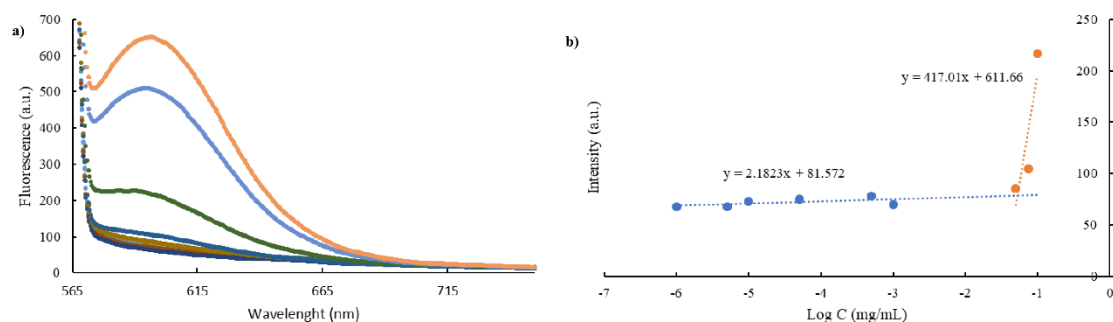
Figure 3. 12 a) Emission spectra of NR ($\lambda_{exc} = 550$ nm) in a solution of a varying concentration of PEG$_{2k}$-BHETE-PLA$_{2k}$ polymer in water. b) Emission intensity at 596.5 nm versus the logarithm of concentration (mg.mL^{-1}) of the polymer.

Table 3. 3 CMC and molar ratio of PEG/PLA of sensitive polymers.

Polymer	CMC (g.L^{-1})
PEG$_{2k}$-BHETE-PLA$_{2k}$	5.27×10^{-2}
PEG$_{5k}$-BHETE-PLA$_{1k}$	7.57×10^{-3}
PEG$_{5k}$-BHETE-PLA$_{2k}$	4.06×10^{-3}
PEG$_{5k}$-BHETE-PLA$_{11k}$	8.08×10^{-3}

The emission intensity graphic of the micelle is in Figure A 8 in the appendix.

The CMC value for the PEG$_{2k}$-*b*-PLA$_{5k}$ micelle was 2.63×10^{-2} g.L^{-1} and for the PEG$_{2k}$-BHETE-PLA$_{2k}$ 5.27×10^{-2} g.L^{-1}, which is a value within the same order of magnitude of other synthesized micelles [137], [48]. The CMC of the synthesized sensitive micelles is in agreement with the literature, where values generally are in the range from 10^{-1} g.L^{-1} to 10^{-3} g.L^{-1} for PEG-PLA block copolymers [108], [223], [224].

Besides the micelle stability, another important factor for drug delivery purposes is the micelle's size. The drug delivery strategy for our micelles is based on the EPR effect, where the particle's size should be between 10 nm and 200 nm. This passive delivery allows the accumulation of polymeric micelles in cancer cells [97]. Micelles' size is influenced by a combination of factors, such as hydrophobic/hydrophilic balance, polymer molecular weight, amount of drug encaged and the preparation method. A summary of PEG-PLA micelles' size is shown in Table 1. 5 in chapter 1.

Micelles could be prepared through several methods, where the most common are: oil-in-water emulsion, solvent evaporation, and dialysis methods. The formation method can directly influence the micelle's size and reproducibility.

PEG-PLA copolymers are soluble in a wide number of organic solvents, such as DCM, chloroform, acetonitrile, acetone, DMF, THF, and DMSO. Thus, from all the possible solvents, we were able to evaluate the formation of micelles of PEG-*b*-PLA/PEG-BHETE-PLA in different methods. Micelles were tested in solvent evaporation (THF, acetone or acetonitrile as solvent), thin film hydration (acetone), direct dissolution and dialysis methods (DMSO). Table 3. 4 shows a summary of the micelle formation experiments.

Table 3. 4 Summary of the results for PEG$_{2k}$-BHETE-PLA$_{2k}$ micelle formation experiments.

Sample	Methodology	Solvent	Addition order and water volume (mL)	Observation
1	Solvent Evaporation	THF 1 mL	1 mL water in solvent	
2	Solvent Evaporation	THF 1 mL	1 mL water in solvent	Ultrasonicated before filtration
3	Solvent Evaporation	THF 2 mL	1 mL water in solvent	
4	Solvent Evaporation	THF 1 mL	1 mL water in solvent	Water addition without stirring
5	Solvent Evaporation	THF 1 mL	1 mL water in solvent	Water addition under magnetic stirring
6	Solvent Evaporation	THF 1 mL	1 mL water in solvent	Water addition under ultrasounds
7*	Solvent Evaporation	THF 1 mL	1 mL water in solvent	Polymer solution was allowed to stir overnight to improve polymer solubility
8*	Solvent Evaporation	Acetone 1 mL	Solvent in 1 mL water	Water addition under magnetic stirring (600 rpm)
9*	Solvent Evaporation	Acetone 1 mL	Solvent in 2 mL water	Water addition under magnetic stirring (600 rpm)
10*	Dialysis	DMSO 1 mL	1 mL water in solvent	Polymer solution added to water under magnetic stirring for 30 min
11*	Solvent Evaporation	Acetone 1 mL	1 mL water in solvent	Polymer solution added to water under magnetic stirring (600 rpm)
12*	Thin-Film hydration	Acetone 1 mL	1 mL water in solvent	Polymer solution allowed to stir overnight. Water addition under ultrasounds
13*	Direct Dissolution	Water 1 mL	1 mL water in solvent	Polymer solution allowed to stir overnight to improve polymer solubility
14*	Solvent Evaporation	Acetonitrile 2 mL	1 mL water in solvent	Water addition under magnetic stirring (600 rpm)

* Polymer used was PEG$_{5k}$-*b*-PLA$_{2k}$ instead of PEG$_{2k}$-BHETE-PLA$_{2k}$ due to the low amount of polymer synthesized

Some details are important in order to anticipate the success of the experiment, simply by visual analysis of the solution. Large particles will lead to a turbid solution or visible aggregated particles. In the case of clear solutions, those were filtered through a Nylon syringe filter of 450 µm. However, in this work, the clear solutions were changed from a colorful (green or orange, if micelles have Ce6 or DOX entrapped, respectively) to a colorless solution after filtration. This fact led to an important question related to the possible interaction between the formed micelles in the solution and the nylon of the filters. When the filter type was changed to a PTFE 450 µm the solutions remained clear and colorful as showed in Figure 3. 13.
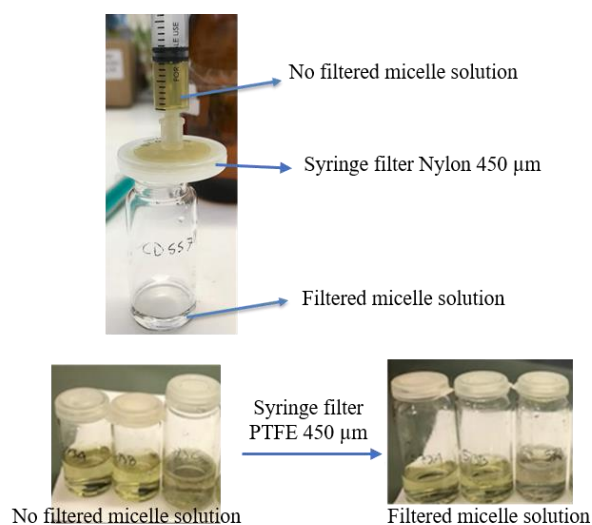
Figure 3. 13 Pictures of micelles before (left) and after (right) passing through the syringe filter.

From the tests carried out, accordingly to Table 3. 4, the conclusion is that the limited solubility of DOX and Ce6 compounds in most common solvents (as THF and acetone) restrict the micelle formation methodology to the use of DMSO. Due to the high boiling point of this solvent, the best method to remove the DMSO from the solution is by the dialysis method. It is noteworthy that Vangeyte *et al.* reported that direct dialysis did not show reproducible results, whereas the solvent evaporation technique showed better results [225]. Nevertheless, most of the DOX-encaged PEG-PLA micelles reported in the literature use the dialysis method. Typically, the DMSO solution containing the polymer and DOX is slowly added dropwise to the stirring water. The resulting suspension is then placed in a dialysis bag (as shown in Table 1. 5 in chapter 1). Following this method, several micelles with sensitive copolymers were prepared and the corresponding hydrodynamic size was analyzed by DLS (Figure 3. 14).
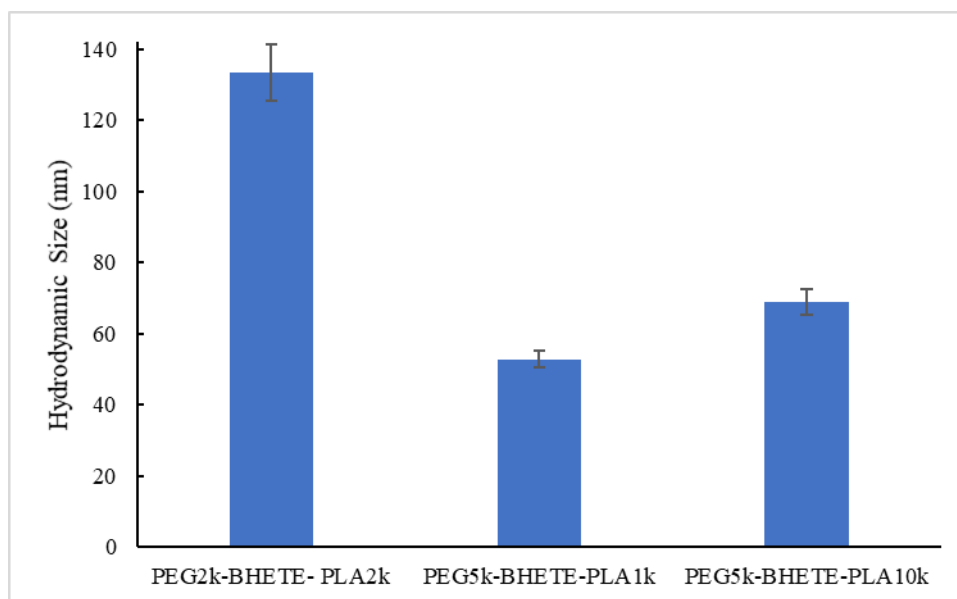
Figure 3. 14 The average hydrodynamic size of micelles formed through dialysis method using sensitive polymers.

The hydrodynamic size of micelles is highly influenced by the molecular weight of the block copolymer [215] and the hydrophobic/hydrophilic balance [80]. The obtained micelle size and the sizing behavior are in agreement with the reported by Wu *et al* for PEG-PLA micelles [226].

The micellization process in a controlled way is the cornerstone of the micelles' applications [227]. A large number of parameters can influence micelle's size and are vastly reported in the literature [100], [228] (Table 1. 5, chapter 1), among them is the order of solvent addition in the micellization process [46] and concentration of polymers [226]. In order to evaluate the effect of these variables, micelles were prepared by the dialysis process with different polymer concentrations, different order of solvent/water addition and stirring speed. The micelles' size was analyzed by DLS. Conditions of micelles' formation and hydrodynamic diameters are shown in Table 3. 5. To analyze the effect of encapsulation in the final size, the experiments were carried out in the presence of the DOX.

Table 3. 5 Hydrodynamic sizes and PDI from DLS analysis of PEG_{2k}-BHETE-PLA_{2k} micelles prepared by the dialysis method with DMSO and 100 wt% of DOX in feeding, using different preparation conditions.

Entry	Conc. of polymer (mg.mL^{-1})	Order of addition	Method of stirring	Size (nm)	PDI
1	2	DMSO to water		276.1 ± 4.747	0.169 ± 0.023
2	1	water to DMSO		232.8 ± 1.007	0.126 ± 0.026
3	1	DMSO to water	I and O	128.0 ± 0.5132	0.138 ± 0.024
4	0.5	water to DMSO		204.2 ± 1.801	0.098 ± 0.031
5	0.5	DMSO to water		123.9 ± 5.622	0.354 ± 0.035
6	0.5	DMSO to water	WO	169.1 ± 0.6928	0.255 ± 0.017
7	0.5	DMSO to water	WO and O	111.6 ± 3.119	0.311 ± 0.011
8	0.5	DMSO to water	O	77.06 ± 1.949	0.318 ± 0.029
9	0.5	DMSO to water	I	270.1 ± 1.710	0.214 ± 0.012
10	0.5	DD	I and O	166.5 ± 2.566	0.141 ± 0.013

DD: micelle made through direct dialysis (solvent was put inside the dialysis bag and dialyzed against water), I: stirring inside the dialysis bag; O: stirring outside the dialysis bag; WO: without agitation in the micelle formation;

The less concentrated polymer solutions (comparing entries 1, 3 and 5 or 2 and 4) showed a smaller hydrodynamic diameter in accordance with the reported in the literature [108], [226]. The dropwise addition of the DMSO-polymer solution in water (entries 3 and 5) forms smaller micelles than the inverse order (entries 2 and 4). These results are in agreement with Vageyte *et al.* study [225] that shows that smaller micelles are obtained adding the DMSO-polymer solution in water.

Ayen *et al.* showed in their work that the stirring of the solution can influence micelles' size [133]. To verify if this occurred in our case, the polymer solution was added in water under stirring (entry 7) and without stirring (entry 6). The influence of stirring was also analyzed in the dialysis process, where solutions were stirred from inside and outside of the dialysis bag (entries 8 and 9). Lastly, the polymer solution was directly added in the dialysis bag, without being previously mixed with water, with agitation from inside and outside of the dialysis bag (entry 10). The smaller size was obtained within the condition corresponding to the micelles formed under stirring in both steps; while adding the polymer solution to water and during the dialysis process (using stirring outside of the bag, entry 8). The hydrodynamic size was ~55% smaller than the sample prepared without stirring (entry 6). This methodology was selected to all further micelles' preparation.

3.1.4 Studies for the Best Photosensitizer

Photosensitizers (PSs) are molecules that are able to produce ROS when activated by light [229]. The PSs of the porphyrin type have several light absorption bands and the higher absorption band (the Soret band) occurs, usually, at the blue wavelength part of the electromagnetic spectrum. However, PSs with red absorption bands are the most valued in the case of tumor therapies by ROS production, due to the deeper penetration of the red-light in comparison to blue light [230].

Below, it is described the preparation of micelles using the PEG_{2k}-BHETE-PLA_{2k} copolymer, with different encaged photosensitizers and the changes in micelles' size after 1 h of irradiation with 650 nm light (80 mW.cm^{-2}). Besides the particle size, another interesting parameter, which can be analyzed from the DLS equipment, is the count rate. To ensure a collection of data statistically significant (e.g. in case of lower concentration) or to avoid damage in the DLS detector (e.g. high concentrated solutions), the equipment automatically selects an attenuator for the signal in order to optimize the amount of light that is used in the measurement. The derivative count rate is a theoretical count rate estimated considering a sample analysis at 100% laser power and zero attenuation conditions. The higher derivative count rate usually denotes higher concentrations, larger particles or both [231]. Contrarily, lower values for the derivative count rate means that the sample is composed of small particles or/and has a low concentration. This parameter is sometimes more important than the value of the particle size. If there is partial destruction of micelles, the mean size value given by the DLS equipment could be the same, since the equipment compensates the less light transmitted by the sample making more effort in terms of attenuation to continue to read the signal. However, when the solution presents less amount of particles the value of the derivative count rate will be lower because a lower response reaches the detector. Figure 3. 15 shows the derivative count rate for PEG_{2k}-BHETE-PLA_{2k} micelles irradiated with a red light in the presence of different PSs.
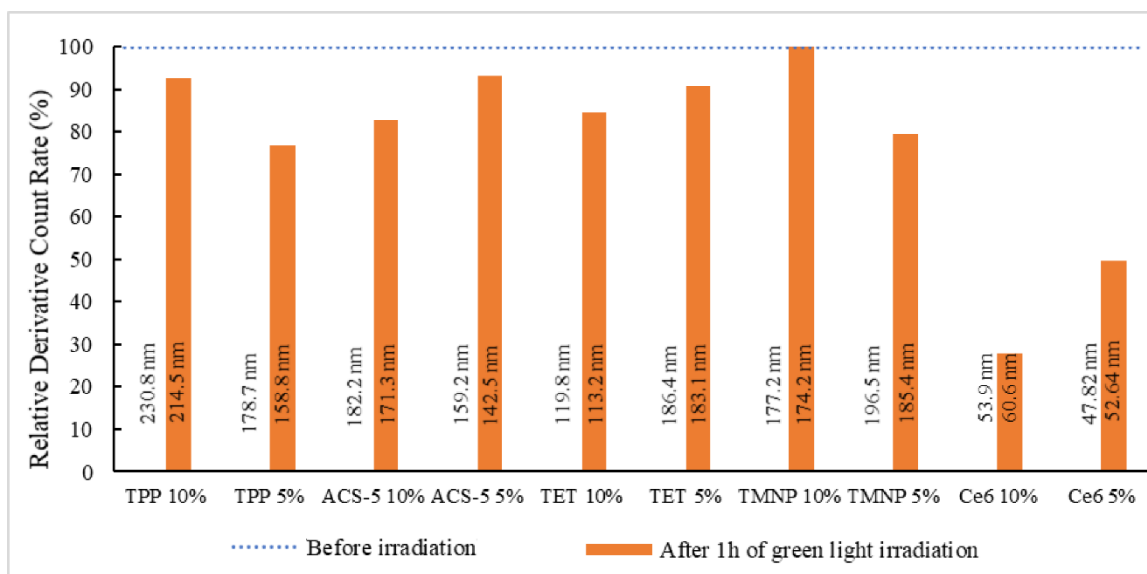
Figure 3. 15 Derivative count rate before and after irradiation of micelles' solution with different PSs. The hydrodynamic size of micelles is shown outside (before irradiation) and inside the bars (after irradiation). *The Ce6 sample was irradiated with a red light. PS structures are shown in Figure A 9 in the appendix.

The derivative count rate of the samples showed in Figure 3. 15 presents a decrease after irradiation. This reduction might indicate the disassembly of micelles after irradiation, evidencing that the number of micelles in the solution was reduced after $^1O_2$ generation by the encaged PS [138], [202], [210], [232]. The decrease in the derivative count rate of the micellar solution with the Ce6 entrapped was more drastic when compared with other samples, probably due to the higher $^1O_2$ quantum yield of this second generation photosensitizer (Appendix, Figure A 10) [181]. Furthermore, Ce6 is frequently used in PDT because: 1) strongly absorbs at the NIR window (around 670 nm); 2) accumulate more effectively in tumors' tissues; 3) rapidly clears from organism [233].

With the aim of evaluating the amount of Ce6 that is encapsulated in micelles, a calibration curve for Ce6 in DMSO was determined. Table A 1 in the appendix shows the values for the calibration curves corresponding to the absorption values and its respective R^2.

The loading capacity of Ce6 was evaluated using the sensitive copolymer PEG$_{2k}$-BHETE-PLA$_{2k}$ based on the calibration curve and this micelle showed a DLC of ~1.7%. The amount of ROS species generated by Ce6 is a key element for the success of the micelle's destruction. Hence, the Ce6 content in micelles needs to be carefully selected. The minimal amount of Ce6 used, to ensure the disassembly of micelles, was evaluated by analyzing the change in the derivative count rate before and after 2 hours of red-light irradiation. The variable mass of the Ce6 used in the experiments is expressed by the initial amount of Ce6 and the amount of used polymer (Figure 3. 16).

98
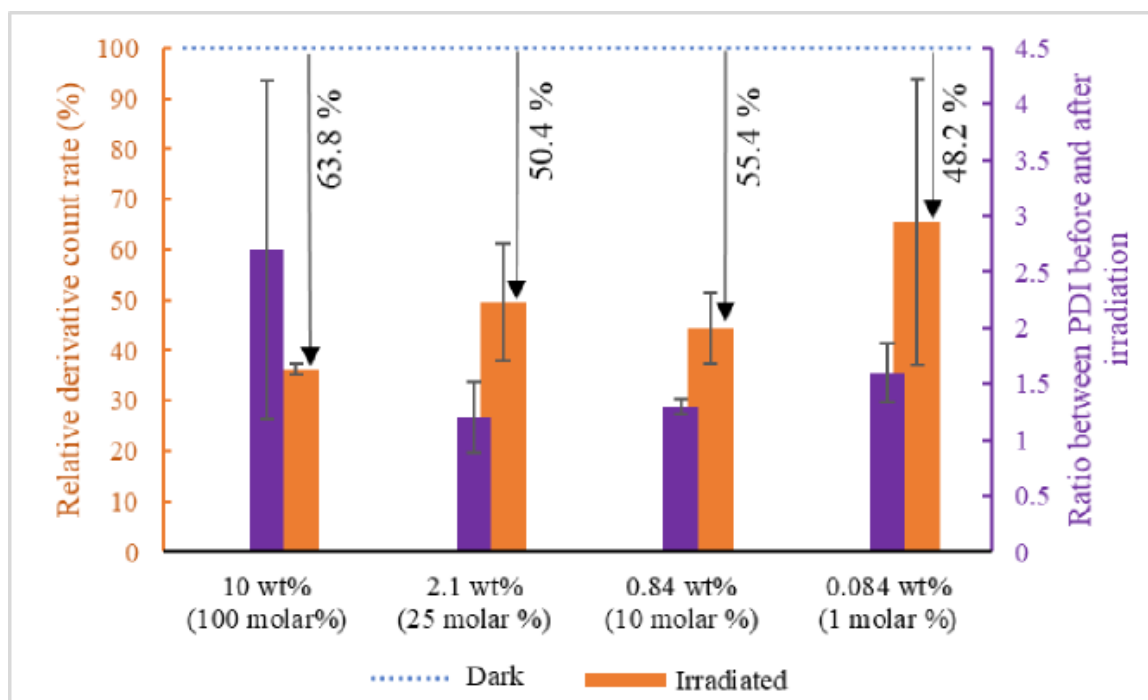
Figure 3. 16 Relative derivative count rate of DLS measurements of micelles after 2 hours of irradiation by red light (650 nm, 80 mW.cm^2), with different amounts of Ce6 (% relatively to mol or weight of polymer). The arrows indicate the percentual of the relative count rate decrease after irradiation. PDI increase after irradiation are also indicated in the graphic.

As expected, in dark conditions micelles seems stable. After irradiation, micelles with Ce6 quantities varying from 100 to 10% of the molar amount of the polymer showed a significant decrease in the derivative count rate until 63.8% of the initial value. However, when the quantity of Ce6 used is reduced to 1%, the decrease in the derivative count rate is 48.2%. The PDI is another parameter which can indicate micelles' disruption. The increase in the PDI value represents a broader distribution of micelles' size. Also, the increase in the PDI relative ratio after light irradiation indicates the occurrence of some disassembly of the micelles. Thus, considering the pronounced decrease in the derivative count rate, the increase in the PDI value after irradiation and the balance in Ce6 amount/cost, a Ce6 molar amount of 10% was selected for the next experiments.

The comparison of the hydrodynamic size of the micelles with different contents and their derivative count rate, before and after irradiation, are shown in Figure 3. 17.
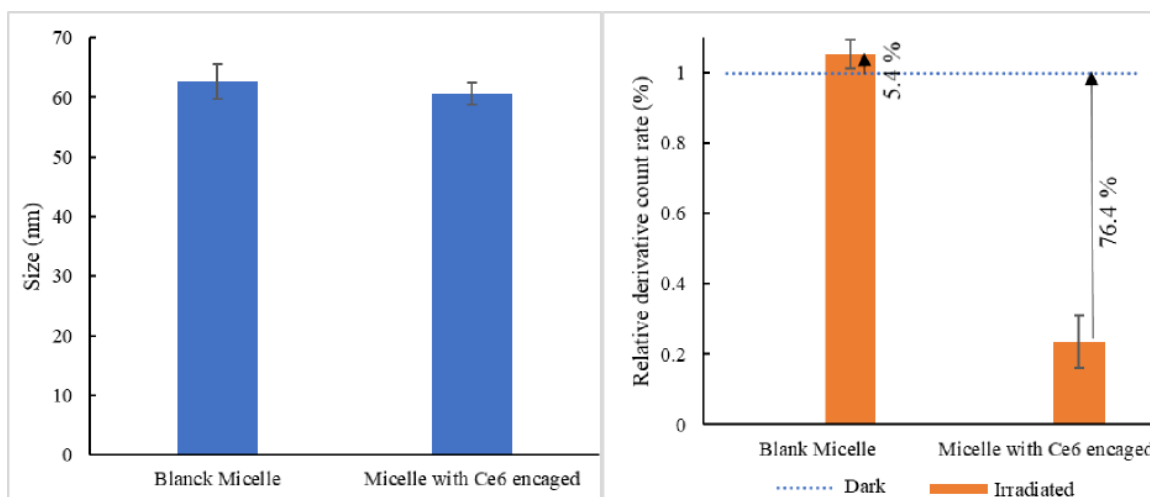
Figure 3. 17 DLS results for PEG_{2k}-BHETE-PLA_{2k} micelles formed by dialysis method. (a) The average hydrodynamic size of micelles according to the encaged compounds. (b) The relative decrease of derivative count rate for micelles under dark and irradiation (2 h of red light) conditions (the arrow and data indicate the percentage of decrease/increase of the derivative count rate).

From Figure 3. 17 (a) it is clearly noted that micelles with the encapsulated Ce6 do not show a significant difference in the hydrodynamic size when compared to bare micelles. After irradiation, only micelles with Ce6 encaged showed a reduction in the derivative count rate (Figure 3. 17, b). As the decrease in the derivative count rate can be directly related to the decrease in micelles' concentration, these values prove the disaggregation potential of the sensitive micelles [138], [210].

The same approach was adopted to other sensitive copolymers. The prepared micelles with Ce6 and DOX were analyzed before and after irradiation. Figure 3. 18 and Table 3. 6 show the DLS results.
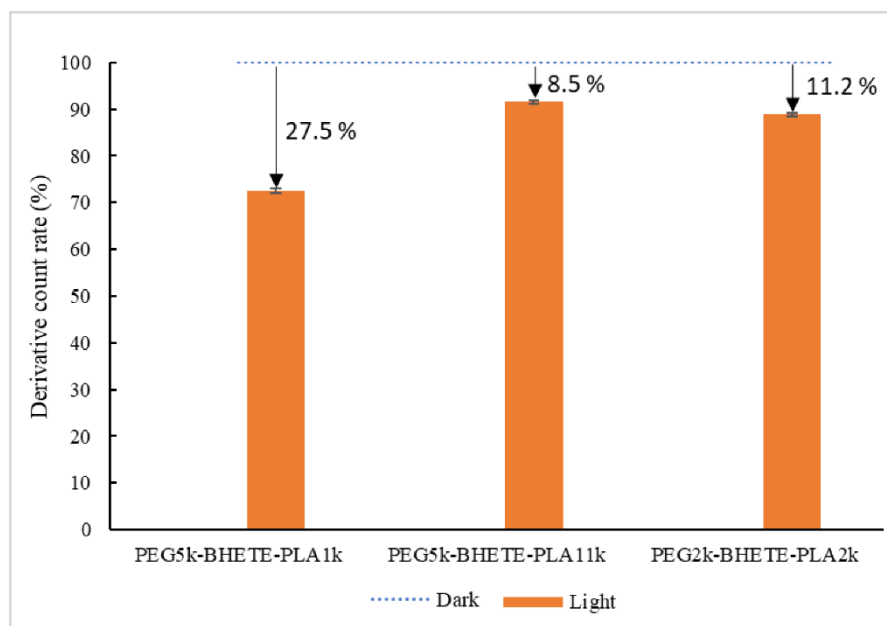
Figure 3. 18 The relative decrease of derivative count rate for micelles under dark and irradiation (30 min of red light) conditions. The arrows highlight the decrease percentage of the derivative count rate.

Table 3. 6 The hydrodynamic size of micelles before and after 2 h of red-light irradiation.

Copolymer	Parameters	Dark	Irradiated
PEG_{2k}-BHETE-PLA_{2k}	Ave Size (nm)	188.2 ± 2.466	164.5 ± 5.268
	PDI	0.165 ± 0.02	0.239 ± 0.021
	Ave Deriv Count Rate (%)	100	54.68
PEG_{5k}-BHETE-PLA_{1k}	Ave Size (nm)	162.7 ± 5.927	165.5 ± 3.024
	PDI	0.136 ± 0.038	0.180 ± 0.039
	Ave Deriv Count Rate (%)	100	26.53
PEG_{5k}-BHETE-PLA_{10k}	Ave Size (nm)	52.46 ± 0.7004	49.77 ± 1.571
	PDI	0.137 ± 0.007	0.171 ± 0.003
	Deriv count rate (%)	100	64.84

After irradiation, the hydrodynamic size of the micelles shows only a slight difference, but the PDI number increases significantly, which proves the increase in the dispersibility of micelles' size, due to a broader size distribution after irradiation. Complementary to these results, the derivative count rate decreases abruptly after irradiation of micelles. The increase in PDI and decrease in the derivative count rate indicate the disaggregation of micelles triggered by light. The fact that the size is preserved, with almost the same value, could indicate that only remained in the solution micelles that do not degrade and maintain their integrity.

Figure 3. 19 shows the kinetics of micelles' disassembly during light irradiation, measured by the value of the derivative count rate.
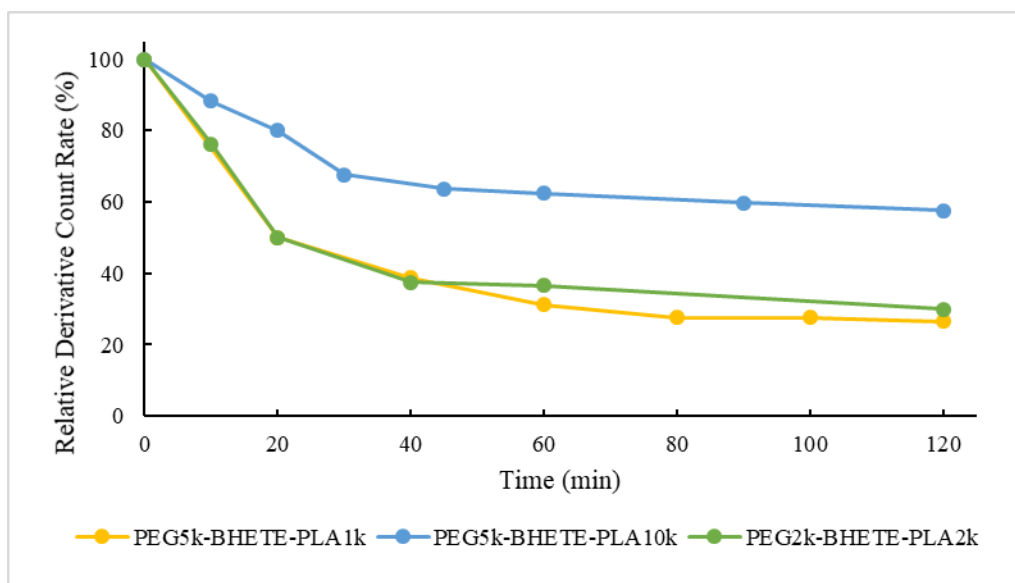
Figure 3. 19 Relative derivative count rate versus irradiation time (red light beam) of sensitive micelles (from different sensitive copolymers) containing Ce6 formed through the dialysis method and DMSO as solvent.

The count rate of the assay decreases with the irradiation time, indicating the reduction in the concentration of nanoparticles due to the disassembly processes [210]. The more prominent decrease of the derivative count rate after the first 20 minutes of irradiation is for PEG_{5k}-BHETE-PLA_{1k} and PEG_{2k}-BHETE-PLA_{2k}. Taking this result into account, these copolymers might have the burst release potential of the nanoparticle activated by light [133]. The disassembly kinetics could be directly related to the length of the hydrophobic block (the micelle core). The smaller molecular weight micelles showed a faster disassembly kinetic profile. This might occur because the smaller length can favor the proximity of the PS and the BHETE sensitive linker.

The disaggregation of micelles activated by light was also confirmed by TEM analysis. Figure 3. 20 and Figure 3. 21 show TEM images of PEG_{2k}-BHETE-PLA_{2k} and PEG_{5k}-BHETE-PLA_{1k}, respectively, before and after irradiation.

102
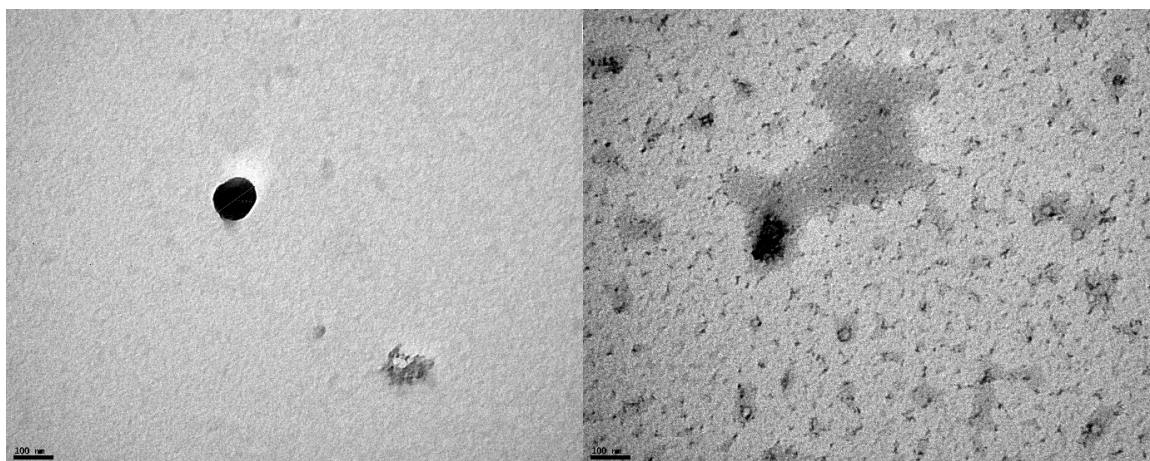
Figure 3. 20 TEM images of PEG$_{2k}$-BHETE-PLA$_{2k}$ before (left) and after (right) red light irradiation (2 h, 650 nm, 80 mW.cm^{-2}).
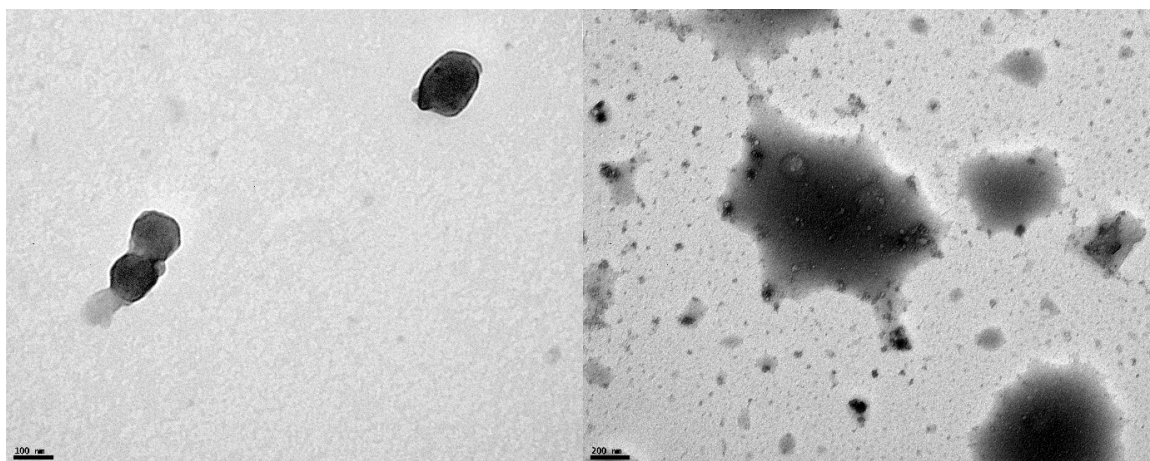
Figure 3. 21 TEM images of PEG$_{5k}$-BHETE-PLA$_{1k}$ before (Left) and after (right) red light irradiation (2 h, 650 nm, 80 mW.cm^{-2}).

TEM images show the spherical aggregated nanoparticles (left image in Figure 3. 20 and Figure 3. 21), however, after micelles underwent the red-light irradiation, the images show smaller particles, disaggregated nanoparticles and small fragments. The TEM image confirms the ability of the nanoparticles to disaggregate through light-stimuli [133].

Another proof for the changes occurring in micelles after irradiation came from NMR experiments. The presence of micellar structures difficult the NMR excitation and the relaxation phenomena of the polymers in the inner core, as well as part of PEG that could be inside the micelle [105], [215]. After excitation, the integration values of the signals corresponding to the polymers must be close to original signals obtained in CDCl$_3$. A solution of PEG$_{5k}$-BHETE-PLA$_{10k}$ micelles in H$_2$O with encaged Ce6 was divided into two equal volumes, one solution was subjected to 2 h of red-light irradiation and other was kept in the dark. The two samples were freeze-dried and resuspended in D$_2$O. Both

103

solutions were analyzed by NMR spectroscopy. Figure 3. 22 shows the NMR spectrum of the two samples.
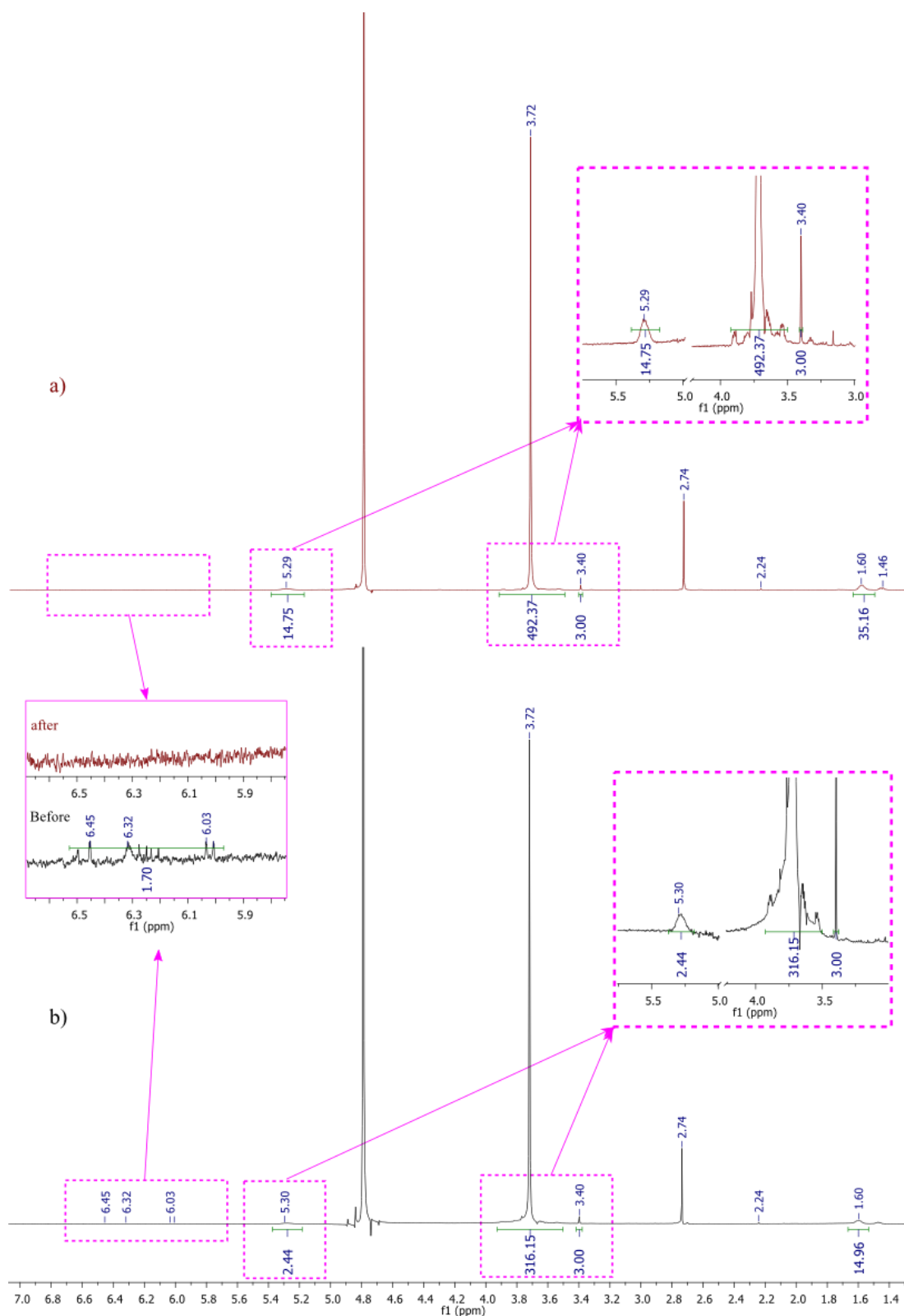
Figure 3. 22 ^{1}H NMR (400 MHz, D$_2$O) spectra of PEG$_{5k}$-BHETE- PLA$_{10k}$ micelle after (a) and before (b) red light irradiation (2 h, 650 nm, 80 mW.cm^{-2}).

The resonance of PEG methyl protons (3.45 ppm) was used as a reference peak. Taking this reference peak, the calculated PEG's molecular weight for the sample before irradiation is ~3.5k. Taking into account that we started with a ~5k PEG sample, this difference is due to the PEG that is incorporated in micelles in a form that is not able to be excited. The same phenomenon occurs for the PLA block, the NMR of the sample before irradiation showed a molecular weight of ~0.17k instead of 10k, which is the value obtained by NMR in chloroform. This proves that almost all the PLA is inside micelles, not sensible to NMR excitation. After irradiation, the size of the PEG calculated from the same signal gives a molecular weight of 5k, which is the expected value. The integration signals for the PLA also increases indicating a molecular weight of PLA of 1k. This is not the original value (10k) but the reason could be the insolubility of PLA in the solvent (D_2O) [105], [215]. The solution, which underwent irradiation, showed no signal of the sensitive segment at the region of 6.5 to 6 ppm and the resonance peak of PEG and PLA present a higher intensity when compared to the reference signal (**CH**$_3$-PEG at 3.40 ppm). This suggests that the micellar structure is in a broader organization, allowing the excitation of a higher number of protons. The NMR results indicate that the break in the sensitive linker occurs but may not be enough to completely destabilize the micelle's structure.

3.1.5 Drug Loading Studies

Drug loading capacity (DLC) and drug loading efficiency (DLE) are important parameters in drug delivery systems and are highly dependent on the polymer structure and its interaction with the drug [234].

The ability of micelles to encapsulate the drug was evaluated using DOX as a drug model. The DLC of DOX in the micelle was estimated through a calibration curve of the DOX solution in DMSO. The DOX solution was diluted several times in order to construct a library of DOX concentrations and fluorescence intensity (Figure A 11 in appendix). The value of the maximum fluorescence intensities emitted for each sample was traced in a chart versus DOX concentration (Figure A 12 in appendix).

The DLC and DLE of micelles were calculated using the equation of the linear fitting of the calibration curve (Figure A 12; y=423320.x -56.069). Sensitive polymers with different chain lengths were used in the micelle formation to evaluate the influence in the DLC of the nanoparticle. Figure 3. 23 shows the graphic of the average DLC of each micelle.
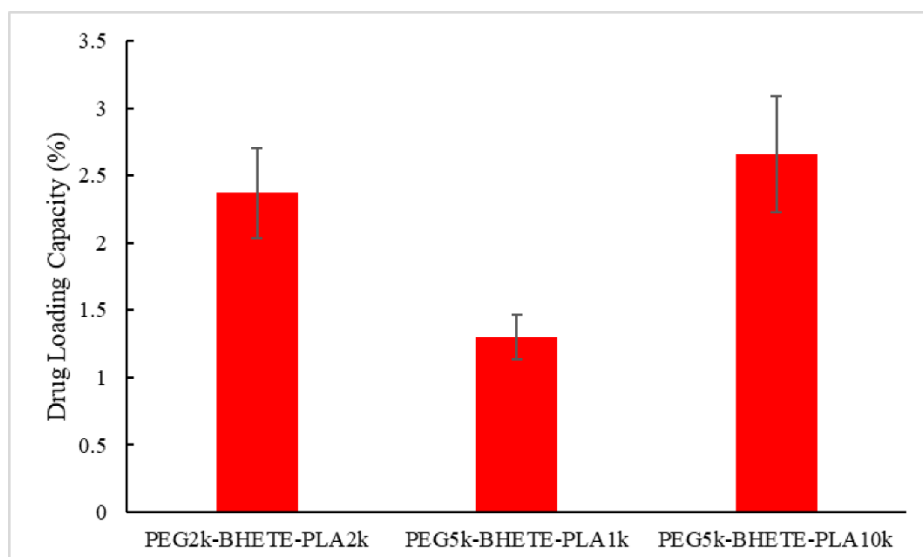
Figure 3. 23 The average drug loading capacity of polymers with different sizes.

The DLC of micelles has a significant variation with the changes in the polymer chain length (ANOVA analysis for the average DLC, a p-value of $1.62*10^{-6}$). The decrease in the molecular weight of the hydrophobic block reduces the DLC. The phenomenon of the physical entrapment of a hydrophobic drug, in the inner core of micelles, is predominantly driven by the interactions between the polymer hydrophobic block and the drug. The PLA compatibility with poorly water-soluble drugs depends, mainly, on the similarity of their structures, polarity and the PLA size [234]. Thus, the increase in the PLA block of the synthesized micelles enhances the hydrophobic interaction with the hydrophobic drug, favoring the encapsulation in the micellization process [48]. The DLC value of the sensitive PEG-PLA micelles agrees with the literature, as shown in Table 3. 7.

Table 3. 7 Literature DLC values of PEG-PLA micelles.

Polymer	DLC (%)	Ref
$(PEG_{1.1k})_3$-PLA_{10k}	5	[46]
PEG_{2k}-PLA_{3k}	2.59	[48]
PEG_{5k}-PLA_{3k}	2.79	
PEG_{2k}-PLA_{5k}	4.65	
PEG_{5k}-PLA_{5k}	3.20	
PEG_{5k}-$PLA_{3.5k*}$	0.9-2.5%	[47]
PEG_{5k}-$PLA_{4.2-5k}$	0.81-2.88	[215]

*Micelles were formed mixed with poly(hydroxypropyl methacrylamide-g-α-tocopheryl succinate)15k in a different ratio

Additionally, the DLE could be a critical factor in micelle systems, especially in the case of expensive drugs as DOX. In order to analyze the DLE of nanoparticles, the micellization process was carried out with DOX amount ranges from 0.5 to 100 wt% of the weighted polymer. Figure 3. 24 shows the DLE results for PEG_{5k}-BHETE-PLA_{1k}.

106
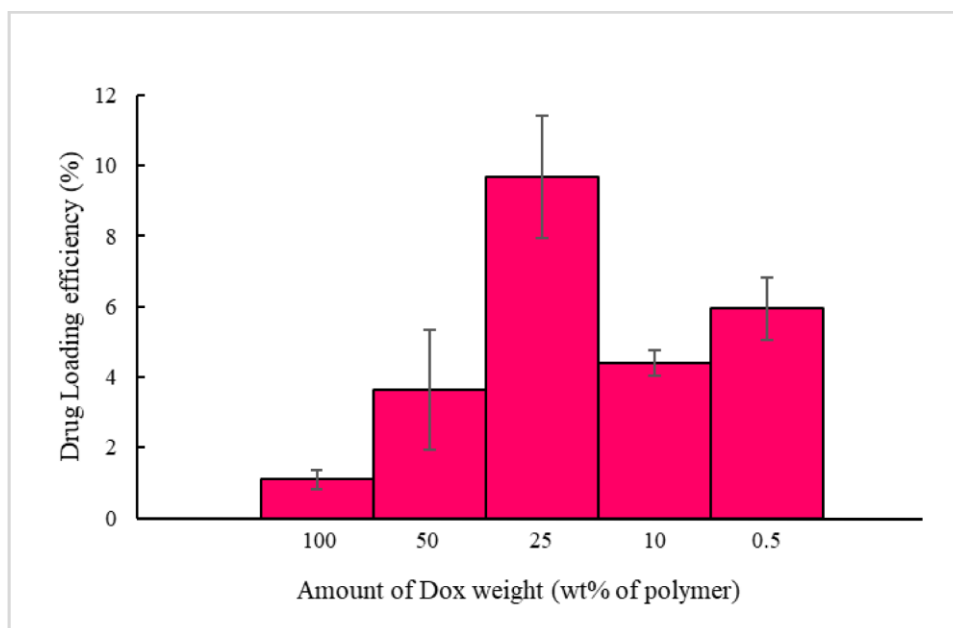
Figure 3. 24 The average drug loading efficiency of PEG$_{5k}$-BHETE-PLA$_{1k}$ micelles.

The most efficient encapsulation occurred when the DOX weight represents 25 wt% of the total polymer mass, showing a DLE of 9.66%, that is almost 9 times higher than micelles formed in the presence of 100 wt% DOX. These results and the appearance of color in the filtered material may indicate high insolubility of DOX and a great tendency to agglomerate during particle formation. The corresponding DLCs for micelles were 1.08 ± 0.27%, 1.82 ± 0.85%, 2.34 ± 0.54%, 0.44 ± 0.04% and 0.30 ± 0.04%, respectively. The conditions that give the highest DLE correspond also to the high value of DLC.

Additionally, the influence of Ce6 in the DOX encapsulation was evaluated. No expressive differences were verified in the average DOX encapsulation capacity and efficiency between micelles with and without Ce6 encaged in the inner core (ANOVA analysis of average values, a p-value of p=0.312, Figure A 13 in appendix). However, the amount of the average Ce6 entrapped in the micelle increased with the presence of DOX in the inner core of the nanoparticle (Figure A 14 in appendix). This factor indicates that the co-loading of the two hydrophobic moieties (Ce6 and DOX) is not conflicted. The observed values are in agreement with the values reported in the literature for the drug loading capacity of PEG-PCL micelles [134], [206].

3.1.6 Drug Release

At this phase, the results point to PEG$_{5k}$-BHETE-PLA$_{1k}$ micelles with better cleavage kinetics and PEG$_{5k}$-BHETE-PLA$_{10k}$ micelles with better DLC. Therefore, both

micelles were analyzed through the fluorimeter technique to evaluate the drug release profile, using DOX as a drug model. The amount of DOX encapsulated was measured by fluorescence, using the maximum intensity absorbed and the equation of linear fitting in the DOX calibration curve (see Figure A 11 and Figure A 12 in Appendix). To prove the drug release ability of the system, the sensitive micelles encapsulating DOX were subjected to irradiation and the DOX release profile was evaluated. For comparison purposes, the DOX release profile of non-irradiated micelles was also studied.

After irradiation, the kinetics of the drug release from micelles should increase due to the disaggregation of micelles and consequently triggering the DOX release from the inner core of the micelle.

The average profile of the kinetics release of the DOX from micelles subjected to light, and the control samples (micelles solutions kept in the dark) were measured through dialysis against water at 37°C, and the profiles are shown in Figure 3. 25 and Figure 3. 26.
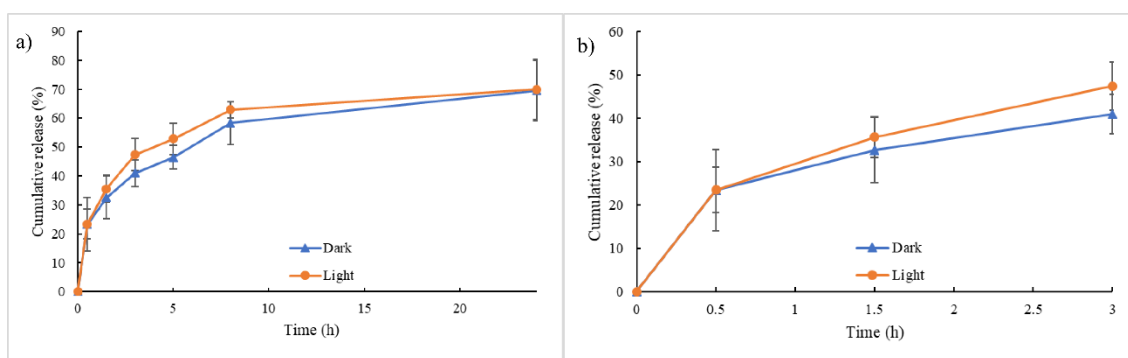
Figure 3. 25 Profile of the release kinetics of the Dox from PEG_{5k}-BHETE-PLA_{1k} sensitive micelle (a) and a zoom of the first 3 h (b). Experiments were carried out by dialysis against water at 37°C.
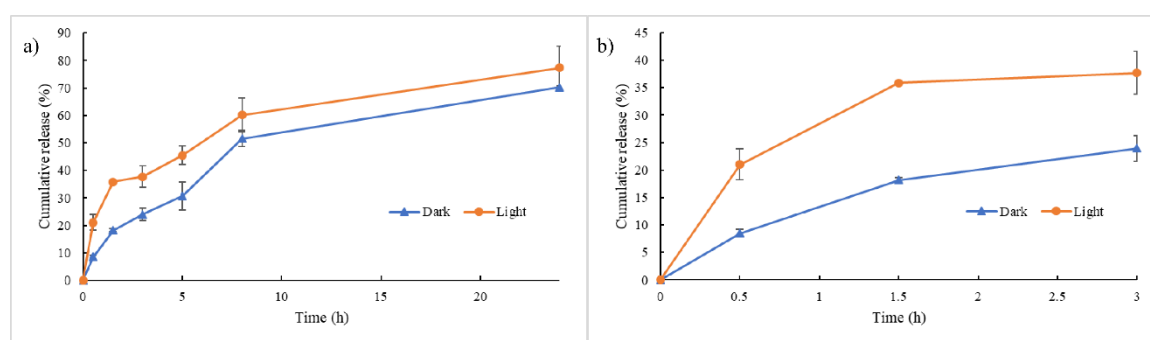
Figure 3. 26 Profile of the release kinetics of the Dox from PEG_{5k}-BHETE-PLA_{10k} sensitive micelle (a) and a zoom of the first 3 h (b). Experiments were carried out by dialysis against water at 37°C.

All samples showed similar behavior for 24 h of release, 70-80% of the encaged DOX was released even for the control sample. The micelle structure is a permeable system and because of that, after a period of time, the drug is released through permeation from the inside of micelle to the exterior [235]. Our developed micelles have the goal to increase

108

the release of drug at a certain moment by using light as a trigger. In this way, we were expecting an increase in the drug release in the first moment after the irradiation of the micelle system. The zoom in the PEG$_{5k}$-BHETE-PLA$_{10k}$ micelles graphics for the first 3 h of dialysis (Figure 3. 26 b) showed a more prominent difference between the irradiated and control samples. The burst release of DOX in the first 30 min from the irradiated samples is justified by the destabilization of the micelles induced by the light. The cleavage of the sensitive segment in each polymer chain leads to the destruction of the amphiphilic character, culminating in the disaggregation of micelles. PEG$_{5k}$-BHETE-PLA$_{10k}$ showed a cumulative DOX release value of 12.5% higher for the irradiated sample (Figure 3. 26). The PEG$_{5k}$-BHETE-PLA$_{1k}$ micelle (Figure 3. 25) showed no significant difference between the irradiated and control samples. The PEG$_{5k}$-BHETE-PLA$_{1k}$ micelle behavior can be justified due to the lower PLA molecular weight, which promotes a rapid release of the drug by disassembly or a more easy diffusion of the DOX [234].

3.1.7 Cellular Studies

For cellular studies, the PEG$_{5k}$-BHETE-PLA$_{10k}$ micelles were synthesized as previously described. After preparation and for better convenience, micelles were used as freeze-dried samples. The micelles used in this stage have the following compositions (Table 3. 8):

Table 3. 8 Amount of polymer and therapeutics used in micelle preparation.

Sample	Polymer (mg)	DOX (mg)	Ce6 (µg)
PEG-BHETE-PLA-DOX-Ce6	10	2.5	40
PEG-BHETE-PLA-DOX	2.8	0.7	-
PEG-BHETE-PLA-Ce6	2.8	-	11.14
PEG-BHETE-PLA	2.8	-	-

Cellular Uptake

A critical factor in the application of nanoparticles as drug delivery systems lies on the cellular internalization. For a safer and efficient treatment, it is important for the therapeutic to be delivered inside the cell's membrane [236]. Due to the fluorescence present in the DOX molecule, its internalization can be evaluated by spectrofluorometry. The cell's membrane is disrupted by an organic solvent which also solubilizes the DOX content. By comparative analysis, the fluorescence of the solution indicates the concentration of the DOX in cells.

The calibration curve of DOX in DMSO was done, in triplicate, and is shown in Figure A 15 and Figure A 16 in the appendix. Table A 2 in the appendix shows the equation of the linear fitting.

To analyze the transportation of DOX to cells mediated by micelles, an uptake assay was carried out and a concentration of 5 μM for the encapsulated DOX was used. The DOX concentration inside cells was measured using maximum intensity of DOX fluorescence (at 591 nm) and taking into account the calibration curve. Figure 3. 27 shows the DOX uptake for each treatment condition for an MCF7 cell line.
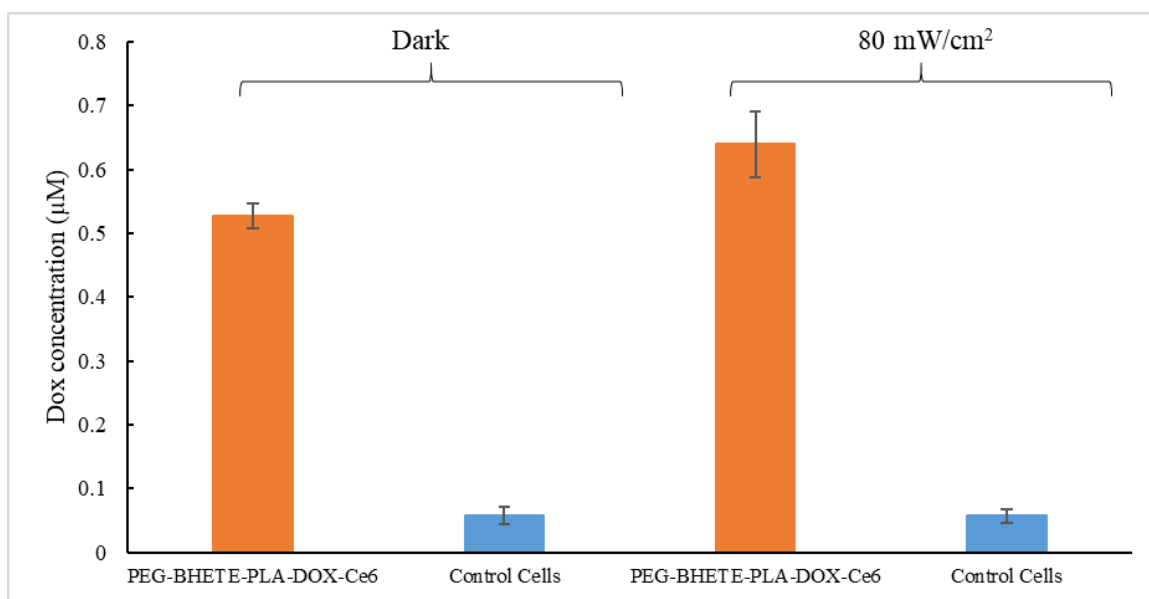
Figure 3. 27 Quantitative studies of average DOX cellular uptake measured by spectrofluorometer at 480 nm under dark and light conditions. In both assays, the cells without therapeutics were used as control. The data bar represents the mean concentration of DOX (N=3) and the error bar.

The uptake assay proves that both DOX (Figure A 17) and PEG-BHETE-PLA-DOX-Ce6 can seep through the cell wall and achieve the cytoplasm of the cells. The light irradiation experiment showed a slight increase in DOX. This is also shown by Pei *et al.* study [237], where thioketal micelles showed a faint difference for DOX content for irradiated and dark MDA-MB-231 cells. The cells treated with free DOX showed a superior DOX uptake than cells treated with the PEG-BHETE-PLA-DOX-Ce6 micelles. This fact could be explained since, in encapsulated form, only 80% of DOX is released after 24 h. Moreover, is important to notice that the PEG shell can hinder the cellular uptake [238]. Sanchez *et al.* [239] showed that the PEG coat reduces cellular internalization from ~ 77% to 23%. This effect is known as PEG dilemma, that improves blood circulation time by avoiding the opsonization (the hydrous character act as a shield to block protein absorption), but also restricts drug internalization by cells. Hence, these results reveal that

DOX can achieve the cytoplasm or nucleus cell, probably due to the light-triggered drug release.

Cytotoxicity assays

The analysis of the *in vitro* cytotoxicity on cell lines can be evaluated through a range of assays and among them are the colorimetric assays, such as, 3-(4,5-dimethythiazol- 2-yl)-2,5- diphenyl tetrazolium bromide (MTT) and the sulforhodamine B (SRB).

The MTT assay evaluates the therapeutics cytotoxicity through the determination of metabolic activity. It measures the conversion of MTT into formazan crystals by the living cells. The NAD(P)H-dependent oxidoreductase enzymes present in the cellular mitochondria reduce the MTT to a deep purple and an insoluble crystalline product, formazan. The absorbance of the dissolved crystals is measured at 570 and 620 nm and indicates the metabolic activity of cells, since the MTT reduction can only occur in metabolically active cells. The level of activity is related to viable cells, giving a measurement of the cellular viability [240].

Three independent experiments were performed in triplicate, as shown in Figure 3. 28.
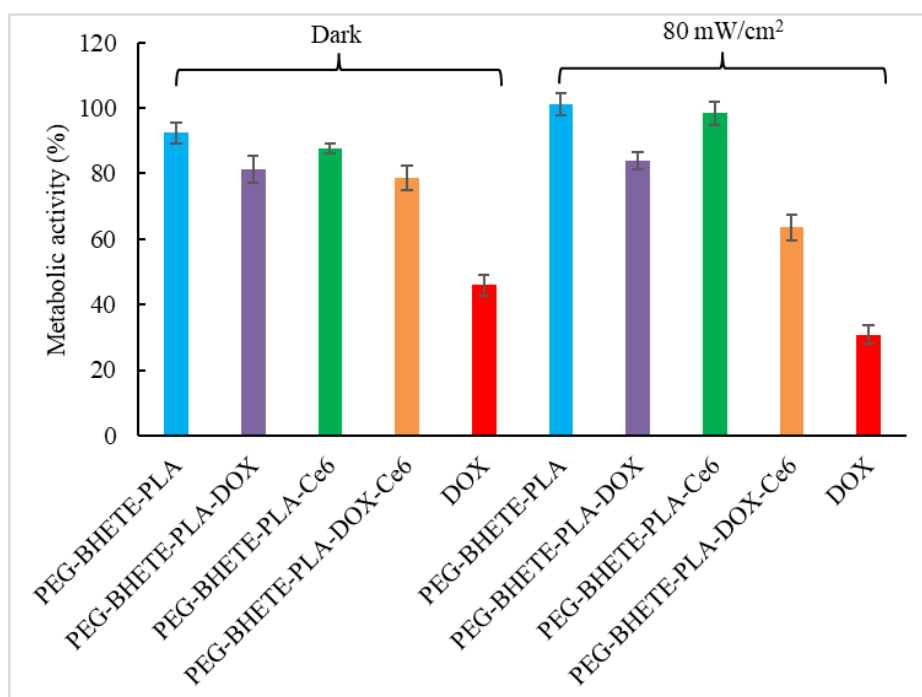
Figure 3. 28 Cell viability of the MCF7 cell line incubated for 24h, after irradiation. Metabolic activity of cells (MTT assay) treated with: free DOX (red), PEG-BHETE-PLA-DOX-Ce6 (orange), PEG-BHETE-PLA-Ce6 (green), PEG-BHETE-PLA-DOX (purple) and PEG-BHETE-PLA (blue) in two different conditions, irradiated and in the dark. Data bars show the mean metabolic activity (N=3) and the error.

Cells treated with PEG-BHETE-PLA and PEG-BHETE-PLA-Ce6 showed no reduction in the mean metabolic activity, evidencing the non-cytotoxicity character of these micelles. Also, the presence of the PS in PEG-BHETE-PLA-Ce6 micelles showed no significant decrease in the metabolic activity of cells submitted to red light irradiation, this occurs because of the low amount of Ce6 in micelles. Cells treated with PEG-BHETE-PLA-DOX showed cytotoxicity in both conditions, under light, and in the dark. Micelles are permeable nanoparticles and the release of DOX is expected even without the light triggering the disassemble of micelles. MCF7 cells treated with PEG-BHETE-PLA-DOX-Ce6 showed a reduction of mean metabolic activity when subjected to light when compared with the dark conditions. Free DOX showed a higher reduction in mean metabolic activity. This fact could be explained due to the incomplete release of DOX content from micelles (in the drug release assay, only 69-80% of DOX was released past 24 h).

The SRB assay determines the drug-induced cytotoxicity and cell proliferation based on the cellular protein content. The SRB is a bright pink aminoxanthene dye with two sulfonic groups that (stoichiometric) bind to basic amino acid residues of proteins (under basic conditions) and then can be extracted using basic conditions. The absorbance of the SRB is measured at 560 and 580nm. As the dye is only carried in attached cells, the amount of bound dye can provide a sensitive linear response with the number of cells and the cellular protein measured [241].

Even though MTT and SRB have slight differences in the cellular viability measurement, they are complementary techniques for this study.

Figure 3. 29 shows the SRB assay for MCF7 cells after treated with therapeutics, kept under dark or irradiated at 80 mW.cm^{-2}.
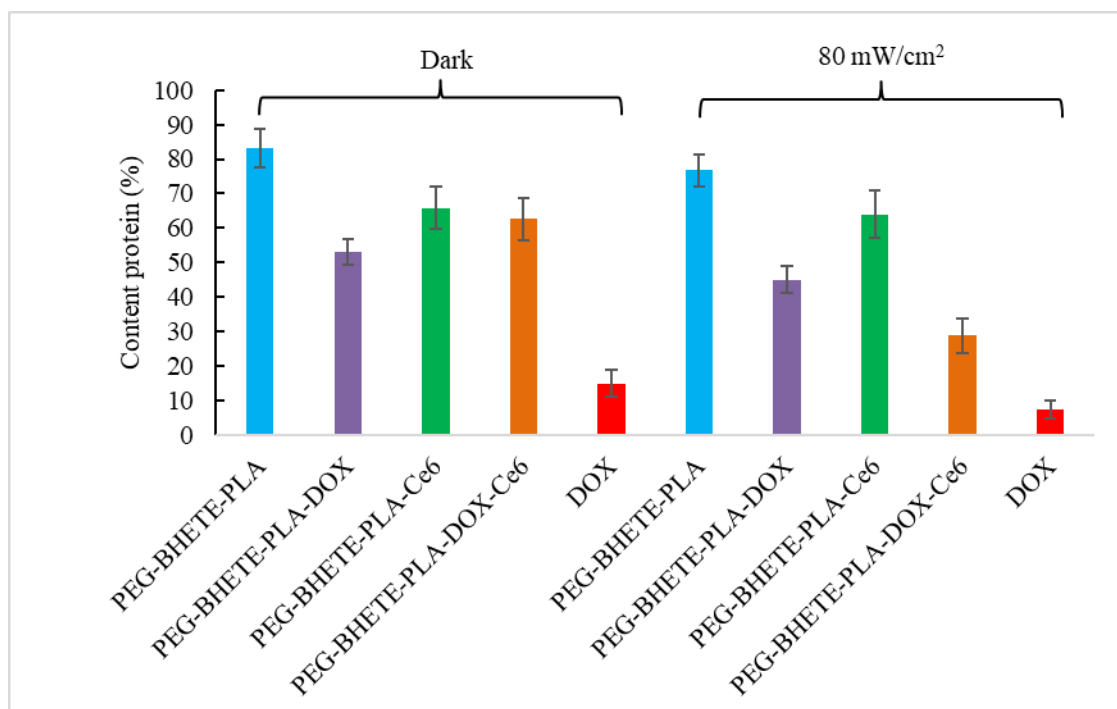
Figure 3. 29 Cell viability of MCF7 cell line (SRB test) after treatment with the therapeutics (2.5 µM). The content protein of cells treated with: DOX free (red); PEG-BHETE-PLA-DOX-Ce6 (orange); PEG-BHETE-PLA-Ce6 (green), PEG-BHETE-PLA-DOX (purple) and PEG-BHETE-PLA (blue), followed by irradiation (10 min with a light intensity of 80 mW.cm^{-2}) or dark conditions. Data bars show the mean content protein (N=3) and the error.

The SRB results confirm the results obtained in the MTT assay which shows that PEG-BHETE-PLA is non-cytotoxic for the cells. The cells treated only with DOX showed a higher reduction in the mean protein content. For MCF7 cells treated with PEG-BHETE-PLA-DOX-Ce6, the reduction in the mean protein content increased for the irradiated samples.

Cell images

In order to visually analyze the behavior of the cells before receiving the therapeutics dose followed by irradiation or kept in the dark, cell images were taken. When the adherent cells (MCF7) present a spread form, they are characterized as living cells, however, when they show a smaller and spherical form, it is indicative of apoptosis and cell deformation.

After treatment with PEG-BHETE-PLA-DOX-Ce6 micelles or DOX free, cells were analyzed by optical microscopy. The images of the cells are shown in Figure 3. 30.

113

	DOX	PEG$_{5k}$-BHETE-PLA$_{10k}$-DOX-Ce6	Control Cells
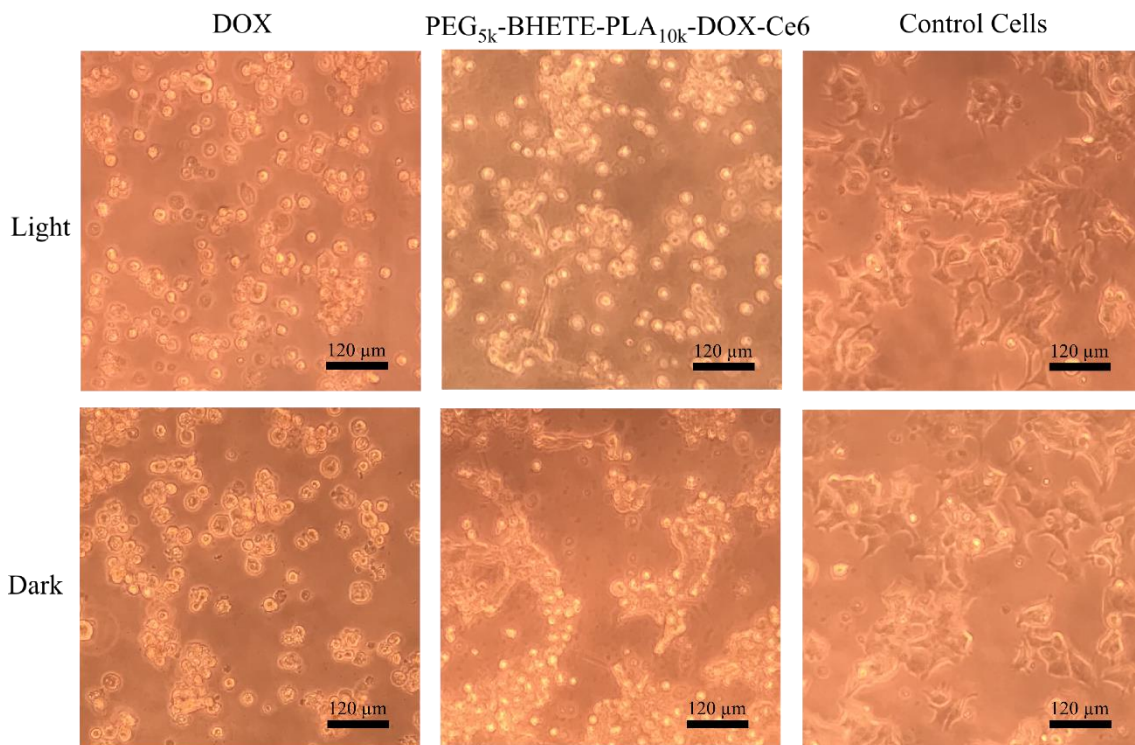
Figure 3. 30 Cell images of the MCF7 cell line after the therapeutics administration, the irradiation treatment and at the end of 24 h of incubation.

In both conditions where free DOX has been dosed, the cells showed spherical form, evidencing the cells' death. This is distinct from the control cells where almost all cells have a spread form, which is characteristic of alive and attached MCF7 cells. Cells treated with PEG-BHETE-PLA-DOX-Ce6 and irradiated exhibit a greater number of cells with a spherical form when compared with cells treated with the same therapeutic but kept in the dark. These pictures evidenced the superior therapeutic effect of the PEG-BHETE-PLA-DOX-Ce6 micelles, that were subjected to the light irradiation and consequently trigger the DOX release.

114

3.2 Preparation of Nanoparticles Based on Light Sensitive Monomers

The results obtained so far with cells and PEG-BHETE-PLA micelles, particularly the observed low effect of light in cellular toxicity, could be explained by the slow DOX release that was observed in preliminary results (Figure 3. 26). This prompt us to develop other more effective release systems based on the sensitive segment.

3.2.1 Synthesis of Poly(1,4-dithio-7,10-dioxa-2-dodecene) (PDDD)

One of the possible reasons for the slow release properties of PEG-BHETE-PLA may be a few numbers of sensitive segments (one per copolymer chain) in the structure. One way to have a faster disaggregation of nanoparticles could be by introducing a higher number of light-sensitive units in the backbone of the polymers [242]. Thus, we hypothesized that the disassembly of the micelles can occur faster if the polymers own more than one sensitive linker moiety per copolymer chain.

A sensitive polymer was synthesized (Scheme 2. 8) using the reaction of the *cis*-1,2-dichloroethene and thiols. Starting from 3,6-dioxane-1,8-octanedithiol and following the protocol for the preparation of BHETE, we obtained the polymeric structure presented in Figure 3. 31.
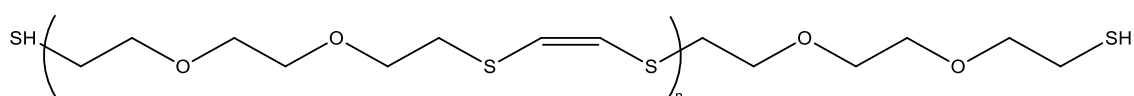
Figure 3. 31 PDDD structure

The polymerization was successful. The divalent monomer can react with the 1,2-cis-dichloroethylene through nucleophilic substitution, leading to the PDDD polymer with a yield of ~50%. PDDD was characterized by FTIR, NMR, and SEC. FTIR spectrum of PDDD is showed in Figure 3. 32.
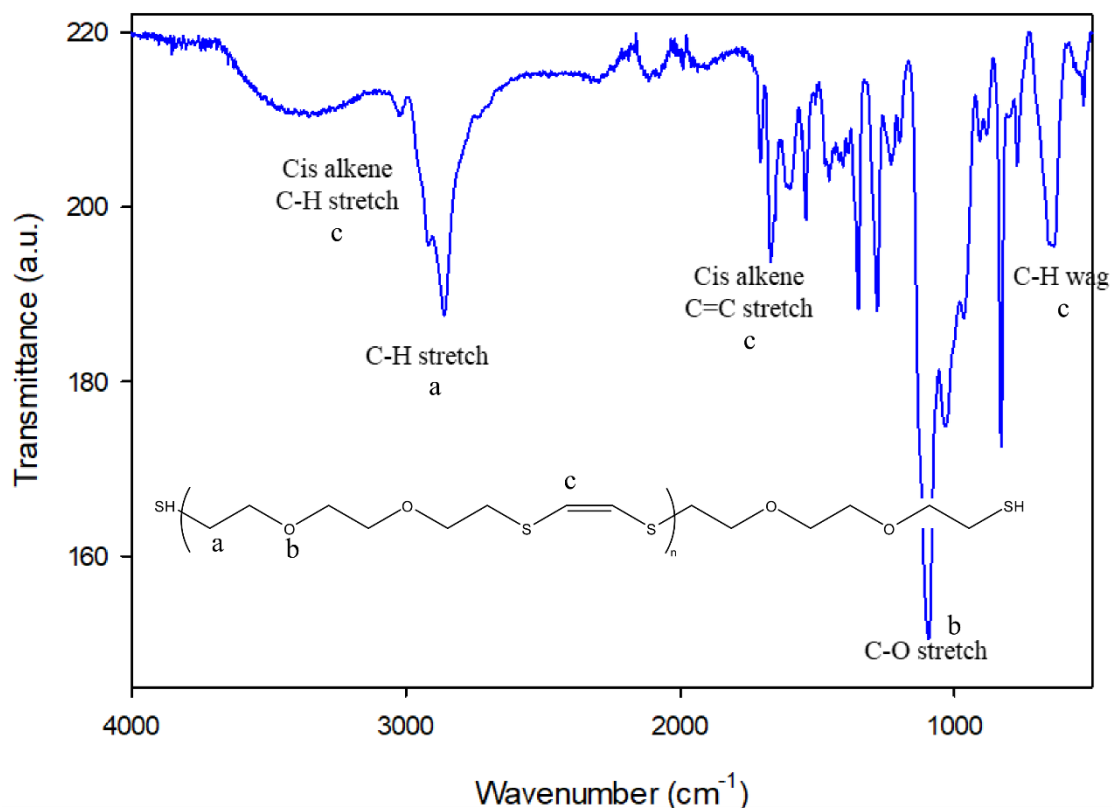
Figure 3. 32 FTIR ATRP of PDDD.

The FTIR spectrum presents the bands of C-H stretch of a *cis* alkene, C-H stretch, C=C stretch of a *cis* alkene, C-O stretch and C-H wag (of *cis* alkene) at 3022, 2847, 1666, 1098 and 631 cm^{-1} respectively, confirming the chemical structure of the PDDD. The ^{1}H NMR spectrum of this polymer is shown in Figure 3. 33.

116
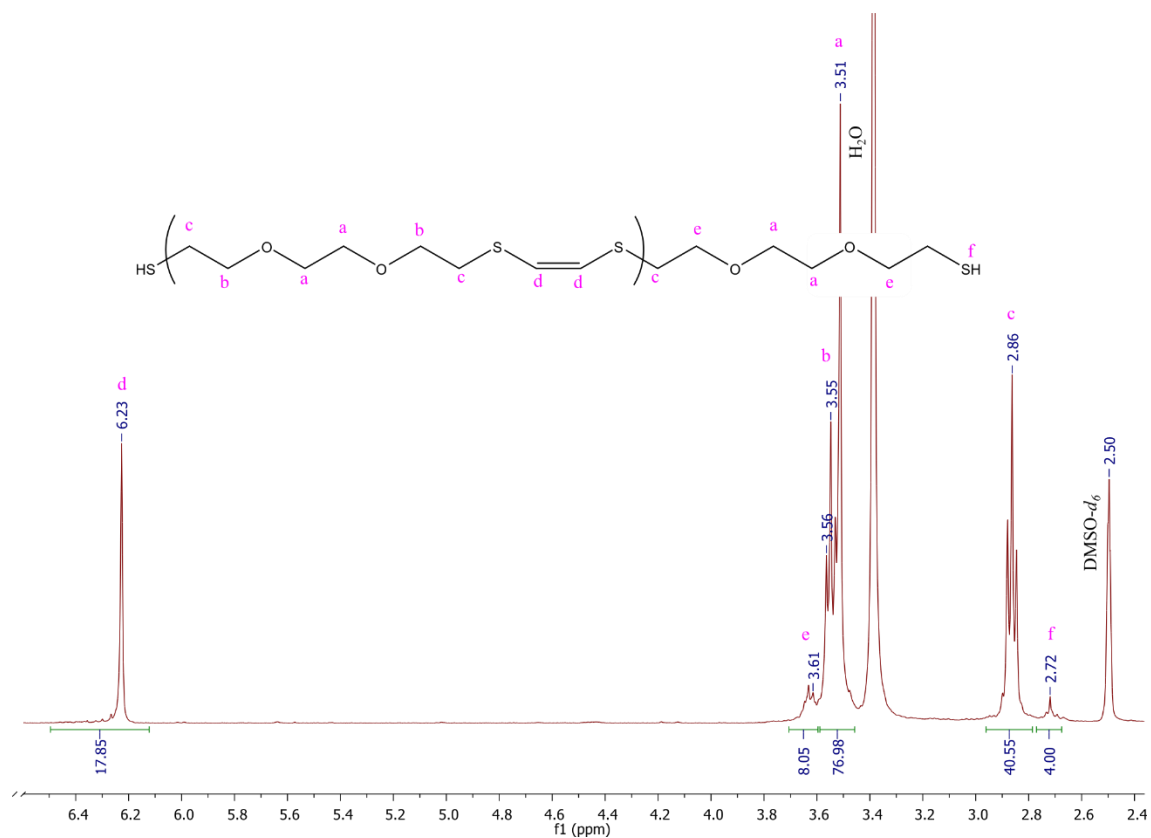
Figure 3. 33 ^{1}H NMR (400 MHz) spectrum of PDDD in DMSO-d_6.

Figure 3. 33 reveals the presence of the sensitive alkene group with a peak at δ=6.23 ppm (-**CH**=**CH**-, **d**). The methylene group of the PDDD, present the chemical shift in the region of 3.8 ppm and 3.4 ppm (-**CH**2-O-C**H**2-, **a** and **b**) and at 3 ppm and 2.8 ppm (-S-**CH**2-, **c**). The thiol proton at the terminal chain showed the signal at δ ~3.61 ppm (-O-C**H**2-, **e**) and at δ ~ 2.72 ppm (SH-C**H**2-, **f**). The molecular weight of the polymer was estimated by comparison of the integration area of the methine group (**d**) and the methylene of the terminal chain (**f**) giving an M$_w$ ~1800 g/mol (9 units).

In order to ensure that the double bond is part of the polymer, a small amount of *cis*-dichloroethene was added to the polymer sample and a new NMR was taken. The signal of the reagent appears at δ = 6.9 ppm, aside from the signal corresponding to the double bond incorporated in the polymer backbone (δ = 6.23 ppm, Figure A 18 in appendix). A ^{13}C NMR spectrum was taken to clarify which is the end group of PDDD. Figure 3. 34 shows the spectrum.
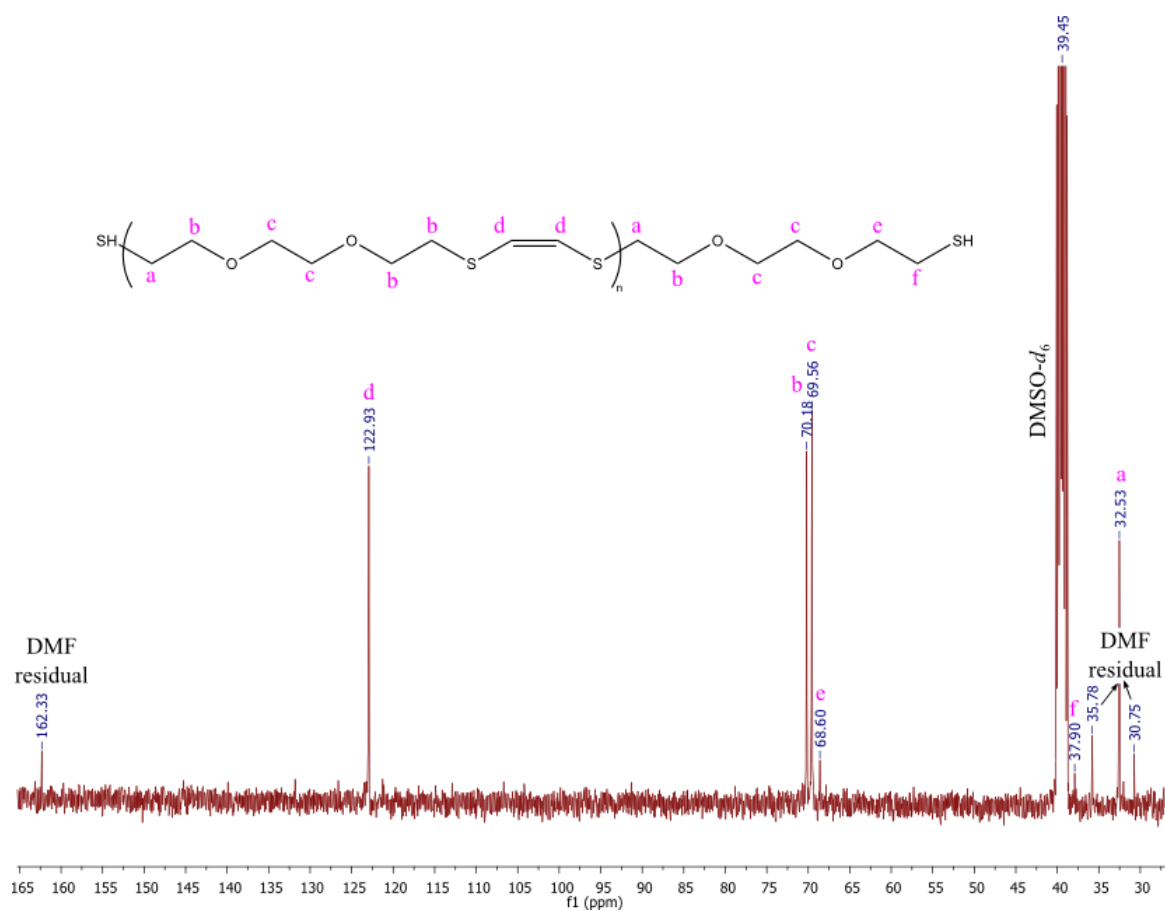
Figure 3. 34 ^{13}C NMR (400 MHz) spectrum of PDDD in DMSO-d_6 with 12 h of acquisition.

The peaks at 37.91 ppm and 68.59 ppm, are related to terminal C**H**$_2$-SH (**f**) and -C**H**2-O (**e**), respectively. The peak identified as **f** suggests the presence of SH as the terminal group.

Size exclusion chromatography analysis was performed and Figure 3. 35 shows the chromatogram.
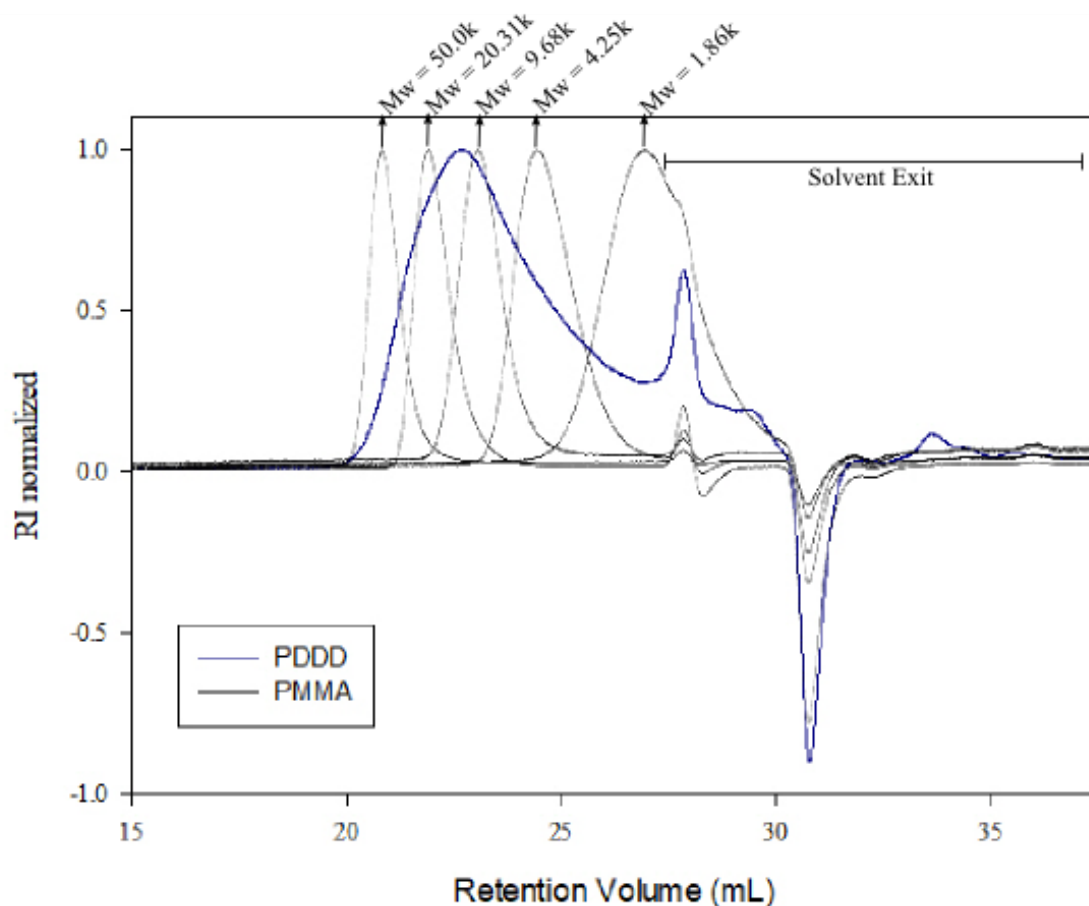
Figure 3. 35 SEC chromatogram of PDDD in DMF comparing with the PMMAs standards.

The molecular weight of the polymer could not be accurately measured by SEC because the elution of the polymer is too close to the eluent exit (between 24 to 37.5 mL). However, this analysis proves the presence of a polymer instead of oligomers ($M_w \sim 5.378k$ if compared with PMMA standards and PDI ~2.265), confirming the success of the polymerization reaction.

Thereafter, the sensitive polymer was subjected to the irradiation test. A polymer solution (in DMF) was split into two vials. One vial solution was mixed with PS (5 wt%) and other was kept without the photosensitizer, as a control sample. Both samples were subjected to red light irradiation (1 h, 650 nm, 80 mW.cm^{-2}). After, the polymer solutions were added dropwise to acetone due to the insolubility of the PDDD polymer in this solvent (Figure 3. 36).
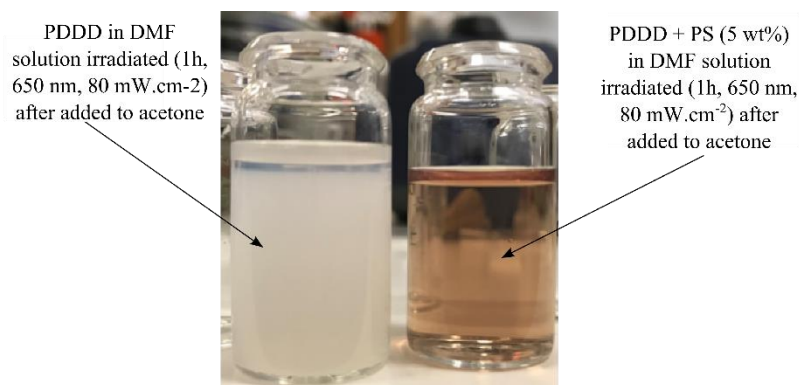
Figure 3. 36 Picture of PDDD solutions without PS (left) and with PS (right) after red light exposition.

In Figure 3. 36 it is clear the difference between the two solutions after irradiation. The polymer without the photosensitizer solution is blurred (vial in the left of the picture), while the solution with photosensitizer is transparent (right). As the PDDD precipitate in acetone, the difference between the two solutions suggests the degradation of the polymer triggered by light in the presence of the PS.

The cleavage ability of the polymer was confirmed by SEC. A solution of PDDD in DMF with Ce6 (10 wt%) was subjected to 8 h of red-light irradiation. A sample of PDDD solution in DMF, that was kept under dark conditions, was used as control. Figure 3. 37 shows the SEC results.
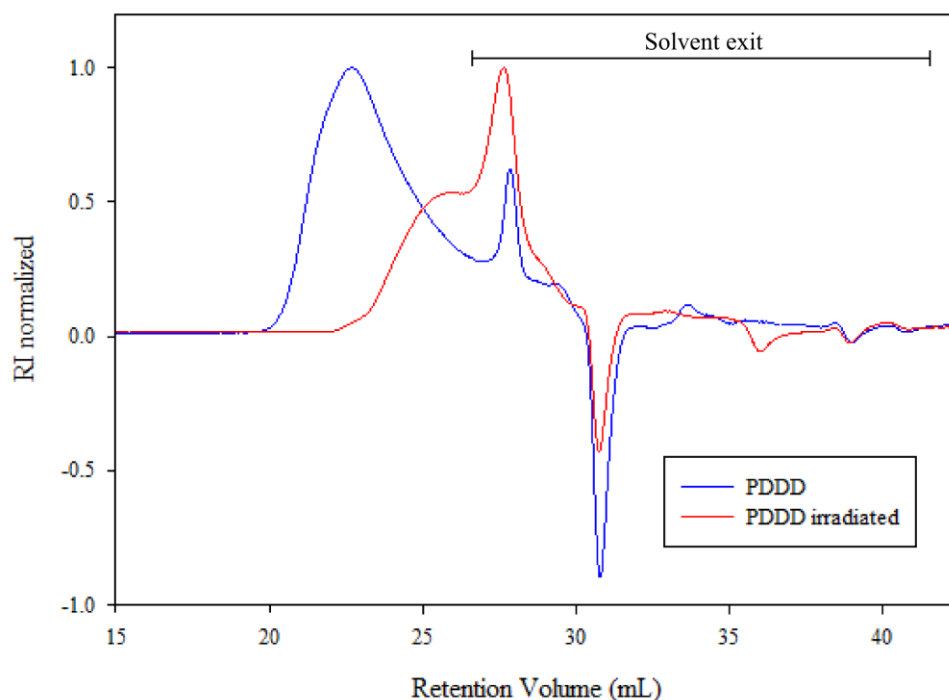
Figure 3. 37 SEC in DMF comparing a sample kept under dark conditions and a sample in a solution with Ce6 and subjected to light irradiation (650 nm, 80 mW.cm^{-2}).

120

After red-light irradiation, the copolymer presents a longer retention time inside the SEC columns than the polymer kept in dark. This behavior indicates the reduction in the copolymer molecular weight caused by the cleavage of the vinylic bonds in the backbone of the sensitive PDDD.

To analyze the influence of the photosensitizer we analyzed the PDDD cleavage ability by NMR technique with the presence of Ce6 as a photosensitizer before and after red light irradiation (650 nm, 80 mW.cm^{-2}). Dibromobenzene was used as the internal standard on NMR spectra (Figure 3. 38).
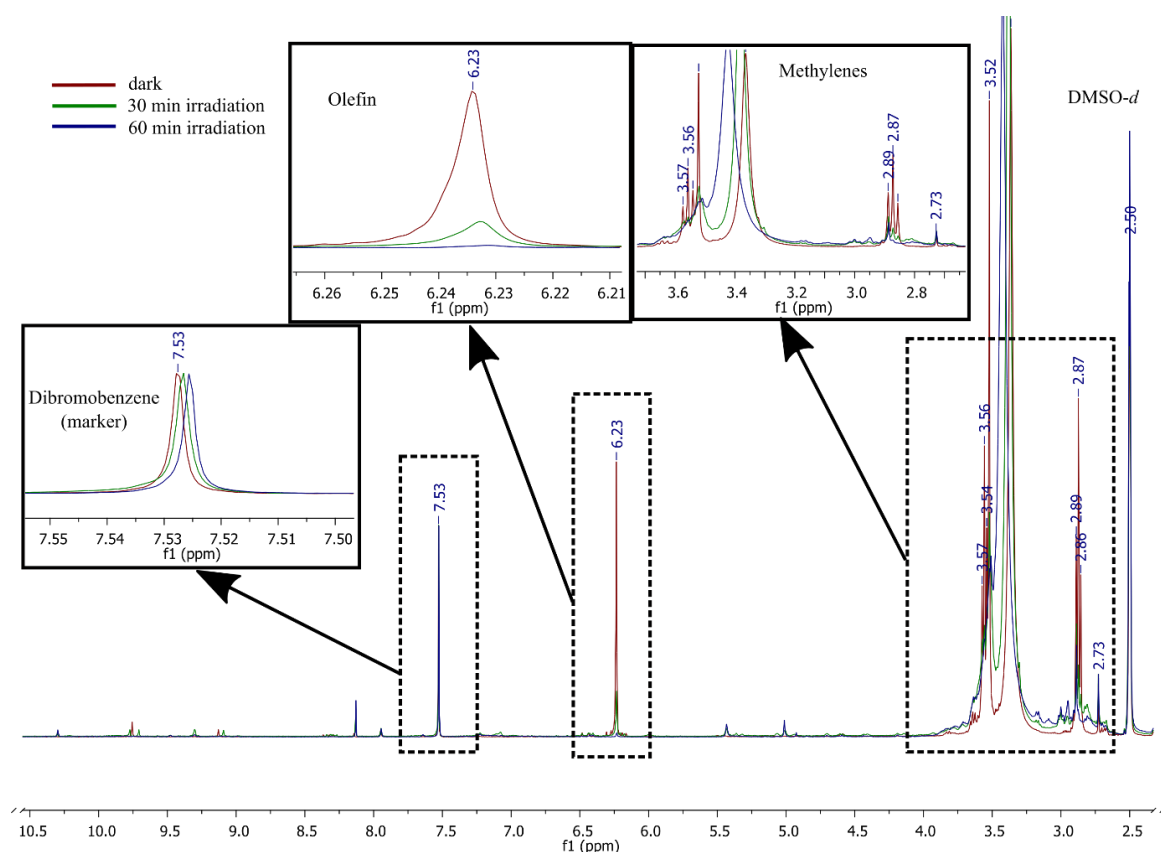
Figure 3. 38 Overlaid ^{1}H NMR spectrums of PDDD in a solution with Ce6 (10 wt%) in DMSO-d_6 before and after the irradiation process.

The chemical shift correspondent to the sensitive olefin at 6.23 ppm strongly decreases after 30 min of irradiation and disappears after 1 h when compared with the dibromobenzene signal (δ ~7.53 ppm). The signal of the protons of the two methylene groups has also been modified by the irradiation time. The NMR analysis proves the ability of the sensitive linker to degrade when exposed to light in the presence of Ce6.

The PDDD has a hydrophobic character, thus a linkage with a hydrophilic polymer provides an amphiphilic character. This property allows it to form nanoparticles by a self-assembly process. Hence, PEG was bonded to the end of the chain of PDDD through a

thiol-ene reaction [208]. In the first step, the hydrophilic $mPEG_{2k}$-OH and $mPEG_{5k}$-OH were functionalized with the acrylate group (mPEG-A, Figure 3. 39 and Scheme 2. 9).

mPEG-OH   +   acryloyl chloride $\longrightarrow$ mPEG-A   +   HCl
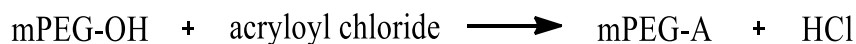
Figure 3. 39 A simple scheme of mPEG-A reaction

The FTIR of mPEGs-A compared with mPEG-OH are shown in Figure 3. 40.
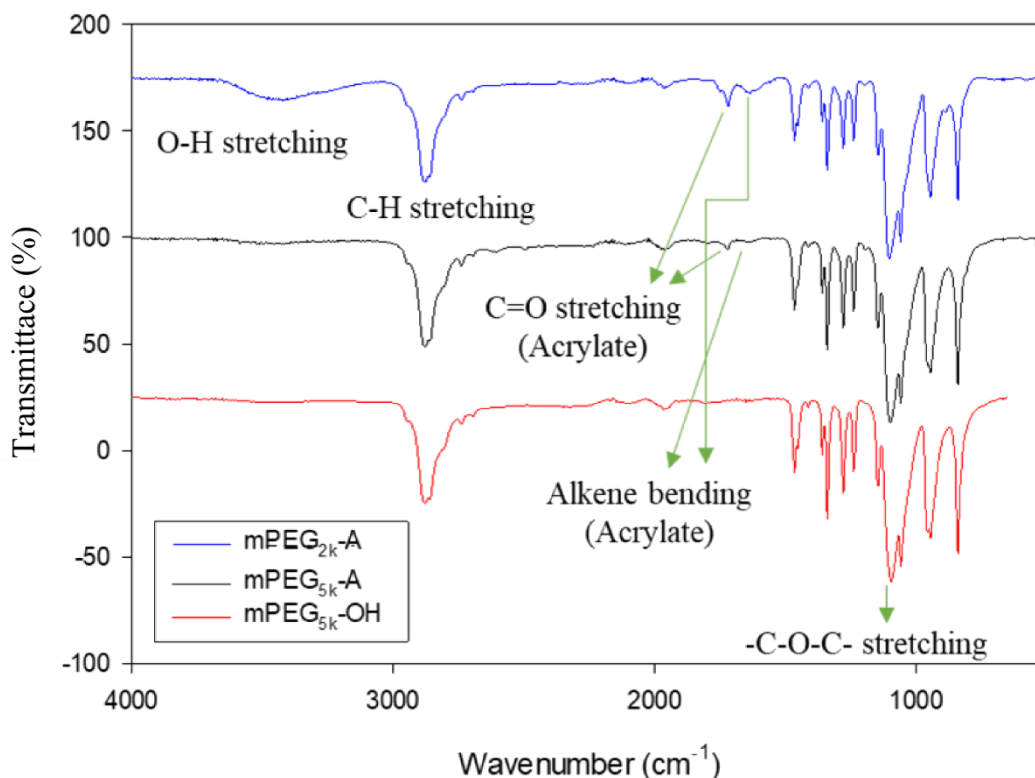
Figure 3. 40 Spectrum of PEG_{5k} and PEG_{2k} acrylate compared with PEG_{5k}-OH.

The characteristic absorption peaks of mPEG-OH are observed in Figure 3. 40 at 3460 cm^{-1} for O-H stretching, 2887 cm^{-1} for C-H stretching, 1461 cm^{-1} for C-H bending and 1099 cm^{-1} for -C-O-C- stretching. In the spectra of the mPEGs-A, the presence of C=O$_{ester}$ stretching band at 1727 cm^{-1} and the alkene bending at 1629 cm^{-1}, confirms the successful modification of mPEG-OH with acrylate groups. Figure 3. 41 and Figure 3. 42 shows the ^{1}H NMR spectra of the synthesized $mPEG_{2k}$-A and $mPEG_{5k}$-A, respectively.
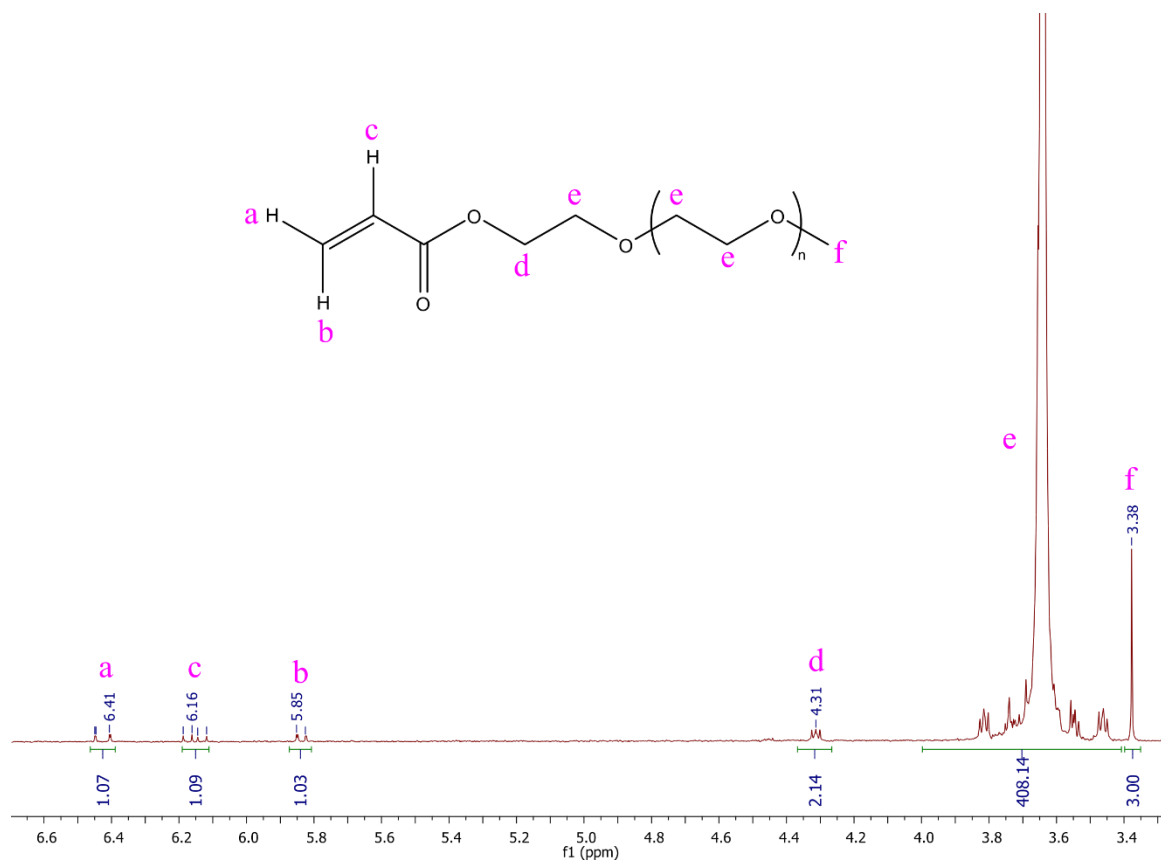
Figure 3. 41 ^{1}H NMR (400 MHz) spectrum of PEG$_{5k}$-A in CDCl$_3$.
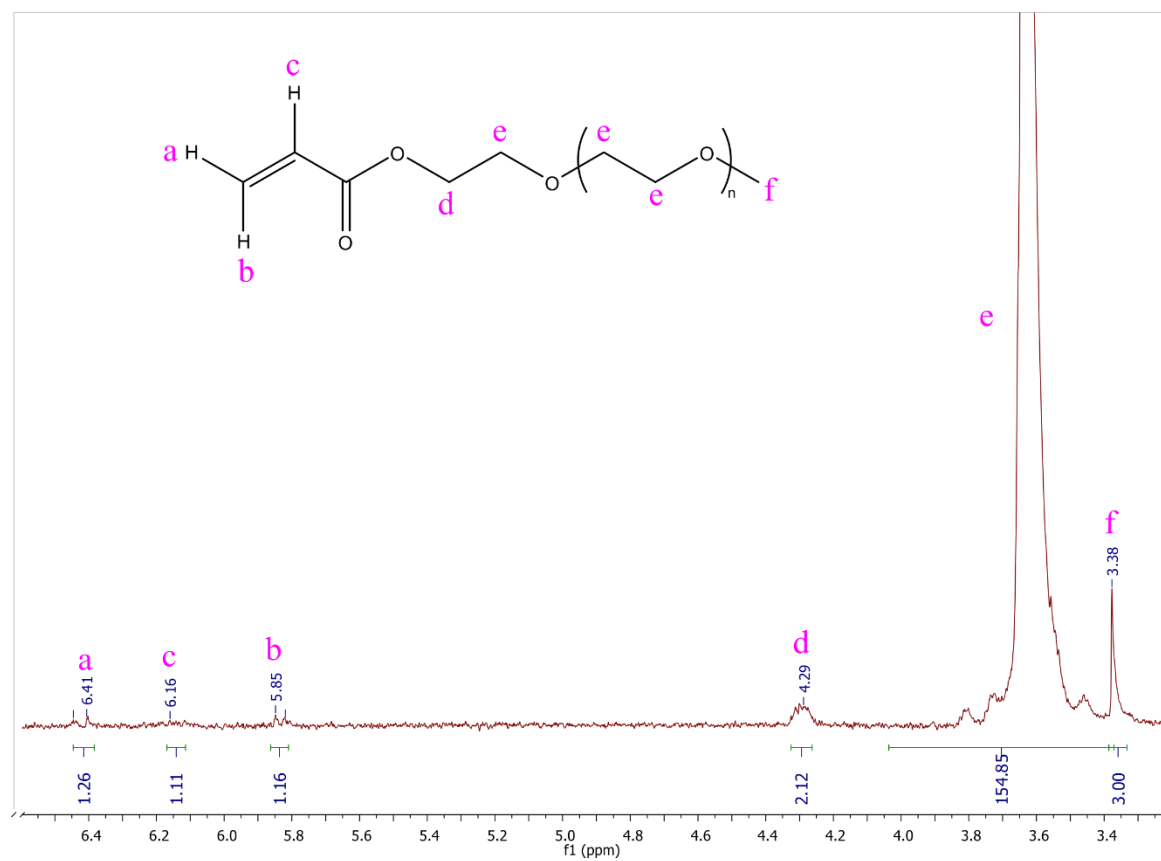
Figure 3. 42 ^{1}H NMR (400 MHz) spectrum of PEG$_{2k}$-A in CDCl$_3$.

The formation of PEG-A was confirmed by the ^{1}H NMR shown in Figure 3. 41 and Figure 3. 42. The spectrum shows the sharp signal of the protons of the methylene groups (-CH2-O-CH2-, **b**) at δ = 3.60 ppm and the characteristic peaks of the methine and methylene protons belonging to the acrylate group (-CH=CH2, **e**, **f** and **g**) in the region of δ = 5.65-6.40 ppm. The signal of the methyl protons (CH$_3$-O-, **a**), at δ = 3.37 ppm, was used to set the integration value and to confirm the polymer molecular weight.

In the second step, PDDD was modified in both extremities with PEG-acrylate in three different molecular weights, namely PEG$_{5k}$-PDDD-PEG$_{5k}$, PEG$_{2k}$-PDDD-PEG$_{2k}$, PEG$_{0.48k}$-PDDD-PEG$_{0.48k}$. The ^{1}H NMR spectrum of PEG$_{0.48k}$-PDDD-PEG$_{0.48k}$ is shown in Figure 3. 43 and the spectra of PEG$_{5k}$-PDDD-PEG$_{5k}$ and PEG$_{2k}$-PDDD-PEG$_{2k}$ are shown in Figure A 19 and Figure A 20 in the appendix, respectively.
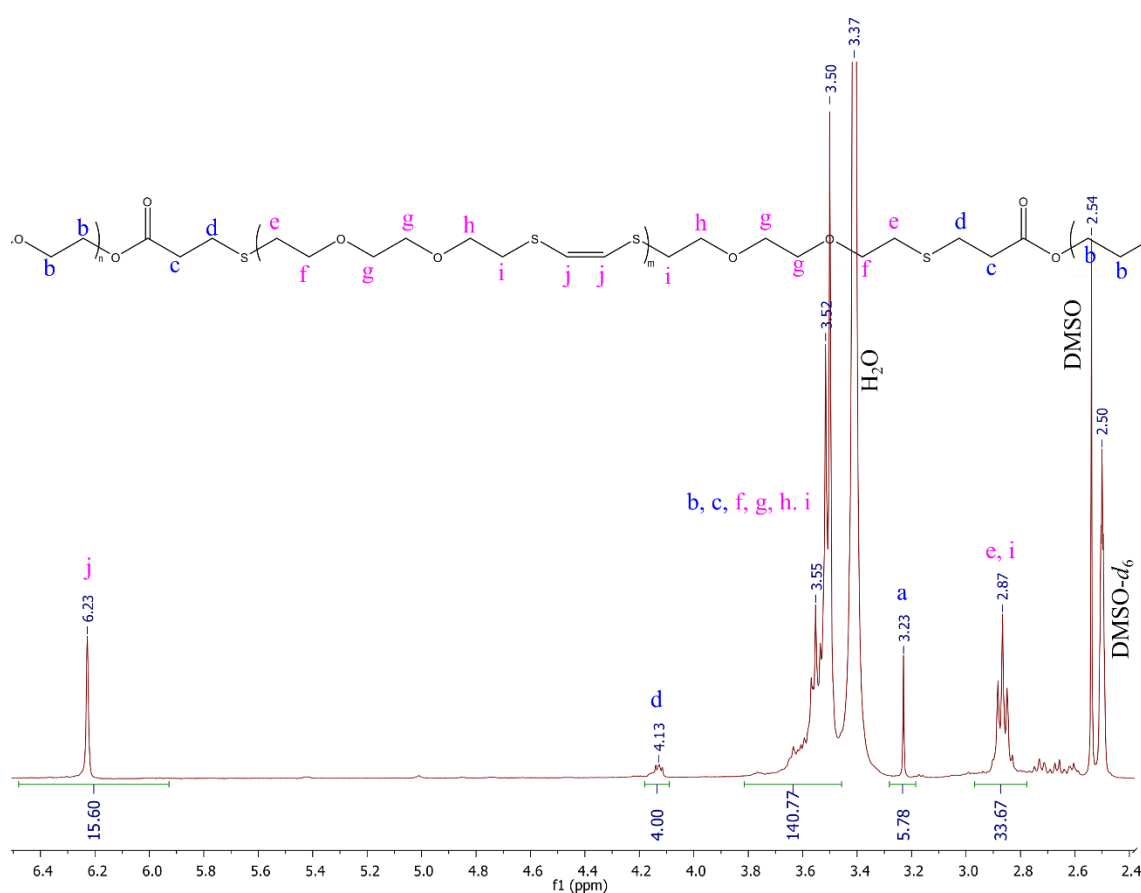
Figure 3. 43 ^{1}H NMR (400 MHz) spectrum of PEG$_{0.48k}$-PDDD- PEG$_{0.48k}$ in DMSO-d_6.

The spectrum reveals the presence of the sensitive alkene group with a peak at δ=6.23 ppm (-CH=CH-, **j**) and the methylene group of the PDDD which presented the chemical shift in the region of 3 ppm and 2.8 ppm (-S-CH2-, **e** and **i**) and 3.8 ppm and 3.4 ppm (-CH2-O-CH2-, **f**, **g**, **h** and **i**). The signal of methylene protons of the PEG chain (**b** and **c**) are overlaid with methylene signals of PDDD (**f**, **g**, **h** and **i**). The methine terminal

124

group of PEG (**a**) presents the chemical shift at 3.33 ppm. The successful synthesis of the PEG$_{0.48k}$-PDDD-PEG$_{0.48k}$ copolymer is evidenced by the resonance peak belonging to the protons of the methylene group, at the linkage between PEG and PDDD polymers (-S-C**H**$_2$-, **d**), and by the disappearance of the peaks ascribed to the methyl and methylene protons of the acrylate groups (-C**H**=C**H**2, **e**, **f** and **g**) in the region of δ = 5.65-6.40 ppm in Figure 3. 41 and Figure 3. 42.

The sensitive copolymers were then analyzed through DMTA to evaluate their glass transition temperature (T_g). Figure 3. 44 shows the thermogram of the sensitive triblock copolymers.
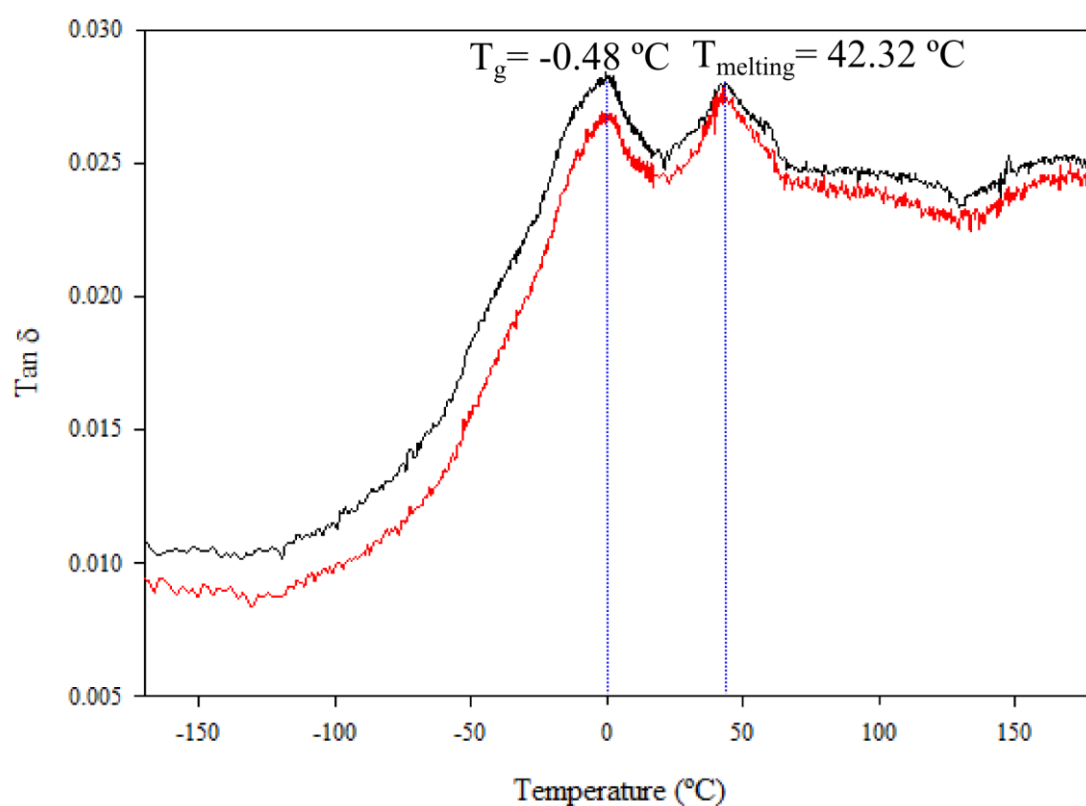
Figure 3. 44 Tan δ traces of PEG$_{5k}$-PDDD-PEG$_{5k}$ copolymer, at 1 and 10 Hz.

The T_g of the samples was determined from the maximum value of tan δ, at 1 Hz [204]. The copolymers showed a T_g at -0.48°C for PEG$_{5k}$-PDDD-PEG$_{5k}$ [243]. It is also possible to see another transition at *ca.* 40 °C (no sensitive to frequency) that can be tentatively ascribed to the melting transition [244]. The single value of the T_g for these copolymers evidence the miscibility of the two blocks in the copolymer.

The introduction of PEG provides the required amphiphilic character to the hydrophobic PDDD block allowing the final copolymers to form micelles by a self-

assembly process. Micelles were formed through the dialysis method (as previously described) using DMSO as a solvent.

In order to evaluate the disassembly process, a solution of micelles was subjected to 2 h of red-light irradiation and analyzed by DLS. Table 3. 9 shows the DLS results.

Table 3. 9 DLS results for size analysis with PEG-PDDD-PEG micelles solutions with 15 wt% of Ce6, before and after red light irradiation (2 h).

Copolymer	Parameters	Dark	Irradiated
PEG_{2k}-PDDD-PEG_{2k}	Ave Size (nm)	97.20 ± 1.118	57.68 ± 0.1721
	Deriv count rate (%)	100	22
	Attenuator	7	8
PEG_{5k}-PDDD-PEG_{5k}	Ave Size (nm)	99.71 ± 2.479	153.0 ± 5.886
	Deriv count rate (%)	100	51
	Attenuator	8	9
$PEG_{0.48k}$-PDDD-$PEG_{0.48k}$	Ave Size (nm)	48.06 ± 0.8047	32.37 ± 0.4550
	Deriv count rate (%)	100	56
	Attenuator	7	7

After irradiation, PEG-PDDD-PEG micelles showed a reduction in the derivative count rate (Table 3. 9). As the decrease in the derivative count rate can be directly related to the decrease in the micelle concentration, these values prove the disaggregation potential of sensitive micelles with Ce6 encaged [184].

3.2.2 Drug Release Study

PEG_{5k}-PDDD-PEG_{5k} and PEG_{2k}-PDDD-PEG_{2k} micelles were analyzed through the fluorimeter technique to evaluate the DOX loading capacity, following the same methodology described for PEG-BHETE-PLA micelles in section 2.3.3. These sensitive micelles present a DLC of $0.86 \pm 0.25\%$ and $1.13 \pm 0.16\%$ for PEG_{2k}-PDDD-PEG_{2k} and PEG_{5k}-PDDD-PEG_{5k}, respectively (Figure A 21 in the appendix). For the evaluation of the drug release profile, the sensitive micelles encapsulating DOX and Ce6 were subjected to irradiation and a dialysis procedure against water at 37ºC. Samples of the micelle solution were measured at pre-determined periods (Section 2.3.4).

The average profile of the kinetics release of the DOX from micelles subjected to light, and the control samples (micelles solutions kept in the dark) are shown in Figure 3. 45 and Figure 3. 46.
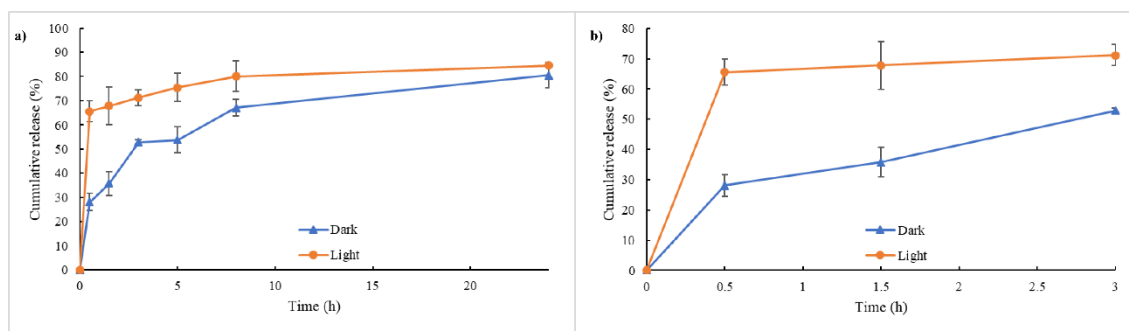
Figure 3. 45 (a) Profile of the release kinetics of the DOX from PEG$_{5k}$-PDDD-PEG$_{5k}$ sensitive micelle and (b) the zoom of the first 3 h.
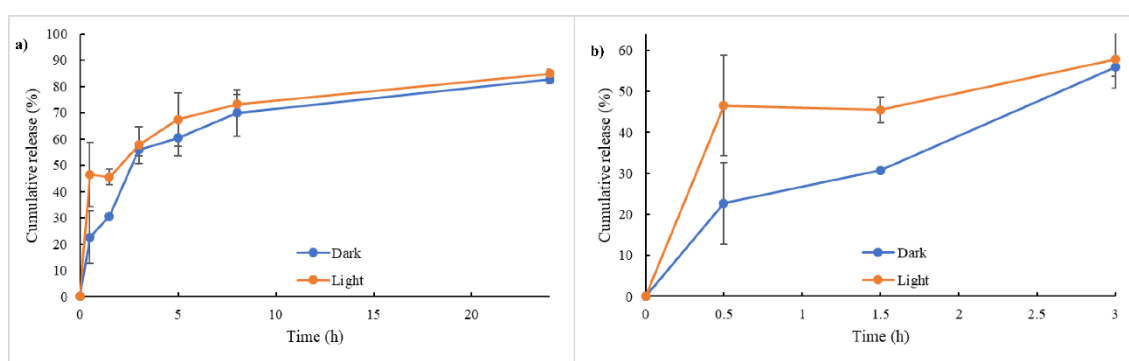
Figure 3. 46 (a) Profile of the release kinetics of the DOX from PEG$_{2k}$-PDDD-PEG$_{2k}$ sensitive micelle and (b) the zoom of the first 3 h.

From Figure 3. 45 and Figure 3. 46, almost all the encaged DOX (>80%), in all samples, was released after 24 h.

For the first 3 h of dialysis (Figure 3. 45 b and Figure 3. 46 b) showed a more prominent difference between the irradiated and control samples. The superior DOX release for the irradiated samples is justified by the destabilization of the micelles induced by the light beam. The irradiated PEG$_{5k}$-PDDD-PEG$_{5k}$ micelles showed a DOX cumulative release 37% higher in the first 30 min when compared with the control sample (Figure 3. 45 a). PEG$_{2k}$-PDDD-PEG$_{2k}$ micelles (Figure 3. 46 a) showed a slower release profile than PEG$_{5k}$-PDDD-PEG$_{5k}$ in the first 30 min. The DOX cumulative release of irradiated micelles was 24% higher than the non-irradiated.

The release profiles of the PEG$_{5k}$-PDDD-PEG$_{5k}$ micelle compared with PEG$_{5k}$-BHETE-PLA$_{10k}$ are shown in Figure 3. 47.
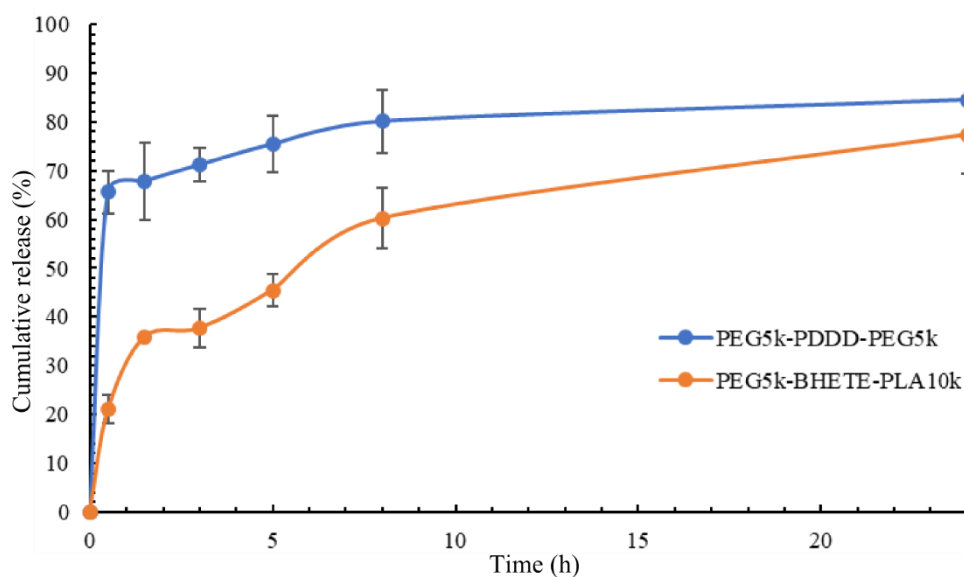
Figure 3. 47 Profile of the DOX release kinetics from the PEG$_{5k}$-PDDD-PEG$_{5k}$ sensitive micelle (blue) and PEG$_{5k}$-BHETE.PLA$_{10k}$ (orange) after irradiation.

Comparing PEG$_{5k}$-PDDD-PEG$_{5k}$ with PEG$_{5k}$-BHETE-PLA$_{10k}$ micelles, the average release of DOX was 3 times higher in the first 30 min and the total average DOX release was 7% higher after 24 h of dialysis for PEG$_{5k}$-PDDD-PEG$_{5k}$. The burst of the drug release of PEG$_{5k}$-PDDD-PEG$_{5k}$ micelles is caused by a larger number of sensitive units in the backbone of PDDD, that promotes a faster disassembly with consequent faster drug release. For drug delivery systems focused on cancer therapy, a fast release of the drug may favor the fast death of tumor cells increasing the success of the treatment and inhibiting the disease growth area [92].

The cytotoxicity of the PEG$_{5k}$-PDDD-PEG$_{5k}$ micelle was tested without any therapeutic encaged through an *in vitro* cells assay (MTT) in an MCF7 cell line as previously described in for PEG-BHETE-PLA micelles (Figure A 22 in the appendix). This experiment shows approximately 100% of metabolic activity, proving the biocompatibility of the copolymer.

3.3 Synthesis of Polymers with Light Sensitive Segments

Another approach was also attempted in the development of light sensitive polymers, using the same family of light sensitive moieties and exploring other functionalities and reactions. Furthermore, a new photodegradable system based in PET RAFT agents was conceptually proved.

128

3.3.1 BCETE Based Poly(Ester Amide)s

Poly(ester amide)s (PEAs) are part of an emerging group of biodegradable-synthetic polymers with a wide range of applications. They are characterized by the presence of ester and amide linkages in the polymer chain. The ester functional group lead into a polymer with biocompatibility, elevated flexibility and ease degradation under physiological conditions. The amide group provides high thermal and mechanical proprieties [245]. These combinations of characteristics and the easy tunability of these properties by the amide /ester bonds content in the polymer make this class of polymer highly required in biomedical applications, especially in tissue engineering and DDSs [246]. Usually, PEAs are synthesized through ROP of a cyclic monomer or polycondensation (e.g. interfacial polymerization) [247].

Our strategy consisted of the introduction of a sensitive bis-(alkylthio) alkene (BATA) segment, here called BCETE, in the poly(ester amide) structure. First, the BCETE segment (Scheme 2. 3 and Scheme 2. 4) was synthesized following the described procedure [205]. The synthesized BCETE was analyzed by FTIR and ^{1}H NMR (Figure 3. 48 and Figure 3. 49, respectively). The ^{13}C NMR of the BCETE is presented in the appendix, Figure A 23 and the melting point was evaluated as 164°C.
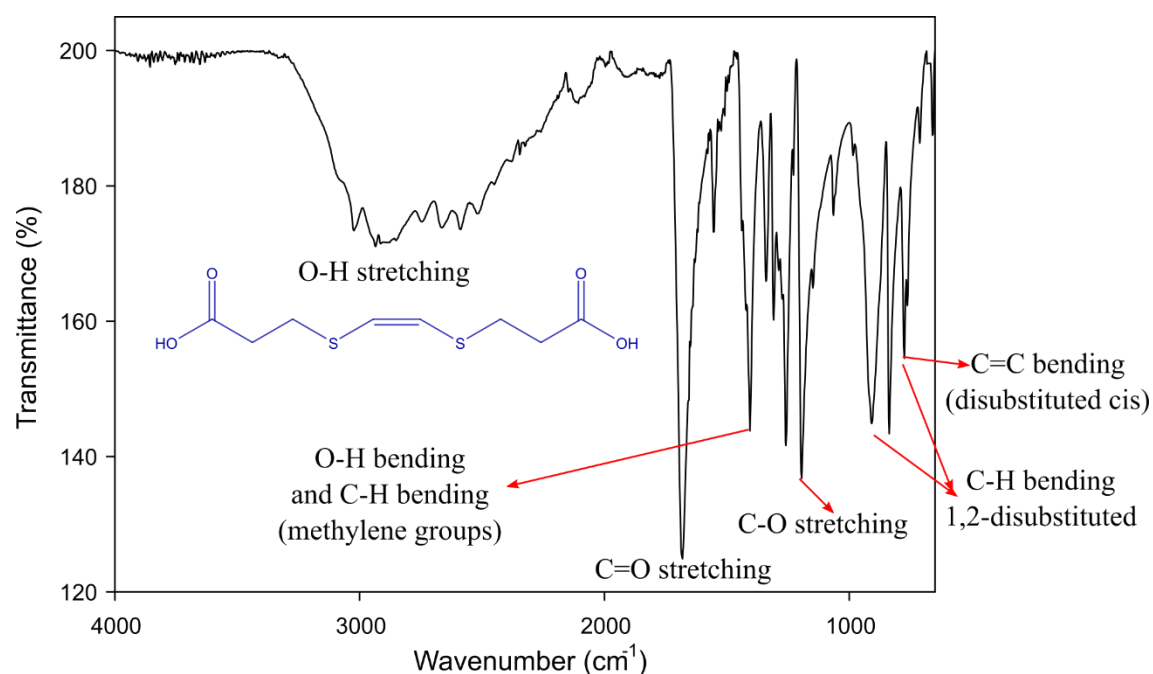
Figure 3. 48 ART-FTIR of BCETE

The FTIR spectrum of the BCETE shows the characteristic frequency band of the carboxylic acid group (very broad band centered at 2867 cm^{-1}) and at 1192 cm^{-1} a band

129

related to the O-H and C-O stretching. The band at 1680 cm^{-1} represents the C=O stretching of carboxylic acid group, the band at 1410 cm^{-1} is characteristic of the O-H bending and C-H bending of the methylene groups. The C-H bending of the 1,2-disubstituted has the transmittance band at 895 and 773 cm^{-1}. This last band also could have contributions of the C=C bending of the *cis* disubstituted transmittance band.
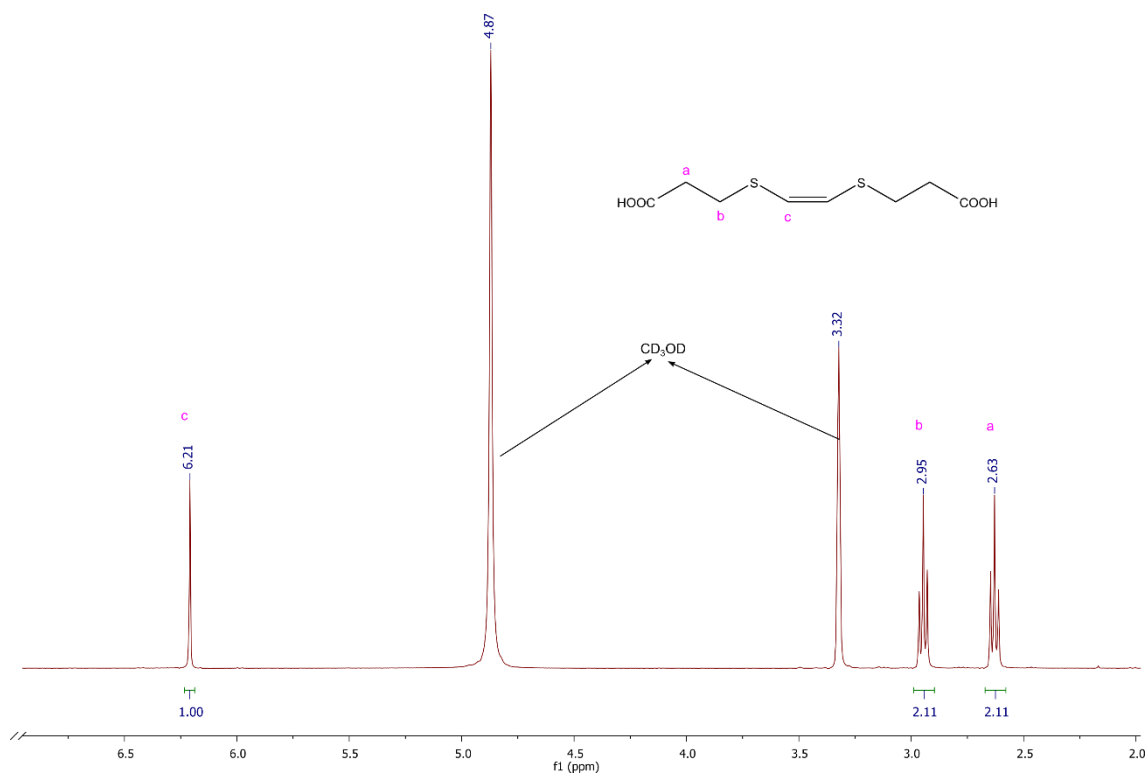
Figure 3. 49 ^{1}H NMR (400 MHz, CD$_3$OD) spectrum of the BCETE.

The resonance peak of the protons of the methylene groups, (-C-**CH**2-, **a**) and (-**CH**2-S-, **b**) are at δ = 2.63 and 2.95 ppm, respectively. The protons of the methine groups (S-**CH**=**CH**-S, **c**) resonates δ = 6.21 ppm. Both the FTIR and ^{1}H NMR spectra are in accordance with the anticipated chemical structure, confirming the successful synthesis of the BCETE sensitive segment.

In order to analyze the sensibility of the BCETE segment to the ^{1}O$_2$ generated by PS under light stimulation, the segment was subjected to 2 h of red-light irradiation (650 nm, 80 mW.cm^{-2}). Figure 3. 50 shows the BCETE ^{1}H NMR after undergoing the ^{1}O$_2$ reaction triggered by red-light.
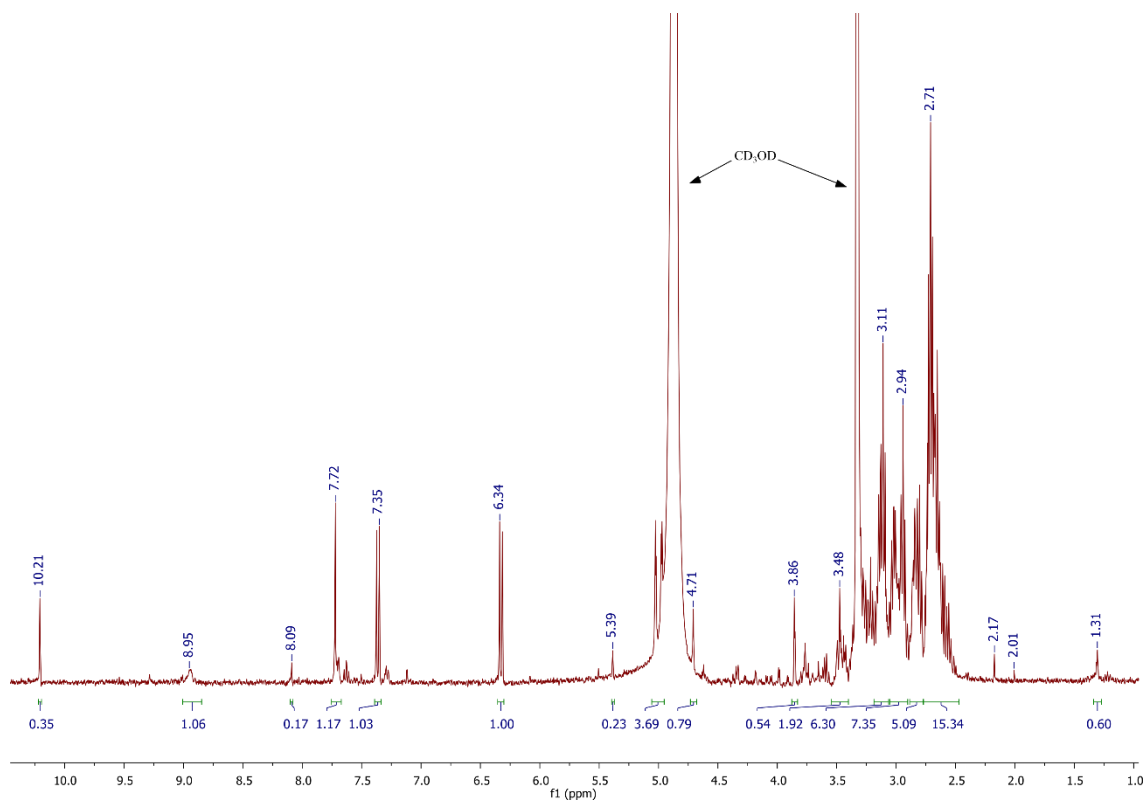
Figure 3. 50 ^{1}H NMR (400 MHz, CD$_3$OD) spectrum of the BCETE in the presence of PS under 2 h of red-light irradiation

Comparing the ^{1}H NMR of Figure 3. 49 and Figure 3. 50, it is clear the difference between the two spectra. The region of 2.25 and 4.0 ppm showed a broad increase in the peaks and the integration area is 9 times bigger than the area of the vinylic protons (at 6.34 ppm). The emergence of these new peaks and the difference in the integration areas suggest the degradation of the BCETE segment after red-light irradiation in the presence of the PS.

The poly(ester amide) could be prepared by the reaction of BCETE with the α-amino acid based diamine through polycondensation. Since these reactions require temperatures above 150 ℃ to occur, it was first necessary to evaluate the degradation temperature of the BCETE. The thermal stability was evaluated by thermogravimetric analysis (TGA), and the thermogravimetric curves are shown in Figure 3. 51.
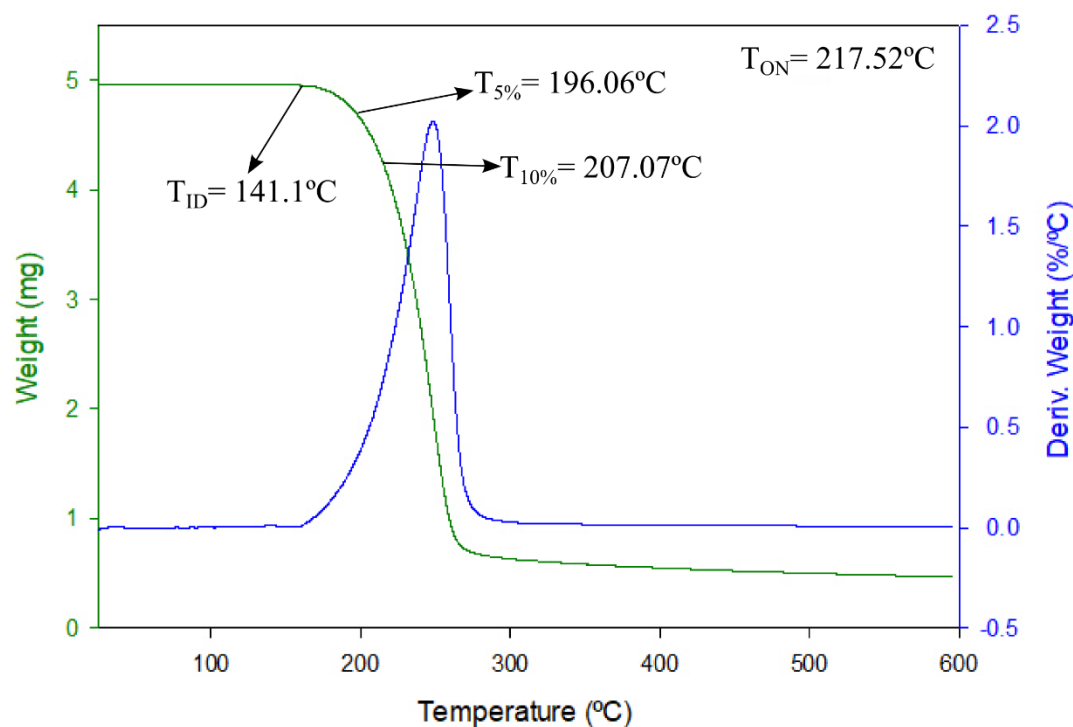
Figure 3. 51 TGA of the BCETE segment. T_{ID} shows the initial temperature of the weight loss, $T_{5\%}$ and $T_{10\%}$ are the temperatures which correspond to 5 and 10% of the BCETE weight loss, respectively. T_{on} shows the temperature of onset.

The TGA measurement shows that BCETE degradation with temperature starts at 141.1°C with more than 58% of degradation occurring at 247.4°C. These results restrict the polymerization of the BCETE to form the PEA with methodologies using mild reaction temperatures.

An interesting approach is the interfacial polymerization that can be carried out at room temperature [247], [248]. In the interfacial polymerization, the polymerization process occurs on the interphase of two immiscible liquids, usually water/organic solvent. The monomers diffuse to the interface due to the difference of the chemical potential between the immiscible phases and the growth of the polymer started. A common reaction involves the diamine and the diacid chloride monomers, which react to form polyamide and hydrogen chloride [138]. The acyl chloride functionalization of the carboxylic acid group can be easily achieved by its reaction with thionyl chloride or oxalyl chloride [247].

Hence, in order to achieve a $^1O_2$-sensitive poly(ester amide), the BCETE is first converted in a diacyl chloride (1,2-bis(chloroalcylethylthio) ethylene, BCAETE), through a nucleophilic reaction with the oxalyl chloride (Scheme 2. 11). The amount of oxalyl chloride reagent and the catalyst (DMF) should be carefully adjusted as the excess of these reagents can degrade the BCAETE. Most of the reactions originate black products which correspond to the degrade materials (^{1}H NMR Figure A 24 in the appendix, the difference

132

among the integration peak of the methine signal at δ=6.16 ppm, 2H, and methylene protons at δ=2.8 to 3.4 ppm, 8H). Following several attempts, the best conditions for the conversion of the carboxylic acid into the diacyl chloride were the 2.5 eq mol of oxalyl chloride and 2 drops of the catalyst (dry DMF). The reaction is carried out in a heterogeneous medium, as the BCETE is not soluble in the DCM. As the nucleophilic substitution occurs, and the diacyl chloride is formed, the solution turns clear, presenting a yellowish-orange color [249]. Due to the high sensitivity of the diacyl chloride molecule, the BCAETE was used without purification. Thus, the synthesized BCAETE was immediately used in the interfacial polymerization with the BAAE. This type of step-growth polymerization occurs in the interface of the organic (DCM-BCAETE)/aqueous solution (water-BAAE). A viscous white-yellowish polymer is instantaneously formed.

The synthesized poly(ester amide) was characterized by FTIR and ^{1}H NMR (Figure 3. 52 and Figure 3. 53).
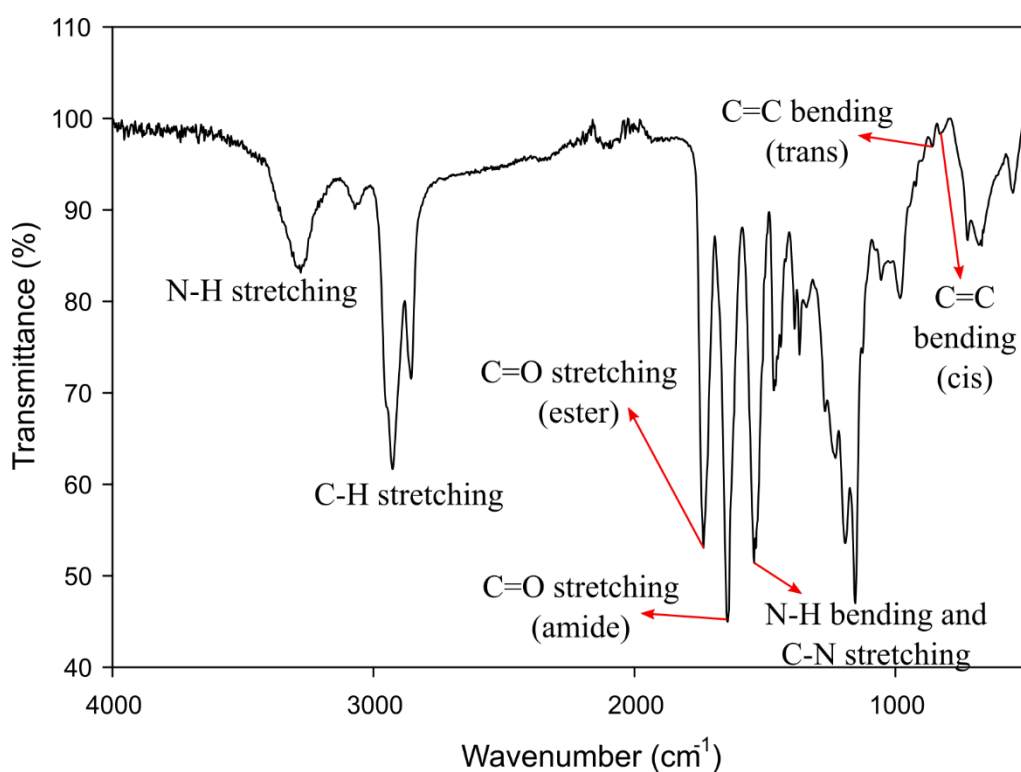
Figure 3. 52 ART-FTIR of the poly(ester amide)
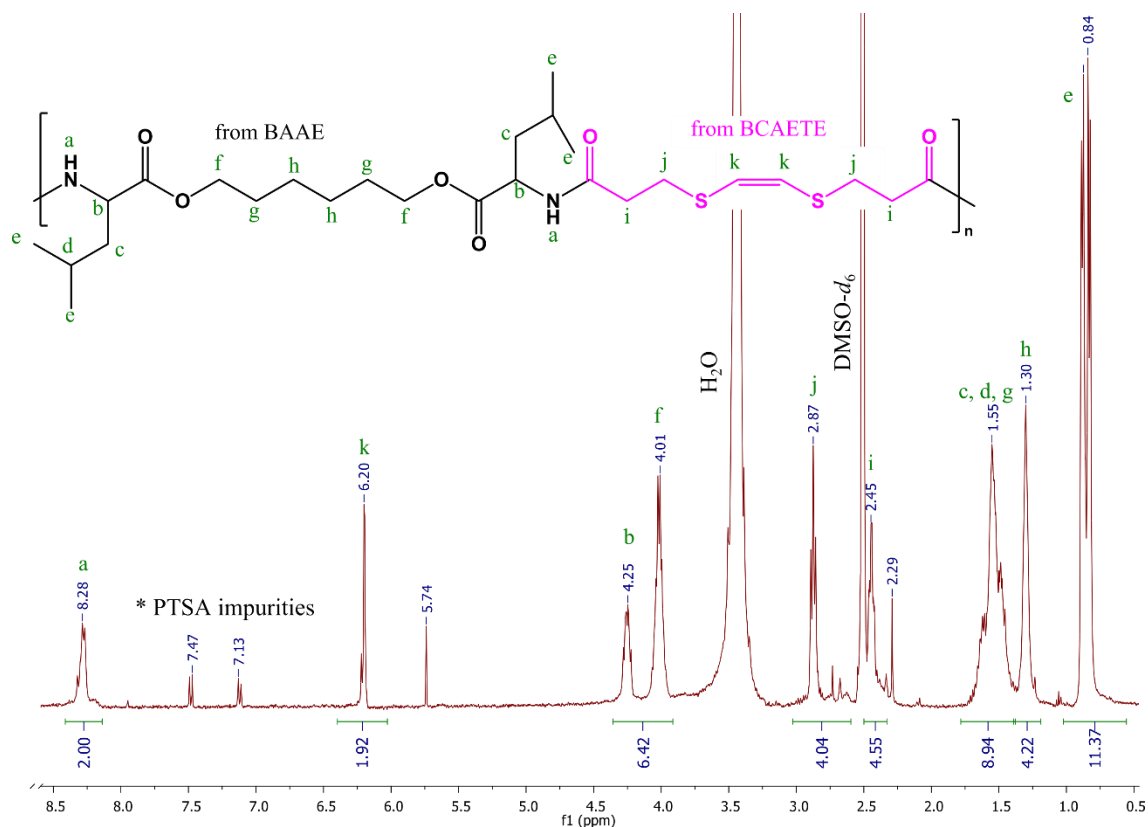
Figure 3. 53 ^{1}H NMR (400 MHz) spectrum of poly(ester amide) in DMSO-d_6 solution.

The bands at 3286.7 cm^{-1}, 1734.8 cm^{-1}, 1630.1 cm^{-1}, 1536.7 cm^{-1}, 861 cm^{-1} and 831 cm^{-1} are the characteristic peaks of poly(ester amide)s. These peaks correspond to the N-H stretching, -C=O stretching (ester), -C=O stretching (amide), C-N stretching and N-H bending, C=C bond *cis* configuration, respectively. In the ^{1}H NMR spectrum, the chemical shift of the BCETE double bond is easily seen through the sharp signal at 6.20 ppm (-**CH**=**CH**-, **k**), as well by the protons of the methylene groups that resonate at 2.87 (-S-**CH2**-, **j**) and 2.44 ppm (-**CH2**-CO-, **i**). The amide proton (**NH**-CO-, **a**) appears at 8.28 ppm and the methyl protons (-CH-(**CH3**)2-, **e**) at 0.84 ppm. The protons of the methine (-C**H**-(CH3)2-, **d**) and methylene groups (-C**H2**-CH-, -O-CH2-C**H2**-, -CH2-(C**H2**)2-CH2, **c, g,** and **h**, respectively) present their characteristic peaks in the region of 1.25 and 1.75 ppm. The protons belonging to the group -**CH₂**-O-C(=O) (**f**) and to the group -C(=O)-**CH**-NH- (**b**) resonate at 3.80 and 4.2 ppm. In summary, the FTIR and ^{1}H NMR spectrum show that the poly(ester amide) comprising the sensitive segment was successfully synthesized.

To investigate the light sensitivity of the obtained poly(ester amide), this sensitive polymer was subjected to red light irradiation with a photosensitizer (Ce6 in 10 wt% of polymer). Figure 3. 54 shows the polymer spectrum before irradiation, after 30 min, 60 min and 90 min of red-light irradiation (650 nm, 80 mW.cm^{-2}), in the presence of Ce6.

134
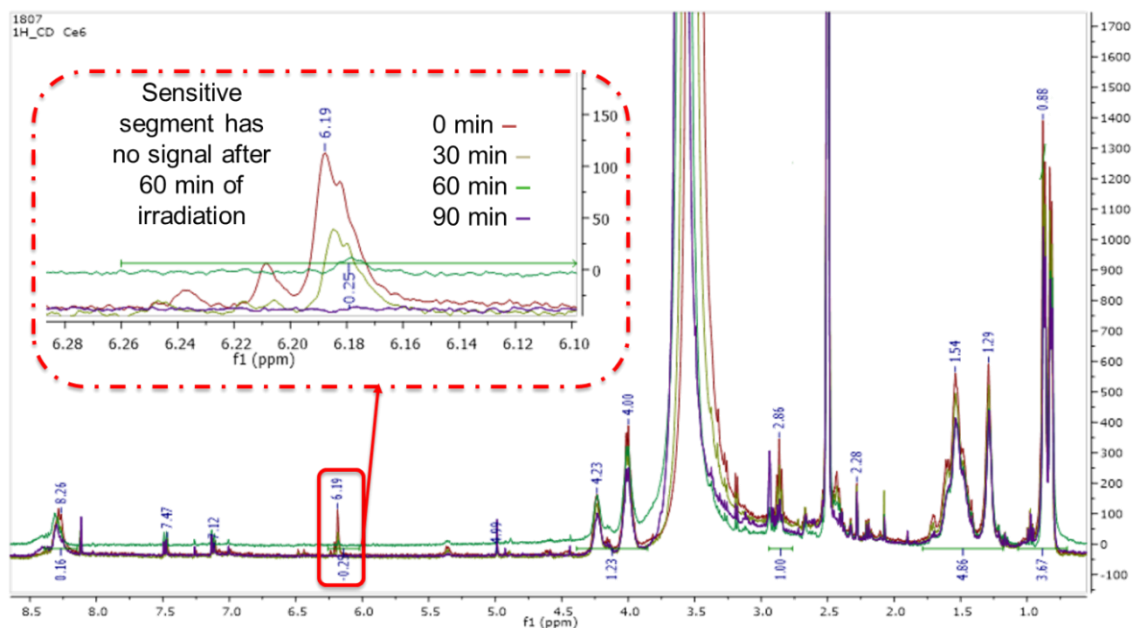
Figure 3. 54 Overlaid ^{1}H NMR (400 MHz) spectra of poly(ester amide) in a solution with Ce6 in DMSO-d_6 before and after undergoing the irradiation process.

The characteristic peak of the sensitive vinylic bond at 6.19 ppm started to disappear after irradiation in the sample with Ce6 (Figure 3. 54), showing no signal after 1 h of light exposition. The absence of the peak corresponding to the olefin group suggests that the sensitive polymer is completely degraded after 1 h of irradiation in a solution with Ce6. For comparison purposes, the poly(ester amide)was irradiated in the same conditions, but without the PS. In this case, the peak ascribed to the protons of the sensitive vinylic bond did not suffer any change (Figure A 25 in appendix).

Considering that the sensitivity of the polymer could be directly related to the number of sensitive units in the polymer backbone, we hypothesized if the response of the polymer could be controlled by adjusting the number of sensitive units present in the poly(ester amide). The presence of a lower number of sensitive units across the polymer backbone would lead to a slower degradation of the polymer. To achieve poly(ester amide)s with different amounts of sensitive segments, sebacoyl chloride was used as the (co) diacyl chloride reagent to replace some/all BCAETE molecules. A library of poly(ester amide)s was synthesized with a molar amount of BCAETE ranging from 0 to 100%, relative to the BAAE. The sebacoyl chloride reagent was added in the DCM solution in such amount that the molar ratio of (sebacoyl chloride+BCAETE):BAAE was maintained in 1:1 (Table 3. 10).

Table 3. 10 Amount of reagents used in the synthesis of poly(ester amide)s.

Sample	BCAETE (mmol)	Oxalyl chloride (mmol)	Sebacoyl Chloride (mmol)	BAAE (mmol)
I	0	0	2.903	2.903
II	0.725	1.814	2.177	2.903
III	1.452	3.629	1.451	2.903
IV	2.177	5.443	0.726	2.903
V	2.177	5.443	0	2.177

The product from the interfacial polymerization was analyzed by FTIR (Figure 3. 55) and NMR (Figure 3. 56).
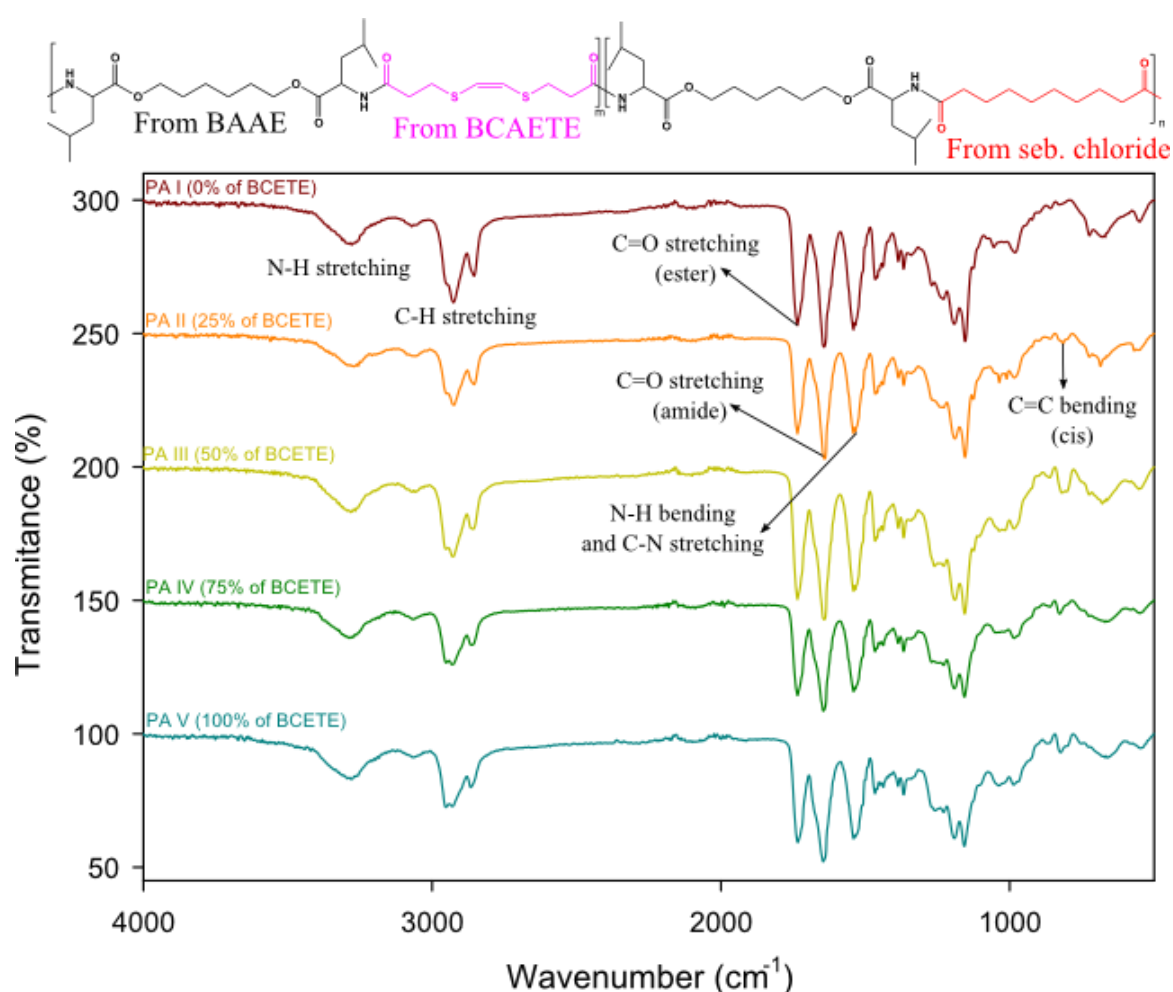
Figure 3. 55 The structure and ATR-FTIR analysis of the poly(ester amide)s PA I to V. Seb. Chloride =Sebacoyl Chloride.

The amide characteristic transmittance bands were identified as N-H stretching at 3300 cm^{-1}, -C=O stretching (ester) at 1724 cm^{-1} and -C=O stretching (amide) at 1622 cm^{-1}, the C-N stretching and N-H bending at 1527 cm^{-1}. These bands prove the formation of

136

the poly(ester amide)s. The signal at 814 cm^{-1} appears only when the sensitive BCETE is added, which is related to the C=C bond of the *cis* isomer configuration of alkene group in the sensitive linker.
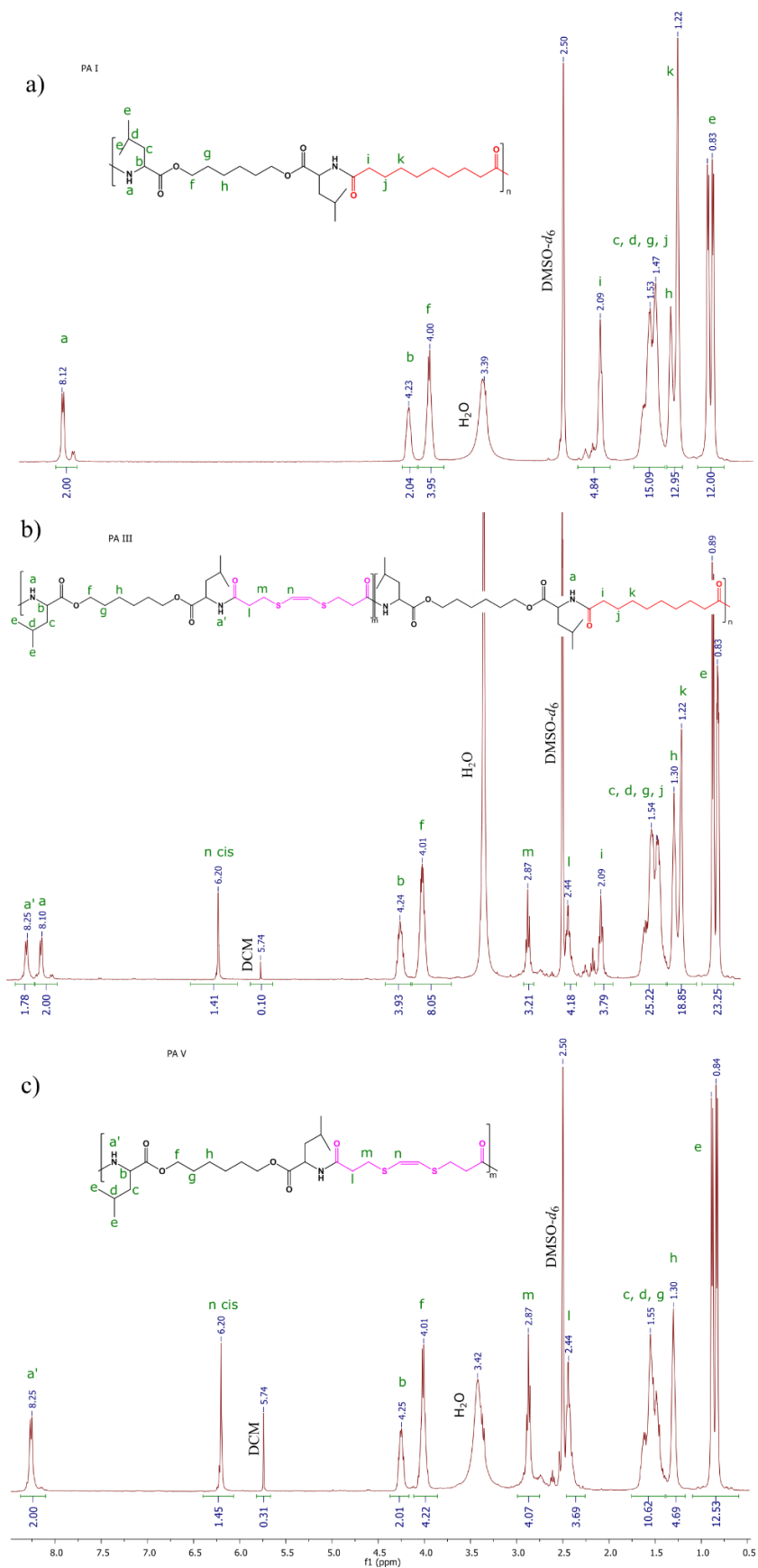
Figure 3. 56 ^{1}H NMR (400 MHz) spectrum of poly(ester amide)s PAI (a), PA III (b) and PA V (c) (0%, 50% and 100% of the BCAETE) in DMSO-d_6. The spectrum of PA II and PA IV are shown in Figure A 26 and Figure A 27 in the appendix.

The resonance peaks related to the BAAE block are found in all spectra. The amide proton (N**H**-CO-, **a**) appears at 8.28 ppm and the methyl protons (-CH-(C**H**3)2-, **e**) at 0.84 ppm, the protons of the methine (-C**H**-(CH3)2-, **d**) and methylene groups (-C**H**2-CH-, -O-CH2-C**H**2-, -CH2-(C**H**2)2-CH2, **c**, **g**, and **h**, respectively) present their characteristic peaks in the region of 1.25 and 1.75 ppm. The protons belonging to the group -**CH₂**-O-C(=O) (**f**) and to the group -C(=O)-**CH**-NH- (**b**) resonate at 3.80 and 4.2 ppm. The polymer block from sebacoyl chloride (spectra a and b in Figure 3. 56) has the methylene protons peak identified at 1.22 ppm (**k**), 2.09 ppm (**i**) and at the region of 1.3 and 1.75 ppm (**j**). In the spectra b and c from Figure 3. 56 the chemical shift of the BCAETE double bond is easily seen through the sharp signal at 6.20 ppm (-C**H**=C**H**-, **k**), and the methylene protons **l** (-C=O-C**H**2-) and **m** (-C**H**2-S-) showed the resonance peak at ca. 2.44 and 2.87 ppm. Noteworthy, the resonance peak of amide proton (**a**) present a slight shift to the most electronegative region in the spectrum (**a'**). This is due to the bond between the poly(ester amide) block (from BAAE) and the sensitive segment (from BCATE). The analysis of the copolymer composition was made through the comparison of the integration value area of the amide proton **a** and **a'**. Table 3. 11 shows the composition of PAs used in the feeding and calculated by the NMR technique for each product.

Table 3. 11 Comparative molar ratio of sebacoyl chloride (Seb Cl) and BCAETE between the feed proportion and the corresponding monomers in final polymers calculated through NMR.

Sample	n (Seb Cl):(BCAETE) feed	n (Seb Cl):(BCAETE) NMR
PA I	1:0	1:0
PA II	0.75:0.25	0.81:0.19
PA III	0.5:0.5	0.53:0.47
PA IV	0.25:0.75	0.28:0.72
PA V	0:1	0:1

In the synthesized polymers, the presence of the two acid derived monomers in the same composition of the initial feed, suggests a similar reactivity of both acyl chlorides.

All the poly(ester amide)s synthesized from the BAAE are soluble in DMSO and the DMF solubility decreases as the BCAETE amount increases in the polymers. The SEC analysis for the determination of the polymers molecular weights is shown in Figure A 28 in the appendix.

The cleavage ability of the poly(ester amide) was proved by a SEC analysis. PA II and PA III were solubilized in DMF and irradiated (8 h, red-light, 80 mW.cm^{-2}) in the presence of Ce6 (10 wt%). For comparison purposes, a solution of PAII and PAIII was kept in the dark. Figure 3. 57 shows the SEC results.
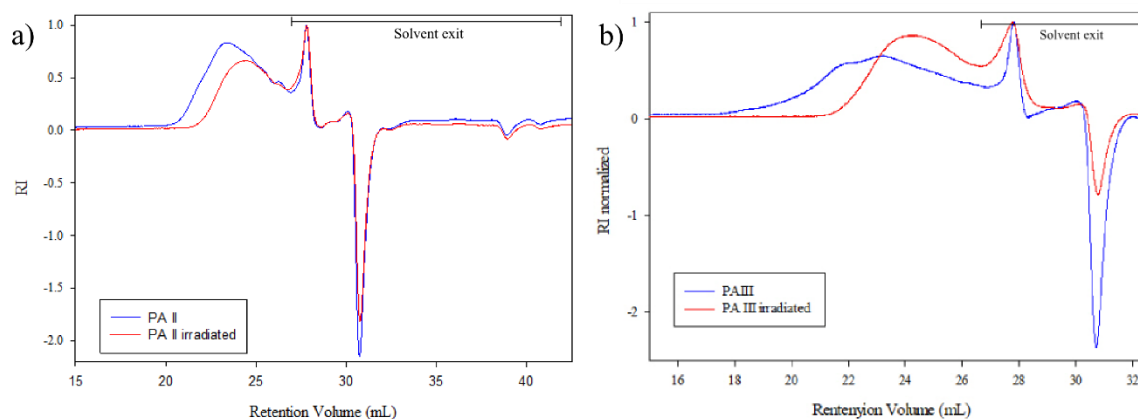
Figure 3. 57 SEC in DMF solution of the PAII (a) and PAIII (b) with and without Ce6 after irradiation (2 h, 650 nm, 80 mW.cm^{-2})

After light irradiation, it is notorious the increase in the retention time of PAII and PAIII, which evidences a reduction in the molecular weight, promoted by the cleavage of the linker by the action of light. The same test was carried out for the non sensitive PAI which showed no shift in the retention volume (Figure A 29 in the appendix), confirming that the light-triggered cleavage is dependent on the presence of the sensitive segment.

3.3.2 Photodegradable System Based on the PET RAFT Agent Process

Looking for different strategies to have a light sensitive segment, an explorative work that could use the Photoinduced Electron Transfer (PET) for Reversible Addition-Fragmentation Chain Transfer (RAFT) polymerization process to create light sensitive segments was carried out.

RAFT polymerization by PET with a photoredox catalyst and a thiocarbonylthiol (TCT) was recently introduced by the Boyer group. The photoredox catalyst (PC) is elevated to an oxidation state in which thiocarbonylthio is reduced to generate a radical anion, resulting in a TCT anion fragmentation and giving an initiating carbon-centered radical. The complete catalytic cycle is made by electron transfer, (re)generating the dormant polymer chain and the photocatalyst coming back to its ground state [250]. Figure 3. 58 shows the scheme of this reaction.

140
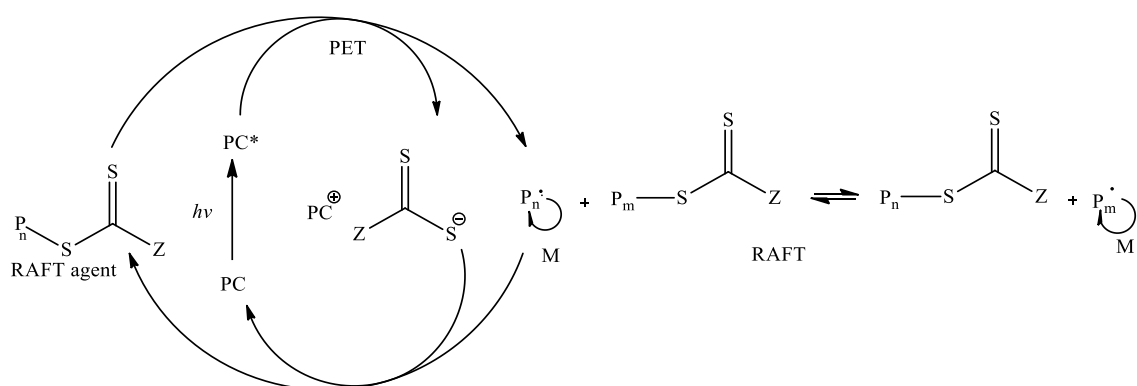
Figure 3. 58 Method of living polymerization via photoredox catalysis, activation of TCT resulting in a single electron reduction of TCT prior to radical polymerization.

The RAFT agent could break into two reactive segments when in contact with a molecule in an excited state, originating a carbon centered radical (P_n.). Thus, if we synthesize a RAFT agent of this kind but with a hydrophobic polymer in one side of the RAFT agent (S side) and a hydrophilic polymer on the other side (Z side), such as PEG-PLA, we could use this cleavage to destabilize any structure. With a PEG-RAFT agent-PLA copolymer, able to form micelle, and a PC, we could generate a new strategy for drug delivery systems. Basically, the RAFT agent cleavage would lead to the destruction of the copolymer amphiphilicity with consequent destabilization of the micelle structure. Figure 3. 59 shows the scheme of the cleavage process with the amphiphilic RAFT agent.
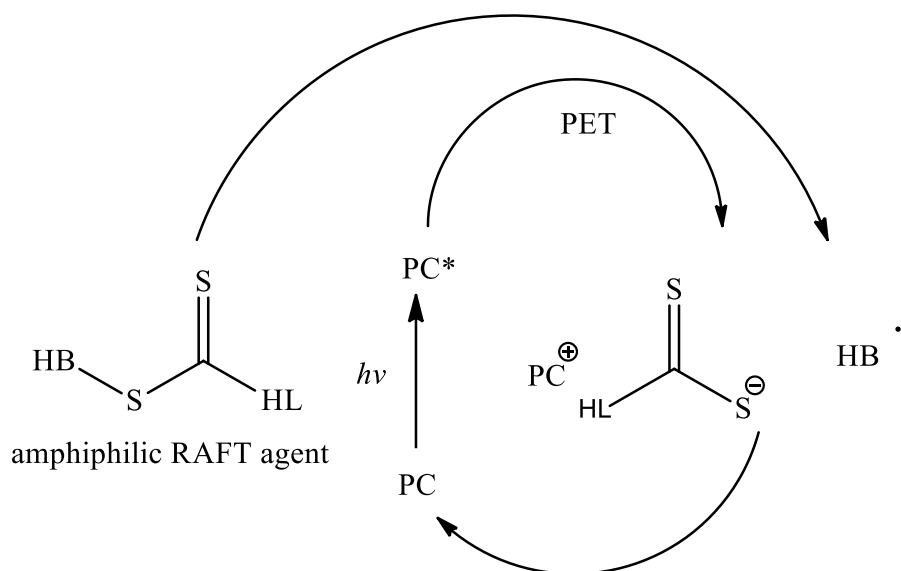
Figure 3. 59 Break of the amphiphilic RAFT agent to separate the hydrophobic (HB) and hydrophilic (HL) part through the PET-RAFT strategy.

The major difference between our approach and PET-RAFT process is that we need to have conditions that allows the HB. radical to be reduced by a reducing agent, otherwise the reactions do not go forward.

DDMAT Cleavage

To evaluate if it is possible to have this kind of cleavage, a proof-of-concept was carried out using a simple RAFT agent, the commercially available 2-(dodecylthiocarbonothioylthio)-2-methylpropionic acid (DDMAT) (Figure 3. 60 shows DDMAT structure).
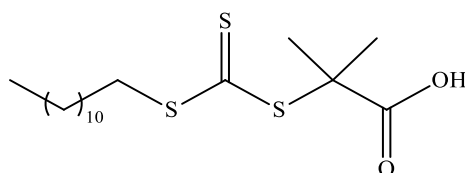
Figure 3. 60 DDMAT structure.

DDMAT was dissolved in deuterated chloroform with TPP porphyrin as PC, exposed to 2 h to red light (635 nm, 3.5 mW.cm^{-2}) and then analyzed by the ^{1}H NMR. DDMAT compound showed no shift or new peaks in the spectrum, indicating that no cleavage occurred. The experiment was repeated using a higher energy power and longer exposition time (4 h of white light, 3.5 mW.cm^{-2}). Unfortunately, the spectrum showed no modification after irradiation. To overcome this issue, TPP was replaced by ZnTPP due to its higher stability and was the PC used by Boyer. However, no difference in the DDMAT structure could be noticed in the spectrum after 2 h of red-light irradiation (635 nm, 3.5 mW.cm^{-2}). Different concentrations of DDMAT and porphyrin were also tried (1:0.0002 and 1:0.002) but the compound did not suffer any structural changes as revealed by the ^{1}H NMR analysis. Figure A 30 in the appendix shows all the ^{1}H NMR spectra.

Taking into account these results, it was hypothesized that if DDMAT was suffering the cleavage into two reactive radicals, but in the absence of a hydrogen donor, the radicals were able to join together again. In order to avoid this reaction, a hydrogen donor must be added to react with the HB radical. Figure 3. 61 shows the scheme of the reaction.
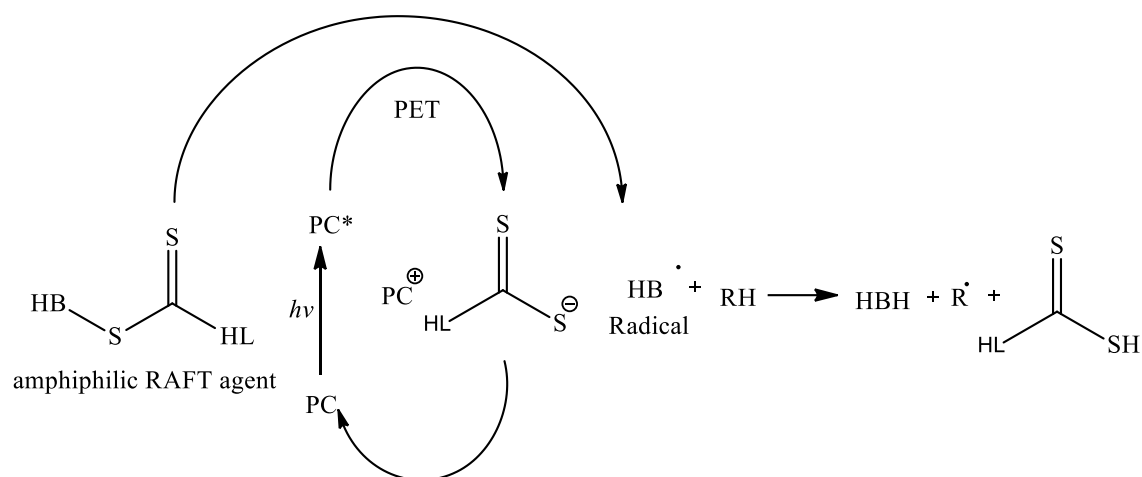
Figure 3. 61 Scheme of the amphiphilic polymer cleavage by the RAFT-PET process in the presence of a hydrogen donor.

Hydroquinone was the first compound tested, but its low solubility in chloroform made no difference in the break reaction. Hence, 2,6 di-tert-butyl-4-methylphenol (TBM) was used to interact with the reactive compound. Despite that, no change in ^{1}H NMR spectrum could be noticed, evidencing the lack of DDMAT break. Figure A 30 in the appendix shows all the spectra.

Thus, it was also hypothesized that if an excess of oxygen is present it would be acting as a quenching agent reacting with PC* avoiding the reaction with DDMAT. Oxygen is a well-known radical scavenger, and can react with the radicals to form peroxy species which inhibit radical polymerizations [251].

Regarding this fact, the DDMAT cleavage test was repeated with TBM in a small vial (2 mL, 60% smaller) to reduce the presence of oxygen and avoiding singlet oxygen quenching reaction. The relative molecular concentration used was 1:1:0.007 [TBM]:[DDMAT]:[ZnTPP] in 4 h of irradiation with white light. Figure 3. 62 shows the spectra.
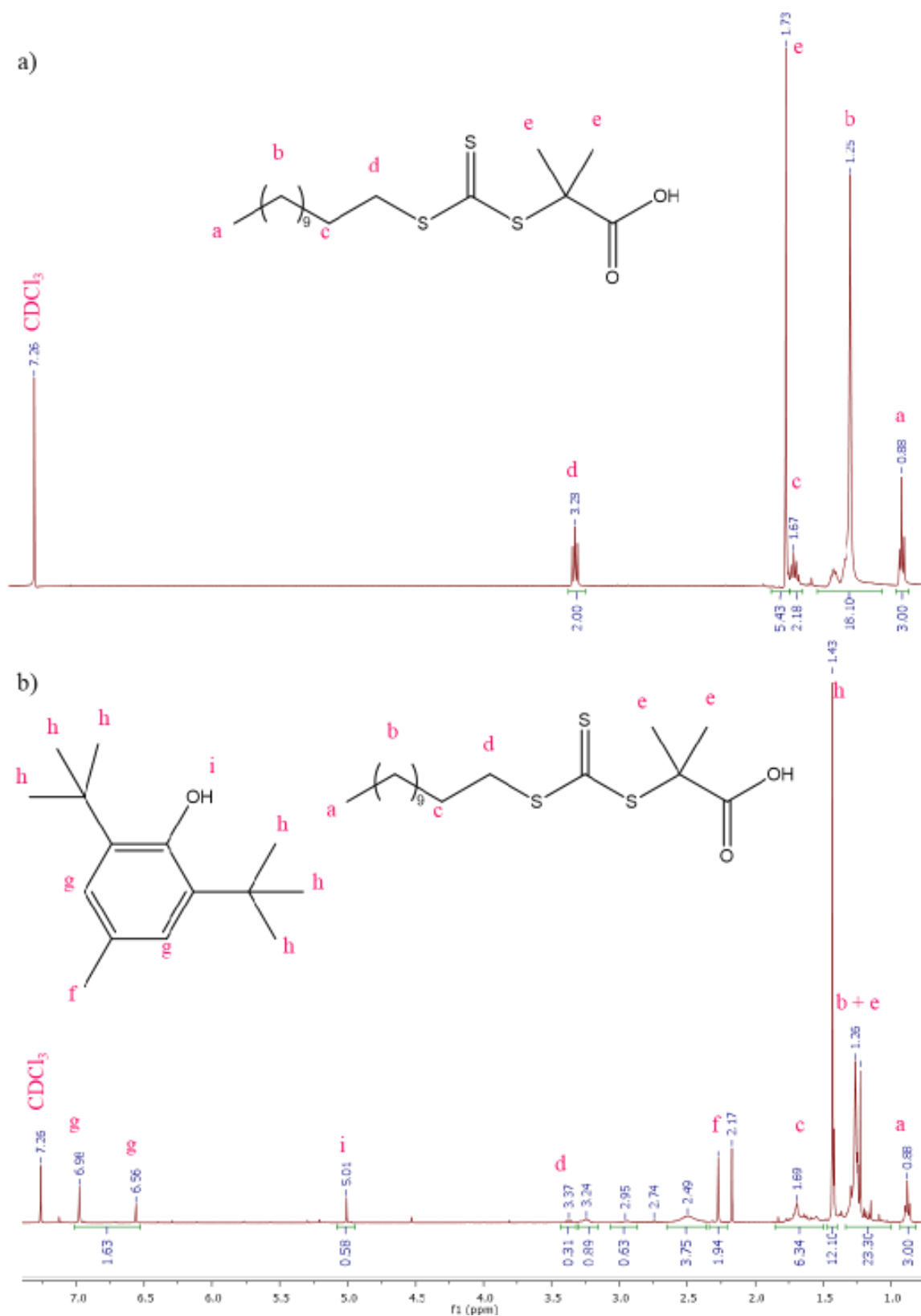
Figure 3. 62 DDMAT breaking test with a molecular rate of 1:1:0.004 ([monomer]:[DDMAT]:[ZnTPP]) after 4 h of white light exposure.

The DDMAT characteristic spectrum (Figure 3. 62, A) has the peaks corresponding to the methylene proton at 3.28 ppm (CH_2 -CH_2-S, **d**); 1.67 ppm (-$(CH_2)_9$-CH_2-, **c**) and 1.25 ppm (-$(CH_2)_9$-, **b**); the methyl protons show the signal at 1.73 ppm (-2CH_3, **e**) and 0.88 ppm (-CH_3, **a**). Figure 3. 62 (b) shows a spectrum much more complex than that of DDMAT with clear differences: the disappearance of signal **e** and signal **d** with the appearance of a new complex set of signals. These set of changes evidenced the degradation of DDMAT.

The break of the TCT moiety present in the DDMAT compound reveals a window of opportunity for a new class of light sensitivity segments. A strategical arrangement with blocks copolymers in the two sides of the TCT group will lead to a light-degradable polymer. Naturally, this process requires more studies to understand if the process works with other RAFT based agents. Also, the cleavage kinetics should be analyzed in order to evaluate the possible advantages over the already existent segments.

4 Conclusions

The aim of this thesis was the development of polymers bearing light-sensitive moieties in their structure and their application in DDSs triggered by light. The light-sensitive moiety used in this work belongs to the vinyl disulfide family. Also, a new concept of the light-sensitive system, based on the PET- RAFT agent process, was described.

The first system studied was based on an amphiphilic block copolymer composed of PEG and PLA, linked by the sensitive moiety (BHETE). The copolymer PEG-BHETE-PLA suffers cleavage when irradiated with a low power light source (3.5 mW.cm^{-2}). Several micelles were formed from different copolymers and some of them showed sizes convenient for targeting, by taking advantage of the EPR effect (< 200 nm). These micelles are able to encage DOX, in fairly good amounts, that are comparable with micellar systems reported in the literature. It is very important to refer that, the simultaneous loading with the PS did not lead to a reduction in the DOX loading. The light-triggered disassembly for Ce6 encaged nanoparticles was proven by the DLS technique. The micelles based on the copolymer with low molecular weight, the PLA (hydrophobic) block (PEG$_{5k}$-BHETE-PLA$_{1k}$), showed a faster disassembly. The drug release tests showed that in these micelles the release of DOX occurs even in dark conditions, a result that might be related with some permeability of the structure. Better control of the DOX release was achieved with PEG$_{5k}$-BHETE-PLA$_{10k}$. *In vitro* assays (MTT and SRB) revealed that the polymeric micelles were non-cytotoxic for the MCF7 cells. However, it was shown that the loaded micelles, when activated by light, enhanced MCF7 tumoral cell death when compared to the inactivated system.

A polymer with a significant increase in light sensible segments in the structure was synthesized (PDDD). In order to reach an amphiphilic structure, the PDDD polymer was linked to hydrophilic PEG, forming an ABA block copolymer. By the DLS technique, the light-triggered disassembly of PEG-PDDD-PEG micelles was proved. Additionally, drug release tests showed that the increase in the number of light-sensitive moieties in the backbone of the polymers resulted in a burst release of DOX when the system was irradiated with light. Also, preliminary *in vitro* cytotoxicity studies (MTT) with the MCF7 cell line have shown that this amphiphilic copolymer did not exert any cytotoxic effect on the cells.

To explore other families of light-responsive polymers, poly(ester amide)s were successfully prepared by interfacial polymerization between a diacyl chloride based on BCETE and an α-amino acid based diamine. The poly(ester amide)s were prepared with different amounts of light-sensitive moieties. The NMR and SEC techniques proved the light sensitivity of the polymer structure. These results are very interesting and could open new avenues in the development of novel light-triggered DDSs.

Another alternative for light-sensitive moiety was hypothesized, inspired by the PET-RAFT strategy. Cleavage of the TCT moiety (in DDMAT structure) in the presence of a hydrogen donor was proved using white-light radiation. This result is very promising and this concept can be used in the development of new light-triggered systems.

In conclusion, this work contributed to the development of new light-sensitive polymers, that have the potential to be used in light-mediated drug delivery systems.

Recommendations for future work

The light-triggered drug delivery systems require a fast and efficient reaction able to completely disintegrate the nanoparticle for a quick drug release, especially when dealing with cancer therapy. It is, also, extremely important that DDSs presents a high drug loading capacity.

To increase the drug loading capacity of micelles, polymers could be functionalized with the drug at the end of the hydrophobic polymer chain. Polymers can be synthesized like a pro-drug or a brush-polymer with groups functionalized with the drug and other groups, to balance the amphiphilic properties.

The study of the influence of the T_g of the block copolymers on the release of drugs would be of interest, since our results showed that, even in dark conditions, some DOX was released. This might be related to the permeation of the drug through the micelles due to the molecular motions of the polymer structure. The increase in the T_g value could reduce the permeability of the micelles, decreasing the off-targeted drug lixiviation from the micelle. An alternative way to minimize this issue, and that is worth being tested, is the possibility of using sensitive crosslinkers in the preparation of the micelles.

In the case of the PDDD polymer, the molecular weight should be increased through, for instance, chain extension reactions. This increase in the polymer length could increase the drug loading capacity, favoring the development of a more efficient DDS.

The insertion of a photosensitizer in the middle of the light-sensitive-hydrophobic block could also contribute to a rapid and efficient cleavage of the polymer.

The poly(ester amide)s synthesis could be further explored in order to control the interfacial polymerization and achieve a light-sensitive polymer with controlled molecular weight and *Đ*. Additionally, the preparation of amphiphilic copolymers based on poly(ester amide)s is worth being tested.

The insertion of the TCT moiety in the middle of an amphiphilic copolymer could favor the self-assembly process to form micelles for drug delivery applications. The cleavage of the TCT moiety should be studied in order to evaluate the cleavage kinetics and compare it with the existing light-sensitive segments.

References

[1]   Y. Zhang, Y. Huang, and S. Li, "Polymeric Micelles: Nanocarriers for Cancer-Targeted Drug Delivery," *AAPS PharmSciTech*, vol. 15, no. 4, pp. 862–871, 2014.

[2]   K. MG, K. V, and H. F, "History and Possible Uses of Nanomedicine Based on Nanoparticles and Nanotechnological Progress," *J. Nanomed. Nanotechnol.*, vol. 06, no. 06, 2015.

[3]   D. Bobo, K. J. Robinson, J. Islam, K. J. Thurecht, and S. R. Corrie, "Nanoparticle-Based Medicines: A Review of FDA-Approved Materials and Clinical Trials to Date," *Pharm. Res.*, vol. 33, no. 10, pp. 2373–2387, 2016.

[4]   J. Li and D. J. Mooney, "Designing hydrogels for controlled drug delivery," *Nat. Rev. Mater.*, vol. 1, no. 12, pp. 1–18, 2016.

[5]   R. Singh and L. J. W., "Nanoparticle-based targeted drug delivery," *Exp. Mol .Pathol.*, vol. 86, no. 3, pp. 215–223, 2009.

[6]   N. Amreddy *et al.*, *Recent Advances in Nanoparticle-Based Cancer Drug and Gene Delivery*, 1st ed., vol. 137. Elsevier Inc., 2018.

[7]   L. R. Peer D, Karp JM, Hong S, Farokhzad OC, Margalit R, "Nano- carriers as an emerging platform for cancer therapy," *Nat Nanotechnol*, vol. 2, no. 12, pp. 751–760, 2007.

[8]   G. Bozzuto and A. Molinari, "Liposomes as nanomedical devices," *Int. J. Nanomedicine*, vol. 10, pp. 975–999, 2015.

[9]   C. Bharti, N. Gulati, U. Nagaich, and A. Pal, "Mesoporous silica nanoparticles in target drug delivery system: A review," *Int. J. Pharm. Investig.*, vol. 5, no. 3, p. 124, 2015.

[10]   S. Sarkar *et al.*, "Advances and Implications in Nanotechnology for Lung Cancer Management," *Curr. Drug Metab.*, vol. 18, no. 33, pp. 30–38, 2017.

[11]   S. Wen, J. Zhou, K. Zheng, A. Bednarkiewicz, X. Liu, and D. Jin, "Advances in highly doped upconversion nanoparticles," *Nat. Commun.*, 2018.

[12]   O. S Vaze, "Pharmaceutical Nanocarriers (Liposomes and Micelles) in Cancer Therapy," *J. Nanomed. Nanotechnol.*, vol. 7, no. 3, 2016.

[13]   D. H. Shin, Y. T. Tam, and G. S. Kwon, "Polymeric micelle nanocarriers in cancer research," *Front. Chem. Sci. Eng.*, vol. 10, no. 3, pp. 348–359, 2016.

[14]   Z. Ahmad, A. Shah, M. Siddiq, and H. B. Kraatz, "Polymeric micelles as drug delivery vehicles," *RSC Adv.*, vol. 4, no. 33, pp. 17028–17038, 2014.

[15]   L. B. Priya, R. Baskaran, and V. V. Padma, "Chapter 21 - Phytonanoconjugates in oral medicine," in *Nanostructures for Oral Medicine*, E. Andronescu and A. M. Grumezescu, Eds. Romenia: Elsevier, 2017, pp. 629–668.

[16]   G. A. Husseini and W. G. Pitt, "Micelles and nanoparticles for ultrasonic drug and gene delivery," *Adv. Drug Deliv. Rev.*, vol. 60, no. 10, pp. 1137–1152, 2008.

[17]   N. Rapoport, R. Gupta, Y. Kim, and B. E. O. Neill, "Polymeric micelles and nanoemulsions as tumor-targeted drug carriers : Insight through intravital imaging," *J. Control. Release*, vol. 206, pp. 153–160, 2015.

[18]   E. Seong, K. Na, and Y. Han, "Doxorubicin loaded pH-sensitive polymeric micelles for reversal of resistant MCF-7 tumor," vol. 103, pp. 405–418, 2005.

[19]   S. K. Singh, S. Singh, J. W. Lillard Jr, and R. Singh, "Drug delivery approaches for breast cancer," *Int. J. Nanomedicine*, vol. 12, pp. 6205–6218, 2017.

[20]   M. Narvekar, H. Y. Xue, J. Y. Eoh, and H. L. Wong, "Nanocarrier for Poorly Water-Soluble Anticancer Drugs—Barriers of Translation and Solutions," *AAPS PharmSciTech*, vol. 15, no. 4, pp. 822–833, 2014.

[21]   A. Gothwal, I. Khan, and U. Gupta, "Polymeric Micelles: Recent Advancements in the Delivery of Anticancer Drugs," *Pharmaceutical Research*, vol. 33, no. 1. 2016.

[22]   S. S. Kulthe, Y. M. Choudhari, N. N. Inamdar, and V. Mourya, "Polymeric micelles: Authoritative aspects for drug delivery," *Des. Monomers Polym.*, vol. 15, no. 5, pp. 465–521, 2012.

[23]   W. Xu, P. Ling, and T. Zhang, "Polymeric micelles, a promising drug delivery system to

enhance bioavailability of poorly water-soluble drugs.," *J. Drug Deliv.*, vol. 2013, no. 1, p. 340315, 2013.

[24] J. Gong, M. Chen, Y. Zheng, S. Wang, and Y. Wang, "Polymeric micelles drug delivery system in oncology," *J. Control. Release*, vol. 159, no. 3, pp. 312–323, 2012.

[25] J. Li, S. Guo, M. Wang, L. Ye, and F. Yao, "Poly(lactic acid)/poly(ethylene glycol) block copolymer based shell or core cross-linked micelles for controlled release of hydrophobic drug," *RSC Adv.*, vol. 5, no. 25, pp. 19484–19492, 2015.

[26] J. Nicolas, S. Mura, D. Brambilla, N. Mackiewicz, and P. Couvreur, "Design, functionalization strategies and biomedical applications of targeted biodegradable/biocompatible polymer-based nanocarriers for drug delivery.," *Chem. Soc. Rev.*, vol. 42, no. 3, pp. 1147–235, 2013.

[27] Y. Lu and K. Park, "Polymeric micelles and alternative nanonized delivery vehicles for poorly soluble drugs," *Int. J. Pharm.*, vol. 453, no. 1, pp. 198–214, 2013.

[28] D. Peer, J. M. Karp, S. Hong, O. C. Farokhzad, R. Margalit, and R. Langer, "Nanocarriers as an emerging platform for cancer therapy," *Nat. Nanotechnol.*, vol. 2, no. 12, pp. 751–760, 2007.

[29] A. S. Deshmukh *et al.*, "Polymeric micelles: Basic research to clinical practice," *Int. J. Pharm.*, vol. 532, no. 1, pp. 249–268, 2017.

[30] J. Blanco, Elvin; Kessinger, Chase W; Sumer, Baran D.; Gao, "Multifunctional Micellar Nanomedicine for Cancer Therapy," *ExpExp Biol Med*, vol. 234, no. 2, pp. 123–131, 2009.

[31] Y. Lu and K. Park, "Polymeric micelles and alternative nanonized delivery vehicles for poorly soluble drugs," *Int. J. Pharm.*, vol. 453, no. 1, pp. 198–214, 2013.

[32] M. Yokoyama, "Polymeric micelles as a new drug carrier system and their required considerations for clinical trials.," *Expert Opin. Drug Deliv.*, vol. 7, no. 2, pp. 145–158, 2010.

[33] H. Cabral and K. Kataoka, "Progress of drug-loaded polymeric micelles into clinical studies," *J. Control. Release*, vol. 190, pp. 465–476, 2014.

[34] C. Oerlemans, W. Bult, M. Bos, G. Storm, J. F. W. Nijsen, and W. E. Hennink, "Polymeric micelles in anticancer therapy: Targeting, imaging and triggered release," *Pharm. Res.*, vol. 27, no. 12, pp. 2569–2589, 2010.

[35] R. Dhar, A. Saneja, P. K. Gupta, and P. N. Gupta, "European Journal of Pharmaceutical Sciences Recent advances in drug delivery strategies for improved therapeutic ef fi cacy of gemcitabine," *Phasci*, vol. 93, pp. 147–162, 2016.

[36] C. L. Ventola, "Progress in Nanomedicine: Approved and Investigational Nanodrugs.," *P T*, vol. 42, no. 12, pp. 742–755, 2017.

[37] J. Song *et al.*, "The power of the ring: A pH-responsive hydrophobic epoxide monomer for superior micelle stability," *Polym. Chem.*, vol. 8, no. 46, pp. 7119–7132, 2017.

[38] K. Letchford and H. Burt, "A review of the formation and classification of amphiphilic block copolymer nanoparticulate structures: micelles, nanospheres, nanocapsules and polymersomes," *Eur. J. Pharm. Biopharm.*, vol. 65, no. 3, pp. 259–269, 2007.

[39] P. Lai, W. Daear, R. Löbenberg, and E. J. Prenner, "Overview of the preparation of organic polymeric nanoparticles for drug delivery based on gelatine, chitosan, poly(d,l-lactide-co-glycolic acid) and polyalkylcyanoacrylate.," *Colloids Surf. B. Biointerfaces*, vol. 118, pp. 154–63, 2014.

[40] K. Zhang *et al.*, "PEG-PLGA copolymers: Their structure and structure-influenced drug delivery applications," *J. Control. Release*, vol. 183, no. 1, pp. 77–86, 2014.

[41] G. Gaucher, M.-H. Dufresne, V. P. Sant, N. Kang, D. Maysinger, and J.-C. Leroux, "Block copolymer micelles: preparation, characterization and application in drug delivery.," *J. Control. Release*, vol. 109, no. 1–3, pp. 169–188, 2005.

[42] U. Kedar, P. Phutane, S. Shidhaye, and V. Kadam, "Advances in polymeric micelles for drug delivery and tumor targeting," *Nanomedicine Nanotechnology, Biol. Med.*, vol. 6, no. 6, pp. 714–729, 2010.

[43] V. J. Stella, R. T. Borchardt, M. J. Hageman, R. Oilyai, and H. Maag, *Nanotechnology in Drug Delivery*. New York: Springer and AAPS Press, 2009.

[44] F. Puoci, *Advanced Polymers in Medicine*. Switzerland: Springer, 2015.

[45] T. Miller *et al.*, "Drug loading of polymeric micelles," *Pharm. Res.*, vol. 30, no. 2, pp. 584–595, 2013.

[46] W. Y. Ayen, K. Garkhal, and N. Kumar, "Doxorubicin-loaded (PEG)3-PLA nanopolymersomes: Effect of solvents and process parameters on formulation development and in vitro study," *Mol. Pharm.*, vol. 8, no. 2, pp. 466–478, 2011.

[47] K.-Y. Lee, Y.-T. Chiu, and C.-L. Lo, "Preparation and characterization of potential doxorubicin-loaded mixed micelles formed from vitamin E containing graft copolymers and PEG-b-PLA diblock copolymers," *RSC Adv.*, vol. 5, no. 102, pp. 83825–83836, 2015.

[48] Q. Yang *et al.*, "Redox-responsive micelles self-assembled from dynamic covalent block copolymers for intracellular drug delivery," *Acta Biomater.*, vol. 17, pp. 193–200, 2015.

[49] W. Chen, F. Meng, R. Cheng, C. Deng, J. Feijen, and Z. Zhong, "Advanced drug and gene delivery systems based on functional biodegradable polycarbonates and copolymers.," *J. Control. Release*, vol. 190, pp. 398–414, 2014.

[50] A. J. R. Lasprilla, G. a R. Martinez, B. H. Lunelli, A. L. Jardini, and R. M. Filho, "Poly-lactic acid synthesis for application in biomedical devices - A review," *Biotechnol. Adv.*, vol. 30, no. 1, pp. 321–328, 2012.

[51] S. Inkinen, M. Hakkarainen, A. C. Albertsson, and A. Södergård, "From lactic acid to poly(lactic acid) (PLA): Characterization and analysis of PLA and Its precursors," *Biomacromolecules*, vol. 12, no. 3, pp. 523–532, 2011.

[52] C. Vasile, *Handbook of Biodegradable Polymers*, no. 0. United Kingdom: rapra technology, 2005.

[53] a. P. Gupta and V. Kumar, "New emerging trends in synthetic biodegradable polymers - Polylactide: A critique," *Eur. Polym. J.*, vol. 43, no. 10, pp. 4053–4074, 2007.

[54] K. Madhavan Nampoothiri, N. R. Nair, and R. P. John, "An overview of the recent developments in polylactide (PLA) research," *Bioresour. Technol.*, vol. 101, no. 22, pp. 8493–8501, 2010.

[55] C. Garofalo *et al.*, "Different insight into amphiphilic PEG-PLA copolymers: Influence of macromolecular architecture on the micelle formation and cellular uptake," *Biomacromolecules*, vol. 15, no. 1, pp. 403–415, 2014.

[56] R. Auras, B. Harte, and S. Selke, "An overview of polylactides as packaging materials," *Macromol. Biosci.*, vol. 4, no. 9, pp. 835–864, 2004.

[57] K. Jelonek, S. Li, X. Wu, J. Kasperczyk, and A. Marcinkowski, "Self-assembled filomicelles prepared from polylactide/poly(ethylene glycol) block copolymers for anticancer drug delivery," *Int. J. Pharm.*, vol. 485, no. 1–2, pp. 357–364, 2015.

[58] S. M. D'Addio *et al.*, "Effects of block copolymer properties on nanocarrier protection from in vivo clearance," *J. Control. Release*, vol. 162, no. 1, pp. 208–217, 2012.

[59] A. Kolate, D. Baradia, S. Patil, I. Vhora, G. Kore, and A. Misra, "PEG - A versatile conjugating ligand for drugs and drug delivery systems," *J. Control. Release*, vol. 192, pp. 67–81, 2014.

[60] M. J. Ernsting, M. Murakami, A. Roy, and S.-D. Li, "Factors Controlling the Pharmacokinetics, Biodistribution and Intratumoral Penetration of Nanoparticles," *J. Control. Release*, vol. 172, no. 3, pp. 782–794, 2013.

[61] F. M. Veronese and G. Pasut, "PEGylation, successful approach to drug delivery," *Drug Discov. Today*, vol. 10, no. 21, pp. 1451–1458, 2005.

[62] T. Ishihara, M. Takahashi, M. Higaki, Y. Mizushima, and T. Mizushima, "Preparation and characterization of a nanoparticulate formulation composed of PEG-PLA and PLA as anti-inflammatory agents," *Int. J. Pharm.*, vol. 385, no. 1–2, pp. 170–175, 2010.

[63] S. a Hagan *et al.*, "Polylactide - Poly (ethylene glycol) Copolymers as Drug Delivery Systems . 1 . Characterization of Water Dispersible Micelle-Forming Systems," *Langmuir*, vol. 12, no. 9, pp. 2153–2161, 1996.

[64] L. Xiong and Z. He, "The Biological Evaluation of the PEG/PLA Amphiphilic Diblock Copolymer," *Polym. Plast. Technol. Eng.*, vol. 49, no. 12, pp. 1201–1206, 2010.

[65] A. Sauer, A. Kapelski, C. Fliedel, S. Dagorne, M. Kol, and J. Okuda, "Structurally well-defined group 4 metal complexes as initiators for the ring-opening polymerization of lactide monomers," *Dalt. Trans.*, vol. 42, no. 25, pp. 9007–9023, 2013.

[66] A. Stopper, J. Okuda, and M. Kol, "Ring-opening polymerization of lactide with Zr complexes of {ONSO} ligands: From heterotactically inclined to isotactically inclined poly(lactic acid)," *Macromolecules*, vol. 45, no. 2, pp. 698–704, 2012.

[67] M. Bouyahyi, N. Ajellal, E. Kirillov, C. M. Thomas, and J. F. Carpentier, "Exploring electronic versus steric effects in stereoselective ring-opening polymerization of lactide and β-butyrolactone with amino-alkoxy- bis(phenolate)-yttrium complexes," *Chem. - A Eur. J.*, vol. 17, no. 6, pp. 1872–1883, 2011.

[68] D. J. Coady, K. Fukushima, H. W. Horn, J. E. Rice, and J. L. Hedrick, "Catalytic insights into acid/base conjugates: Highly selective bifunctional catalysts for the ring-opening polymerization of lactide," *Chem. Commun.*, vol. 47, no. 11, pp. 3105–3107, 2011.

[69] H. A. Brown, A. G. De Crisci, J. L. Hedrick, and R. M. Waymouth, "Amidine-mediated zwitterionic polymerization of lactide," *ACS Macro Lett.*, vol. 1, no. 9, pp. 1113–1115, 2012.

[70] H. Qian, A. R. Wohl, J. T. Crow, C. W. MacOsko, and T. R. Hoye, "A strategy for control of 'random' copolymerization of lactide and glycolide: Application to synthesis of PEG- b -PLGA block polymers having narrow dispersity," *Macromolecules*, vol. 44, no. 18, pp. 7132–7140, 2011.

[71] N. Kang, M. È. Perron, R. E. Prud'Homme, Y. Zhang, G. Gaucher, and J. C. Leroux, "Stereocomplex block copolymer micelles: Core-shell nanostructures with enhanced stability," *Nano Lett.*, vol. 5, no. 2, pp. 315–319, 2005.

[72] N. Nasongkla *et al.*, "Multifunctional Polymeric Micelles as Cancer-Targeted, MRI-Ultrasensitive Drug Delivery Systems," *Nano Lett.*, vol. 6, no. 11, pp. 3–6, 2006.

[73] M. Alibolandi, M. Ramezani, K. Abnous, F. Sadeghi, and F. Hadizadeh, "Comparative evaluation of polymersome versus micelle structures as vehicles for the controlled release of drugs," *J. Nanoparticle Res.*, vol. 17, no. 2, 2015.

[74] M. Theerasilp and N. Nasongkla, "Comparative studies of poly(ε-caprolactone) and poly(D,L-lactide) as core materials of polymeric micelles.," *J. Microencapsul.*, vol. 30, no. 4, pp. 390–7, 2013.

[75] M. Alibolandi, F. Sadeghi, S. H. Sazmand, S. M. Shahrokhi, M. Seifi, and F. Hadizadeh, "Synthesis and self-assembly of biodegradable polyethylene glycol-poly (lactic acid) diblock copolymers as polymersomes for preparation of sustained release system of doxorubicin," *Int. J. Pharm. Investig.*, vol. 5, no. 3, pp. 134–141, 2015.

[76] A. Ouahab, N. Cheraga, V. Onoja, Y. Shen, and J. Tu, "Novel pH-sensitive charge-reversal cell penetrating peptide conjugated PEG-PLA micelles for docetaxel delivery: In vitro study," *Int. J. Pharm.*, vol. 466, no. 1–2, pp. 233–245, 2014.

[77] Z. Fan *et al.*, "Adding Vitamin E-TPGS to the Formulation of Genexol-PM: Specially Mixed Micelles Improve Drug-Loading Ability and Cytotoxicity against Multidrug-Resistant Tumors Significantly," *PLoS One*, vol. 10, no. 4, p. e0120129, 2015.

[78] M. Longmire, P. L. Choyke, and H. Kobayashi, "Clearance Properties of Nano-sized Particles and Molecules as Imaging Agents: Considerations and Caveats," *Nanomedicine (lond)*, vol. 3, no. 5, pp. 703–717, 2012.

[79] H. M. Aliabadi, S. Elhasi, A. Mahmud, R. Gulamhusein, P. Mahdipoor, and A. Lavasanifar, "Encapsulation of hydrophobic drugs in polymeric micelles through co-solvent evaporation: The effect of solvent composition on micellar properties and drug loading," *Int. J. Pharm.*, vol. 329, no. 1–2, pp. 158–165, 2007.

[80] E. Pişkin, X. Kaitian, E. B. Denkbaş, and Z. Küçükyavuz, "Novel PDLLA/PEG copolymer micelles as drug carriers," *J. Biomater. Sci. Polym. Ed.*, vol. 7, no. 4, pp. 359–373, 1995.

[81] R. Z. Xiao, Z. W. Zeng, G. L. Zhou, J. J. Wang, F. Z. Li, and A. M. Wang, "Recent advances in PEG-PLA block copolymer nanoparticles," *Int. J. Nanomedicine*, vol. 5, no. 1, pp. 1057–1065, 2010.

[82] C. O. Rangel-Yagui, a. Pessoa-Jr, and D. Blankschtein, "Two-Phase Aqueous Micellar Systems - an Alternative Method for Protein Purification," *Brazilian J. Chem. Eng.*, vol. 21, no. 04, pp. 531–544, 2004.

[83] D. J. Adams *et al.*, "On the mechanism of formation of vesicles from poly(ethylene oxide)-block-poly(caprolactone) copolymers," *Soft Matter*, vol. 5, no. 16, pp. 3086–3096, 2009.

[84] C. Allen, D. Maysinger, and A. Eisenberg, "Nano-engineering block copolymer aggregates for drug delivery," *Colloids Surfaces B Biointerfaces*, vol. 16, no. 1–4, pp. 3–27, 1999.

[85] Y. A. N. Geng, P. Dalhaimer, S. Cai, R. Tsai, T. Minko, and D. E. Discher, "Shape effects of filaments versus spherical particles in flow and drug delivery," *Nat. Nanotechnol.*, vol. 2, no. 4, pp. 249–255, 2007.

[86] K. Kataoka, A. Harada, and Y. Nagasaki, "Block copolymer micelles for drug delivery: Design, characterization and biological significance," *Adv. Drug Deliv. Rev.*, vol. 64, no. SUPPL., pp. 37–48, 2012.

[87] M. Talelli, M. Barz, C. J. F. Rijcken, F. Kiessling, W. E. Hennink, and T. Lammers, "Core-crosslinked polymeric micelles: Principles, preparation, biomedical applications and clinical translation," *Nano Today*, vol. 10, no. 1, pp. 93–117, 2015.

[88] Y. Kim, M. H. Pourgholami, D. L. Morris, and M. H. Stenzel, "Effect of cross-linking on the performance of micelles as drug delivery carriers: A cell uptake study," *Biomacromolecules*, vol. 13, no. 3, pp. 814–825, 2012.

[89] Y. Li, X. R. Qi, Y. Maitani, and T. Nagai, "PEG-PLA diblock copolymer micelle-like nanoparticles as all-trans-retinoic acid carrier: in vitro and in vivo characterizations.," *Nanotechnology*, vol. 20, no. 5, p. 055106, 2009.

[90] L. Yang, Z. Zhao, J. Wei, A. El, and S. Li, "Micelles formed by self-assembling of polylactide / poly (ethylene glycol) block copolymers in aqueous solutions," vol. 314, pp. 470–477, 2007.

[91] S. C. Owen, D. P. Y. Chan, and M. S. Shoichet, "Polymeric micelle stability," *Nano Today*, vol. 7, no. 1, pp. 53–65, 2012.

[92] Y. Zhang *et al.*, "Strategies for improving the payload of small molecular drugs in polymeric micelles," *J. Control. Release*, vol. 261, pp. 352–366, 2017.

[93] T. Govender *et al.*, "Defining the drug incorporation properties of PLA-PEG nanoparticles," *Int. J. Pharm.*, vol. 199, no. 1, pp. 95–110, 2000.

[94] S. Lv *et al.*, "High Drug Loading and Sub-Quantitative Loading Efficiency of Polymeric Micelles Driven by Donor-Receptor Coordination Interactions," *J. Am. Chem. Soc.*, vol. 140, no. 4, pp. 1235–1238, 2018.

[95] M. Meunier, A. Goupil, and P. Lienard, "Predicting drug loading in PLA-PEG nanoparticles," *Int. J. Pharm.*, vol. 526, no. 1–2, pp. 157–166, 2017.

[96] M. Hans, K. Shimoni, D. Danino, S. J. Siegel, and A. Lowman, "Synthesis and Characterization of mPEG - PLA Prodrug Micelles," pp. 2708–2717, 2005.

[97] S. Puntawee *et al.*, "Solubility enhancement and in vitro evaluation of PEG- b -PLA micelles as nanocarrier of semi-synthetic andrographolide analogue for cholangiocarcinoma chemotherapy," *Pharm. Dev. Technol.*, vol. 00, no. 00, pp. 1–8, 2015.

[98] Y. Shi, H. Zhu, Y. Ren, K. Li, B. Tian, and J. Han, "Preparation of protein-loaded PEG-PLA micelles and the effects of ultrasonication on particle size," *Colloid Polym. Sci.*, pp. 259–266, 2017.

[99] T. M. Popiolski *et al.*, "Preparation of Polymeric Micelles of Poly (Ethylene Oxide- b - Lactic Acid) and their Encapsulation With Lavender Oil," vol. 19, no. 6, pp. 1356–1365, 2016.

[100] Z. Daman *et al.*, "Polymeric Micelles of PEG-PLA Copolymer as a Carrier for Salinomycin Against Gemcitabine-Resistant Pancreatic Cancer," pp. 3756–3767, 2015.

[101] H. Danafar *et al.*, "Drug-conjugated PLA – PEG – PLA copolymers : a novel approach for controlled delivery of hydrophilic drugs by micelle formation Drug-conjugated PLA – PEG – PLA copolymers : a novel approach for controlled delivery of hydrophilic drugs by micelle formation," vol. 7450, no. January, 2016.

[102] T. Riley *et al.*, "Physicochemical Evaluation of Nanoparticles Assembled from Poly (lactic acid) - Poly (ethylene glycol) (PLA - PEG) Block Copolymers as Drug Delivery Vehicles," no. 16, pp. 3168–3174, 2001.

[103] Y. Li, X. R. Qi, Y. Maitani, and T. Nagai, "PEG – PLA diblock copolymer micelle-like nanoparticles as all-trans-retinoic acid carrier : in vitro and in vivo characterizations," 2009.

[104] and S. S. D. T. Riley, C. R. Heald, S. Stolnik, M. C. Garnett, L. Illum, "Core-Shell Structure of PLA-PEG Nanoparticles Used for Drug Delivery," *langmuir*, no. 19, pp. 8428–8435,

2003.

[105] K. Jelonek, S. Li, J. Kasperczyk, X. Wu, and A. Orchel, "Effect of polymer degradation on prolonged release of paclitaxel from fi lomicelles of polylactide / poly (ethylene glycol) block copolymers," *Mater. Sci. Eng. C*, vol. 75, pp. 918–925, 2017.

[106] Z. Zhang *et al.*, "Cellular uptake and intracellular trafficking of PEG- b -PLA polymeric micelles," *Biomaterials*, vol. 33, no. 29, pp. 7233–7240, 2012.

[107] K. M. Huh, S. C. Lee, Y. W. Cho, J. Lee, J. H. Jeong, and K. Park, "Hydrotropic polymer micelle system for delivery of paclitaxel," vol. 101, pp. 59–68, 2005.

[108] S. S. Venkatraman, P. Jie, F. Min, B. Yin, C. Freddy, and G. Leong-huat, "Micelle-like nanoparticles of PLA – PEG – PLA triblock copolymer as chemotherapeutic carrier," vol. 298, pp. 219–232, 2005.

[109] Y. Yamamoto, Y. Nagasaki, Y. Kato, and Y. Sugiyama, "Long-circulating poly (ethylene glycol)– poly (D , L -lactide) block copolymer micelles with modulated surface charge," vol. 77, pp. 27–38, 2001.

[110] G. He, L. L. Ma, J. Pan, and S. Venkatraman, "ABA and BAB type triblock copolymers of PEG and PLA : A comparative study of drug release properties and ' stealth ' particle characteristics," vol. 334, pp. 48–55, 2007.

[111] L. Yang, X. Wu, F. Liu, Y. Duan, and S. Li, "Novel Biodegradable Polylactide / poly (ethylene glycol) Micelles Prepared by Direct Dissolution Method for Controlled Delivery of Anticancer Drugs," vol. 26, no. 10, pp. 2332–2342, 2009.

[112] L. Yang, X. Qi, P. Liu, A. El, and S. Li, "Aggregation behavior of self-assembling polylactide / poly (ethylene glycol) micelles for sustained drug delivery," *Int. J. Pharm.*, vol. 394, no. 1–2, pp. 43–49, 2010.

[113] L. Yang, A. El, and S. Li, "In vitro degradation behavior of poly (lactide)– poly (ethylene glycol) block copolymer micelles in aqueous solution," *Int. J. Pharm.*, vol. 400, no. 1–2, pp. 96–103, 2010.

[114] S. Mura, J. Nicolas, and P. Couvreur, "Stimuli-responsive nanocarriers for drug delivery.," *Nat. Mater.*, vol. 12, no. 11, pp. 991–1003, 2013.

[115] P. Xiao, J. Zhang, J. Zhao, and M. H. Stenzel, "Light-induced release of molecules from polymers," *Prog. Polym. Sci.*, vol. 74, pp. 1–33, 2017.

[116] Y. Zhao, "Light-Responsive Block Copolymer Micelles," *Macromolecules*, vol. 45, pp. 3647–3657, 2012.

[117] N. Fomina, J. Sankaranarayanan, and A. Almutairi, "Photochemical mechanisms of light-triggered release from nanocarriers," *Adv. Drug Deliv. Rev.*, vol. 64, no. 11, pp. 1005–1020, 2012.

[118] G. Shim *et al.*, "Light-switchable systems for remotely controlled drug delivery," *J. Control. Release*, no. May, pp. 0–1, 2017.

[119] J. Olejniczak, C. J. Carling, and A. Almutairi, "Photocontrolled release using one-photon absorption of visible or NIR light," *J. Control. Release*, vol. 219, pp. 18–30, 2015.

[120] A. Y. Rwei, W. Wang, and D. S. Kohane, "Photoresponsive nanoparticles for drug delivery," *Nano Today*, vol. 10, no. 4, pp. 451–467, 2015.

[121] N. Rahoui, B. Jiang, N. Taloub, and Y. D. Huang, "Spatio-temporal control strategy of drug delivery systems based nano structures," *J. Control. Release*, vol. 255, no. January, pp. 176–201, 2017.

[122] S. Wu and H. J. Butt, "Near-Infrared-Sensitive Materials Based on Upconverting Nanoparticles," *Adv. Mater.*, vol. 28, no. 6, pp. 1208–1226, 2016.

[123] A. P. Castano, T. N. Demidova, and M. R. Hamblin, "Mechanisms in photodynamic therapy: Part one - Photosensitizers, photochemistry and cellular localization," *Photodiagnosis Photodyn. Ther.*, vol. 1, no. 4, pp. 279–293, 2004.

[124] M. Dichiara *et al.*, "Recent advances in drug discovery of phototherapeutic non-porphyrinic anticancer agents," *Eur. J. Med. Chem.*, vol. 142, pp. 459–485, 2017.

[125] O. V Gerasimov, J. A. Boomer, M. M. Qualls, and D. H. Thompson, "Cytosolic drug delivery using pH-and light-sensitive liposomes," *Adv. Drug Deliv. Rev.*, vol. 38, no. 3, pp. 317–338, 1999.

[126] K. Deng *et al.*, "Recent Progress in Near Infrared Light Triggered Photodynamic Therapy,"
156

Small, vol. 13, no. 44, pp. 1–27, 2017.

[127] W. Sharman, C. Allen, and van Lier JE, "Photodynamic therapeutics: basic principles and clinical applications.," *Drug Discov. Today*, vol. 4, no. 11, pp. 507–517, 1999.

[128] H. Abrahamse, C. A. Kruger, S. Kadanyo, and A. Mishra, "Nanoparticles for Advanced Photodynamic Therapy of Cancer," *Photomed. Laser Surg.*, vol. 35, no. 11, pp. 581–588, 2017.

[129] H. J. Cho, M. Chung, and M. S. Shim, "Engineered photo-responsive materials for near-infrared-triggered drug delivery," *J. Ind. Eng. Chem.*, vol. 31, pp. 15–25, 2015.

[130] B. M. Lamb and C. F. Barbas III, "Selective arylthiolane deprotection by singlet oxygen: a promising tool for sensors and prodrugs," *Chem. Commun. Chem. Commun*, vol. 3196, no. 51, pp. 3196–3199, 2015.

[131] M. Zamadar *et al.*, "Photosensitizer drug delivery via an optical fiber," *J. Am. Chem. Soc.*, vol. 133, no. 20, pp. 7882–7891, 2011.

[132] G. Saravanakumar, J. Lee, J. Kim, and W. J. Kim, "Visible light-induced singlet oxygen-mediated intracellular disassembly of polymeric micelles co-loaded with a photosensitizer and an anticancer drug for enhanced photodynamic therapy," *Chem. Commun.*, vol. 51, no. 49, pp. 9995–9998, 2015.

[133] G. Saravanakumar *et al.*, "Miktoarm Amphiphilic Block Copolymer with Singlet Oxygen-Labile Stereospecific β-aminoacrylate Junction: Synthesis, Self-assembly, and Photodynamically Triggered Drug Release," *Biomacromolecules*, vol. 19, no. 6, pp. 2202–2213, 2018.

[134] Z. Cao *et al.*, "ROS-Sensitive Polymeric Nanocarriers with Red Light-Activated Size Shrinkage for Remotely Controlled Drug Release," *Chem. Mater.*, vol. 30, no. 2, pp. 517–525, 2018.

[135] X. Cheng *et al.*, "Dual pH and oxidation-responsive nanogels crosslinked by diselenide bonds for controlled drug delivery," *Polym. (United Kingdom)*, vol. 101, pp. 370–378, 2016.

[136] F. Fan, L. Wang, F. Li, Y. Fu, and H. Xu, "Stimuli-Responsive Layer-by-Layer Tellurium-Containing Polymer Films for the Combination of Chemotherapy and Photodynamic Therapy," *ACS Appl. Mater. Interfaces*, vol. 8, no. 26, pp. 17004–17010, 2016.

[137] K. Kim, C.-S. Lee, and K. Na, "Light-controlled reactive oxygen species (ROS)-producible polymeric micelles with simultaneous drug-release triggering and endo/lysosomal escape," *Chem. Commun.*, vol. 52, no. 13, pp. 2839–2842, 2016.

[138] X. Li *et al.*, "Singlet oxygen-responsive micelles for enhanced photodynamic therapy," *J. Control. Release*, vol. 260, no. February, pp. 12–21, 2017.

[139] V. C. Anderson and D. H. Thompson, "Triggered release of hydrophilic agents from plasmalogen liposomes using visible light or acid.," *Biochim. Biophys. Acta*, vol. 1109, pp. 33–42, 1992.

[140] M. Y. Jiang and D. Dolphin, "Site-Specific Prodrug Release Using Visible Light," *J. Am. Chem. Soc.*, vol. 130, no. 13, pp. 4236–4237, 2008.

[141] C. S. Jin and G. Zheng, "Liposomal nanostructures for photosensitizer delivery," *Lasers Surg. Med.*, vol. 43, no. 7, pp. 734–748, 2011.

[142] K. Berg *et al.*, "Photochemical internalization: A novel technology for delivery of macromolecules into cytosol," *Cancer Res.*, vol. 59, no. 6, pp. 1180–1183, 1999.

[143] K. A. Carter *et al.*, "Porphyrin-phospholipid liposomes permeabilized by near-infrared light," *Nat. Commun.*, vol. 5, pp. 1–11, 2014.

[144] C. Alvarez-lorenzo, L. Bromberg, and A. Concheiro, "Review Light-sensitive Intelligent Drug Delivery Systems †," *Photochem. Photobiol.*, vol. 85, pp. 848–860, 2009.

[145] L. A. Scherrer and R. W. Gross, "Subcellular distribution, molecular dynamics and catabolism of plasmalogens in myocardium," *Mol. Cell. Biochem.*, vol. 88, no. 1–2, pp. 97–105, 1989.

[146] I. O. L. Bacellar, T. M. Tsubone, C. Pavani, and M. S. Baptista, "Photodynamic efficiency: From molecular photochemistry to cell death," *Int. J. Mol. Sci.*, vol. 16, no. 9, pp. 20523–20559, 2015.

[147] B. Q. Spring *et al.*, "A photoactivable multi-inhibitor nanoliposome for tumour control and simultaneous inhibition of treatment escape pathways," *Nat nanotechnol*, vol. 11, no. 4, pp.

378–387, 2016.

[148] C. Zhang *et al.*, "A Light Responsive Nanoparticle-Based Delivery System Using Pheophorbide A Graft Polyethylenimine for Dendritic Cell-Based Cancer Immunotherapy," *Mol. Pharm.*, vol. 14, no. 5, pp. 1760–1770, 2017.

[149] L. Rhodes, E. Saga, and M. Trotta, *Photodynamic Medicine From Bench to Clinic*. Photochem. Photobiol. Sci., 2016,15, 8-9, 2016.

[150] P. K. Selbo *et al.*, "Photochemical internalization provides time- and space-controlled endolysosomal escape of therapeutic molecules," *J. Control. Release*, vol. 148, no. 1, pp. 2–12, 2010.

[151] O. J. Norum, P. K. Selbo, A. Weyergang, K. E. Giercksky, and K. Berg, "Photochemical internalization (PCI) in cancer therapy: From bench towards bedside medicine," *J. Photochem. Photobiol. B Biol.*, vol. 96, no. 2, pp. 83–92, 2009.

[152] N. Nishiyama, Y. Morimoto, W. D. Jang, and K. Kataoka, "Design and development of dendrimer photosensitizer-incorporated polymeric micelles for enhanced photodynamic therapy," *Adv. Drug Deliv. Rev.*, vol. 61, no. 4, pp. 327–338, 2009.

[153] W. Chen, W. Deng, and E. M. Goldys, "Light-Triggerable Liposomes for Enhanced Endolysosomal Escape and Gene Silencing in PC12 Cells," *Mol. Ther. - Nucleic Acids*, vol. 7, no. June, pp. 366–377, 2017.

[154] H. Park, W. Park, and K. Na, "Doxorubicin loaded singlet-oxygen producible polymeric micelle based on chlorine e6 conjugated pluronic F127 for overcoming drug resistance in cancer," *Biomaterials*, vol. 35, no. 27, pp. 7963–7969, 2014.

[155] P. Shum, J. M. Kim, and D. H. Thompson, "Phototriggering of liposomal drug delivery systems," *Adv. Drug Deliv. Rev.*, vol. 53, no. 3, pp. 273–284, 2001.

[156] D. H. Thompson, O. V. Gerasimov, J. J. Wheeler, Y. Rui, and V. C. Anderson, "Triggerable plasmalogen liposomes: Improvement of system efficiency," *Biochim. Biophys. Acta - Biomembr.*, vol. 1279, no. 1, pp. 25–34, 1996.

[157] J. Yang and N. L. Bauld, "Synthesis of cis - and trans -1 , 2-Diphenoxyethenes and p , p ′ - Disubstituted Diaryloxyethenes," *j. Org. Chem.*, vol. 64, no. 25, pp. 9251–9253, 1999.

[158] a Ruebner, Z. Yang, D. Leung, and R. Breslow, "A cyclodextrin dimer with a photocleavable linker as a possible carrier for the photosensitizer in photodynamic tumor therapy.," *Proc. Natl. Acad. Sci. U. S. A.*, vol. 96, no. 26, pp. 14692–14693, 1999.

[159] S. D. P. Baugh, Z. Yang, D. K. Leung, D. M. Wilson, and R. Breslow, "Cyclodextrin dimers as cleavable carriers of photodynamic sensitizers," *J. Am. Chem. Soc.*, vol. 123, no. 50, pp. 12488–12494, 2001.

[160] J. Lee, J. Park, K. Singha, and W. J. Kim, "Mesoporous silica nanoparticle facilitated drug release through cascade photosensitizer activation and cleavage of singlet oxygen sensitive linker," *Chem. Commun.*, vol. 49, no. 15, p. 1545, 2013.

[161] J. Liu *et al.*, "Light-controlled drug release from singlet-oxygen sensitive nanoscale coordination polymers enabling cancer combination therapy," *Biomaterials*, vol. 146, pp. 40–48, 2017.

[162] R. S. Murthy, M. Bio, and Y. You, "Low energy light-triggered oxidative cleavage of olefins," *Tetrahedron Lett.*, vol. 50, no. 9, pp. 1041–1044, 2009.

[163] A. Dinache *et al.*, "Photosensitized cleavage of some olefins as potential linkers to be used in drug delivery," *Appl. Surf. Sci.*, vol. 417, pp. 136–142, 2017.

[164] M. Bio, G. Nkepang, and Y. You, "Click and photo-unclick chemistry of aminoacrylate for visible light-triggered drug release," *Chem. Commun.*, vol. 48, no. 52, pp. 6517–6519, 2012.

[165] G. Nkepang, P. K. Pogula, M. Bio, and Y. You, "Synthesis and singlet oxygen reactivity of 1,2-diaryloxyethenes and selected sulfur and nitrogen analogs," *Photochem. Photobiol.*, vol. 88, no. 3, pp. 753–759, 2012.

[166] A. M. L. Hossion, M. Bio, G. Nkepang, S. G. Awuah, and Y. You, "Visible light controlled release of anticancer drug through double activation of prodrug," *ACS Med. Chem. Lett.*, vol. 4, no. 1, pp. 124–127, 2013.

[167] M. Bio, P. Rajaputra, G. Nkepang, S. G. Awuah, A. M. L. Hossion, and Y. You, "Site-specific and far-red-light-activatable prodrug of combretastatin A-4 using photo-unclick chemistry," *J. Med. Chem.*, vol. 56, no. 10, pp. 3936–3942, 2013.

[168] P. Rajaputra, M. Bio, G. Nkepang, P. Thapa, S. Woo, and Y. You, "Anticancer drug released from near IR-activated prodrug overcomes spatiotemporal limits of singlet oxygen," *Bioorganic Med. Chem.*, vol. 24, no. 7, pp. 1540–1549, 2016.

[169] G. Nkepang, M. Bio, P. Rajaputra, S. G. Awuah, and Y. You, "Folate receptor-mediated enhanced and specific delivery of far-red light-activatable prodrugs of combretastatin A-4 to FR-positive tumor," *Bioconjug. Chem.*, vol. 25, no. 12, pp. 2175–2188, 2014.

[170] Y. Yuan, C.-J. Zhang, S. Xu, and B. Liu, "A self-reporting AIE probe with a built-in singlet oxygen sensor for targeted photodynamic ablation of cancer cells," *Chem. Sci.*, vol. 7, no. 3, pp. 1862–1866, 2016.

[171] P. P. S. Colonna, N. Caggero, G. Carrea, "Enantio and Diastereoselectivity of Cyclohexanone Monooxygenase Catalyzed Oxidation of 1,3-Dithioacetals.," *Tetrahedron: Asymmetry*, vol. 7, no. 2, pp. 565–570, 1996.

[172] A. K. Shukla, M. Verma, and K. N. Singh, "Superoxide induced deprotection of 1,3-dithiolanes: A convenient method of dedithioacetalization," *Indian J. Chem. - Sect. B Org. Med. Chem.*, vol. 43, no. 8, pp. 1748–1752, 2004.

[173] N. G. Ganguly; and S. K. Barik, "A Facile Mild Deprotection Protocol for 1,3-Dithianes and 1,3-Dithiolanes with 30% Hydrogen Peroxide and Iodine Catalyst in Aqueous Micellar System," *Synthesis (Stuttg).*, vol. 8, pp. 1393–1399, 2009.

[174] N. M. D. S. Wilson, G. Dalmasso, L. Wang, S. V. Sitaraman, D. Merlin, "Orally delivered thioketal-nanoparticles loaded with TNFα-siRNA target inflammation and inhibit gene expression in the intestines," *Nat Mater*, vol. 11, no. 9, pp. 923–928, 2010.

[175] M. S. Shim and Y. Xia, "A reactive oxygen species (ROS)-responsive polymer for safe, efficient, and targeted gene delivery in cancer cells," *Angew. Chemie - Int. Ed.*, vol. 52, no. 27, pp. 6926–6929, 2013.

[176] Y. Yuan, J. Liu, and B. Liu, "Conjugated-polyelectrolyte-based polyprodrug: Targeted and image-guided photodynamic and chemotherapy with on-demand drug release upon irradiation with a single light source," *Angew. Chemie - Int. Ed.*, vol. 53, no. 28, pp. 7163–7168, 2014.

[177] L. H. Liu *et al.*, "A Red Light Activatable Multifunctional Prodrug for Image-Guided Photodynamic Therapy and Cascaded Chemotherapy," *Adv. Funct. Mater.*, vol. 26, no. 34, pp. 6257–6269, 2016.

[178] Q. Pei *et al.*, "Light-Activatable Red Blood Cell Membrane-Camouflaged Dimeric Prodrug Nanoparticles for Synergistic Photodynamic/Chemotherapy," *ACS Nano*, vol. 12, no. 2, pp. 1630–1641, 2018.

[179] G. L. Seah, J. S. Kim, J. H. Yu, and Y. S. Nam, "Light-Triggered Tumor Targeted Delivery of Anticancer Therapeutics Using ROS-sensitive Polymeric Micelles," in *2016 CRS Annual Meeting Presentations Seattle, Washington*, 2016.

[180] G. L. Seah *et al.*, "Low-power and low-drug-dose photodynamic chemotherapy via the breakdown of tumor-targeted micelles by reactive oxygen species," *J. Control. Release*, vol. 286, pp. 240–253, 2018.

[181] C. Yue *et al.*, "Near-infrared light triggered ros-activated theranostic platform based on ce6-cpt-ucnps for simultaneous fluorescence imaging and chemo-photodynamic combined therapy," *Theranostics*, vol. 6, no. 4, pp. 456–469, 2016.

[182] X. Wang, G. Meng, S. Zhang, and X. Liu, "A Reactive 1O2-Responsive Combined Treatment System of Photodynamic and Chemotherapy for Cancer," *Sci. Rep.*, vol. 6, no. June, pp. 2–10, 2016.

[183] J. Li *et al.*, "Light-Triggered Clustered Vesicles with Self-Supplied Oxygen and Tissue Penetrability for Photodynamic Therapy against Hypoxic Tumor," *Adv. Funct. Mater.*, vol. 27, no. 33, pp. 1–13, 2017.

[184] L. Liu, R. Wang, C. Wang, J. Wang, L. Chen, and J. Cheng, "Light-triggered release of drug conjugates for an efficient combination of chemotherapy and photodynamic therapy," *Biomater. Sci.*, vol. 6, no. 5, pp. 997–1001, 2018.

[185] H. Xu, W. Cao, and X. Zhang, "Selenium-containing polymers: Promising biomaterials for controlled release and enzyme mimics," *Acc. Chem. Res.*, vol. 46, no. 7, pp. 1647–1658, 2013.

[186] W. Cao *et al.*, "Coordination-responsive selenium-containing polymer micelles for controlled drug release," *Chem. Sci.*, vol. 3, no. 12, pp. 3403–3408, 2012.

[187] N. Ma, Y. Li, H. Xu, Z. Wang, and X. Zhang, "Dual redox responsive assemblies formed from diselenide block copolymers," *J. Am. Chem. Soc.*, vol. 132, no. 2, pp. 442–443, 2010.

[188] V. G. Deepagan *et al.*, "In situ diselenide-crosslinked polymeric micelles for ROS-mediated anticancer drug delivery," *Biomaterials*, vol. 103, pp. 56–66, 2016.

[189] P. Han *et al.*, "Oxidation-responsive micelles based on a selenium-containing polymeric superamphiphile," *Langmuir*, vol. 26, no. 18, pp. 14414–14418, 2010.

[190] N. Ma, Y. Li, H. Ren, H. Xu, Z. Li, and X. Zhang, "Selenium-containing block copolymers and their oxidation-responsive aggregates," *Polym. Chem.*, vol. 1, no. 10, pp. 1609–1614, 2010.

[191] W. Zhou *et al.*, "Selenium-Containing Polymer@Metal-Organic Frameworks Nanocomposites as an Efficient Multiresponsive Drug Delivery System," *Adv. Funct. Mater.*, vol. 27, no. 6, p. 1605465, 2017.

[192] H. Ren, Y. Wu, N. Ma, H. Xu, and X. Zhang, "Side-chain selenium-containing amphiphilic block copolymers: redox-controlled self-assembly and disassembly," *Soft Matter*, vol. 8, no. 5, pp. 1460–1466, 2012.

[193] S. Zhai, X. Hu, Y. Hu, B. Wu, and D. Xing, "Visible light-induced crosslinking and physiological stabilization of diselenide-rich nanoparticles for redox-responsive drug release and combination chemotherapy," *Biomaterials*, vol. 121, pp. 41–54, 2017.

[194] P. Han *et al.*, "Red light responsive diselenide-containing block copolymer micelles," *J. Mater. Chem. B*, no. 1, pp. 740–743, 2013.

[195] H. Ren *et al.*, "Visible-light-induced disruption of diselenide-containing layer-by-layer films: Toward combination of chemotherapy and photodynamic therapy," *Small*, vol. 9, no. 23, pp. 3981–3986, 2013.

[196] C. Sun, S. Ji, F. Li, and H. Xu, "Diselenide-Containing Hyperbranched Polymer with Light-Induced Cytotoxicity," *ACS Appl. Mater. Interfaces*, vol. 9, no. 15, pp. 12924–12929, 2017.

[197] R. Fang, H. Xu, W. Cao, L. Yang, and X. Zhang, "Reactive oxygen species (ROS)-responsive tellurium-containing hyperbranched polymer," *Polym. Chem.*, vol. 6, no. 15, pp. 2817–2821, 2015.

[198] W. Cao, L. Wang, and H. Xu, "Selenium/tellurium containing polymer materials in nanobiotechnology," *Nano Today*, vol. 10, no. 6, pp. 717–736, 2015.

[199] W. Cao, Y. Gu, T. Li, and H. Xu, "Ultra-sensitive ROS-responsive tellurium-containing polymers," *Chem. Commun.*, vol. 51, no. 32, pp. 7069–7071, 2015.

[200] F. Li, T. Li, W. Cao, L. Wang, and H. Xu, "Near-infrared light stimuli-responsive synergistic therapy nanoplatforms based on the coordination of tellurium-containing block polymer and cisplatin for cancer treatment," *Biomaterials*, vol. 133, pp. 208–218, 2017.

[201] X. Zhang *et al.*, "Pharmaceutical Micelles Featured with Singlet Oxygen-Responsive Cargo Release and Mitochondrial Targeting for Enhanced Photodynamic Therapy," *Nanotechnology*, vol. 29, p. 255101, 2018.

[202] L. Wang *et al.*, "Mechanistic insight into the singlet oxygen-triggered expansion of hypoxia-responsive polymeric micelles," *Biomater. Sci.*, vol. 6, no. 7, pp. 1712–1716, 2018.

[203] J. tang, Shaosheng; Peng, Chuanqi; Xu, Jing;Du, Bujie; Wang, Qingxiao; VinluanIII, Rodrigo D.;Yu, Mengxiao; Kim, Moon j.; Zheng, "Tailoring Renal Clearance and Tumor Targeting of Ultrasmall Metal Nanoparticles with Particle Density Shaoheng Access," *Angew Chem Int Ed Engl*, vol. 55, no. 52, pp. 16039–16043, 2016.

[204] M. L. Lamas *et al.*, "Towards the development of electrospun mats from poly(ε-caprolactone)/poly(ester amide)s miscible blends," *Polym. (United Kingdom)*, vol. 150, pp. 343–359, 2018.

[205] J. Lee, J. Park, K. Singha, and W. J. Kim, "Mesoporous silica nanoparticle facilitated drug release through cascade photosensitizer activation and cleavage of singlet oxygen sensitive linker.," *Chem. Commun. (Camb).*, vol. 49, no. 15, pp. 1545–1547, 2013.

[206] G. Saravanakumar, J. Lee, J. Kim, and W. J. Kim, "Visible light-induced singlet oxygen-mediated intracellular disassembly of polymeric micelles co-loaded with a photosensitizer and an anticancer drug for enhanced photodynamic therapy," *Chem. Commun.*, vol. 51, no.

49, pp. 9995–9998, 2015.

[207] S. Sundararajan, A. B. Samui, and P. S. Kulkarni, "Synthesis and characterization of poly(ethylene glycol) acrylate (PEGA) copolymers for application as polymeric phase change materials (PCMs)," *React. Funct. Polym.*, vol. 130, no. January, pp. 43–50, 2018.

[208] C. F. Frias, A. C. Fonseca, J. F. J. Coelho, and A. C. Serra, "Straightforward functionalization of acrylated soybean oil by Michael-addition and Diels-Alder reactions," *Ind. Crops Prod.*, vol. 64, pp. 33–38, 2015.

[209] A. P. Goodwin, J. L. Mynar, Y. Ma, G. R. Fleming, and J. M. J. Fréchet, "Synthetic micelle sensitive to IR light via a two-photon process," *J. Am. Chem. Soc.*, vol. 127, no. 28, pp. 9952–9953, 2005.

[210] P. Han *et al.*, "Red light responsive diselenide-containing block copolymer micelles," *J. Mater. Chem. B*, vol. 1, no. 6, p. 740, 2013.

[211] L. Meng, W. Huang, D. Wang, X. Huang, X. Zhu, and D. Yan, "Chitosan-based nanocarriers with ph and light dual response for anticancer drug delivery," *Biomacromolecules*, vol. 14, no. 8, pp. 2601–2610, 2013.

[212] A. P. Goodwin, J. L. Mynar, Y. Ma, G. R. Fleming, and J. M. J. Fre, "Synthetic Micelle Sensitive to IR Light via a Two-Photon Process," pp. 9952–9953, 2005.

[213] A. Al Samad *et al.*, "PCL–PEG graft copolymers with tunable amphiphilicity as efficient drug delivery systems," *J. Mater. Chem. B*, vol. 4, no. 37, pp. 6228–6239, 2016.

[214] N. Fomina, C. McFearin, M. Sermsakdi, O. Edigin, and A. Almutairi, "UV and near-IR triggered release from polymeric nanoparticles," *J. Am. Chem. Soc.*, vol. 132, no. 28, pp. 9540–9542, 2010.

[215] P. Pan, G. Shan, Y. Bao, M. Fujita, and M. Maeda, "Core − Shell Structure, Biodegradation, and Drug Release Behavior of Poly(lactic acid)/Poly(ethylene glycol) Block Copolymer Micelles Tuned by Macromolecular Stereostructure," 2015.

[216] E. Q. Rosenthal and C. Wesdemiotis, "Green Polymer Chemistry: Living Dithiol Polymerization via Cyclic Intermediates," 2012.

[217] E. Themistou, G. Battaglia, and S. P. Armes, "Facile synthesis of thiol-functionalized amphiphilic polylactide–methacrylic diblock copolymers," *Polym. Ch*, vol. 5, pp. 1405–1417, 2014.

[218] K. E. B. Doncom, L. D. Blackman, D. B. Wright, M. I. Gibson, and R. K. O. Reilly, "Dispersity effects in polymer self-assemblies: a matter of hierarchical control," *chem soc rev*, vol. 46, pp. 4119–4134, 2017.

[219] C. G. Dariva, J. F. J. Coelho, and A. C. Serra, "Near infrared light-triggered nanoparticles using singlet oxygen photocleavage for drug delivery systems," *J. Control. Release*, vol. 294, no. December 2018, pp. 337–354, 2019.

[220] H. Hu, X. Wang, K. I. Lee, K. Ma, H. Hu, and J. H. Xin, "Graphene oxide-enhanced sol-gel transition sensitivity and drug release performance of an amphiphilic copolymer-based nanocomposite," *Sci. Rep.*, vol. 6, no. July, pp. 1–11, 2016.

[221] R. Mathiyalagan *et al.*, "Protopanaxadiol aglycone ginsenoside-polyethylene glycol conjugates: synthesis, physicochemical characterizations, and in vitro studies," *Artif. Cells, Nanomedicine Biotechnol.*, vol. 44, no. 8, pp. 1803–1809, 2016.

[222] Z. Hami, M. Amini, M. Ghazi-Khansari, S. M. Rezayat, and K. Gilani, "Doxorubicin-conjugated PLA-PEG-Folate based polymeric micelle for tumor-targeted delivery: Synthesis and in vitro evaluation," *DARU, J. Pharm. Sci.*, vol. 22, no. 1, pp. 1–7, 2014.

[223] A. V Kabanov, E. V Batrakova, and V. Yu, "Pluronic block copolymer as novel polymer therapeutics for drug and gene delivery," *J. Control. Release*, vol. 82, pp. 189–212, 2002.

[224] Z. Hami, M. Amini, M. Ghazi-Khansari, S. M. Rezayat, and K. Gilani, "Synthesis and in vitro evaluation of a pH-sensitive PLA-PEG-folate based polymeric micelle for controlled delivery of docetaxel," *Colloids Surfaces B Biointerfaces*, vol. 116, pp. 309–317, 2014.

[225] P. Vangeyte, S. Gautier, and R. Jérôme, "About the methods of preparation of poly(ethylene oxide)-b-poly(ε- caprolactone) nanoparticles in water - Analysis by dynamic light scattering," *Colloids Surfaces A Physicochem. Eng. Asp.*, vol. 242, no. 1–3, pp. 203–211, 2004.

[226] X. Wu, A. El Ghzaoui, and S. Li, "Anisotropic Self-Assembling Micelles Prepared by the

Direct Dissolution of PLA / PEG Block Copolymers with a High PEG Fraction," pp. 8000–8008, 2011.

[227] S. J. Rowan, "Micelles make a living," *Nat. Mater.*, vol. 8, no. 2, pp. 89–91, 2009.

[228] C. Garofalo *et al.*, "Different Insight into Amphiphilic PEG-PLA Copolymers: In fl uence of Macromolecular Architecture on the Micelle Formation and Cellular Uptake," 2014.

[229] L. F. De Freitas and M. R. Hamblin, "Chapter 1 - Antimicrobial photoinactivation with functionalized fullerenes," in *Nanobiomaterials in Antimicrobial Therapy - Applications of Nanobiomaterials Volume 6*, no. 0, 2016, pp. 1–17.

[230] K. Svanberg and N. Bendsoe, "25 - Photodynamic therapy for human malignancies with superficial and interstitial illumination," *Lasers Med. Appl. - Diagnostics, Ther. Surg.*, no. 1, pp. 760–778, 2013.

[231] U. Nobbmann, "DERIVED COUNT RATE – WHAT IS IT?," *Malvern Panalytical*, 2015. [Online]. Available: https://www.materials-talks.com/blog/2015/06/11/derived-count-rate-what-is-it/.

[232] J. M. Chem, G. Liu, C. Chen, D. Li, S. Wang, and J. Ji, "Near-infrared light-sensitive micelles for enhanced intracellular drug delivery †," pp. 16865–16871, 2012.

[233] K. Zhang *et al.*, "Efficacy of Chlorin e6-Mediated Sono-Photodynamic Therapy on 4T1 Cells," *Cancer Biother. Radiopharm.*, vol. 29, no. 1, pp. 42–52, 2013.

[234] H. Cho, J. Gao, and G. S. Kwon, "PEG- b -PLA micelles and PLGA- b -PEG- b -PLGA sol – gels for drug delivery," *J. Control. Release*, vol. 240, pp. 191–201, 2016.

[235] J. Wang *et al.*, "Poly(ethylene glycol)-polylactide micelles for cancer therapy," *Front. Pharmacol.*, vol. 9, no. MAR, pp. 1–15, 2018.

[236] S. Behzadi *et al.*, "Cellular uptake of nanoparticles: journey inside the cell," vol. 46, no. 14, 2017.

[237] P. Pei, C. Sun, W. Tao, J. Li, X. Yang, and J. Wang, "Biomaterials ROS-sensitive thioketal-linked polyphosphoester-doxorubicin conjugate for precise phototriggered locoregional chemotherapy," *Biomaterials*, vol. 188, no. October 2018, pp. 74–82, 2019.

[238] Y. Fang *et al.*, "Cleavable PEGylation : a strategy for overcoming the ' PEG dilemma ' in efficient drug delivery," *Drug Deliv.*, vol. 0, no. 0, pp. 22–32, 2017.

[239] L. Sanchez, Y. Yi, and Y. Yu, "Effect of partial PEGylation on particle uptake by macrophages," pp. 288–297, 2017.

[240] J. Van Meerloo, G. J. L. Kaspers, and J. Cloos, "Cell Sensitivity Assays : The MTT Assay," vol. 731, pp. 237–245.

[241] V. Vichai and K. Kirtikara, "Sulforhodamine B colorimetric assay for cytotoxicity screening," vol. 1, no. 3, pp. 1112–1116, 2006.

[242] A. Traeger *et al.*, "Photocontrolled Release of Chemicals from Nano- and Microparticle Containers," *Angew. Chemie Int. Ed.*, vol. 57, no. 9, pp. 2479–2482, 2017.

[243] PerkinElmer, "Tg and Melting Point of a Series of Polyethylene Glycols Using the Material Pocket," 2011.

[244] Polysciences, "Poly(ethylene glycol) [MW 1,000] _ Polysciences, Inc." 2019.

[245] A. C. Fonseca, M. H. Gil, and P. N. Simões, "Biodegradable poly(ester amide)s - A remarkable opportunity for the biomedical area: Review on the synthesis, characterization and applications," *Prog. Polym. Sci.*, vol. 39, no. 7, pp. 1291–1311, 2014.

[246] Z. Guan and H. Zeng, "Direct Synthesis of Polyamides via Catalytic Dehydrogenation of Diols and Diamines," *J. Am. Chem. Soc.*, vol. 133, no. 5, pp. 1159–1161, 2011.

[247] A. Rodriguez-Galan, L. Franco, and J. Puiggali, "Degradable poly(ester amide)s for biomedical applications," *Polymers (Basel).*, vol. 3, no. 1, pp. 65–99, 2011.

[248] M. Winnacker and B. Rieger, "Poly(ester amide)s: Recent insights into synthesis, stability and biomedical applications," *Polym. Chem.*, vol. 7, no. 46, pp. 7039–7046, 2016.

[249] J. M. Fang, P. A. Fowler, J. Tomkinson, and C. A. S. Hill, "The preparation and characterisation of a series of chemically modi ® ed potato starches," vol. mi, pp. 245–252, 2002.

[250] T. G. McKenzie *et al.*, "Beyond Traditional RAFT: Alternative Activation of Thiocarbonylthio Compounds for Controlled Polymerization," *Adv. Sci.*, vol. 3, no. 9, pp. 1–9, 2016.

[251] J. Phommalysack-lovan, Y. Chu, and C. Boyer, "PET-RAFT polymerisation : towards green and precision polymer manufacturing," pp. 6591–6606, 2018.

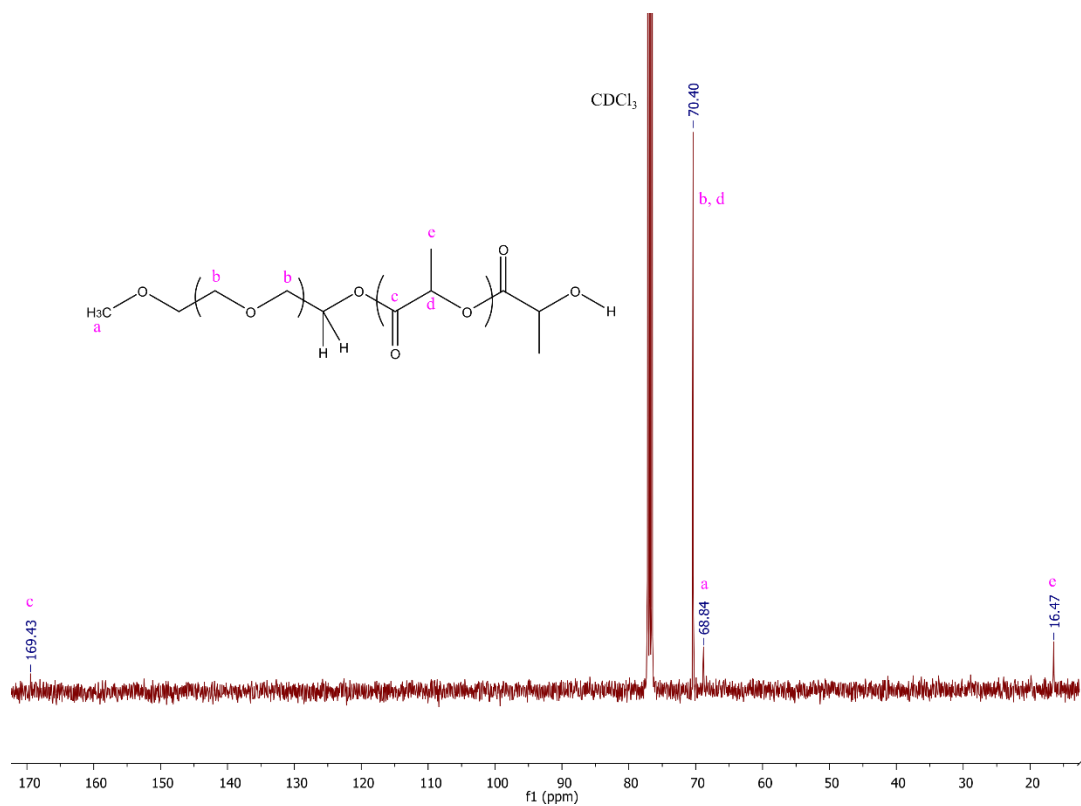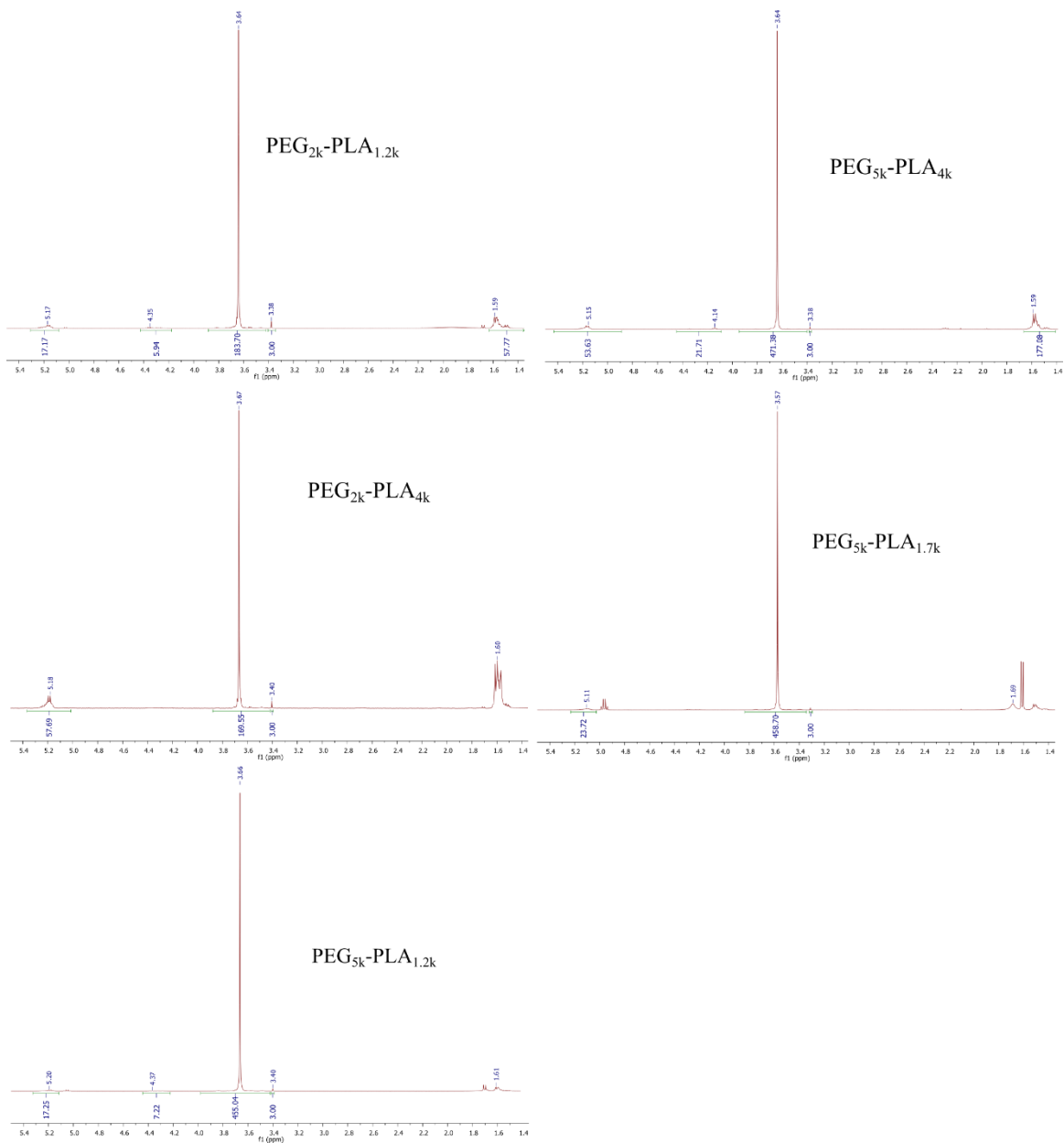Figure A 1 ^{13}C NMR (400 MHz) spectrum of PEG$_{5k}$-PLA$_{5k}$ in CDCl$_3$.

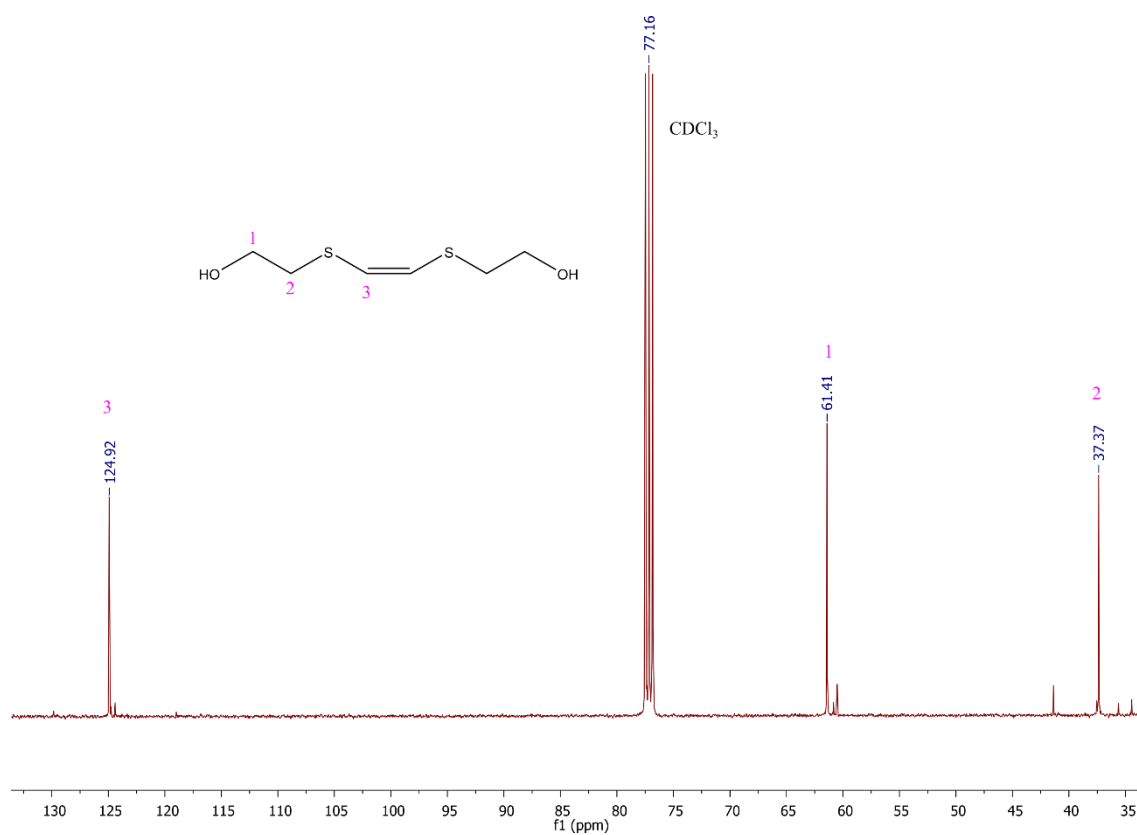Figure A 2 ^{1}H NMR (400 MHz) spectrum of PEGs-PLAs in CDCl$_3$.

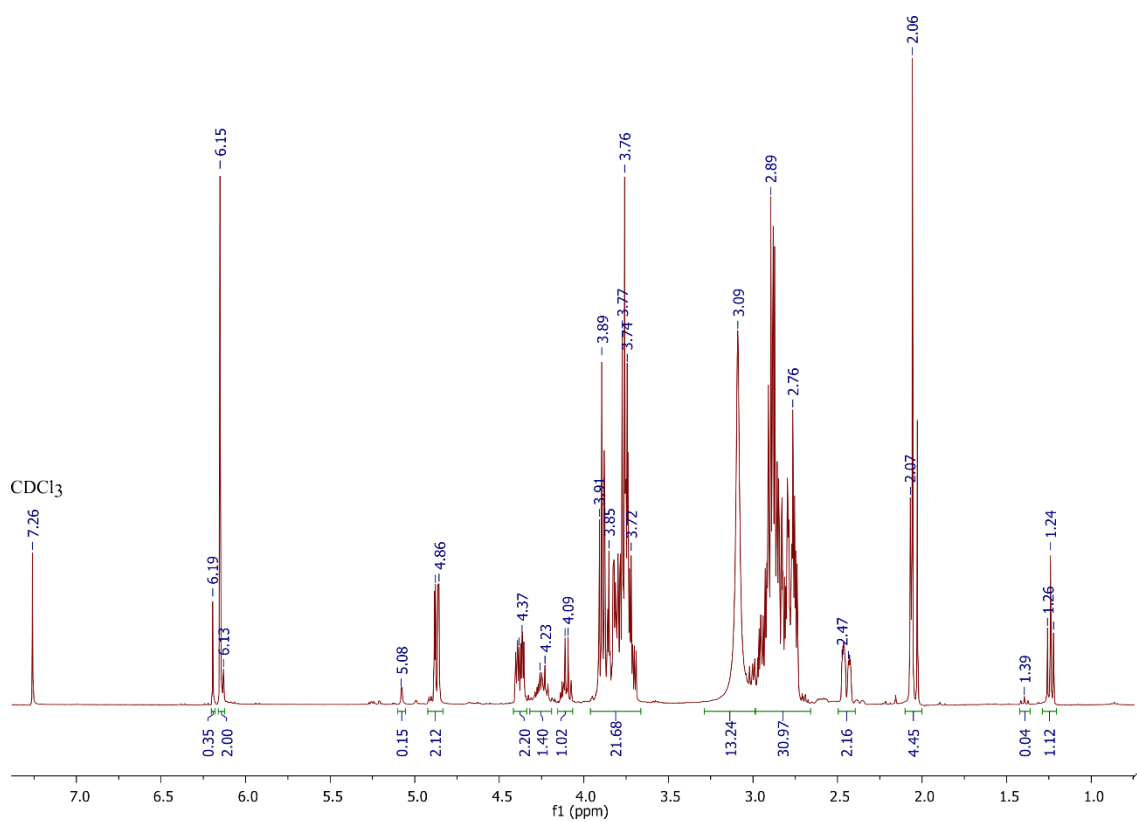Figure A 3. ^{13}C NMR (400 MHz) spectrum of BHETE in CDCl$_3$.

Figure A 4. ^{1}H NMR (400 MHz) spectrum of the degraded BHETE in CDCl$_3$ after purification through the chromatography column (ethyl acetate and hexane, 3:1, were used as mobile phase).
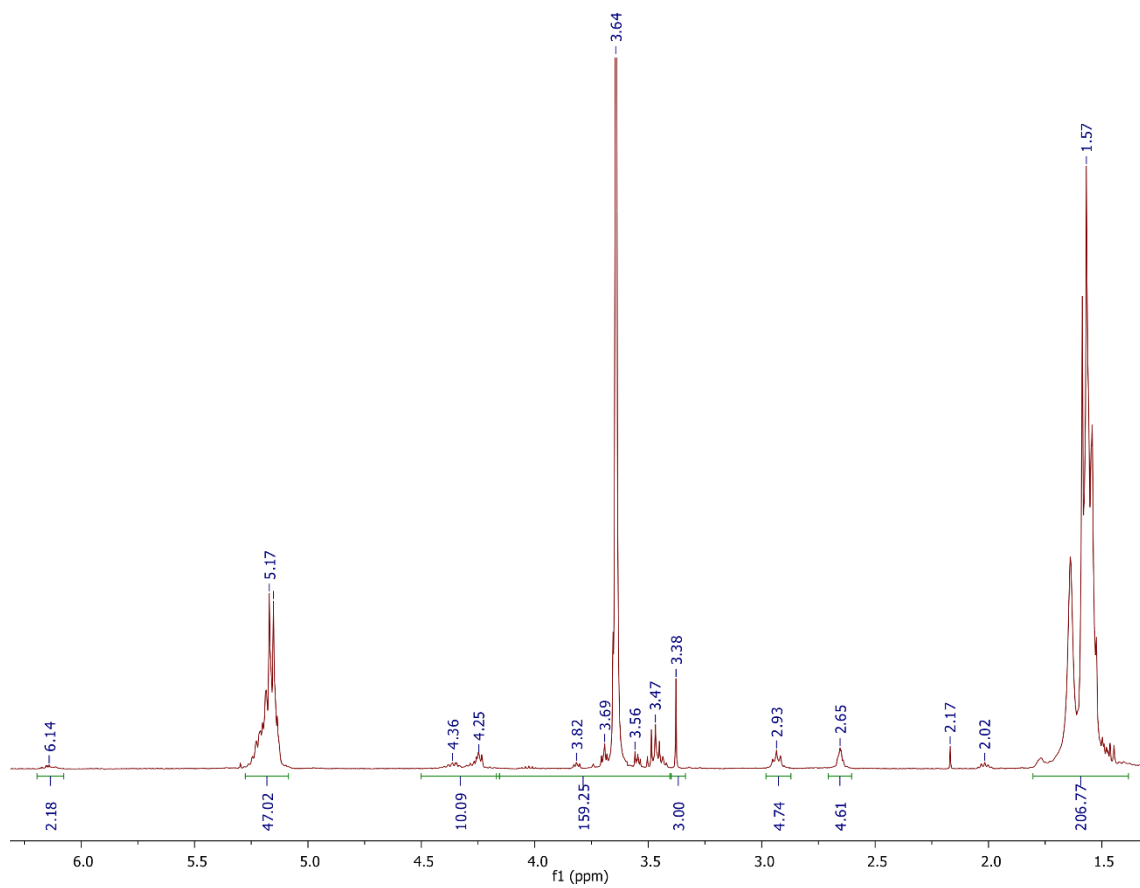
Figure A 5 ^{1}H NMR (400 MHz, CDCl$_3$) spectrum of amphiphilic sensitive polymer PEG$_{2k}$-BHETE-PLA$_{2k}$.
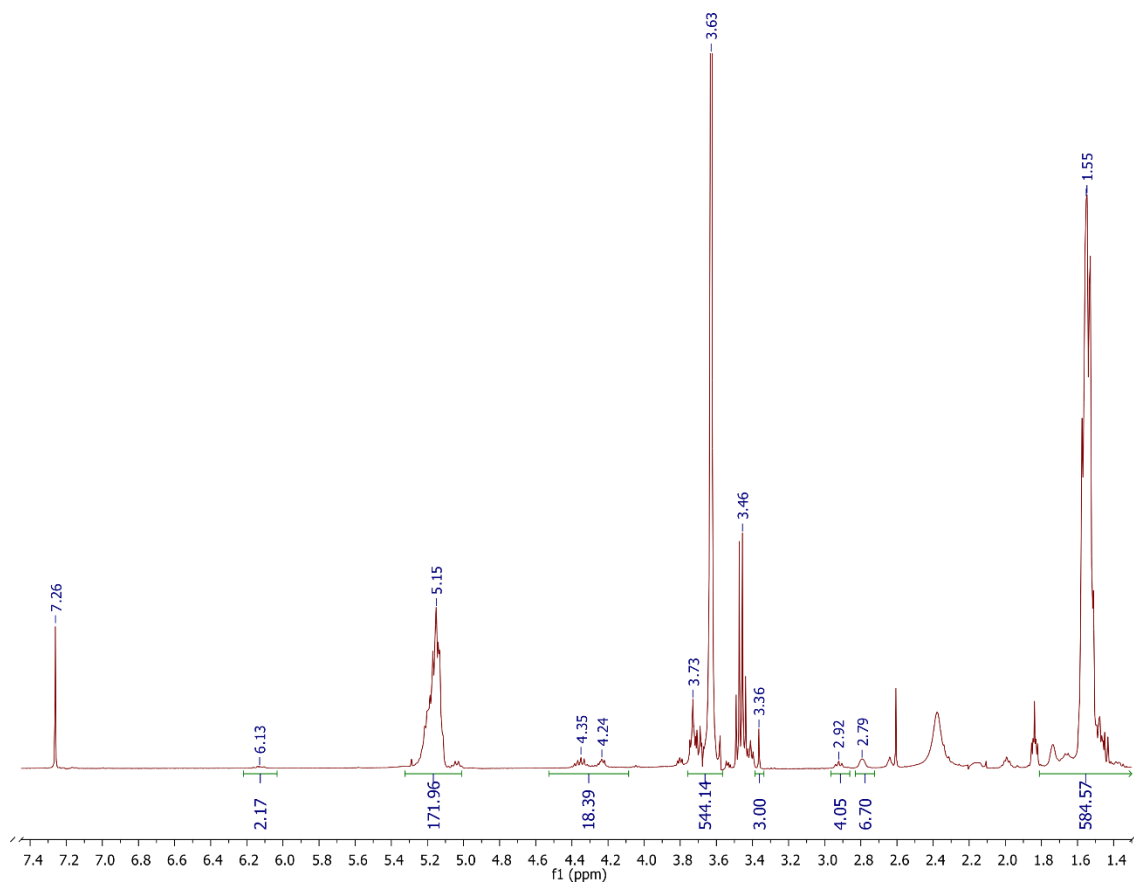
Figure A 6 ^{1}H NMR (400 MHz, CDCl$_3$) spectrum of amphiphilic sensitive polymer PEG$_{5k}$-BHETE-PLA$_{10k}$.
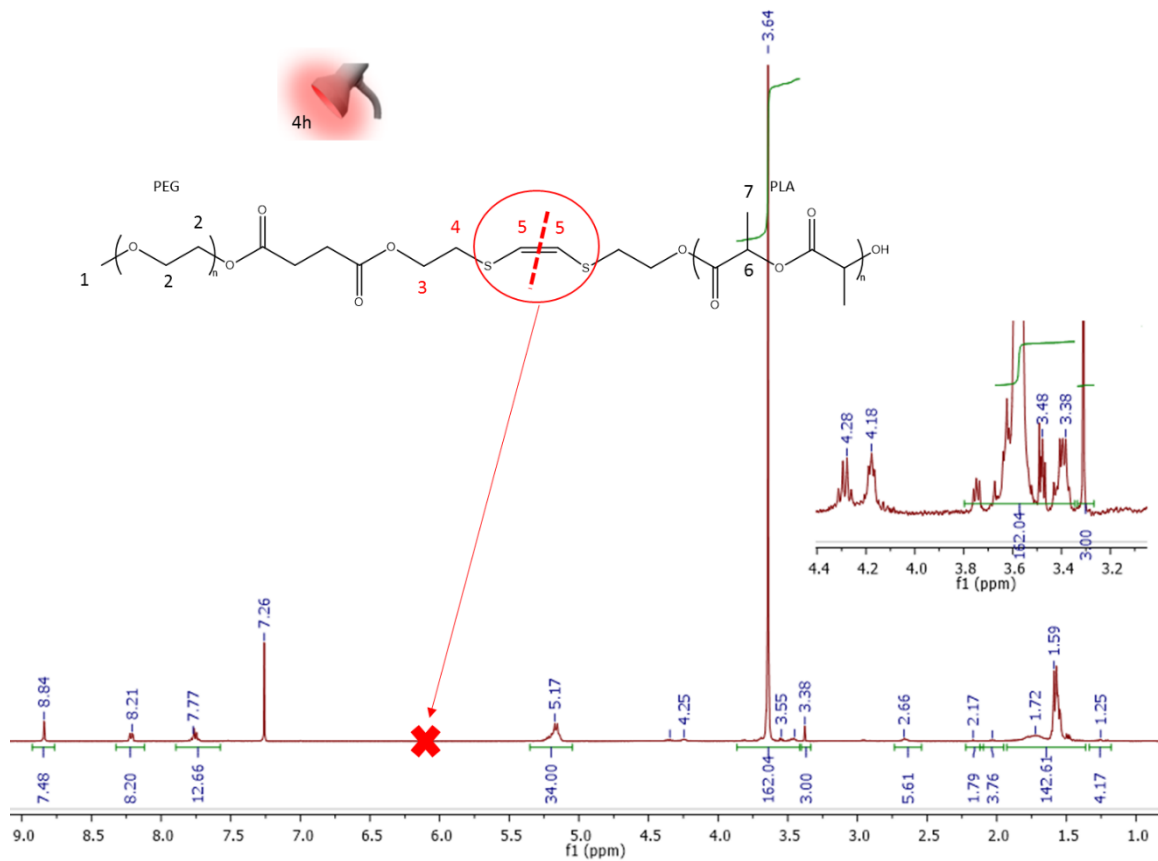
Figure A 7. ^{1}H NMR (400 MHz, CDCl$_3$) spectrum of the amphiphilic sensitive polymer after 4 h of red-light irradiation (635 nm, 3.6 mW.cm^{-2}) in the solution of CDCl$_3$ and 10 wt% (respect to polymer) of PS.
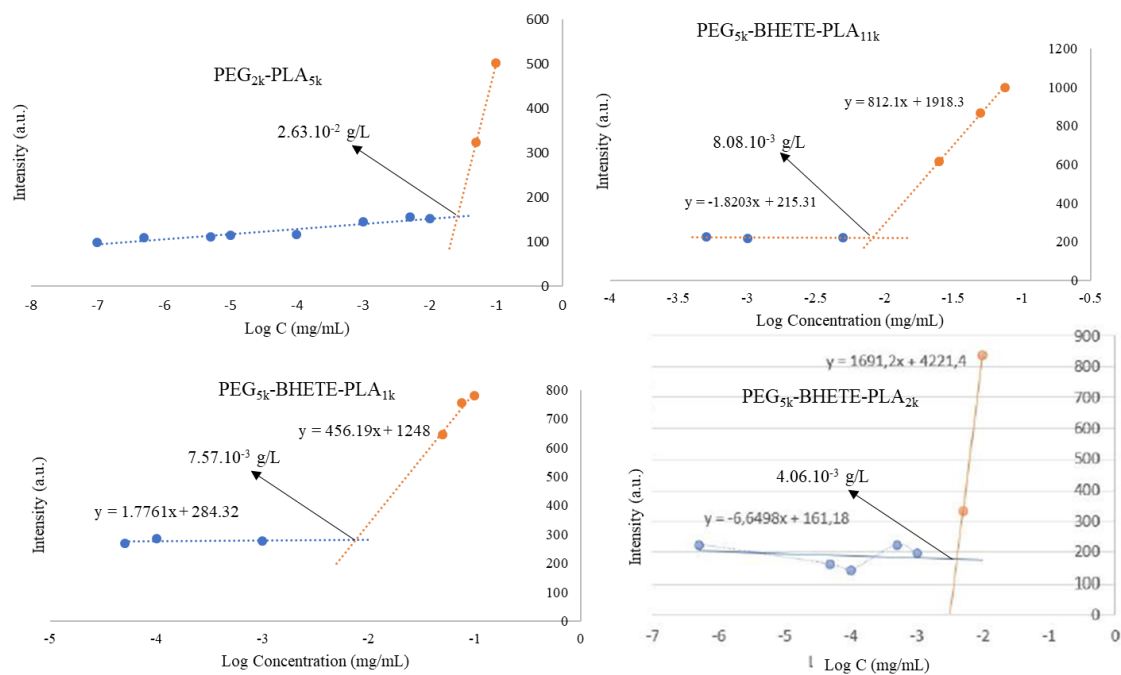
Figure A 8 CMC of PEG-BHETE-PLA micelles
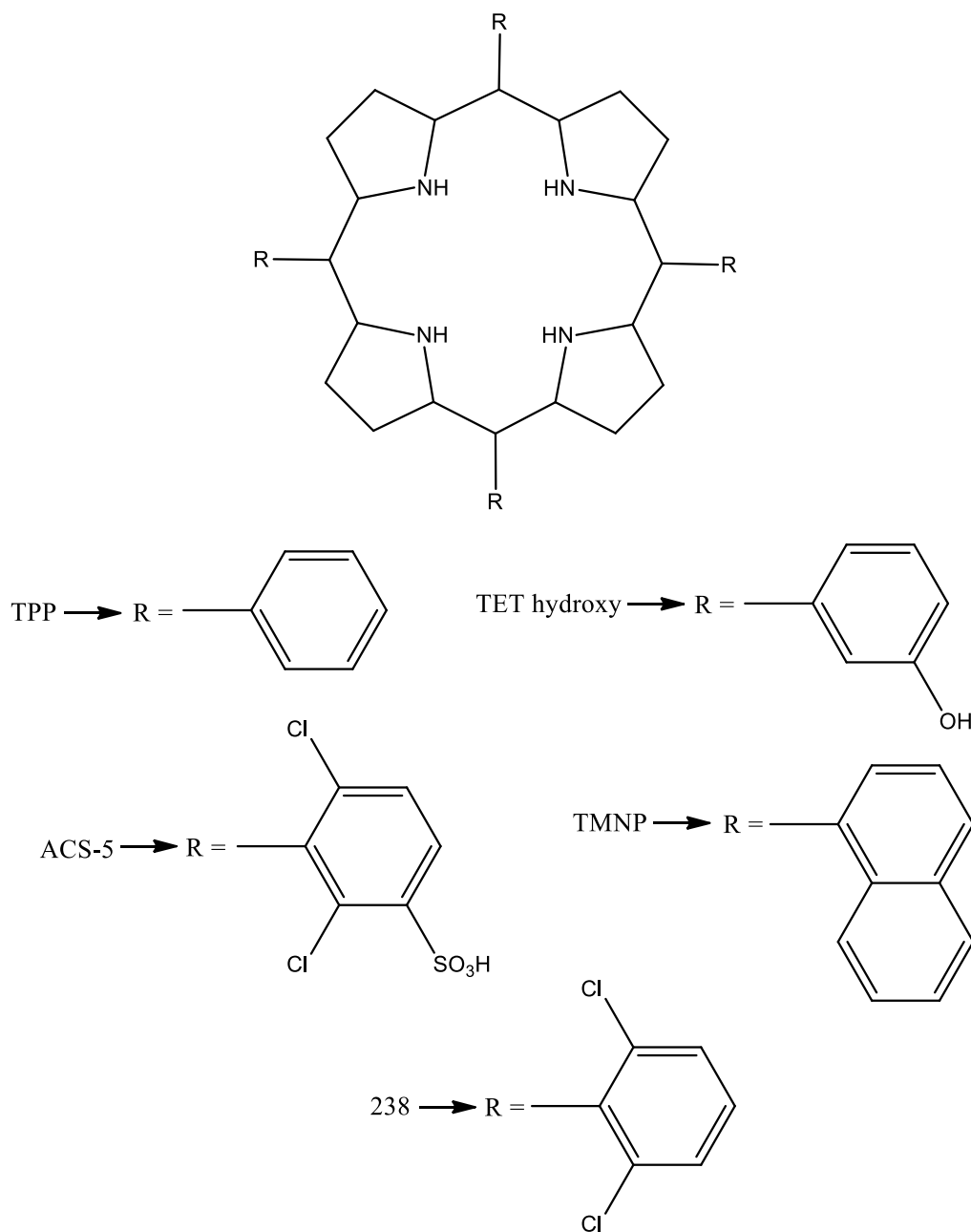
Figure A 9 PSS structures (TPP = *meso*-tetraphenyl-porphyrin; TET hydroxy = *meso*-tetra(3-hydroxyphenyl) porphyrin; ACS-5 = *meso*-tetra(2,6-dichloro-3-sulphonic acid phenyl) porphyrin; TMNP = *meso*-tetra(1-naphtyl) porphyrin; 238= *meso*-tetra(2,6-dichlorophenyl) porphyrin
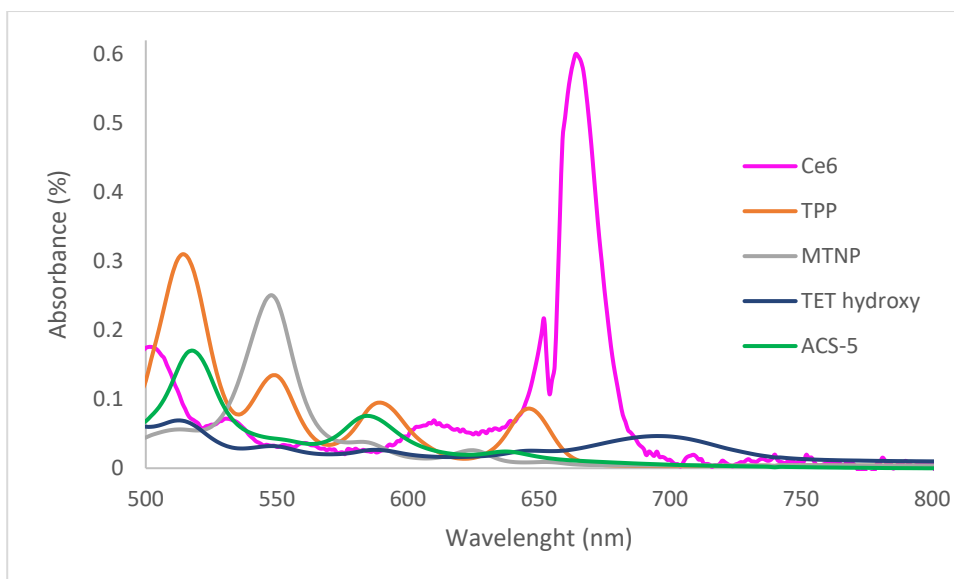
Figure A 10 Absorbance spectrum of photosensitizers in $CHCl_3$ (ACS and Ce6 were analyzed in water and DMSO, respectively, as they are not soluble in $CHCl_3$). The lasers available for the irradiation experiments has a wavelength of 650 nm, with a red beam light

Table A 1 Linear fitting and R^2 for Ce6 calibration curve at 405 nm for each assay

	Linear fitting (405 nm)	R^2
Calibration Curve	y = 177.86x + 0.0057	0.9956
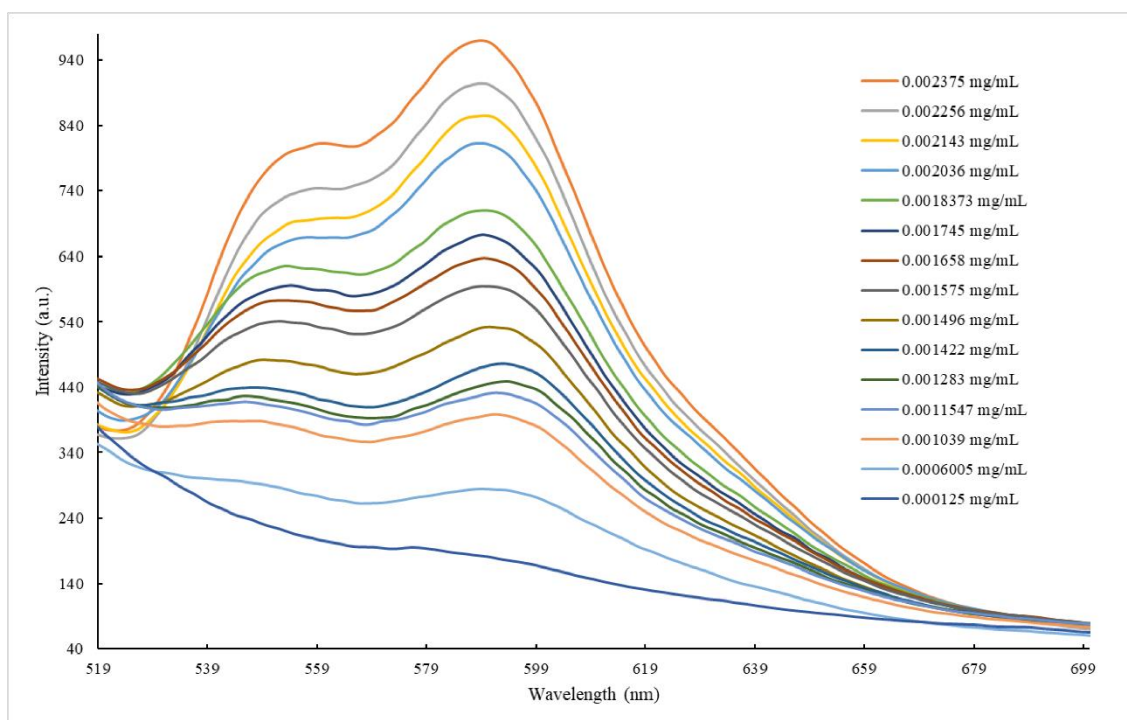
Figure A 11 Fluorescence emitted for DOX in DMSO solution in concentration rage from $0.6*10^{-3}$ to $2.3*10^{-3}$ mg.mL^{-1}. Emission at 480 nm
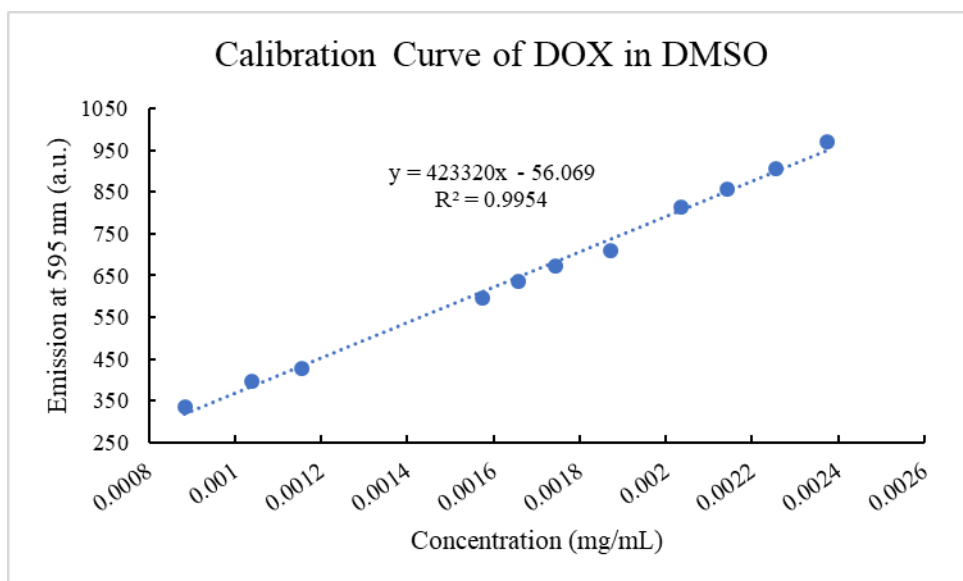
Figure A 12. Maximum emission fluorescence intensity (at 595 nm) versus solution concentration.
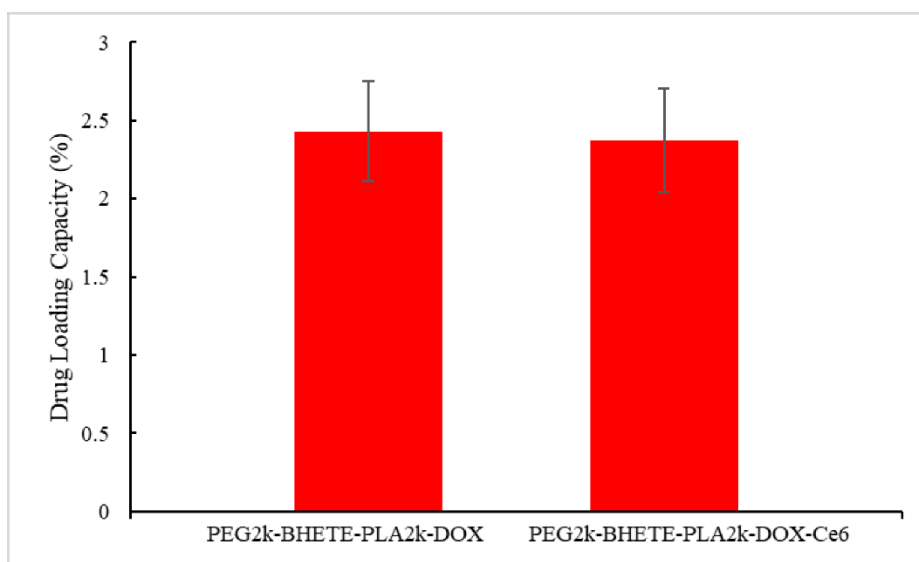
Figure A 13 The average DOX loading capacity of PEG_{2k}-BHETE-PLA_{2k} with and without Ce6 encaged. (N>3)
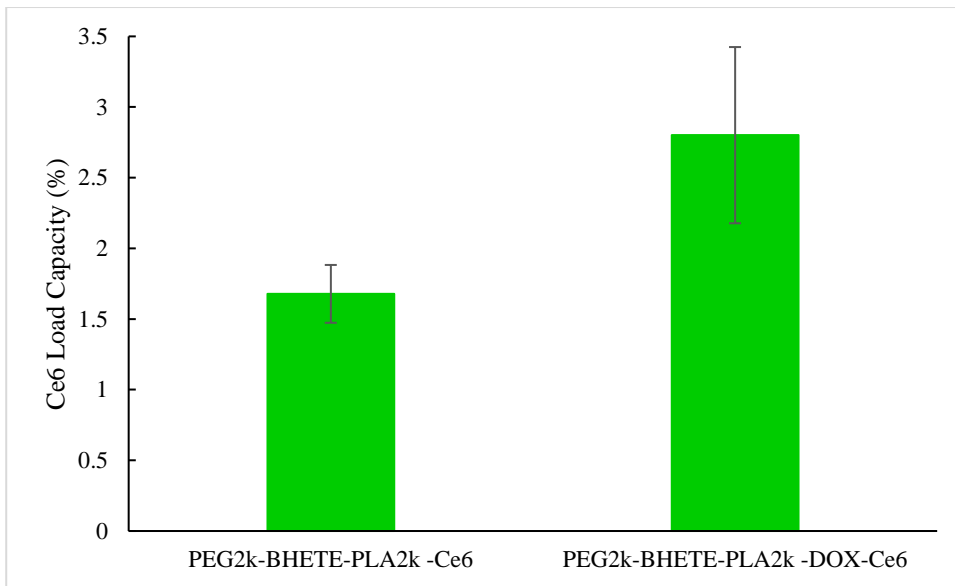
Figure A 14 The Ce6 average loading content for micelles
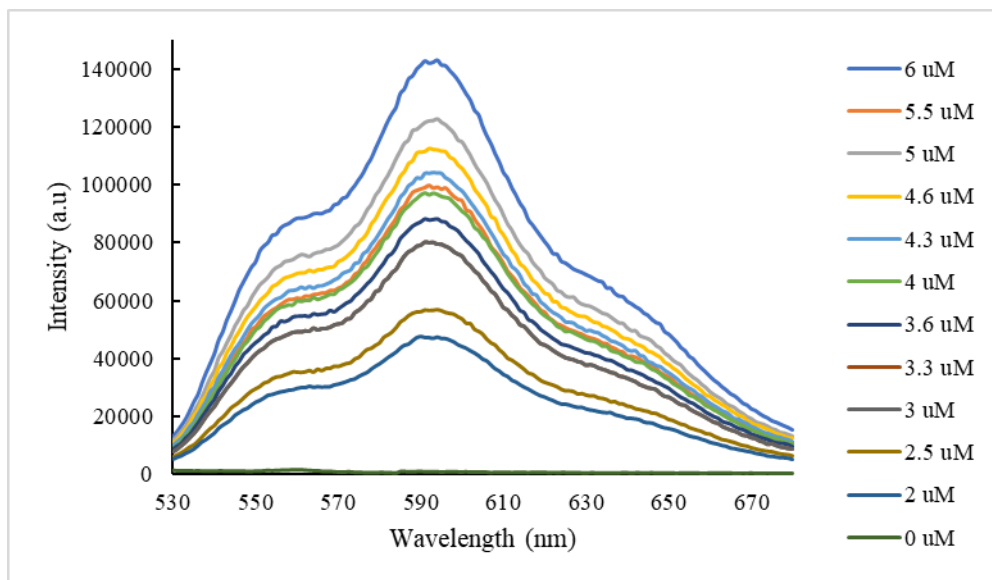
Figure A 15 The spectrum of fluorescence emission of DOX in DMSO solution in different molar concertation.
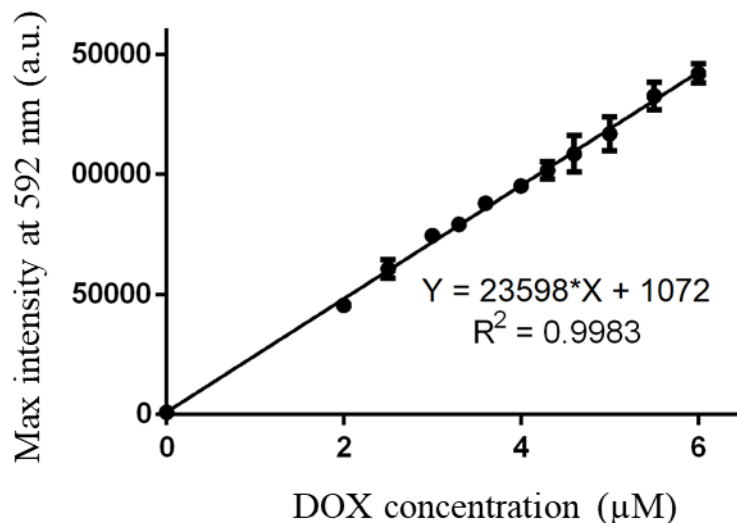
Figure A 16 Standard curve of DOX in DMSO. The linear fitting of DOX was made by the maximum intensity point of the DOX fluorescence emission spectrum versus molar concentration of calibration solutions.

Table A 2 Equation of each DOX calibration curve.

Calibration curve	Equation	R^2
average	y = 23589x + 1072	0.9983
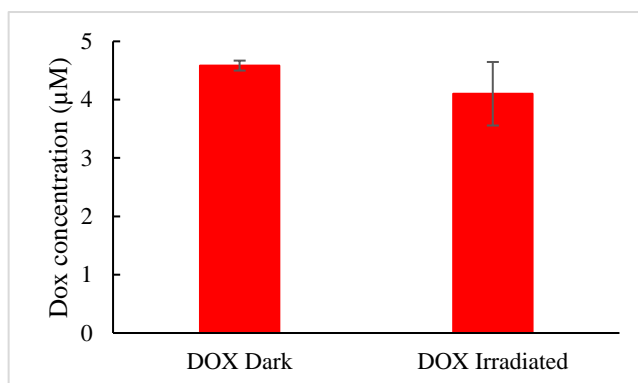
Figure A 17 The average cellular uptake of DOX for dosed without polymeric micelles
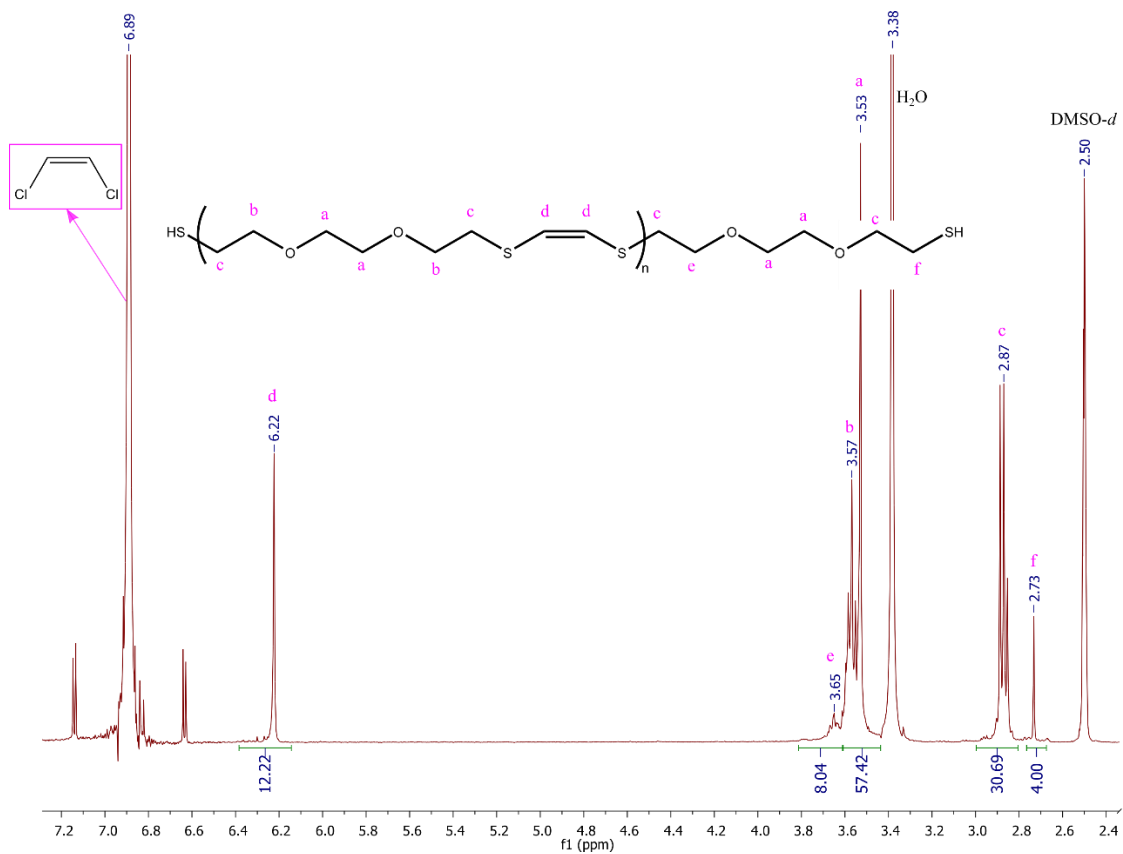
Figure A 18 ^{1}H NMR (400 MHz, DMSO-d_6) spectrum of PDDD and *cis*-dichloroethene.
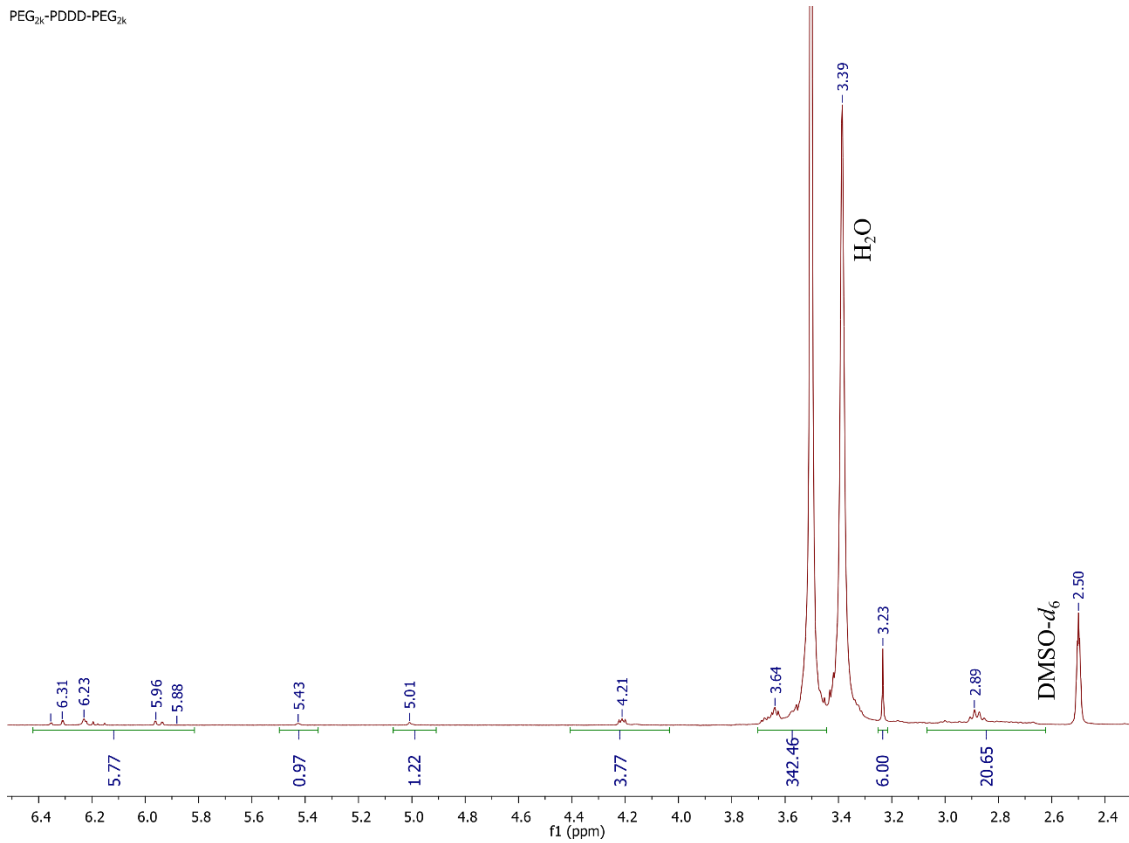
Figure A 19 ^{1}H NMR (400 MHz, DMSO-d_6) spectrum of PEG$_{2k}$-PDDD-PEG$_{2k}$.

176
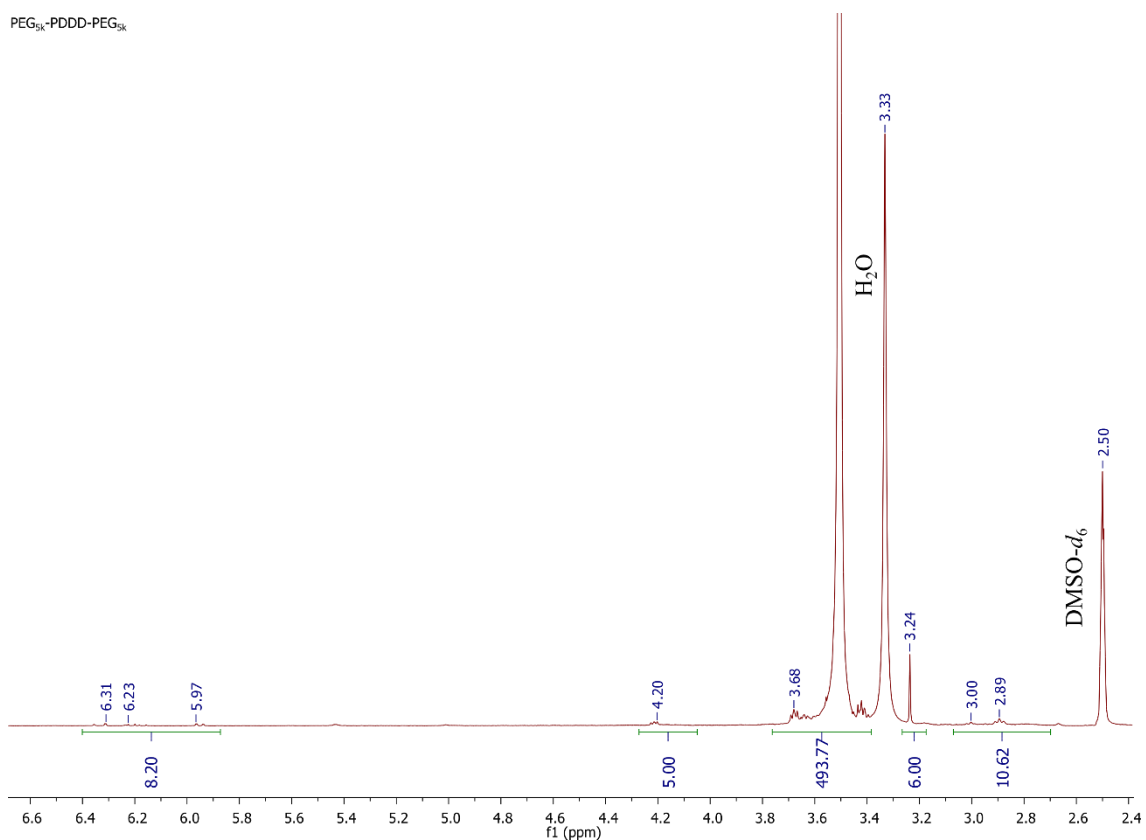
PEG$_{5k}$-PDDD-PEG$_{5k}$

Figure A 20 ^{1}H NMR (400 MHz, DMSO-d_6) spectrum of PEG$_{5k}$-PDDD-PEG$_{5k}$.
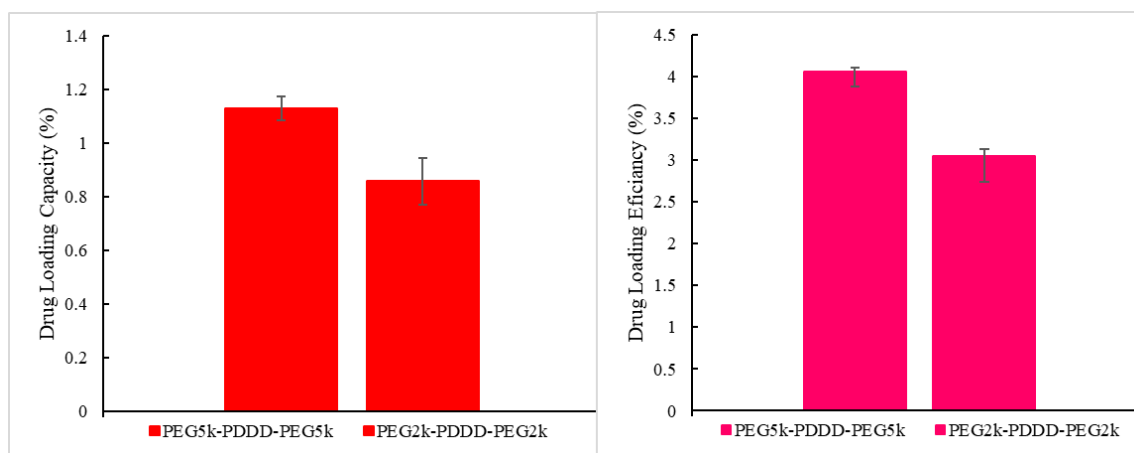
Figure A 21 The average DLC and DLE for PEG$_{5k}$-PDDD-PEG$_{5k}$ and PEG$_{2k}$-PDDD-PEG$_{2k}$
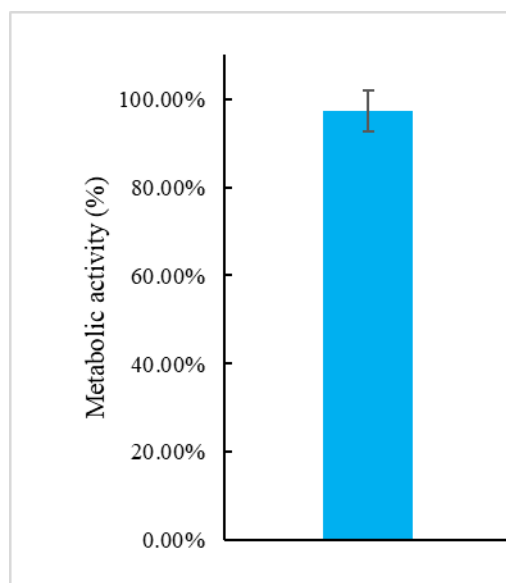
Figure A 22 MTT assay of PEE$_{5k}$-PDDD-PEG$_{5k}$ micelles using MCF7 cells. Data bar shows the average metabolic activity of cells (N=2).
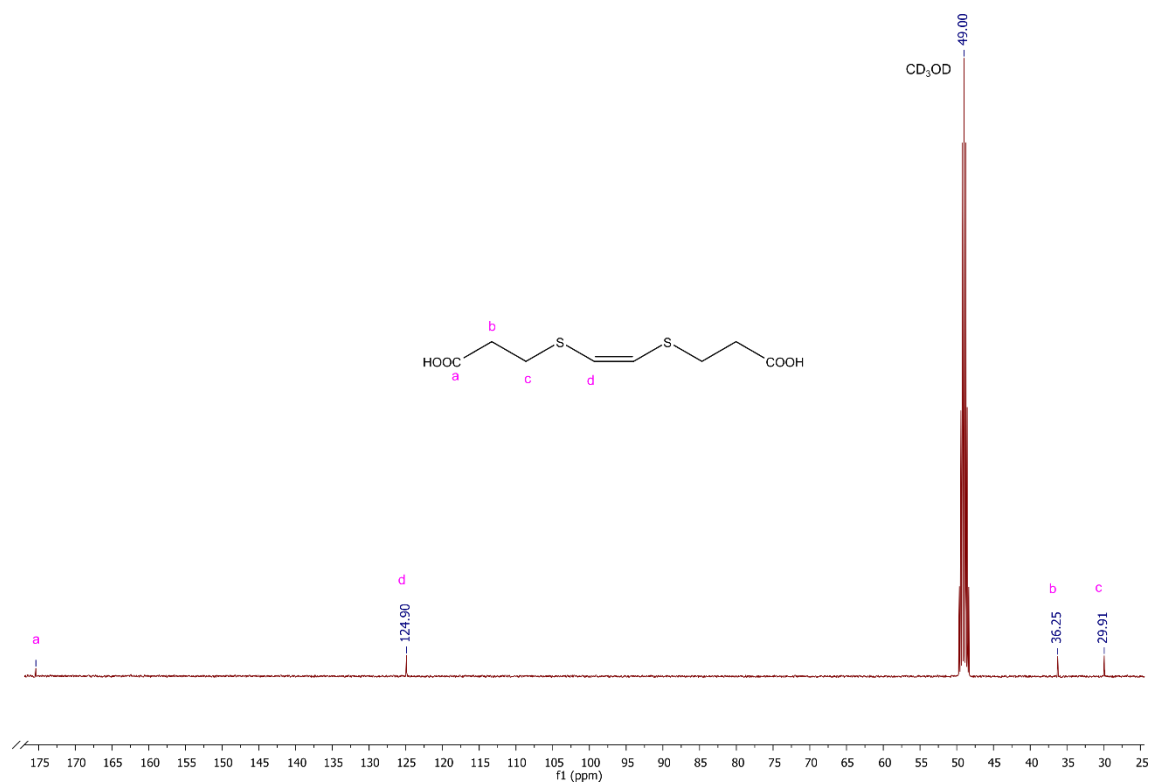
Figure A 23 ^{13}C NMR (400 MHz, CD$_3$OD) spectrum of the BCETE
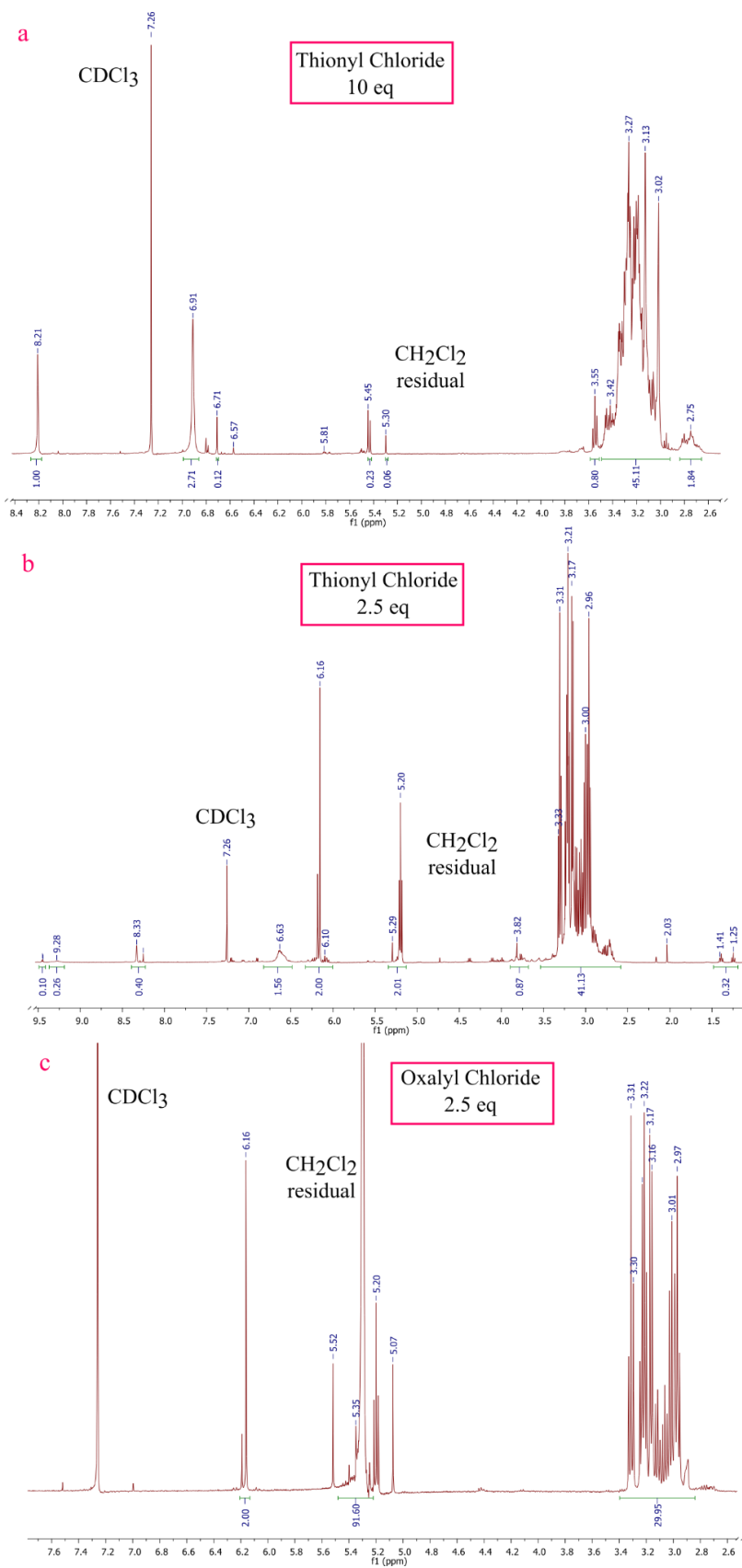
Figure A 24 ^{1}H NMR (400 MHz, CDCl$_3$) spectrum of BCETE after reacted with thionyl chloride or oxalyl chloride.
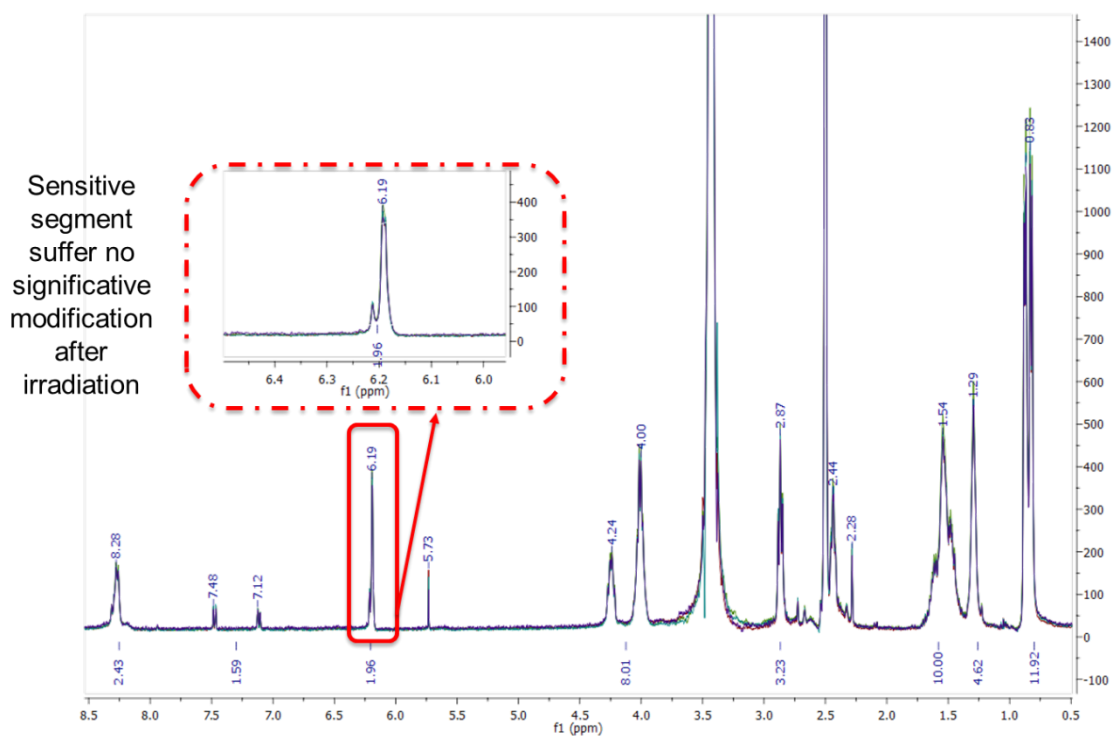
Figure A 25 Overlaid ^{1}H NMR (400 MHz) spectrums of poly(ester amide) in a DMSO-d_6 solution without Ce6, before and after undergoes irradiation process
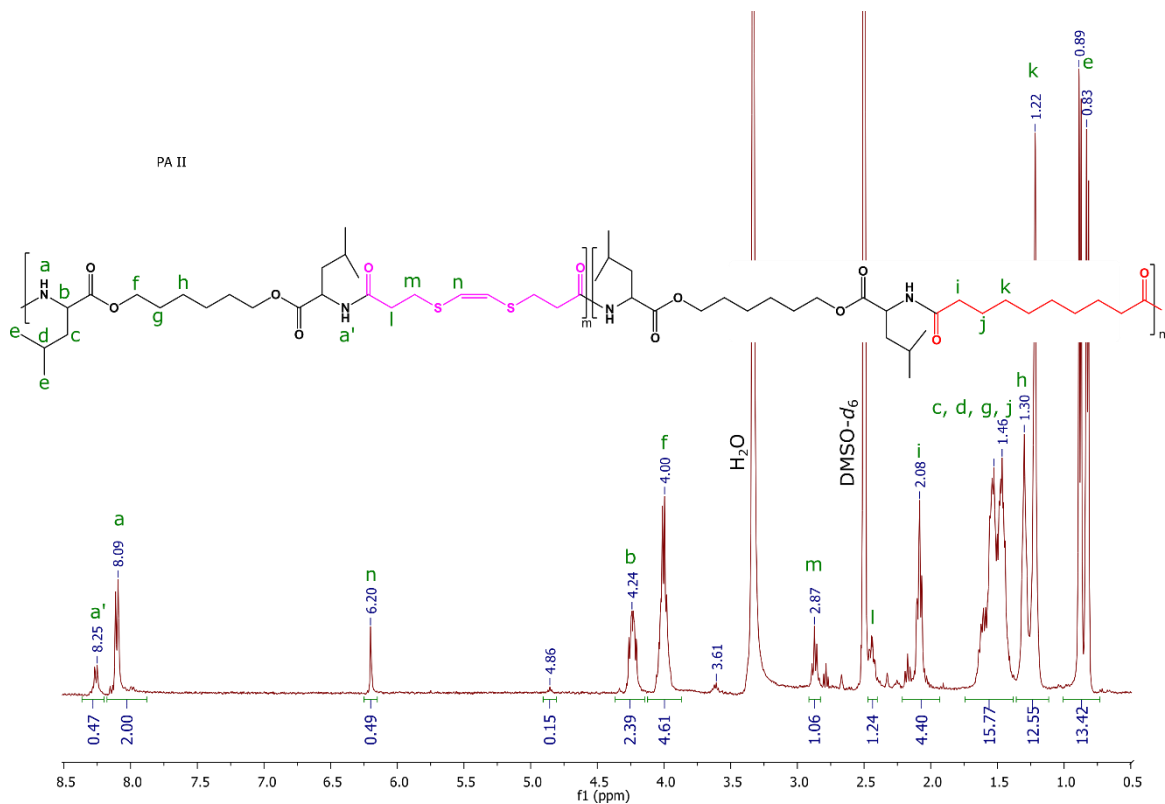

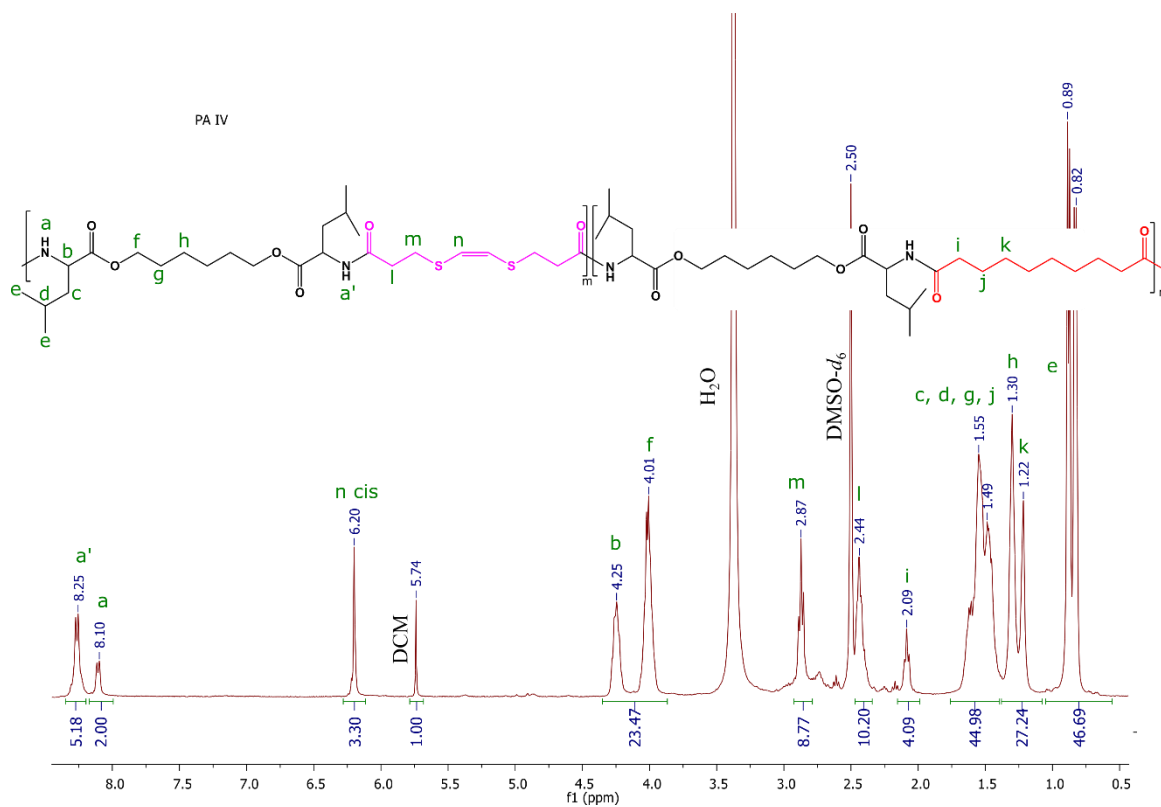Figure A 26 ^{1}H NMR (400 MHz) spectrum of poly(ester amide) 25% of the linker in DMSO-d_6.

180

Figure A 27 ^{1}H NMR (400 MHz) spectrum of poly(ester amide) 75% of the linker in DMSO-d_6.

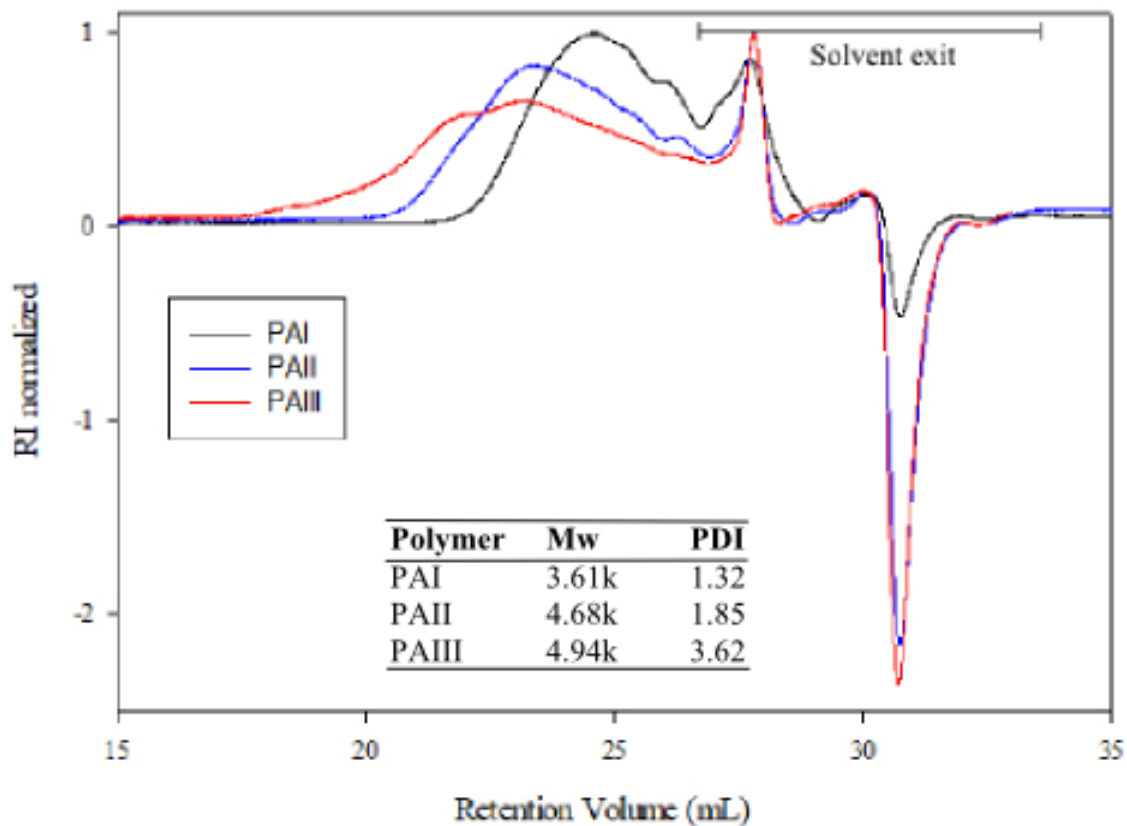| Polymer	Mw	PDI
PAI	3.61k	1.32
PAII	4.68k	1.85
PAIII	4.94k	3.62

Figure A 28 SEC in DMF solution of PAI, PAII and PAIII. The inset table shows the calculated molecular weight and PDI using the conventional calibration.
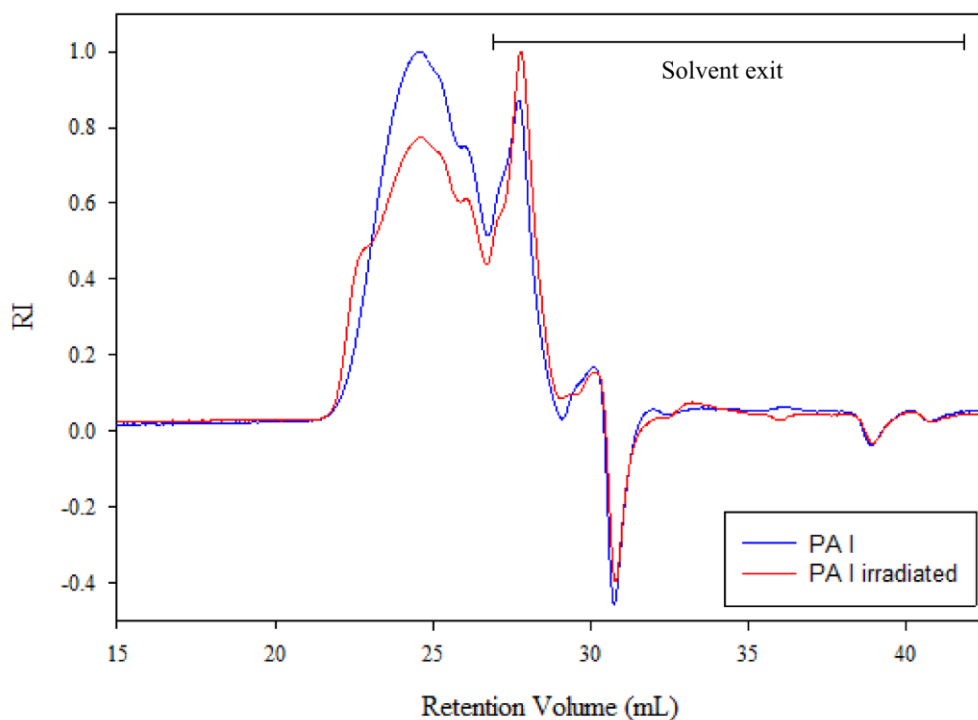
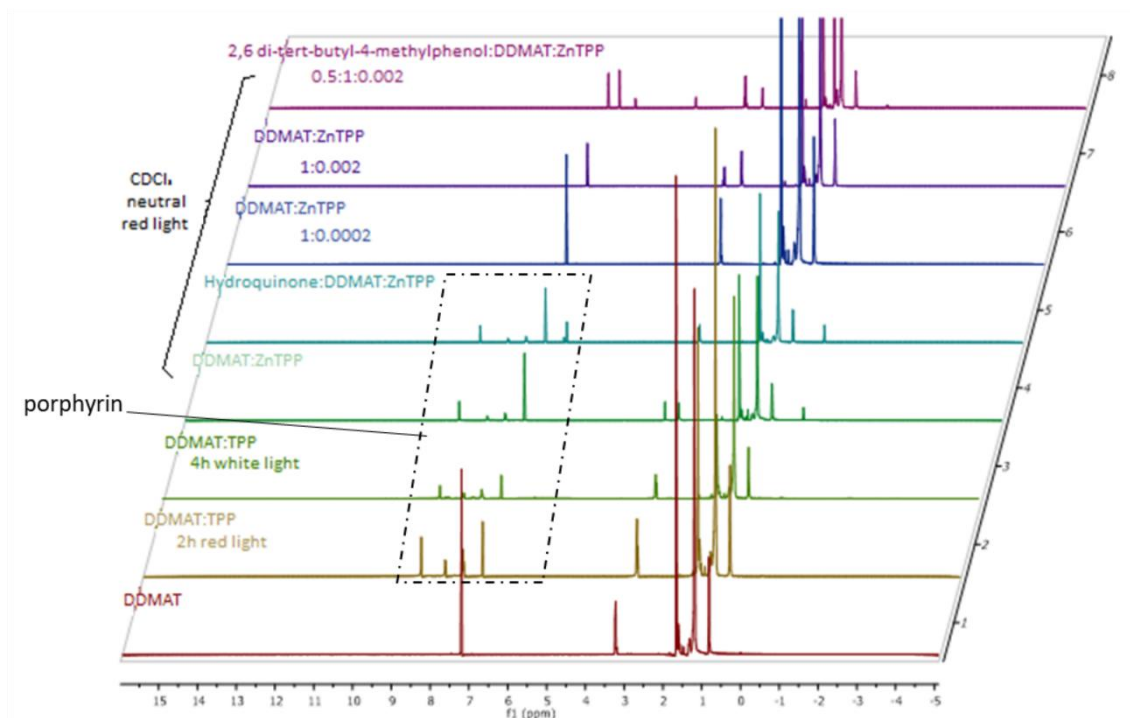Figure A 29 SEC in DMF solution of the PAI and PAI with Ce6 after irradiation (2 h, 650 nm, 80 mW.cm^{-2})

Figure A 30 ^{1}H NMR (400 MHz) spectrum of DDMAT in different concentrations in CDCl$_3$. DDMAT characteristic peaks are in the zone between δ= 3.40 and 3.30 ppm **CH**2-S; δ= 1.70 and 1.60 ppm -(CH2)9-**CH**2-; δ= 1.70 and 1.25 ppm-(**CH**2)9-; δ= 1.80 and 1.70 ppm -**CH**3 ramification and δ= 0.95 and 0.84 ppm -**CH**3 terminal group.